NATIONAL CENTER FOR EARTHQUAKE
ENGINEERING RESEARCH
State University of New York at Buffalo

PRACTICAL CONSIDERATIONS FOR STRUCTURAL CONTROL: SYSTEM UNCERTAINTY, SYSTEM TIME DELAY, AND TRUNCATION OF SMALL CONTROL FORCES

by

J.N. Yang and A. Akbarpour
Department of Civil, Mechanical and Environmental Engineering
The George Washington University
Washington, D.C. 20052

Technical Report NCEER-87-0018

August 10, 1987

This research was conducted at George Washington University and was partially supported by the National Science Foundation under Grant No. ECE 86-07591.

NOTICE

This report was prepared by The George Washington University as a result of research sponsored by the National Center for Earthquake Engineering Research (NCEER) and the National Science Foundation. Neither NCEER, associates of NCEER, its sponsors, The George Washington University, nor any person acting on their behalf:

a. makes any warranty, express or implied, with respect to the use of any information, apparatus, method, or process disclosed in this report or that such use may not infringe upon privately owned rights; or

b. assumes any liabilities of whatsoever kind with respect to the use of, or the damages resulting from the use of, any information, apparatus, method or process disclosed in this report.

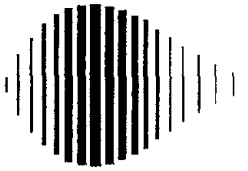

PRACTICAL CONSIDERATIONS FOR STRUCTURAL CONTROL: SYSTEM UNCERTAINTY, SYSTEM TIME DELAY, AND TRUNCATION OF SMALL CONTROL FORCES

by

J.N. Yang[1] and A. Akbarpour[2]

August 10, 1987

Technical Report NCEER-87-0018

NCEER Contract Number 86-3021

NSF Master Contract Number ECE-86-07591

and

NSF Grant No. ECE-85-21496

1 Professor, Dept. of Civil, Mechanical and Environmental Engineering, George Washington University

2 Graduate Research Assistant, Dept. of Civil, Mechanical and Environmental Engineering, George Washington University

NATIONAL CENTER FOR EARTHQUAKE ENGINEERING RESEARCH
State University of New York at Buffalo
Red Jacket Quadrangle, Buffalo, NY 14261

50272-101

REPORT DOCUMENTATION PAGE	1. REPORT NO. NCEER-87-0018	2.	3. Recipient's Accession No. PB88 163738/AS
4. Title and Subtitle: Practical Considerations for Structural Control: System Uncertainty, System Time Delay, and Truncation of Small Control Forces.			5. Report Date: August 10, 1987 6.
7. Author(s): J.N. Yang and A. Akbarpour			8. Performing Organization Rept. No.
9. Performing Organization Name and Address: National Center for Earthquake Engineering Research, SUNY/Buffalo, Red Jacket Quadrangle, Buffalo, NY 14261			10. Project/Task/Work Unit No. 11. Contract(C) or Grant(G) No. (C) ECE-85-21496 (G) 86-3021
12. Sponsoring Organization Name and Address: Same as box 9.			13. Type of Report & Period Covered: Technical Report 14.

15. Supplementary Notes

This research was conducted at George Washington University and was partially supported by the National Science Foundation under Grant No. ECE 86-07591.

16. Abstract (Limit: 200 words)

For practical application of structural control system, various important factors should be considered, including the system time delay, uncertainty in structural identification, truncation of small control forces, etc. A sensitivity study is conducted to investigate the effects of these factors on the control system of structures. THe influence of system time delay, estimation errors for structural parameters and elimination of small control forces on the efficiency of the control system depends upon the particular control algorithm used. Four control algorithms practical for applications to earthquake-excited structures have been studied. These include the Riccati closed-loop control algorithm and three instantaneous optimal control algorithms recently proposed. The methodologies for the sensitivity analysis are presented. Both the active tendon control system and the active mass damper have been considered. Numerical examples are worked out to demonstrate the criticality and tolerance of these factors for practical implementation of active control systems.

17. Document Analysis a. Descriptors

b. Identifiers/Open-Ended Terms

STRUCTURAL CONTROL
CONTROL ALGORITHMS
SEISMIC RELIABILITY ANALYSIS
EARTHQUAKE ENGINEERING
STRUCTURAL ANALYSIS

c. COSATI Field/Group

18. Availability Statement	19. Security Class (This Report)	21. No. of Pages
Release unlimited	unclassified	159
	20. Security Class (This Page) unclassified	22. Price

ABSTRACT

For practical application of structural control system, various important factors should be considered, including the system time delay, uncertainty in structural identification, truncation of small control forces, etc. A sensitivity study is conducted to investigate the effects of these factors on the control system of structures. The influence of system time delay, estimation errors for structural parameters and elimination of small control forces on the efficiency of the control system depends upon the particular control algorithm used. Four control algorithms practical for applications to earthquake-excited structures have been studied. These include the Riccati closed-loop control algorithm and three instantaneous optimal control algorithms recently proposed. The methodologies for the sensitivity analysis are presented. Both the active tendon control system and the active mass damper have been considered. Numerical examples are worked out to demonstrate the criticality and tolerance of these factors for practical implementation of active control systems.

TABLE OF CONTENTS

LIST OF ILLUSTRATIONS

LIST OF ILLUSTRATIONS (Continued)

LIST OF ILLUSTRATIONS (Continued)

LIST OF ILLUSTRATIONS (Continued)

LIST OF ILLUSTRATIONS (Continued)

LIST OF ILLUSTRATIONS (Continued)

LIST OF ILLUSTRATIONS (Continued)

LIST OF TABLES

I. INTRODUCTION

The use of protective systems, such as passive or active devices, to improve the reliability and safety of structures subjected to severe environmental loads, such as strong earthquakes, wind turbulences, etc. has received increasing attention recently. One potentially promising protective system is the active control device [e.g., Refs. 1-24] In this regard, considerable research efforts have been made for active control of seismic-excited building structures both theoretically and experimentally [e.g., 1-24]. In particular, new optimal control algorithms practical for applications to earthquake-excited structures have been proposed [17-18] and verified experimentally [4, 5]. Most studies in active control of civil engineering structures, however, are based on ideal control environments in the sense that the structural system can be identified precisely and the system time delay is negligible.

Even under well-controlled laboratory environments, the experimental results differ from those computed theoretically, and the experimental control efficiency is lower than the theoretical one [4, 5]. This can be attributed to several factors, such as system time delay, uncertainty in structural identification, software and hardware control devices, etc. For practical implementation of active control systems to full-scale structures, such important problems as system time delay, identification of structural parameters, etc., should be studied [24]. The investigation of these problems can be made theoretically by conducting a sensitivity study to determine their criticality and tolerance for the design of a control system.

The knowledge of a structural model and its parameters, such as stiffnesses, damping coefficients, and natural frequencies, should be given in the design of a control system. These parameters should be obtained via

a set of measurements for an as built structure. In practice, however, these parameters are estimated and their estimations involve errors and uncertainties. Thus, the efficiency of a control system depends on how closely these estimated parameter values approximate the actual ones. Likewise, the structural characteristics are affected by the service environments and they may change with service time. Any change in structural parameters may cause a change in controlled quantities. Thus, the uncertainties involved in the estimation of structural parameters may result in an adverse effect on the efficiency of the active control system.

Time delay exists within the control system, because of the following operations: (i) taking measurements of the response vector and/or the earthquake base accelerations and processing them, (ii) computing the required active control forces, (iii) generating signals to activate control devices, and (iv) generating the required magnitude of control force (i.e., the reaction time for the controller). Whether system time delay is detrimental to the control system and to what extent a time delay is tolerable for a particular control algorithm should be examined. Preliminary investigations in this regard have been made in Ref. 1.

When a structure is exposed to an earthquake, the time history of the active control force contains many cycles of small amplitudes. Because of limitations of actuators, it may be desirable to eliminate those control forces with magnitude smaller than a certain value. The effect of truncating small control forces on the structural response and the efficiency of the control system should be investigated.

The objective of this report is to investigate the effect of (i) uncertainty in structural identification, (ii) system time delay, and (iii) truncation of small control forces, on the efficiency of the active control system. A sensitivity study is conducted to study the effect and

criticality of these factors on the control system with respect to various control algorithms. Four control algorithms that have been demonstrated to be feasible and practical for earthquake-excited structures are investigated herein. These include the Riccati closed-loop control algorithm and three instantaneous optimal control algorithms recently proposed [17-18]. The methodology for the sensitivity analysis associated with each control algorithm is presented. Both the active tendon control system and the active mass damper have been considered. Numerical examples are worked out to demonstrate the tolerance of a control system for system time delay, estimation error for structural parameters, and truncation of small control forces.

II. CONTROL ALGORITHMS IN IDEAL ENVIRONMENTS

The method of analysis for investigating the influence of various factors described above on the control system varies with respect to the particular control algorithm used. Hence, the following control algorithms practical for applications to seismic-excited structures will be investigated separately. These include the Riccati closed-loop control algorithm and three instantaneous optimal control algorithms proposed recently [17-18].

For simplicity, consider a shear beam type building structure implemented by an active tendon control system as shown in Fig. 1. The structure is idealized by an n degrees of freedom system and subjected to a one-dimensional earthquake ground acceleration $\ddot{X}_0(t)$. The matrix equation of motion can be expressed as [e.g., 17-19]

$$\dot{\underset{\sim}{Z}}(t) = \underset{\sim}{A}\,\underset{\sim}{Z}(t) + \underset{\sim}{B}\,\underset{\sim}{U}(t) + \underset{\sim}{W}_1\,\ddot{X}_0(t) \tag{2.1}$$

with the initial condition $\underset{\sim}{Z}(0) = 0$. In Eq. (2.1), $\underset{\sim}{Z}(t)$ = 2n state vector, $\underset{\sim}{U}(t)$ = r dimensional control vector, $\underset{\sim}{A}$ = (2nx2n) system matrix, $\underset{\sim}{B}$ = (2nxr) matrix specifying the location of active controllers, and $\underset{\sim}{W}_1$ is an appropriate 2n vector [see Ref. 17 for these matrices]. In what follows, an under bar denotes a vector or matrix and a prime denotes the transpose of a vector or matrix.

Let $\underset{\sim}{\theta}$ be a (2nx2n) diagonal matrix consisting of complex eigenvalues θ_j (j = 1, 2,..., 2n) of matrix $\underset{\sim}{A}$, and $\underset{\sim}{T}$ be a (2nx2n) modal matrix consisting of the corresponding eigenvectors of $\underset{\sim}{A}$. Then, the solution of the equation of motion, Eq. (2.1), can be obtained numerically as [17]

$$\underset{\sim}{Z}(t) = \underset{\sim}{T}\,\underset{\sim}{D}(t-\Delta t) + \frac{\Delta t}{2}\left[\underset{\sim}{B}\,\underset{\sim}{U}(t) + \underset{\sim}{W}_1\,\ddot{X}_0(t)\right] \tag{2.2}$$

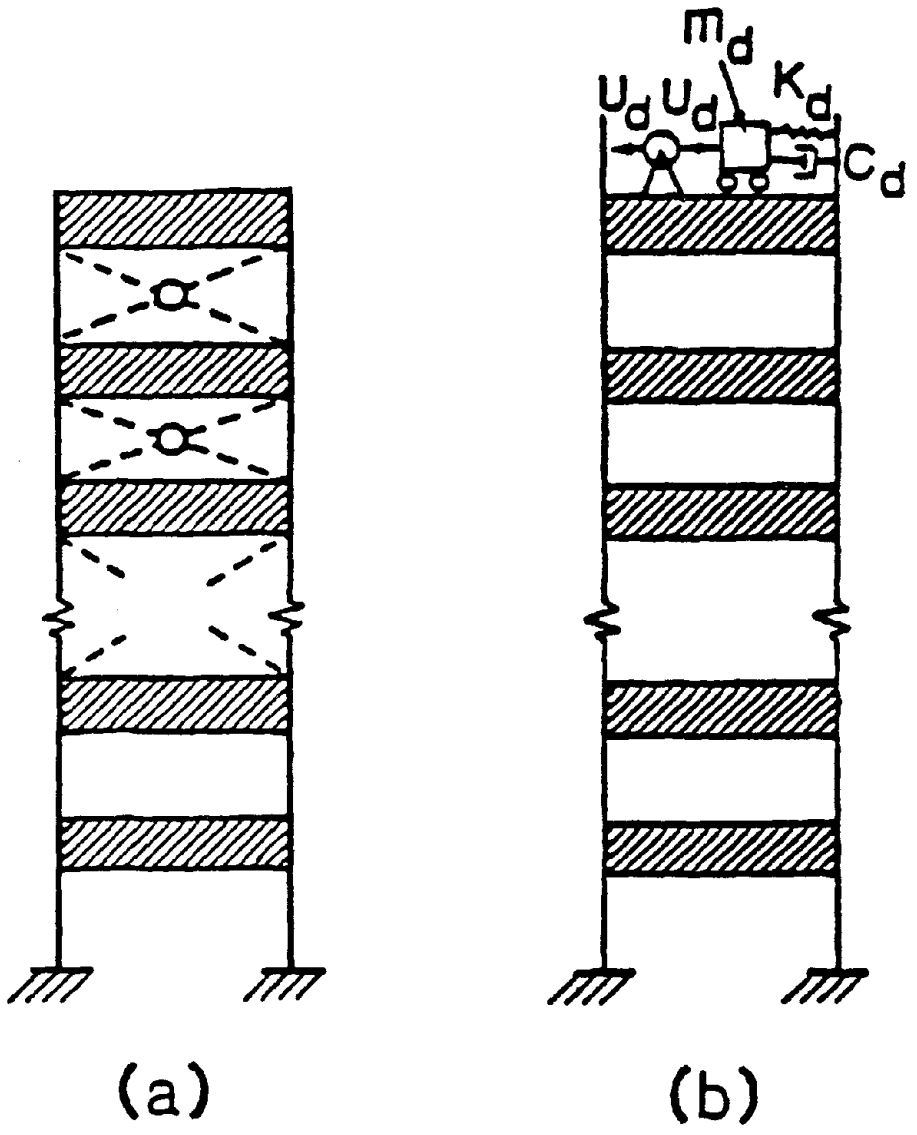

Fig. 1: Structural Model of a Multi-Story Building with Active Control System; (a) Active Tendon Control System; (b) Active Mass Damper

in which Δt is the integration step,

$$\underset{\sim}{D}(t-\Delta t) = e^{\underset{\sim}{\theta}\Delta t}\ \underset{\sim}{T}^{-1}\left\{\underset{\sim}{Z}(t-\Delta t) + \frac{\Delta t}{2}\left[\underset{\sim}{B}\ \underset{\sim}{U}(t-\Delta t) + \underset{\sim}{W}_1\ \ddot{X}_0(t-\Delta t)\right]\right\} \qquad (2.3)$$

is a vector containing all elements evaluated at $t-\Delta t$, and $e^{\underset{\sim}{\theta}\Delta t}$ is a (2nx2n) diagonal matrix with the jth diagonal element being $\exp[\theta_j \Delta t]$.

A time dependent performance index J(t) has been proposed recently by Yang, et al for optimizing the control system [17-19]

$$J(t) = \underset{\sim}{Z}'(t)\ \underset{\sim}{Q}\ \underset{\sim}{Z}(t) + \underset{\sim}{U}'(t)\ \underset{\sim}{R}\ \underset{\sim}{U}(t) \qquad (2.4)$$

in which $\underset{\sim}{Q}$ is a (2nx2n) positive semi-definite weighting matrix, and $\underset{\sim}{R}$ is a (rxr) positive definite weighting matrix. The three instantaneous optimal control algorithms to be investigated later are obtained by minimizing Eq. (2.4) subjected to the constraint of the equations of motion, Eq. (2.2), [17-18].

On the other hand, the classical performance index J is defined as the integral of J(t) over the time duration t_f longer than that of the earthquake excitation, i.e.,

$$J = \int_0^{t_f} J(t)\ dt \qquad (2.5)$$

As mentioned previously, the sensitivity of the control system with respect to various factors described above depends on the individual control algorithm. Further, the method of sensitivity analysis differs for each control algorithm. To facilitate the derivation of the solutions for each control algorithm in different environments, the four control algorithms in

ideal control environments, i.e., without system time delay, structural uncertainty, and truncation of control forces, will be summarized in the *following. For detail derivations, the reader is referred to Refs.* 17-18.

2.1 **Riccati Closed-Loop Control**: When the classical performance index J defined above, Eq. (2.5), is minimized subjected to the equation of motion, Eq. (2.1), and the external excitation $\ddot{X}_0(t)$ is disregarded, the so-called Riccati closed-loop control has been derived [Ref. 17-18]. For Riccati closed-loop control in ideal environments, the control vector $\underset{\sim}{U}(t)$ is regulated by the measured response state vector $\underset{\sim}{Z}(t)$,

$$\underset{\sim}{U}(t) = -\frac{1}{2} \underset{\sim}{R}^{-1} \underset{\sim}{B}' \underset{\sim}{P} \underset{\sim}{Z}(t) \tag{2.6}$$

in which $\underset{\sim}{P}$ is a (2nx2n) Riccati matrix computed from the following matrix Riccati equation

$$\underset{\sim}{P} \underset{\sim}{A} - \frac{1}{2} \underset{\sim}{P} \underset{\sim}{B} \underset{\sim}{R}^{-1} \underset{\sim}{B}' \underset{\sim}{P} + \underset{\sim}{A}' \underset{\sim}{P} + 2 \underset{\sim}{Q} = 0 \tag{2.7}$$

Although the Riccati matrix is time dependent, it has been shown in Refs. 17-18 that the constant Riccati matrix is an excellent approximation for earthquake excitations. The response state vector $\underset{\sim}{Z}(t)$ is computed numerically from the equation of motion

$$\dot{\underset{\sim}{Z}}(t) = \underset{\sim}{A} \underset{\sim}{Z}(t) + \underset{\sim}{B} \underset{\sim}{U}(t) + \underset{\sim}{W}_1 \ddot{X}_0(t) \tag{2.8}$$

A block diagram for the Riccati closed-loop control algorithm is displayed in Fig. 2.

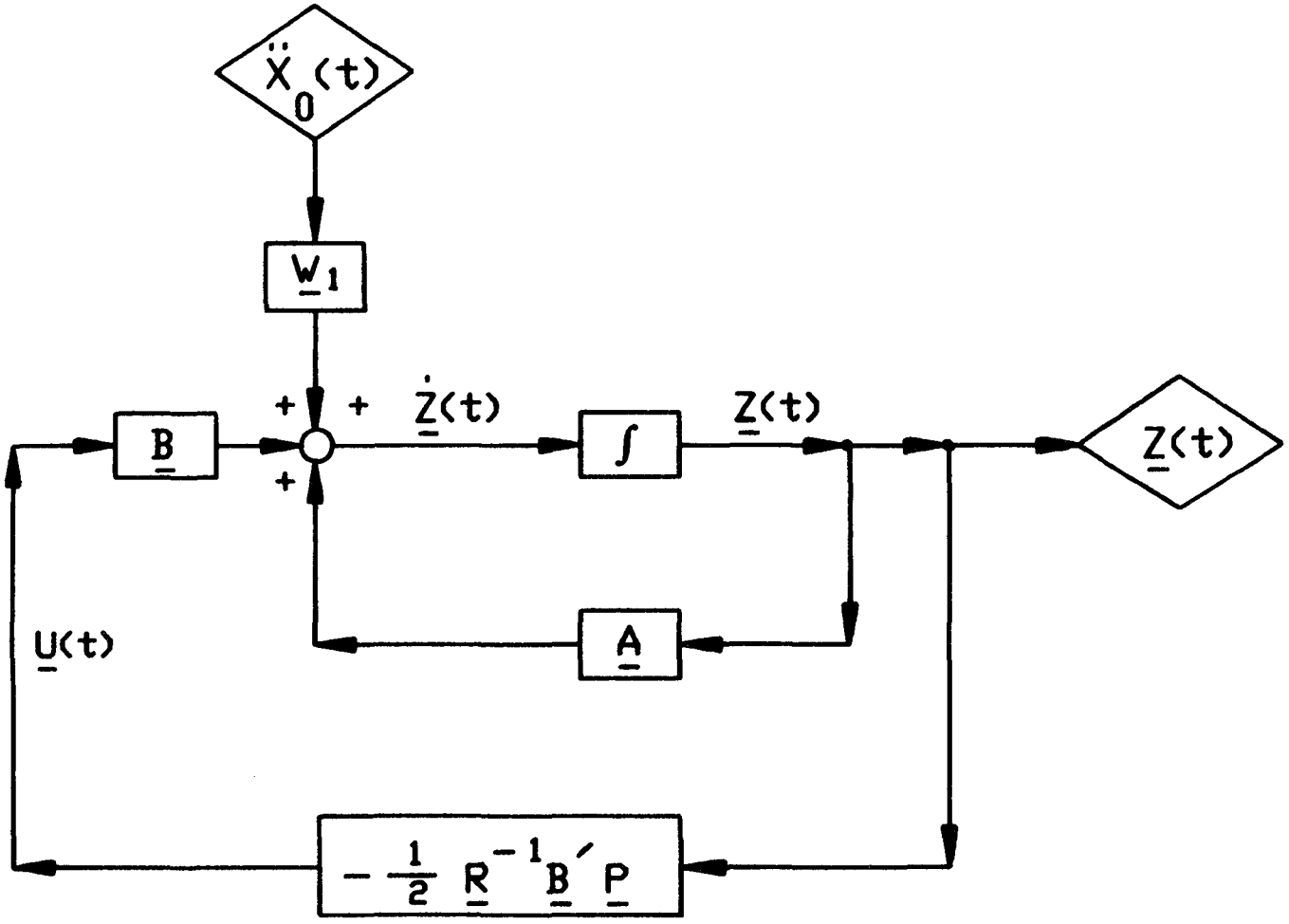

Fig. 2 : Block Diagram For Riccati Closed-Loop Control.

2.2. Instantaneous Optimal Closed-Loop Control: The so-called instantaneous optimal closed-loop control algorithm is obtained by minimizing the time dependent performance index J(t), Eq. (2.4), subjected to the constraint of the equations of motion, Eq. (2.2), and assuming that the control vector $\underset{\sim}{U}(t)$ is regulated by the measured response state vector [17-18]. For such a control algorithm, the control vector $\underset{\sim}{U}(t)$ is related to the feedback state vector $\underset{\sim}{Z}(t)$ as

$$\underset{\sim}{U}(t) = \underset{\sim}{G}\ \underset{\sim}{Z}(t) \tag{2.9}$$

in which the gain matrix $\underset{\sim}{G}$ is given by

$$\underset{\sim}{G} = -(\Delta t/2)\ \underset{\sim}{R}^{-1}\ \underset{\sim}{B}'\ \underset{\sim}{Q} \tag{2.10}$$

The response state vector $\underset{\sim}{Z}(t)$ is computed numerically using the following discretized equation of motion

$$\underset{\sim}{Z}(t) = \underset{\sim}{T}\ \underset{\sim}{D}(t-\Delta t) + (\Delta t/2)\left[\ \underset{\sim}{B}\ \underset{\sim}{U}(t) + \underset{\sim}{W}_1\ \ddot{X}_0(t)\ \right] \tag{2.11}$$

where $\underset{\sim}{D}(t-\Delta t)$ is the vector denoting the system's boundary conditions at time $t-\Delta t$ given by Eq. (2.3). A block diagram describing such a control algorithm is shown in Fig. 3.

2.3 Instantaneous Optimal Open-Loop Control: Based on the instantaneous optimal open-loop control algorithm, the control vector $\underset{\sim}{U}(t)$ is computed on-line, real-time, using the sensed base acceleration, $\ddot{X}_0(t)$, at time t as follows [17-18]

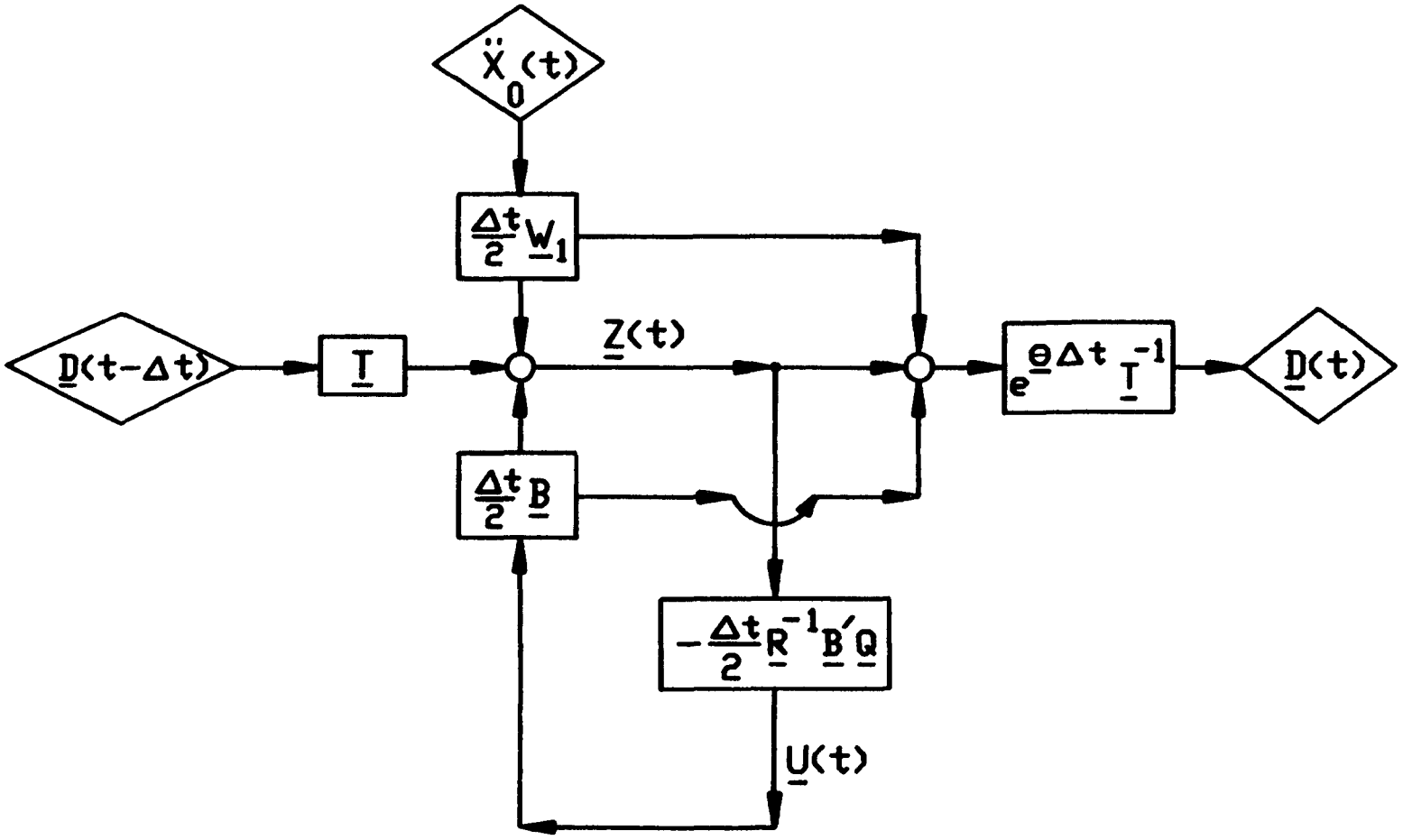

Fig. 3 : Block Diagram For Instantaneous Optimal Closed-Loop Control

$$\underset{\sim}{U}(t) = \underset{\sim}{L}\ \underset{\sim}{G}(t) \tag{2.12}$$

in which

$$\underset{\sim}{L} = \left[(\Delta t/2)^2\ \underset{\sim}{B}'\ \underset{\sim}{Q}\ \underset{\sim}{B} + \underset{\sim}{R} \right]^{-1} \tag{2.13}$$

$$\underset{\sim}{G}(t) = -(\Delta t/2)\ \underset{\sim}{B}'\ \underset{\sim}{Q}\ \underset{\sim}{T}\ \underset{\sim}{D}(t-\Delta t) - (\Delta t/2)^2\ \underset{\sim}{B}'\ \underset{\sim}{Q}\ \underset{\sim}{W}_1\ \ddot{X}_0(t) \tag{2.14}$$

where $\underset{\sim}{D}(t-\Delta t)$ is defined by Eq. (2.3). The response state vector $\underset{\sim}{Z}(t)$ is given by

$$\underset{\sim}{Z}(t) = \underset{\sim}{T}\ \underset{\sim}{D}(t-\Delta t) + (\Delta t/2)\ \underset{\sim}{B}\ \underset{\sim}{L}\ \underset{\sim}{G}(t) + (\Delta t/2)\ \underset{\sim}{W}_1\ \ddot{X}_0(t) \tag{2.15}$$

A block diagram for the instantaneous optimal open-loop control algorithm in ideal environments is displayed in Fig. 4.

2.4 Instantaneous Optimal Closed-Open-Loop Control: For the instantaneous optimal closed-open-loop control algorithm, the control vector $\underset{\sim}{U}(t)$ is regulated by both the measured base acceleration, $\ddot{X}_0(t)$, and the feedback state vector, $\underset{\sim}{Z}(t)$, as follows [17-18]

$$\underset{\sim}{U}(t) = (\Delta t/4)\underset{\sim}{R}^{-1}\ \underset{\sim}{B}'\left[\underset{\sim}{\Lambda}\ \underset{\sim}{Z}(t) + \tilde{\underset{\sim}{q}}(t) \right] \tag{2.16}$$

in which $\tilde{\underset{\sim}{\Lambda}}$ is a (2nx2n) constant gain matrix representing the closed-loop portion of the control force, and $\tilde{\underset{\sim}{q}}(t)$ is a 2n vector denoting the open-loop portion of the control force,

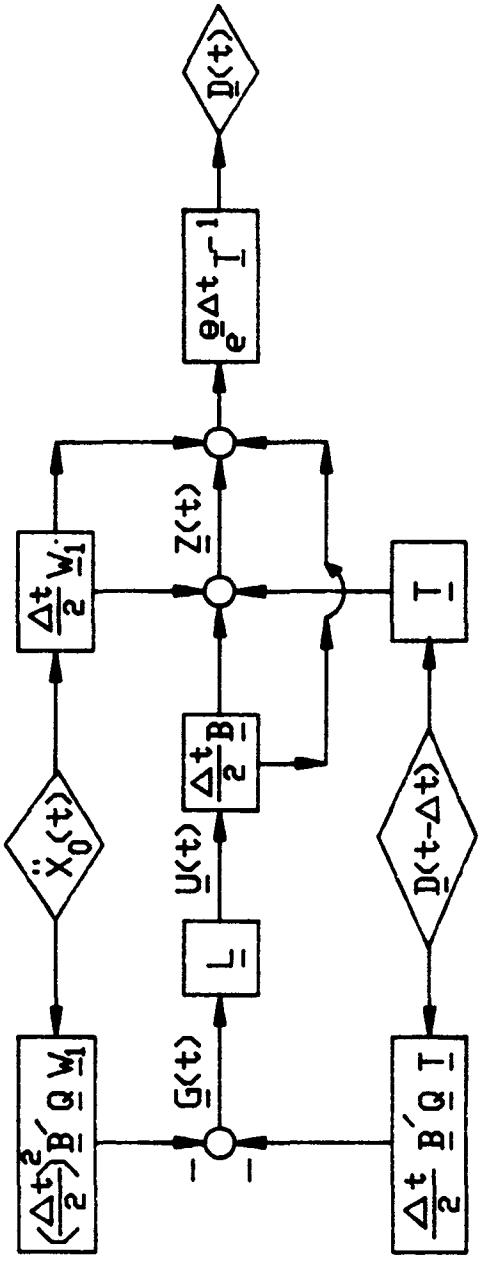

Fig. 4 : Block Diagram For Instantaneous Optimal Open-Loop Control.

$$\tilde{\underline{g}}(t) = \tilde{\underline{\Lambda}} \left[\underline{T} \, \underline{D}(t-\Delta t) + (\Delta t/2)\underline{W}_1 \, \ddot{X}_0(t) \right] \tag{2.17}$$

$$\tilde{\underline{\Lambda}} = - \left[\frac{(\Delta t)^2}{8} \, \underline{Q} \, \underline{B} \, \underline{R}^{-1} \, \underline{B}' + \underline{I} \right]^{-1} \underline{Q} \tag{2.18}$$

The response state vector $\underline{Z}(t)$ is calculated numerically as

$$\underline{Z}(t) = \underline{T} \, \underline{D}(t-\Delta t) + (\Delta t/2) \left[\underline{B} \, \underline{U}(t) + \underline{W}_1 \, \ddot{X}_0(t) \right] \tag{2.19}$$

A block diagram describing the instantaneous optimal closed-open-loop control algorithm in ideal environments is shown in Fig. 5.

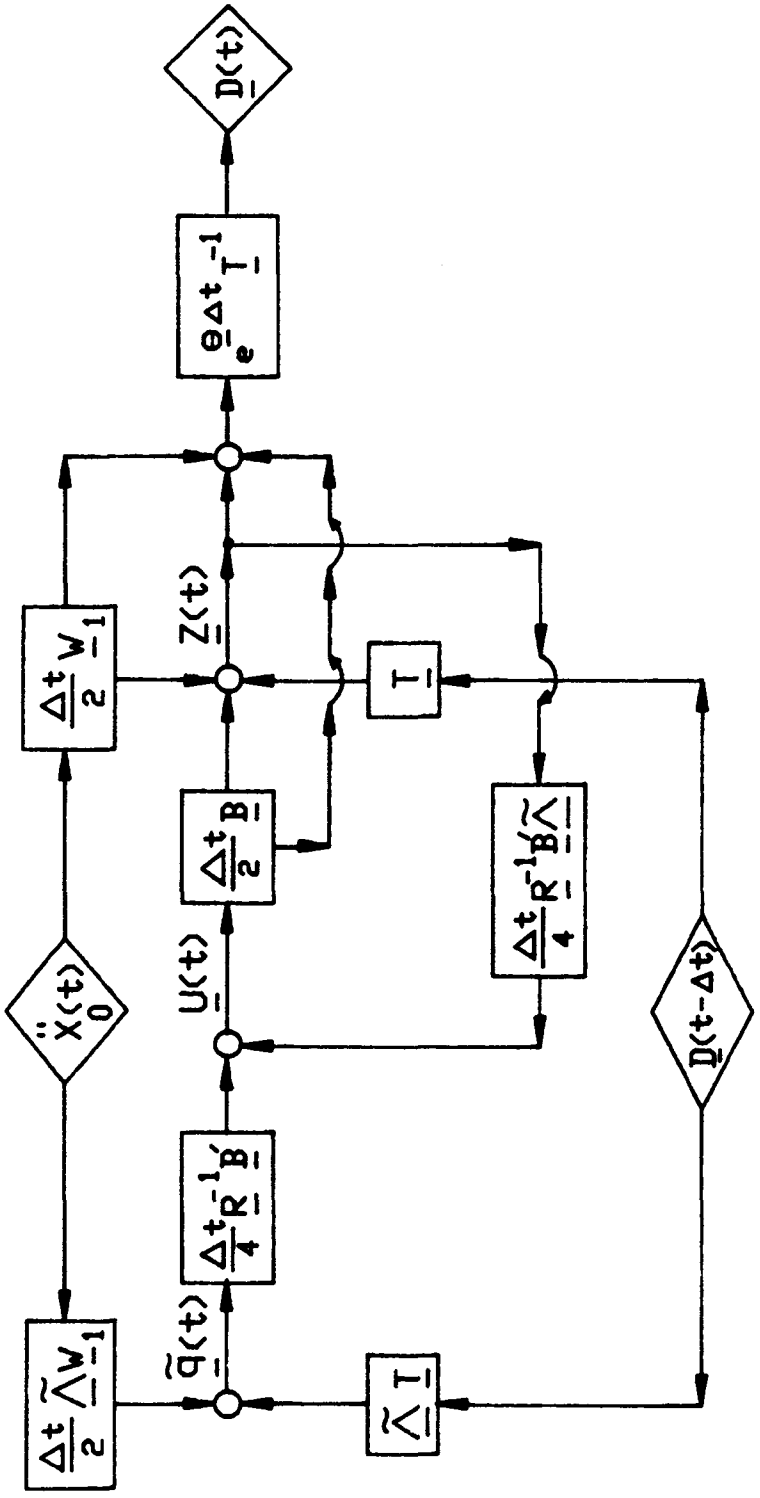

Fig. 5 : Block Diagram For Instantaneous Optimal Closed-Open-Loop Control

III. STRUCTURAL CONTROL WITH SYSTEM UNCERTAINTY

When the structural parameters, such as stiffnesses, natural frequencies, damping ratios, etc., involve uncertainties, the response state vector $\underset{\sim}{Z}(t)$ and the control vector $\underset{\sim}{U}(t)$ deviate from the solutions derived above in ideal environments. The solutions for $\underset{\sim}{Z}(t)$ and $\underset{\sim}{U}(t)$ for a control system with estimation errors in structural parameters will be derived in this section.

The system matrix $\underset{\sim}{A}$ represents the structural characteristics and the elements of matrix $\underset{\sim}{A}$ are functions of structural parameters, including masses, stiffnesses, and dampings. In reality, structural (system) parameters can not be identified precisely and they involve considerable statistical variabilities. As a result, the actual $\underset{\sim}{A}$ matrix is unknown. Let $\underset{\sim}{A}^*$ be the best estimate of the system matrix $\underset{\sim}{A}$. Of course, $\underset{\sim}{A}^*$ deviates from $\underset{\sim}{A}$ and the extent of deviation with respect to the degradation of the control efficiency will be studied.

3.1 Riccati Closed-Loop Control: With the estimated system matrix $\underset{\sim}{A}^*$, the estimated Riccati matrix, denoted by $\underset{\sim}{P}^*$, is computed from Eq. (2.7) in which $\underset{\sim}{A}$ replaced by $\underset{\sim}{A}^*$, i.e.,

$$\underset{\sim}{P}^* \underset{\sim}{A}^* - \frac{1}{2} \underset{\sim}{P}^* \underset{\sim}{B} \underset{\sim}{R}^{-1} \underset{\sim}{B}' \underset{\sim}{P}^* + \underset{\sim}{A}^{*\prime} \underset{\sim}{P}^* + 2 \underset{\sim}{Q} = 0 \tag{3.1}$$

The control vector $\underset{\sim}{U}(t)$ is computed using $\underset{\sim}{P}^*$ and the measured state vector $\underset{\sim}{Z}(t)$ as,

$$\underset{\sim}{U}(t) = - \frac{1}{2} \underset{\sim}{R}^{-1} \underset{\sim}{B}' \underset{\sim}{P}^* \underset{\sim}{Z}(t) \tag{3.2}$$

The equations of motion for the entire structural system is obtained by substituting Eq. (3.2) into Eq. (2.1) as follows

$$\underset{\sim}{\dot{Z}}(t) = \tilde{\underset{\sim}{A}}\ \underset{\sim}{Z}(t) + \underset{\sim}{W}_1\ \ddot{X}_0(t) \tag{3.3}$$

in which $\tilde{\underset{\sim}{A}}$ is a (2n x 2n) matrix given by

$$\tilde{\underset{\sim}{A}} = \underset{\sim}{A} - \frac{1}{2}\ \underset{\sim}{B}\ \underset{\sim}{R}^{-1}\ \underset{\sim}{B}'\ \underset{\sim}{P}^{*} \tag{3.4}$$

Thus, the state vector $\underset{\sim}{Z}(t)$ can be computed numerically using Eq. (3.3) as follows

$$Z(t) = \tilde{\underset{\sim}{T}}\ e^{\tilde{\theta}\Delta t}\ \tilde{\underset{\sim}{T}}^{-1}\left[\underset{\sim}{Z}(t-\Delta t) + (\Delta t/2)\ \underset{\sim}{W}_1\ \ddot{X}_0(t-\Delta t)\right] + (\Delta t/2)\ \underset{\sim}{W}_1\ \ddot{X}_0(t) \tag{3.5}$$

in which $\exp(\tilde{\underset{\sim}{\theta}}\Delta t)$ is a (2nx2n) diagonal matrix with the jth diagonal element being $\exp(\tilde{\theta}_j \Delta t)$, where $\tilde{\theta}_j$ is the jth eigenvalue of $\tilde{\underset{\sim}{A}}$. In Eq. (3.5), $\tilde{\underset{\sim}{T}}$ is the modal matrix consisting of eigenvectors of $\tilde{\underset{\sim}{A}}$ matrix.

A block diagram for simulating the entire control process with uncertainties in structural parameters is displayed in Fig. 6.

3.2 <u>Instantaneous Optimal Closed-Loop Control</u>: For the instantaneous optimal closed-loop control algorithm, the control vector is related to the feedback state vector $\underset{\sim}{Z}(t)$ through a gain matrix $\underset{\sim}{G}$, Eq. (2.9). The gain matrix $\underset{\sim}{G}$ given by Eq. (2.10) is, however, not a function of the system matrix $\underset{\sim}{A}$. Hence, both the control vector $\underset{\sim}{U}(t)$ and the gain matrix $\underset{\sim}{G}$ are not functions of structural parameters. Therefore, instantaneous optimal closed-loop control is independent of the uncertainties involved in

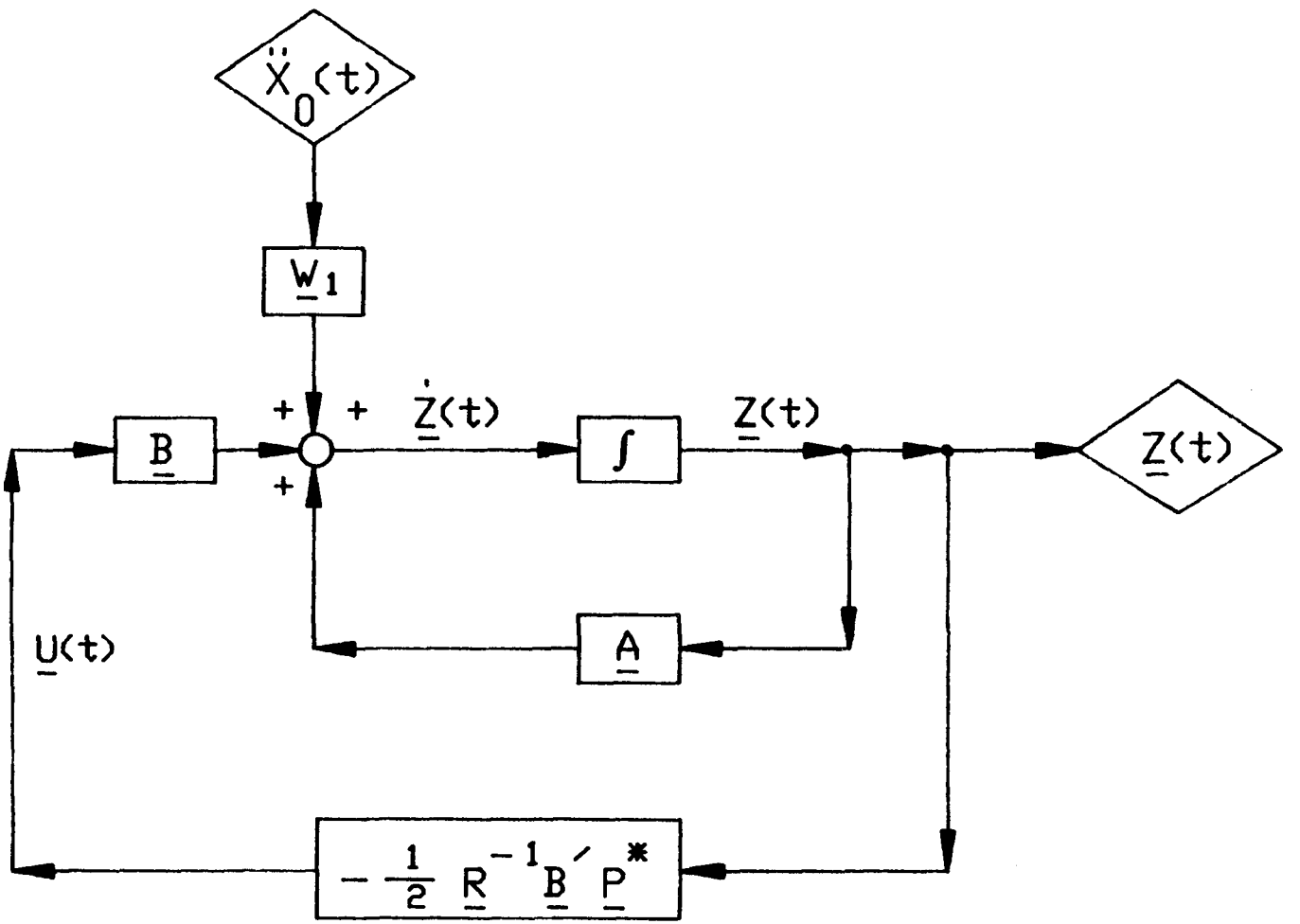

Fig. 6 : Block Diagram For Riccati Closed-Loop Control With Uncertainties In Structural Identification.

determining structural parameters, such as stiffnesses, dampings, natural frequencies, etc. In other words, whether the structural parameters are estimated accurately or not the control efficiency is not affected.

3.3 Instantaneous Optimal Open-Loop Control: Based on the instantaneous optimal open-loop control algorithm without system uncertainty, the control vector $\underset{\sim}{U}(t)$ is computed from the sensed ground acceleration, $\ddot{X}_0(t)$, at time t and the calculated vector $\underset{\sim}{D}(t-\Delta t)$, see Eqs. (2.12)-(2.14) and Eq. (2.3). The vector $\underset{\sim}{D}(t-\Delta t)$ is a function of the state vector $\underset{\sim}{Z}(t-\Delta t)$, where $\underset{\sim}{Z}(t-\Delta t)$ is estimated rather than measured for the open-loop control algorithm. Further, the response state vector $\underset{\sim}{Z}(t)$ is estimated numerically from Eq. (2.15) rather than being measured.

When the structural parameters involve uncertainties, the estimated system matrix $\underset{\sim}{A}^*$, rather than the true matrix $\underset{\sim}{A}$, is used for computing the state vectors, $\underset{\sim}{Z}^*(t-\Delta t)$ and $\underset{\sim}{Z}^*(t)$, as well as vectors $\underset{\sim}{D}^*(t-\Delta t)$ and $\underset{\sim}{U}^*(t)$. Thus, the estimated equation of motion is given as follows

$$\dot{\underset{\sim}{Z}}^*(t) = \underset{\sim}{A}^* \underset{\sim}{Z}^*(t) + \underset{\sim}{B} \underset{\sim}{U}^*(t) + \underset{\sim}{W}_1 \ddot{X}_0(t) \; ; \quad \underset{\sim}{Z}^*(0) = 0 \tag{3.6}$$

Let $\underset{\sim}{\theta}^*$ be a (2nx2n) diagonal matrix consisting of complex eigenvalues θ_j^* (j = 1, 2,..., 2n) of matrix $\underset{\sim}{A}^*$, and $\underset{\sim}{T}^*$ be a (2nx2n) modal matrix consisting of eigenvectors of $\underset{\sim}{A}^*$. Then, the solution of Eq. (3.6), can be obtained numerically as

$$\underset{\sim}{Z}^*(t) = \underset{\sim}{T}^* \underset{\sim}{D}^*(t-\Delta t) + (\Delta t/2) \left[\underset{\sim}{B} \underset{\sim}{U}^*(t) + \underset{\sim}{W}_1 \ddot{X}_0 \right] \tag{3.7}$$

in which

$$\underset{\sim}{D}^*(t-\Delta t) = e^{\underset{\sim}{\theta}^*\Delta t}\ [\underset{\sim}{T}^*]^{-1}\left\{\underset{\sim}{Z}^*(t-\Delta t) + (\Delta t/2)\left[\underset{\sim}{B}\ \underset{\sim}{U}^*(t-\Delta t) + \underset{\sim}{W}_1\ \ddot{X}_0(t-\Delta t)\right]\right\} \tag{3.8}$$

and the estimated control vector $\underset{\sim}{U}^*(t)$ applied to the structure is

$$\underset{\sim}{U}^*(t) = \underset{\sim}{L}\ \underset{\sim}{G}^*(t) \tag{3.10}$$

where $\underset{\sim}{L}$ is given by Eq. (2.13) and

$$\underset{\sim}{G}^*(t) = -(\Delta t/2)\ \underset{\sim}{B}'\ \underset{\sim}{Q}\ \underset{\sim}{T}^*\ \underset{\sim}{D}^*(t-\Delta t) - (\Delta t/2)^2\ \underset{\sim}{B}'\ \underset{\sim}{Q}\ \underset{\sim}{W}_1\ \ddot{X}_0(t) \tag{3.11}$$

Thus, the control vector $\underset{\sim}{U}^*(t)$ and the estimated response state vector $\underset{\sim}{Z}^*(t)$ can be computed numerically from Eqs. (3.7)-(3.11). A block diagram for such a control operation is shown on the left hand side of Fig. 7.

Note that the estimated control vector $\underset{\sim}{U}^*(t)$ is actually applied to the structure, whereas the estimated state vector, $\underset{\sim}{Z}^*(t)$, that is computed for the purpose of estimating the control vector $\underset{\sim}{U}^*(t)$, is not the actual response state vector. The actual response state vector $\underset{\sim}{Z}(t)$, can be synthesized using the actual system matrix $\underset{\sim}{A}$ as well as the control vector $\underset{\sim}{U}^*(t)$ that is applied to the structure as follows:

$$\dot{\underset{\sim}{Z}}(t) = \underset{\sim}{A}\ \underset{\sim}{Z}(t) + \underset{\sim}{B}\ \underset{\sim}{U}^*(t) + \underset{\sim}{W}_1\ \ddot{X}_0(t) \quad ; \quad \underset{\sim}{Z}(0) = 0 \tag{3.12}$$

or

$$\underset{\sim}{Z}(t) = \underset{\sim}{T}\ \underset{\sim}{D}(t-\Delta t) + (\Delta t/2)\left[\ \underset{\sim}{B}\ \underset{\sim}{U}^*(t) + \underset{\sim}{W}_1\ \ddot{X}_0(t)\ \right] \tag{3.13}$$

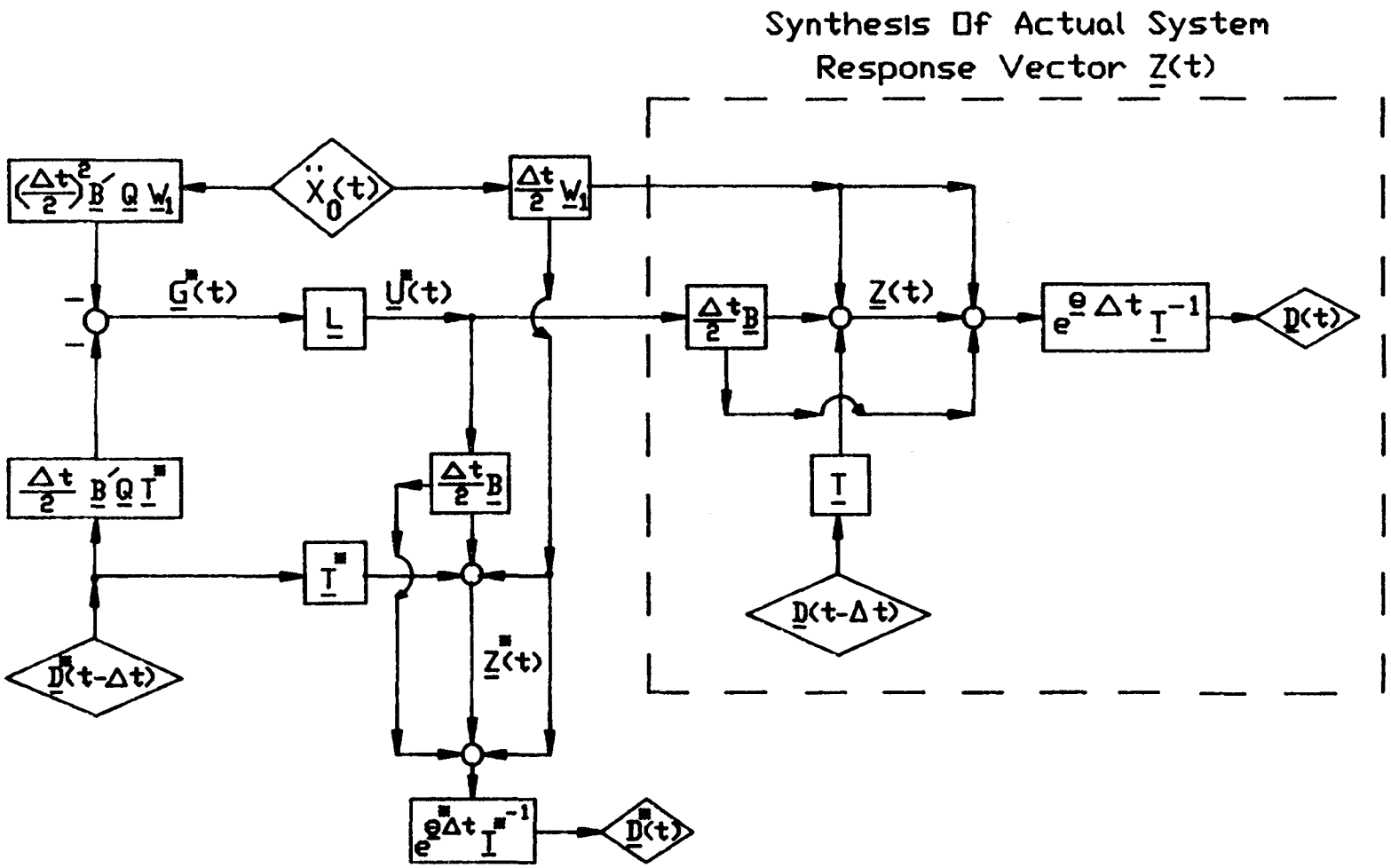

Fig. 7 : Block Diagram For Instantaneous Optimal Open-Loop Control With Uncertainties In Structural Identification.

where

$$\underset{\sim}{D}(t-\Delta t) = e^{\underset{\sim}{\theta}\Delta t}\ \underset{\sim}{T}^{-1}\left\{\underset{\sim}{Z}(t-\Delta t) + (\Delta t/2)\left[\underset{\sim}{B}\ \underset{\sim}{U}^{*}(t-\Delta t) + \underset{\sim}{W}_1\ \ddot{X}_0(t-\Delta t)\right]\right\} \qquad (3.14)$$

It should be mentioned that the system matrix $\underset{\sim}{A}$ is unknown. However, for the purpose of investigating the effect of uncertainty in structural identification, the actual response state vector $\underset{\sim}{Z}(t)$ is synthesized using the $\underset{\sim}{A}$ matrix. A block diagram for the synthesis of the actual response state vector $\underset{\sim}{Z}(t)$ is shown on the right hand side of Fig. 7.

3.4 Instantaneous Optimal Closed-Open-Loop Control: For instantaneous optimal closed-open-loop control without system uncertainty, the control vector $\underset{\sim}{U}(t)$ is regulated by the response state vector $\underset{\sim}{Z}(t)$ and the measured earthquake base acceleration given by Eqs. (2.16)-(2.18).

With system uncertainties, the best estimate, $\underset{\sim}{A}^{*}$, for the system matrix $\underset{\sim}{A}$ should be used in computing the control vector $\underset{\sim}{U}(t)$. Thus, the estimated control vector to be applied to the structure, $\underset{\sim}{U}^{*}(t)$, is given by

$$\underset{\sim}{U}^{*}(t) = (\Delta t/4)\underset{\sim}{R}^{-1}\ \underset{\sim}{B}'\ \left[\tilde{\underset{\sim}{\Lambda}}\ \underset{\sim}{Z}(t) + \tilde{\underset{\sim}{q}}^{*}(t)\right] \qquad (3.15)$$

in which the response state vector $\underset{\sim}{Z}(t)$ is measured. In Eq. (3.15), $\tilde{\underset{\sim}{q}}^{*}(t)$ is a 2n vector representing the contribution from open-loop control, which is computed based on the estimated system matrices $\underset{\sim}{A}^{*}$ and its modal matrix $\underset{\sim}{T}^{*}$, i.e.,

$$\tilde{\underset{\sim}{q}}^{*}(t) = \tilde{\underset{\sim}{\Lambda}}\ \left[\underset{\sim}{T}^{*}\ \underset{\sim}{D}^{*}(t-\Delta t) + (\Delta t/2)\ \underset{\sim}{W}_1\ \ddot{X}_0(t)\right] \qquad (3.16)$$

in which $\tilde{\underset{\sim}{\Lambda}}$ is given by Eq. (2.18) and $\underset{\sim}{D}^{*}(t-\Delta t)$ is estimated as follows

$$\underset{\sim}{D}^*(t-\Delta t) = e^{\underset{\sim}{\theta}^*\Delta t}\ [\underset{\sim}{T}^*]^{-1}\left\{\underset{\sim}{Z}(t-\Delta t) + (\Delta t/2)\left[\underset{\sim}{B}\ \underset{\sim}{U}^*(t-\Delta t) + \underset{\sim}{W}_1\ddot{X}_0(t-\Delta t)\right]\right\} \tag{3.17}$$

The actual response state vector $\underset{\sim}{Z}(t)$ that is measured during the control operation can be synthesized using the true system matrix $\underset{\sim}{A}$ as well as the control vector $\underset{\sim}{U}^*(t)$ computed above, i.e.,

$$\dot{\underset{\sim}{Z}}(t) = \underset{\sim}{A}\ \underset{\sim}{Z}(t) + \underset{\sim}{B}\ \underset{\sim}{U}^*(t) + \underset{\sim}{W}_1\ \ddot{X}_0(t) \tag{3.18}$$

and the numerical solution of Eq. (3.18) can be written as

$$\underset{\sim}{Z}(t) = \underset{\sim}{T}\ \underset{\sim}{D}(t-\Delta t) + (\Delta t/2)\left[\ \underset{\sim}{B}\ \underset{\sim}{U}^*(t) + \underset{\sim}{W}_1\ \ddot{X}_0(t)\ \right] \tag{3.19}$$

in which $\underset{\sim}{D}(t-\Delta t)$ is synthesized again using the true system matrix $\underset{\sim}{A}$, i.e.,

$$\underset{\sim}{D}(t-\Delta t) = e^{\underset{\sim}{\theta}\Delta t}\ \underset{\sim}{T}\left\{\underset{\sim}{Z}(t-\Delta t) + (\Delta t/2)\left[\underset{\sim}{B}\ \underset{\sim}{U}^*(t-\Delta t) + \underset{\sim}{W}_1\ \ddot{X}_0(t-\Delta t)\right]\right\} \tag{3.20}$$

The computational procedures for determining $\underset{\sim}{U}^*(t)$ and for synthesizing $\underset{\sim}{Z}(t)$ are summarized in the following. First, $\underset{\sim}{Z}(t)$ is computed by substituting Eq. (3.15) into Eq. (3.19). Second, $\underset{\sim}{U}^*(t)$ is obtained by substituting the computed $\underset{\sim}{Z}(t)$ obtained above into Eq. (3.15). A block diagram for the synthesis of the entire control operation is presented in Fig. 8, when the system identification involves uncertainties.

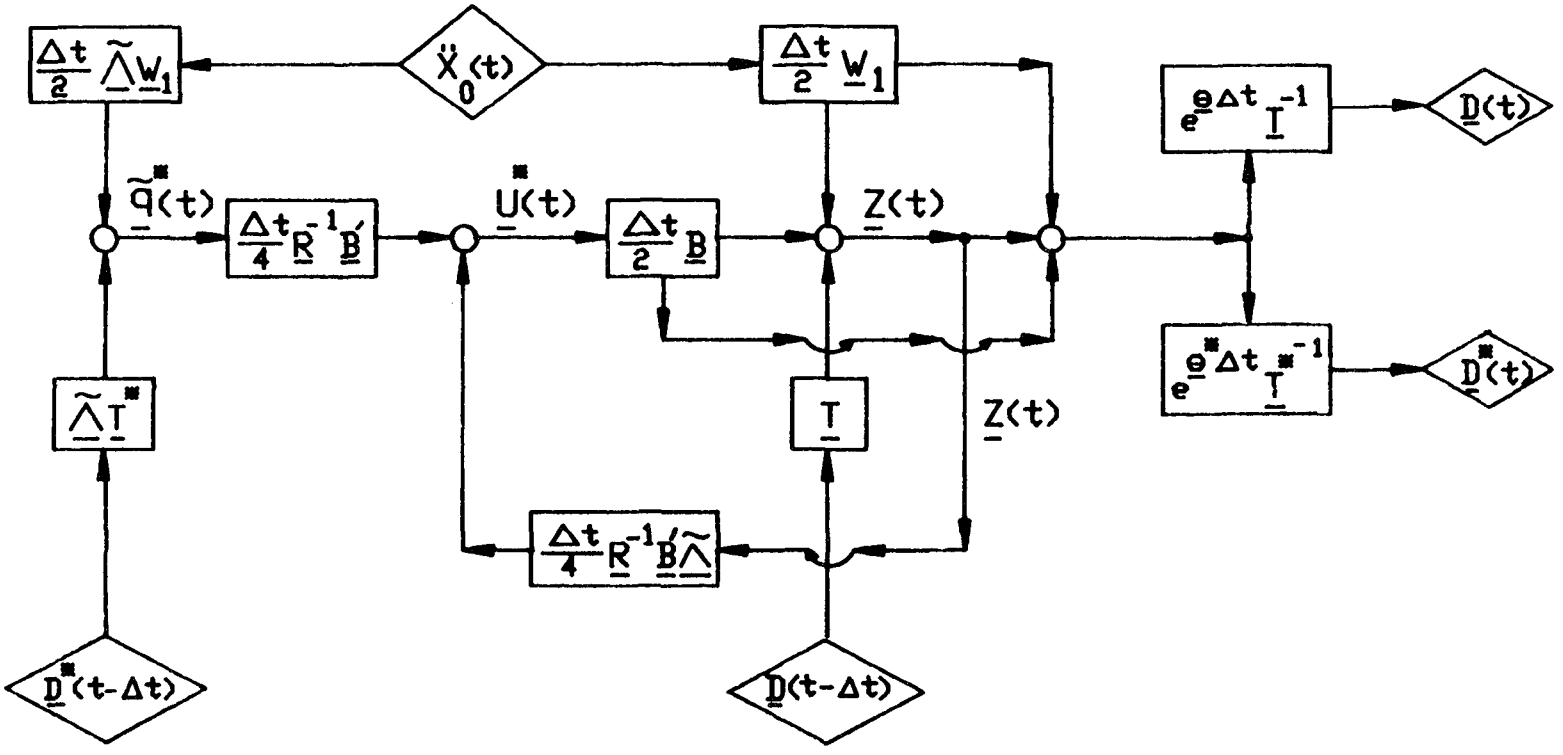

Fig. 8 : Block Diagram For Instantaneous Optimal Closed-Open-Loop Control With Uncertainties In Structural Identification.

IV. STRUCTURAL CONTROL WITH SYSTEM TIME DELAY

Four control algorithms without system time delay have been summarized in Section II. With a system time delay, the response state vector $\underset{\sim}{Z}(t)$ and the control vector $\underset{\sim}{U}(t)$ will deviate from those given in Section II. The solution for $\underset{\sim}{Z}(t)$ and $\underset{\sim}{U}(t)$ using each control algorithm with a system time delay will be derived in the following.

Let τ be the time delay for the control vector $\underset{\sim}{U}(t)$. In other words, the control vector $\underset{\sim}{U}(t-\tau)$ is applied to the structural system at time t, such that the equation of motion becomes

$$\dot{\underset{\sim}{Z}}(t) = \underset{\sim}{A}\ \underset{\sim}{Z}(t) + \underset{\sim}{B}\ \underset{\sim}{U}(t-\tau) + \underset{\sim}{W}_1\ \ddot{X}_0(t) \tag{4.1}$$

4.1 Riccati Closed-Loop Control: For Riccati closed-loop control, the gain matrix, denoted by $\underset{\sim}{G}$, is constant, i.e.,

$$\underset{\sim}{U}(t) = \underset{\sim}{G}\ \underset{\sim}{Z}(t) = -\frac{1}{2}\ \underset{\sim}{R}^{-1}\ \underset{\sim}{B}'\underset{\sim}{P}\ \underset{\sim}{Z}(t) \tag{4.2}$$

in which $\underset{\sim}{G} = -\ (1/2)\ \underset{\sim}{R}^{-1}\ \underset{\sim}{B}'\ \underset{\sim}{P}$. Hence, the equation of motion is given by

$$\dot{\underset{\sim}{Z}}(t) = \underset{\sim}{A}\ \underset{\sim}{Z}(t) + \underset{\sim}{B}\ \underset{\sim}{G}\ \underset{\sim}{Z}(t-\tau) + \underset{\sim}{W}_1\ \ddot{X}_0(t) \tag{4.3}$$

Eq. (4.3) can be integrated step-by-step with an integration inteval Δt if the response state vector, $\underset{\sim}{Z}(t-\tau)$, at $t-\tau$ is known. For simplicity, the integration step size Δt is chosen to be equal to the time delay τ, i.e., $\Delta t = \tau$. Thus, the numerical solution for Eq. (4.3) can be expressed similar to Eqs. (2.2) and (2.3) as

$$\underset{\sim}{Z}(t) = \underset{\sim}{T}\, e^{\underset{\sim}{\theta}\tau}\, \underset{\sim}{T}^{-1} \left\{ \underset{\sim}{Z}(t-\tau) + (\tau/2) \left[\underset{\sim}{B}\, \underset{\sim}{G}\, \underset{\sim}{Z}(t-2\tau) + \underset{\sim}{W}_1\, \ddot{X}_0(t-\tau) \right] \right\}$$

$$+ (\tau/2) \left[\underset{\sim}{B}\, \underset{\sim}{G}\, \underset{\sim}{Z}(t-\tau) + \underset{\sim}{W}_1\, \ddot{X}_0(t) \right] \tag{4.4}$$

The response state vector, $\underset{\sim}{Z}(t)$, for a control system with a time delay τ can be computed step-by-step using Eq. (4.4). A block diagram for such computations is shown in Fig. 9.

4.2 **Instantaneous Optimal Closed-Loop Control:** For instantaneous optimal closed-loop control, the gain matrix, denoted by $\underset{\sim}{S}$, is constant, i.e.,

$$\underset{\sim}{U}(t) = \underset{\sim}{S}\, \underset{\sim}{Z}(t) \tag{4.5}$$

in which

$$\underset{\sim}{S} = -(\Delta t/2)\, \underset{\sim}{R}^{-1}\, \underset{\sim}{B}'\, \underset{\sim}{Q} \tag{4.6}$$

For a time delay τ, the equation of motion is given by Eq. (4.1), where $\underset{\sim}{U}(t-\tau)$ is obtained from Eq. (4.5) with t being replaced by $t-\tau$. If the numerical integration step Δt is chosen to be equal to the time delay τ for simplicity, then the response state vector $\underset{\sim}{Z}(t)$ for a control system with a time delay τ can be computed numerically similar to Eq. (4.4) as follows

$$\underset{\sim}{Z}(t) = \underset{\sim}{T}\, e^{\underset{\sim}{\theta}\tau}\, \underset{\sim}{T}^{-1} \left\{ \underset{\sim}{Z}(t-\tau) + (\tau/2) \left[\underset{\sim}{B}\, \underset{\sim}{S}\, \underset{\sim}{Z}(t-2\tau) + \underset{\sim}{W}_1\, \ddot{X}_0(t-\tau) \right] \right\}$$

$$+ (\tau/2) \left[\underset{\sim}{B}\, \underset{\sim}{S}\, \underset{\sim}{Z}(t-\tau) + \underset{\sim}{W}_1\, \ddot{X}_0(t) \right] \tag{4.7}$$

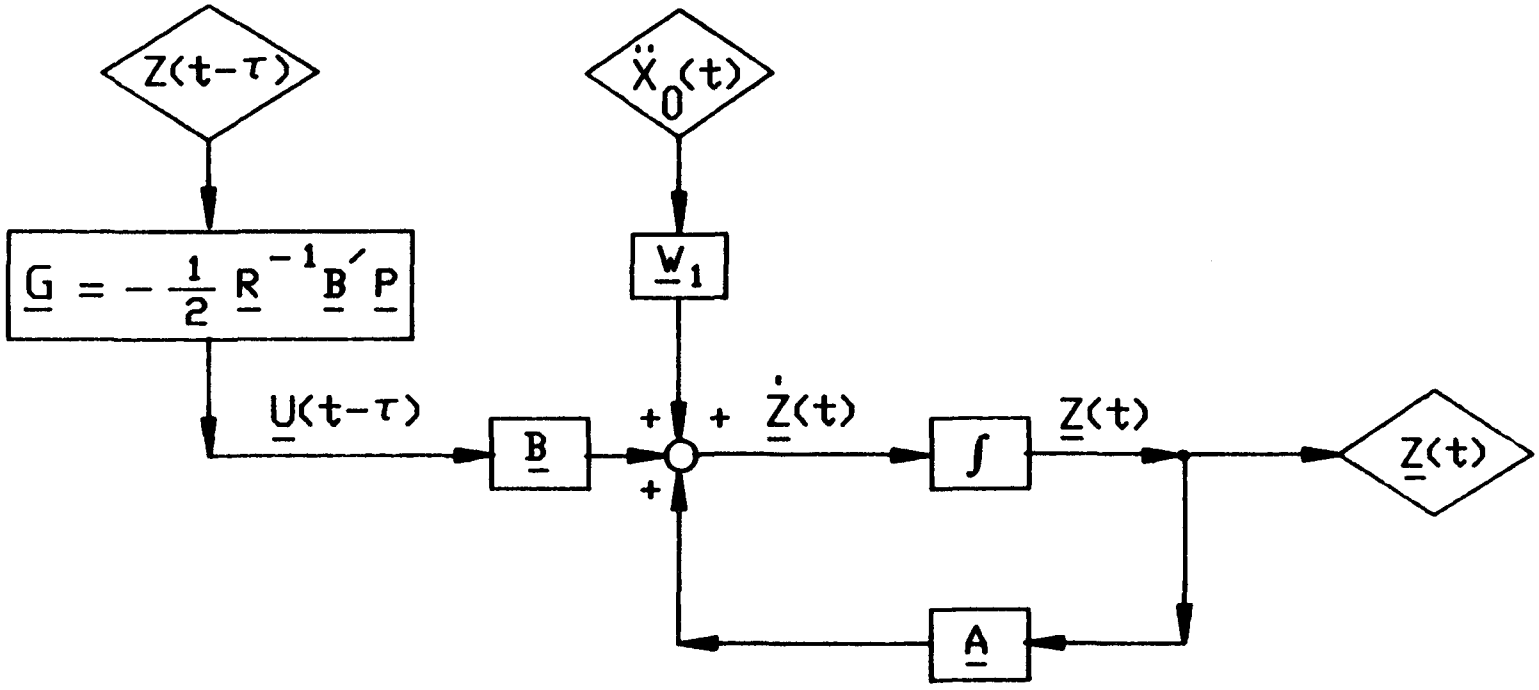

Fig. 9 : Block Diagram For Riccati Closed-Loop Control With Time Delay.

Eq. (4.7) is similar to Eq. (4.4) as expected, because both control algorithms described above are closed-loop control. A block diagram for the instantaneous optimal closed-loop control algorithm with a time delay τ is shown in Fig. 10.

4.3 Instantaneous Optimal Open-Loop Control: Based on the instantaneous optimal open-loop control algorithm the control vector $\underset{\sim}{U}(t)$ is computed from the sensed ground acceleration, $\ddot{X}_0(t)$, at time t, and the calculated vector $\underset{\sim}{D}(t-\Delta t)$, Eq. (2.12), at $t-\Delta t$. Unlike closed-loop control, the response state vector $\underset{\sim}{Z}(t)$ is not measured in open-loop control operation. Instead, $\underset{\sim}{Z}(t)$ is estimated without considering system time delay. This is because, in reality, the magnitude of time delay is unknown.

With a system time delay τ, let the estimated response state vector be denoted by $\underset{\sim}{Z}^*(t)$, and the corresponding estimated quantity at the previous time step $t-\Delta t$ be denoted by $\underset{\sim}{D}^*(t-\Delta t)$. Of course $\underset{\sim}{Z}^*(t)$ and $\underset{\sim}{D}^*(t-\Delta t)$ are different from the actual $\underset{\sim}{Z}(t)$ and $\underset{\sim}{D}(t-\Delta t)$. In actual operation, the control vector, denoted by $\underset{\sim}{U}^*(t)$, is computed from $\underset{\sim}{Z}^*(t)$ and $\underset{\sim}{D}^*(t-\Delta t)$, whereas the estimated response state vector $\underset{\sim}{Z}^*(t)$ is computed as

$$\underset{\sim}{Z}^*(t) = \underset{\sim}{T}\ \underset{\sim}{D}^*(t-\Delta t) + (\Delta t/2)\left[\ \underset{\sim}{B}\ \underset{\sim}{U}^*(t) + \underset{\sim}{W}_1\ \ddot{X}_0(t)\ \right] \qquad (4.8)$$

The block diagram shown on the left hand side of Fig. 11 illustrates the operation described above at $t-\Delta t$.

For simplicity of computation, the integration time step Δt is chosen to be identical to the time delay τ, i.e., $\Delta t = \tau$. Because of time delay, the control vector at $t-\tau$, $\underset{\sim}{U}^*(t-\tau)$, is applied to the structure at time t,

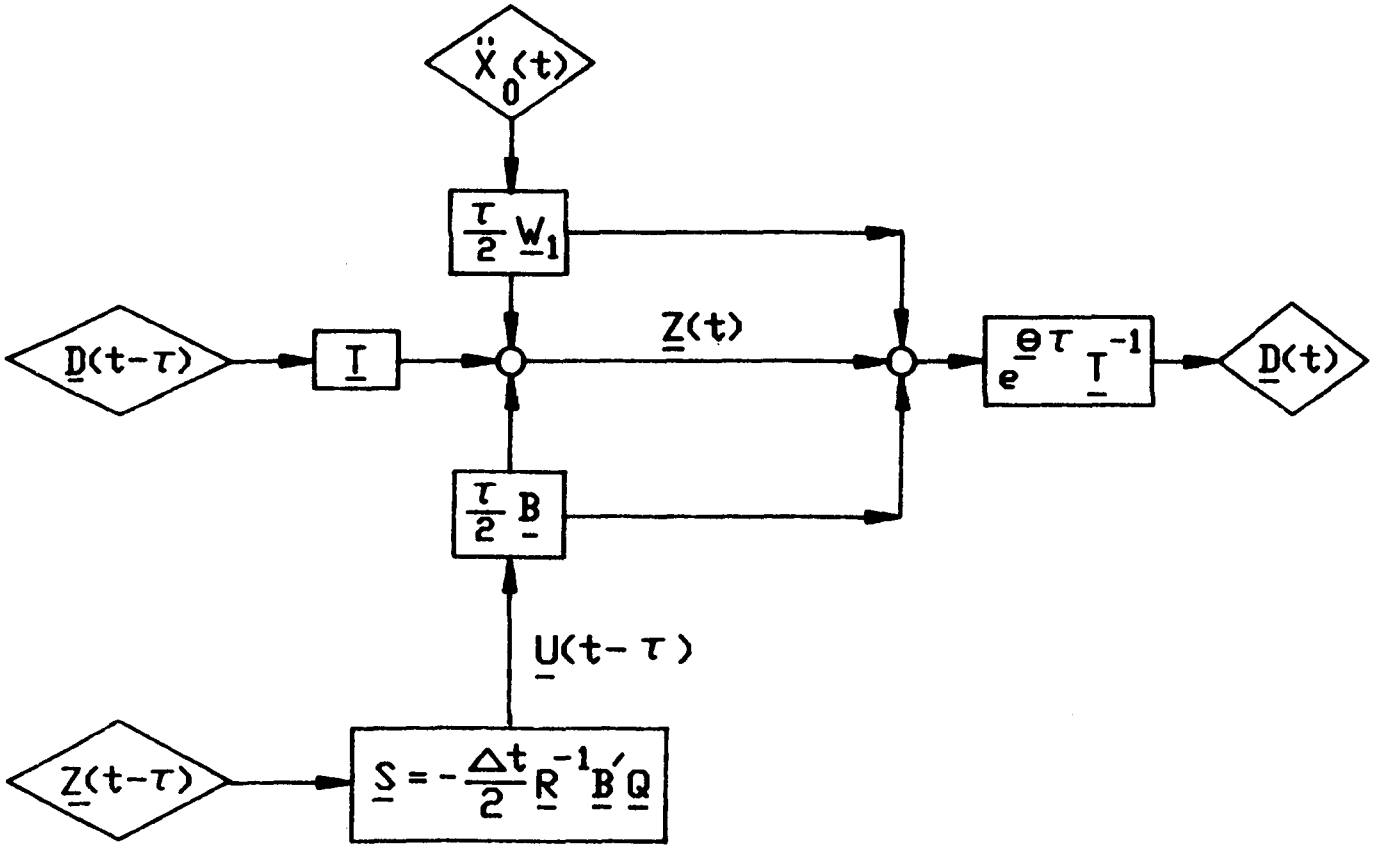

Fig. 10 : Block Diagram For Instantaneous Optimal Closed-Loop Control With Time Delay.

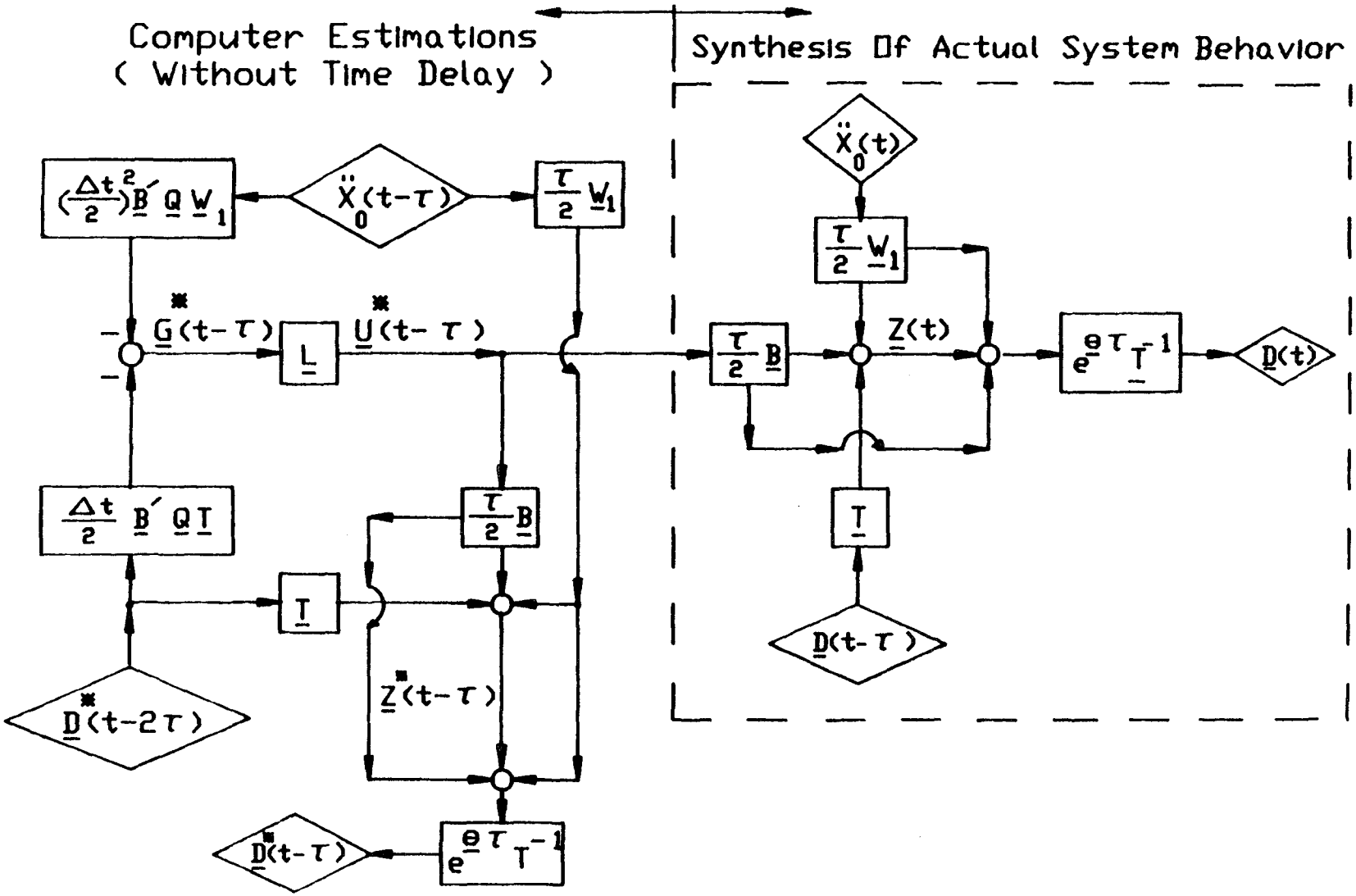

Fig. 11 : Block Diagram For Instantaneous Optimal Open-Loop Control With Time Delay.

and the actual response state vector $\underset{\sim}{Z}(t)$ can be synthesized as shown on the right hand side of the block diagrams depicted in Fig. 11.

The estimated control vector $\underset{\sim}{U}^*(t-\tau)$, that is applied to the structure at time t, is given by [see Fig. 11]

$$\underset{\sim}{U}^*(t-\tau) = \underset{\sim}{L}\ \underset{\sim}{G}^*(t-\tau) \tag{4.9}$$

in which $\underset{\sim}{L}$ is given by Eq. (2.13) and

$$\underset{\sim}{G}^*(t-\tau) = -(\Delta t/2)\ \underset{\sim}{B}'\ \underset{\sim}{Q}\ \underset{\sim}{T}\ \underset{\sim}{D}^*(t-2\tau) - (\Delta t/2)^2\ \underset{\sim}{B}'\ \underset{\sim}{Q}\ \underset{\sim}{W}_1\ \ddot{X}_0(t-\tau) \tag{4.10}$$

where

$$\underset{\sim}{D}^*(t-2\tau) = e^{\underset{\sim}{\theta}\tau}\ \underset{\sim}{T}^{-1}\left\{\underset{\sim}{Z}^*(t-2\tau) + (\tau/2)\left[\underset{\sim}{B}\ \underset{\sim}{U}^*(t-2\tau) + \underset{\sim}{W}_1\ \ddot{X}_0(t-2\tau)\right]\right\} \tag{4.11}$$

involves quantities estimated at $t-2\tau$ or $t-2\Delta t$. The response state vector $\underset{\sim}{Z}^*(t-\Delta t)$ estimated at $t-\Delta t$ or $t-\tau$ is computed by substituting Eq. (4.9) into Eq. (4.8) with $\Delta t = \tau$

$$\underset{\sim}{Z}^*(t-\tau) = \underset{\sim}{T}\ \underset{\sim}{D}^*(t-2\tau) + (\tau/2)\ \underset{\sim}{B}\ \underset{\sim}{L}\ \underset{\sim}{G}^*(t-\tau) + (\tau/2)\ \underset{\sim}{W}_1\ \ddot{X}_0(t-\tau) \tag{4.12}$$

The estimated control vector $\underset{\sim}{U}^*(t-\tau)$ with a time delay τ is actually applied to the structure at time t. The actual response of the structure can be synthesized numerically using the equation of motion, Eq. (4.1) as

$$\underset{\sim}{Z}(t) = \underset{\sim}{T}\ \underset{\sim}{D}(t-\tau) + (\tau/2)\ \underset{\sim}{B}\ \underset{\sim}{U}^*(t-\tau) + (\tau/2)\ \underset{\sim}{W}_1\ \ddot{X}_0(t) \tag{4.13}$$

where

$$\underset{\sim}{D}(t-\tau) = e^{\underset{\sim}{\theta}\tau}\ \underset{\sim}{T}^{-1}\left\{\underset{\sim}{Z}(t-\tau) + (\tau/2)\left[\underset{\sim}{B}\ \underset{\sim}{U}^{*}(t-2\tau) + \underset{\sim}{W}_1\ \ddot{X}_0(t-\tau)\right]\right\} \qquad (4.14)$$

A step-by-step numerical computation with the step size $\Delta t = \tau$ can be carried out to determine the actual response state vector $\underset{\sim}{Z}(t)$. A block diagram showing the computer estimation of the control vector $\underset{\sim}{U}^{*}(t-\tau)$ and the synthesis of the actual system behavior is displayed in Fig. 11.

4.4 Instantaneous Optimal Closed-Open-Loop Control: For instantaneous optimal closed-open-loop control without system time delay, the control vector $\underset{\sim}{U}(t)$ is regulated by the response state vector $\underset{\sim}{Z}(t)$ and the measured earthquake base acceleration as shown in Eqs. (2.16)-(2.19). The response state vector $\underset{\sim}{Z}(t)$ and the earthquake ground acceleration $\ddot{X}_0(t)$ are measured from which the control vector $\underset{\sim}{U}(t)$ is computed. This is different from open-loop control in which the response state vector $\underset{\sim}{Z}(t)$ and the control vector $\underset{\sim}{U}(t)$ are estimated. As a result, the problem of time delay for the closed-open-loop control is, in general, expected to be less serious than the open-loop control.

With a time delay τ, the control vector $\underset{\sim}{U}(t-\tau)$ is actually applied to the structure at time t. Choosing the integration interval Δt to be equal to τ, i.e., $\Delta t = \tau$, the response vector is computed as

$$\underset{\sim}{Z}(t) = \underset{\sim}{T}\ \underset{\sim}{D}(t-\tau) + (\tau/2)\left[\underset{\sim}{B}\ \underset{\sim}{U}(t-\tau) + \underset{\sim}{W}_1\ \ddot{X}_0(t)\right] \qquad (4.15)$$

in which the control vector $\underset{\sim}{U}(t-\tau)$ at $t-\tau$ is given by

$$\underset{\sim}{U}(t-\tau) = (\Delta t/4)\ \underset{\sim}{R}^{-1}\ \underset{\sim}{B}'\ \left[\tilde{\underset{\sim}{\Lambda}}\ \underset{\sim}{Z}(t-\tau) + \tilde{\underset{\sim}{q}}\ (t-\tau)\right] \tag{4.16}$$

where

$$\tilde{\underset{\sim}{q}}(t-\tau) = \tilde{\underset{\sim}{\Lambda}}\ \left[\underset{\sim}{T}\ \underset{\sim}{D}(t-2\tau) + (\Delta t/2)\ \underset{\sim}{W}_1\ \ddot{X}_0(t-\tau)\right] \tag{4.17}$$

$$\underset{\sim}{Z}(t-\tau) = \underset{\sim}{T}\ \underset{\sim}{D}(t-2\tau) + (\tau/2)\ \left[\underset{\sim}{B}\ \underset{\sim}{U}(t-2\tau) + \underset{\sim}{W}_1\ \ddot{X}_0(t-\tau)\right] \tag{4.18}$$

$$\underset{\sim}{D}(t-2\tau) = e^{\underset{\sim}{\theta}\tau}\ \underset{\sim}{T}^{-1}\left\{\underset{\sim}{Z}(t-2\tau) + (\tau/2)\ \left[\underset{\sim}{B}\ \underset{\sim}{U}(t-3\tau) + \underset{\sim}{W}_1\ \ddot{X}_0(t-2\tau)\right]\right\} \tag{4.19}$$

A step-by-step numerical computation can be carried out easily with a step size τ for the determination of $\underset{\sim}{Z}(t)$ and $\underset{\sim}{U}(t)$. A block diagram for the entire operation of the control system using the instantaneous optimal closed-open-loop control algorithm with a system time delay is shown in Fig. 12.

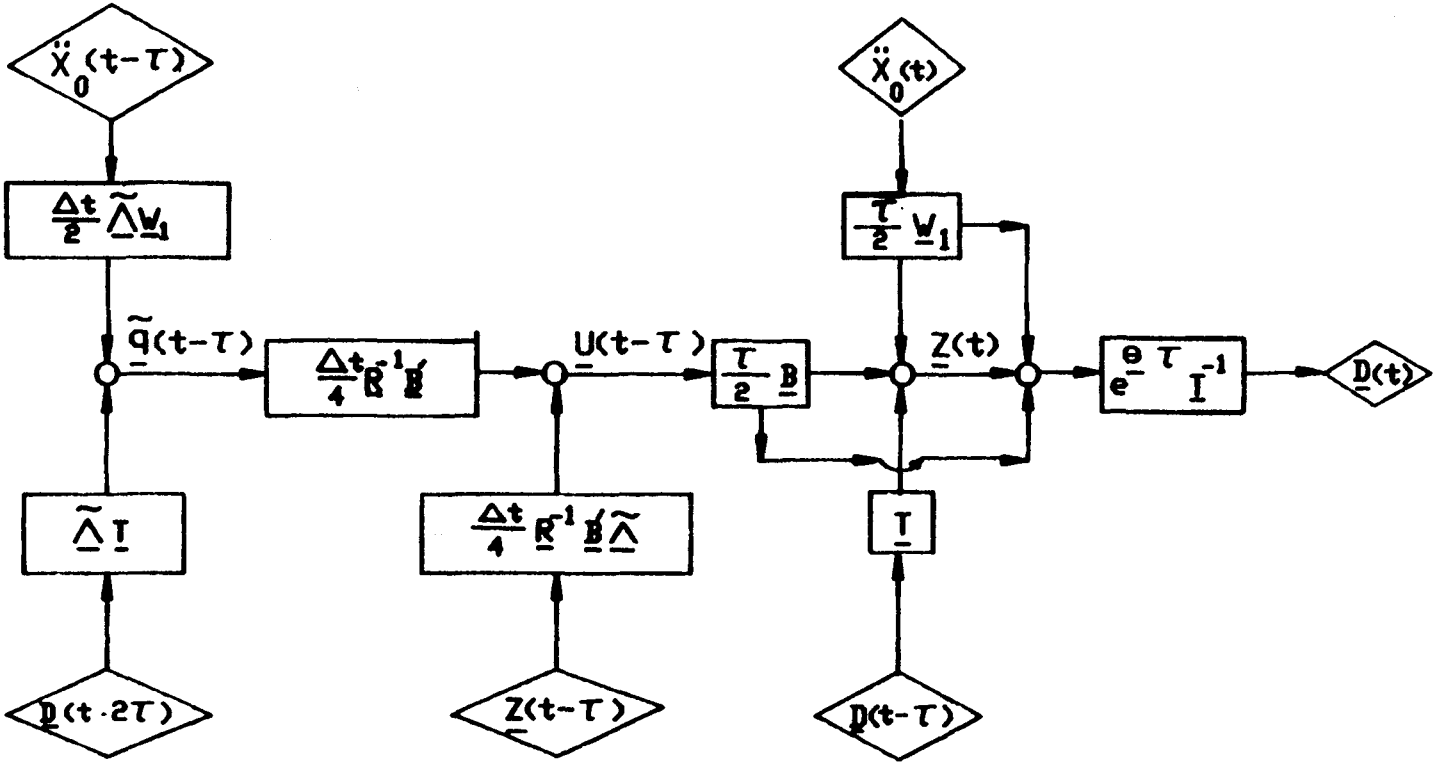

Fig. 12 : Block Diagram For Instantaneous Optimal Closed-Open -Loop Control With Time Delay.

V. TRUNCATION OF SMALL CONTROL FORCES

Under earthquake excitations, the time history of active control forces involve many cycles of small amplitude. Because of limitations of actuators, it may be desirable to eliminate all cycles of control forces with amplitudes smaller than a certain value, thus simplifying the control operation. When small control forces are truncated, not only the behavior of the structure under control will be different, but also the control forces will deviate from the results presented in section II. In this section, the response state vector $\underset{\sim}{Z}(t)$ and the required control vector $\underset{\sim}{U}(t)$ will be derived, when control forces smaller than a certain value are eliminated.

5.1 Riccati Closed-Loop Control: Based on Riccati closed-loop control, the response state vector $\underset{\sim}{Z}(t)$ is measured and the control vector $\underset{\sim}{U}(t)$ is computed from $\underset{\sim}{Z}(t)$, i.e.,

$$\underset{\sim}{U}(t) = \underset{\sim}{G}\ \underset{\sim}{Z}(t) \tag{5.1}$$

in which

$$\underset{\sim}{G} = -\frac{1}{2}\ \underset{\sim}{R}^{-1}\ \underset{\sim}{B}'\ \underset{\sim}{P} \tag{5.2}$$

Let ϵ be a preselected value such that any control force smaller than ϵ will be truncated, i.e., will be set to be zero. This is equivalent to pass the control vector $\underset{\sim}{U}(t)$ through a filter, such that any element of $\underset{\sim}{U}(t)$ becomes zero if it is smaller than ϵ, and it is unaffected if larger than ϵ. Then, the resulting control vector from the filter, denoted by $\underset{\sim}{U}^*(t)$, is

applied to the structure. The process is repeated for every time instant t throughout the entire episode of the earthquake.

For the analytical/numerical investigation, the entire operations described above can be simulated to determine the response state vector $\underset{\sim}{Z}(t)$ and the control vector $\underset{\sim}{U}^*(t)$. A block diagram for such a simulation the entire control operation is shown in Fig. 13.

The response state vector $\underset{\sim}{Z}(t)$ is obtained from the equations of motion,

$$\dot{\underset{\sim}{Z}}(t) = \underset{\sim}{A}\,\underset{\sim}{Z}(t) + \underset{\sim}{B}\,\underset{\sim}{U}^*(t) + \underset{\sim}{W}_1\,\ddot{X}_0(t) \tag{5.3}$$

in which $\underset{\sim}{U}^*(t)$ is the truncated control vector actually applied to the structure,

$$\underset{\sim}{U}^*(t) = \underset{\sim}{\delta}\,\underset{\sim}{U}(t) \tag{5.4}$$

where $\underset{\sim}{U}(t)$ is the untruncated control vector computed from the response vector $\underset{\sim}{Z}(t)$ given by Eqs. (5.1) and (5.2), and $\underset{\sim}{\delta}$ is a nonlinear operator indicating the truncation effect.

The nonlinear truncation operator $\underset{\sim}{\delta}$ can be represented by a (rxr) diagonal matrix with the diagonal elements given as follows

$$\begin{aligned} \delta_{ii} &= 1 \qquad \text{if } U_i(t) > \epsilon \\ &= 0 \qquad \text{if } U_i(t) \le \epsilon \end{aligned} \tag{5.5}$$

in which $U_i(t)$ is the ith element of $\underset{\sim}{U}(t)$.

The response vector $\underset{\sim}{Z}(t)$ and the control vector $\underset{\sim}{U}^*(t)$ applied to the

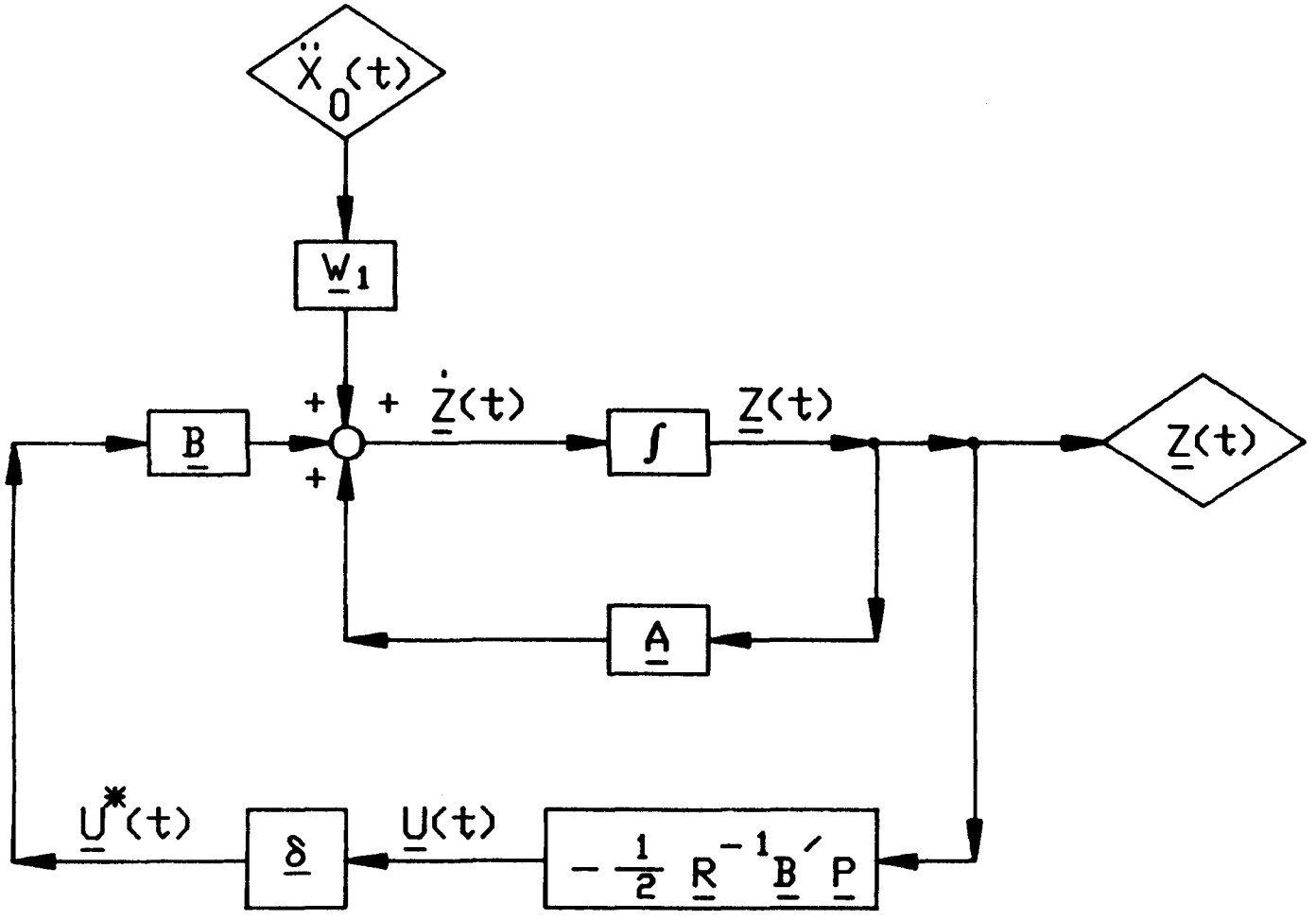

Fig. 13 : Block Diagram For Riccati Closed-Loop Control With Elimination Of Small Control Forces.

structure can be solved using the system of equations in Eqs. (5.1)-(5.5). However, the system of equations is nonlinear because the operator $\underset{\sim}{\delta}$ is nonlinear. As a result, the following iterative procedures are used to determine the state vector $\underset{\sim}{Z}(t)$ and the control vector $\underset{\sim}{U}^*(t)$.

(i) The response state vector $\underset{\sim}{Z}(t)$ is computed from Eq. (5.3) by use of the untruncated control vector $\underset{\sim}{U}(t)$, i.e., $\underset{\sim}{U}^*(t) = \underset{\sim}{U}(t)$. In other words, $\underset{\sim}{U}^*(t)$ in Eq. (5.3) is replaced by $\underset{\sim}{G}\ \underset{\sim}{Z}(t)$, Eq. (5.1),

(ii) $\underset{\sim}{U}(t)$ is computed from $\underset{\sim}{Z}(t)$ obtained in step (i) using Eq. (5.1),

(iii) $\underset{\sim}{U}^*(t)$ is obtained from $\underset{\sim}{U}(t)$ using Eqs. (5.4)-(5.5), and

(iv) The response state vector $\underset{\sim}{Z}(t)$ is computed from Eq. (5.3) using $\underset{\sim}{U}^*(t)$ obtained in step (iii).

The iterative procedure is repeated until both vectors $\underset{\sim}{Z}(t)$ and $\underset{\sim}{U}^*(t)$ converge. In general, $\underset{\sim}{Z}(t)$ and $\underset{\sim}{U}^*(t)$ converge rapidly and few cycles of iteration are sufficient. Such an interative procedure is repeated for every time instant t to obtain the time histories of $\underset{\sim}{Z}(t)$ and $\underset{\sim}{U}^*(t)$.

5.2 **Instantaneous Optimal Closed-Loop Control**: The control operation using the instantaneous optimal closed-loop control algorithm is essentially identical to that of the Riccati closed-loop control, except that the gain matrix, $\underset{\sim}{S}$, is different, i.e.,

$$\underset{\sim}{U}(t) = \underset{\sim}{S}\ \underset{\sim}{Z}(t) \tag{5.6}$$

where

$$\underset{\sim}{S} = -(\Delta t/2)\ \underset{\sim}{R}^{-1}\ \underset{\sim}{B}'\ \underset{\sim}{Q} \tag{5.7}$$

In simulating the entire control operation using the instantaneous optimal closed-loop control algorithm, the following equation for computing $\underset{\sim}{Z}(t)$ is employed, Eq. (2.2),

$$\underset{\sim}{Z}(t) = \underset{\sim}{T}\ \underset{\sim}{D}(t-\Delta t) + (\Delta t/2)\left[\ \underset{\sim}{B}\ \underset{\sim}{U}^{*}(t) + \underset{\sim}{W}_1\ \ddot{X}_0(t)\ \right] \tag{5.8}$$

in which $\underset{\sim}{U}^{*}(t)$ is given by Eqs. (5.4) and (5.5), and

$$\underset{\sim}{D}(t-\Delta t) = e^{\underset{\sim}{\theta}\Delta t}\ \underset{\sim}{T}^{-1}\left\{\underset{\sim}{Z}(t-\Delta t) + (\Delta t/2)\ \left[\underset{\sim}{B}\ \underset{\sim}{U}^{*}(t-\Delta t) + \underset{\sim}{W}_1\ \ddot{X}_0(t-\Delta t)\right]\right\} \tag{5.9}$$

Thus, instead of Eq. (5.3), Eqs. (5.8) and (5.9) are used in conjunction with Eqs. (5.4)-(5.7) for iteration and simulation. Again, the iterative procedure converges very rapidly. A block diagram for simulating the response state vector $\underset{\sim}{Z}(t)$ and the control vector $\underset{\sim}{U}^{*}(t)$ is shown in Fig. 14.

5.3 **Instantaneous Optimal Open-Loop Control**: For instantaneous optimal open-loop control, the operation for the truncation of small control forces is identical to that described previously. The difference between the present control algorithm and the closed-loop control algorithm is that the response state vector $\underset{\sim}{Z}(t)$ is computed rather than measured. Because of such a difference, the iterative procedure is not necessary in simulating the response state vector $\underset{\sim}{Z}(t)$ and the control vector $\underset{\sim}{U}^{*}(t)$. The following equations can be used directly to compute $\underset{\sim}{U}^{*}(t)$ and $\underset{\sim}{Z}(t)$ at each time instant t.

$$\underset{\sim}{U}(t) = \underset{\sim}{L}\ \underset{\sim}{G}(t) \tag{5.10}$$

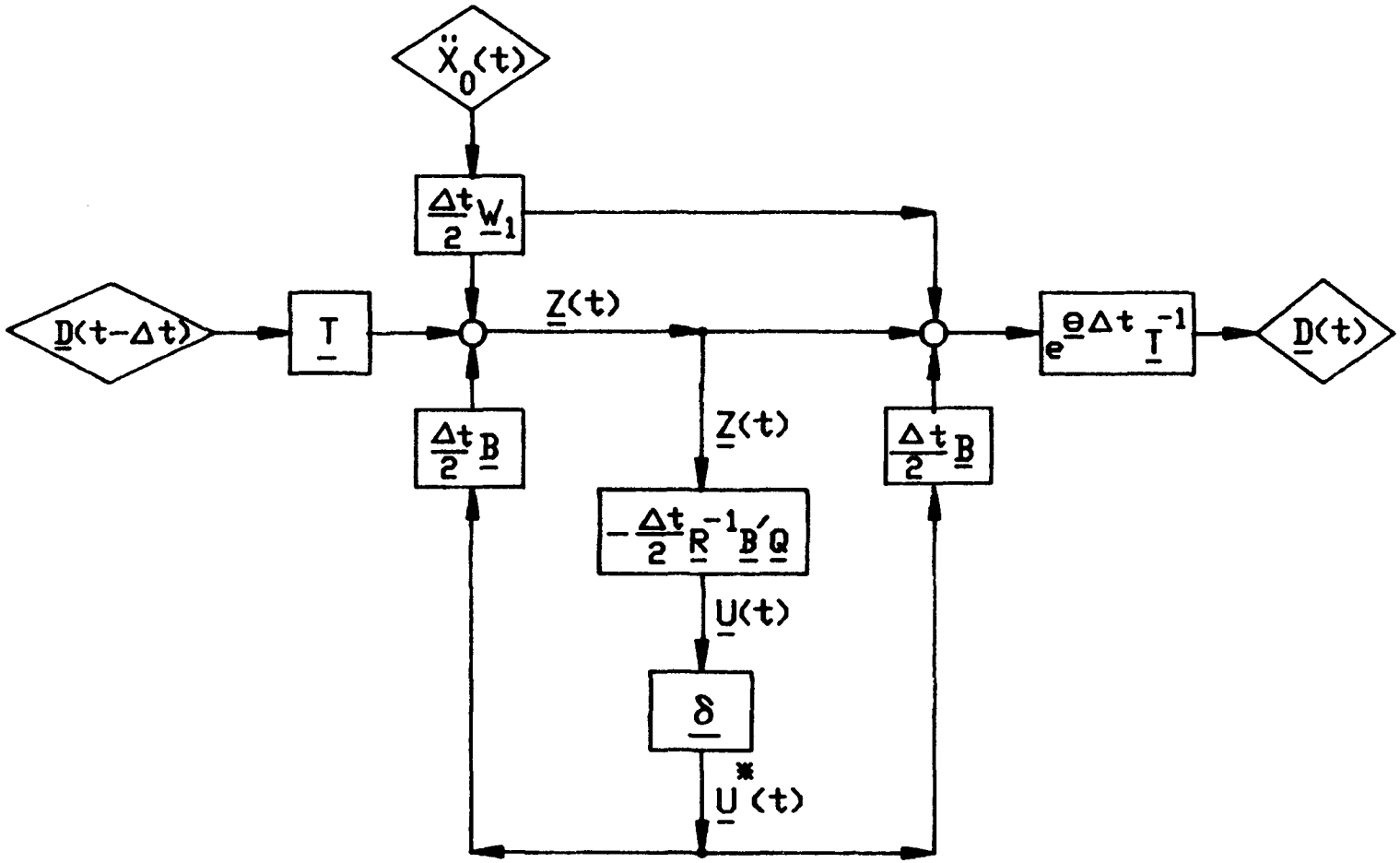

Fig. 14 : Block Diagram For Instantaneous Optimal Closed-Loop Control With Elimination Of Small Control Forces.

$$\underset{\sim}{G}(t) = -(\Delta t/2)\ \underset{\sim}{B}'\ \underset{\sim}{Q}\ \underset{\sim}{T}\ \underset{\sim}{D}(t-\Delta t) - (\Delta t/2)^2\ \underset{\sim}{B}'\ \underset{\sim}{Q}\ \underset{\sim}{W}_1\ \ddot{X}_0(t) \tag{5.11}$$

$$\underset{\sim}{D}(t-\Delta t) = e^{\underset{\sim}{\theta}\Delta t}\ \underset{\sim}{T}^{-1} \left\{ \underset{\sim}{Z}(t-\Delta t) + (\Delta t/2) \left[\underset{\sim}{B}\ \underset{\sim}{U}^*(t-\Delta t) + \underset{\sim}{W}_1\ \ddot{X}_0(t-\Delta t) \right] \right\} \tag{5.12}$$

$$\underset{\sim}{U}^*(t) = \underset{\sim}{\delta}\ \underset{\sim}{U}(t) \tag{5.13}$$

$$\underset{\sim}{Z}(t) = \underset{\sim}{T}\ \underset{\sim}{D}(t-\Delta t) + (\Delta t/2) \left[\underset{\sim}{B}\ \underset{\sim}{U}^*(t) + \underset{\sim}{W}_1\ \ddot{X}_0(t) \right] \tag{5.14}$$

A block diagram for simulating the control operation is shown in Fig. 15.

5.4 <u>Instantaneous Optimal Closed-Open-Loop Control</u>: By use of the instantaneous optimal closed-open-loop control algorithm, the response state vector $\underset{\sim}{Z}(t)$ is measured, whereas the control vector $\underset{\sim}{U}^*(t)$ depends on the measured $\underset{\sim}{Z}(t)$. In other words, both $\underset{\sim}{Z}(t)$ and $\underset{\sim}{U}^*(t)$ are coupled in the simulation process. Hence, the iterative procedure described previously is needed. The equations used for the simulation of $\underset{\sim}{Z}(t)$ and $\underset{\sim}{U}^*(t)$ are given in the following

$$\underset{\sim}{Z}(t) = \underset{\sim}{T}\ \underset{\sim}{D}(t-\Delta t) + (\Delta t/2) \left[\underset{\sim}{B}\ \underset{\sim}{U}^*(t) + \underset{\sim}{W}_1\ \ddot{X}_0(t) \right] \tag{5.15}$$

$$\underset{\sim}{U}^*(t) = \underset{\sim}{\delta}\ \underset{\sim}{U}(t) \tag{5.16}$$

$$\underset{\sim}{U}(t) = (\Delta t/4)\ \underset{\sim}{R}^{-1}\ \underset{\sim}{B}' \left[\tilde{\underset{\sim}{\Lambda}}\ \underset{\sim}{Z}(t) + \tilde{\underset{\sim}{q}}(t) \right] \tag{5.17}$$

$$\tilde{\underset{\sim}{q}}(t) = \tilde{\underset{\sim}{\Lambda}} \left[\underset{\sim}{T}\ \underset{\sim}{D}(t-\Delta t) + (\Delta t/2)\ \underset{\sim}{W}_1\ \ddot{X}_0(t) \right] \tag{5.18}$$

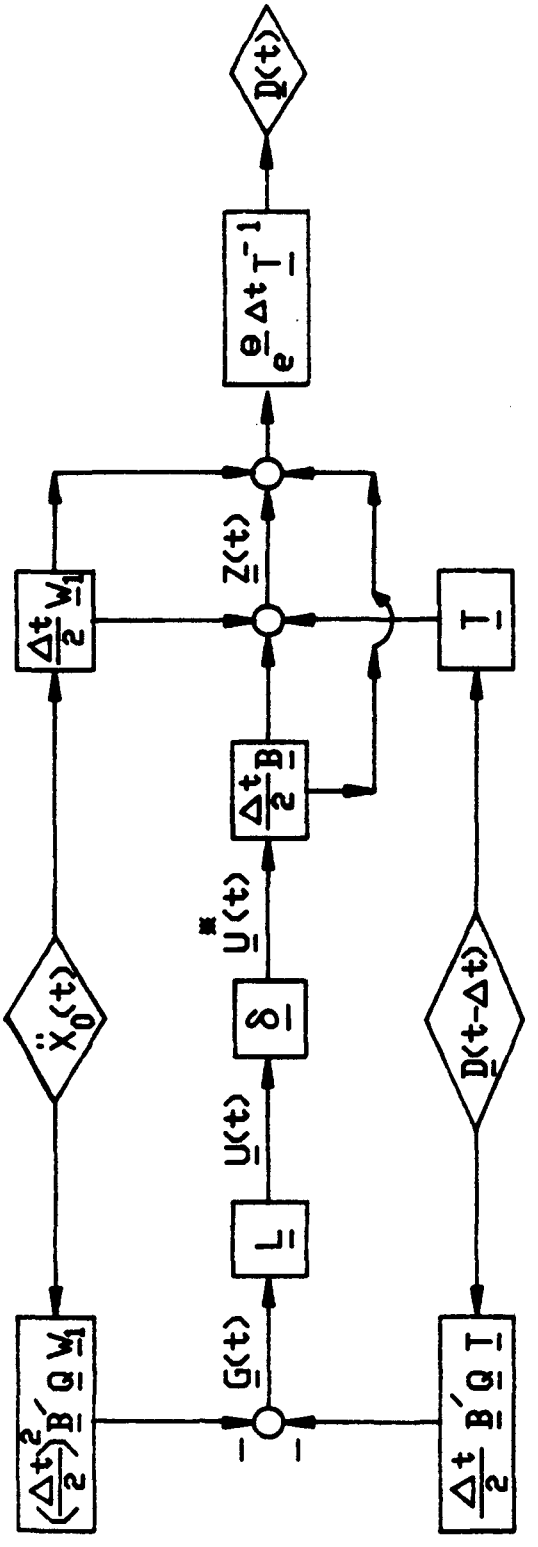

Fig. 15 - Block Diagram For Instantaneous Optimal Open-Loop Control With Elimination Of Small Control Forces.

$$\underset{\sim}{D}(t-\Delta t) = e^{\underset{\sim}{\theta}\Delta t}\ \underset{\sim}{T}^{-1}\left\{\underset{\sim}{Z}(t-\Delta t) + (\Delta t/2)\left[\underset{\sim}{B}\ \underset{\sim}{U}^{*}(t-\Delta t) + \underset{\sim}{W}_1\ \ddot{X}_0(t-\Delta t)\right]\right\} \qquad (5.19)$$

The iterative procedures for determining $\underset{\sim}{Z}(t)$ and $\underset{\sim}{U}^{*}(t)$ are described in the following

(i) The initial solutions for $\underset{\sim}{Z}(t)$ and $\underset{\sim}{U}(t)$ are obtained by setting $\underset{\sim}{U}^{*}(t) = \underset{\sim}{U}(t)$ and using Eqs. (5.15) and (5.17)

(ii) With $\underset{\sim}{U}(t)$ determined in (i), $\underset{\sim}{U}^{*}(t)$ is computed from Eq. (5.16)

(iii) $\underset{\sim}{Z}(t)$ is obtained from Eq. (5.15) using $\underset{\sim}{U}^{*}(t)$ determined in (ii) and

(iv) $\underset{\sim}{U}(t)$ is computed from $\underset{\sim}{Z}(t)$ using Eq. (5.17).

The iterative procedure is repeated until $\underset{\sim}{Z}(t)$ and $\underset{\sim}{U}^{*}(t)$ converge. Again, numerical results indicate that $\underset{\sim}{Z}(t)$ and $\underset{\sim}{U}^{*}(t)$ converge rapidly. A block diagram for such a simulation procedure is shown in Fig. 16.

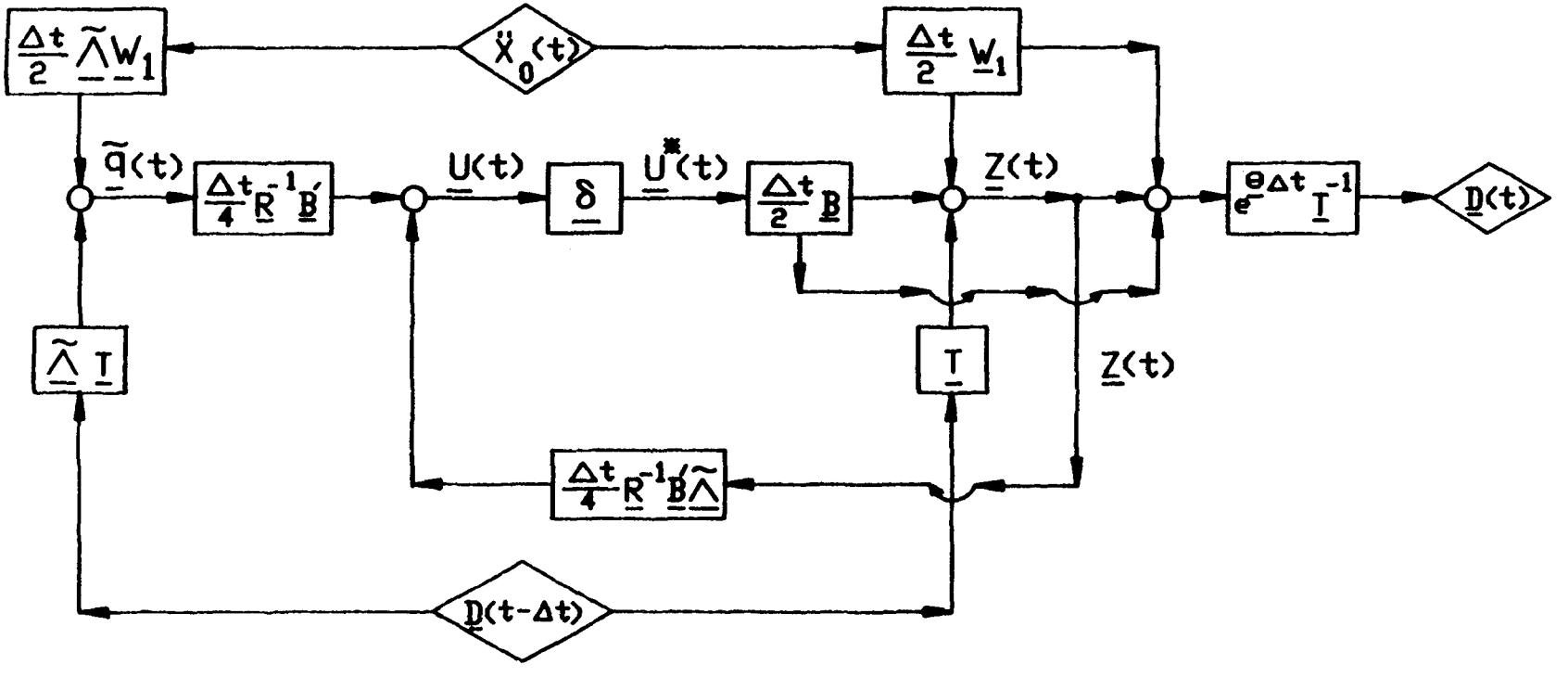

Fig. 16 : Block Diagram For Instantaneous Optimal Closed-Open-Loop Control With Elimination Of Small Control Forces.

VI. NUMERICAL EXAMPLES

To demonstrate the sensitivity and criticality of the active control system with respect to the variant from ideal control environments, extensive numerical examples are worked out in this section. In particular, two configurations of the active control system will be considered, including the active tendon control system and active mass damper. A simulated earthquake ground acceleration shown in Fig. 17 is considered as the input excitation.

An eight-story building in which every story unit is identically constructed is considered for illustrative purposes. The structural properties of each story are: m = floor mass = 345.6 tons; k = elastic stiffness = 3.404×10^5 KN/m; and c = internal damping coefficient = 2,937 tons/sec. that corresponds to a 2% damping for the first vibrational mode of the entire building. The external damping is assumed to be zero. The computed natural frequencies are 5.79, 17.18, 27,98, 37.82, 46.38, 53.36, 58.53, and 61.69 rad/sec.

Without control system, the top floor relative displacement with respect to the ground and the base shear force of the building are shown in Fig 18.

6.1 Ideal Control Environments: Two examples, one with an active tendon control system and another with an active mass damper, will be illustrated in the following under ideal control environments. Ideal control environments refer to the control situation without system time delay and free of estimation errors for structural parameters. The structural response quantities and required active control forces under ideal control environments will be presented in this subsection. These will serve as bases for comparing the corresponding results when control environments

deviate from ideal ones, including system time delay, uncertainty in structural identification, and truncation of small control forces.

Example 1: Active Tendon Control System

Suppose four active tendon controllers are installed in the lowest four story units and the angle of inclination of the tendons with respect to the floor is 25^{o}. The dimension of the weighting matrices $\underset{\sim}{Q}$ and $\underset{\sim}{R}$ are (16x16) and (4x4), respectively. For Riccati closed-loop control, both $\underset{\sim}{Q}$ and $\underset{\sim}{R}$ matrices are chosen to be diagonal matrices with elements $Q_{ii} = Q^{*} = 1.3 \times 10^{5}$ (for i = 1, 2, ...8), Q_{jj}=0 (for j = 9, 10,...16), and $R_{11} = R_{22} = R_{33} = R_{44} = 10^{-4}$.

With the application of instantaneous optimal control algorithms, the weighting matrix $\underset{\sim}{R}$ is identical to the one given above. However, the (16x16) weighting matrix $\underset{\sim}{Q}$ will be partitioned more efficiently as follows

$$\underset{\sim}{Q} = \alpha \left[\begin{array}{c|c} \underset{\sim}{0} & \underset{\sim}{0} \\ \hline \underset{\sim}{Q}_{21} & \underset{\sim}{Q}_{22} \end{array}\right] \tag{6.1}$$

in which $\underset{\sim}{Q}_{21}$ and $\underset{\sim}{Q}_{22}$ are (8x8) matrices and α is a constant. Note that $\underset{\sim}{Q}_{11}$ and $\underset{\sim}{Q}_{12}$ do not contribute to the active control force and, hence, they are chosen to be zero [17, 18]. The choice of $\underset{\sim}{Q}_{21}$ and $\underset{\sim}{Q}_{22}$ requires some considerations as discussed in Ref. 17. For simplicity, $\underset{\sim}{Q}_{21}$ and $\underset{\sim}{Q}_{22}$ are chosen to be equal, i.e., $\underset{\sim}{Q}_{21} = \underset{\sim}{Q}_{22} = \underset{\sim}{Q}^{*}$. The elements of $\underset{\sim}{Q}^{*}$, denoted by $Q^{*}(i,j)$, are given in the following; $Q^{*}(i,j) = j$ for $i \leq 4$ and $Q^{*}(i,j) = 0$ for $i > 4$. For a 68% reduction of the building response, a value of 5,000 is used for α.

The time histories of (i) the top floor relative displacement to the ground, (ii) the base shear force, and (iii) the control force from the

lowest controller, are shown in Fig. 19, when the Riccati closed-loop control algorithm is used.

Under ideal control environments, it has been shown in Refs. 17-18 that the control efficiencies for three instantaneous optimal control algorithms are identical. In other words, the resulting structural response quantities and required active control forces for these three control algorithms are identical. The time histories of the response quantities and the required active control force from the lowest controller are shown in Fig. 20, when one of the instantaneous optimal control algorithms is used. The maximum values of the time histories shown in Figs. 18 to 20 are tabulated in Table 1.

Example 2: Active Mass Damper

The same example as the previous one is considered except that, instead of the active tendon control system an active mass damper is installed on the top floor of the building as shown in Fig. 1(b). The properties of the active mass damper are m_d = mass of the damper = 29.63 tons, c_d = damping of the damper = 25 tons/sec., k_d = stiffness of the damper = 957.2 KN/m. Note that the mass m_d is 2% of the generalized mass associated with the first vibrational mode, the frequency of the damper is 98% of the first natural frequency of the building, and the damping coefficient of the damper is approximately 7.3%. In the present situation, the weighting matrix $\underset{\sim}{R}$ consists of only one element, i.e., $\underset{\sim}{R} = R$, whereas the dimension of $\underset{\sim}{Q}$ matrix is (18x18).

For Riccati closed-loop control, the weighting matrix $\underset{\sim}{Q}$ is considered as a diagonal matrix with $Q_{ii} = 1.3 \times 10^5$ (for i=1, 2, ..., 8), and $Q_{jj} = 0$ (for j = 9, 10, ..., 18). The element of $\underset{\sim}{R}$ is 10^{-3}.

In applying instantaneous optimal control algorithms, $\underset{\sim}{R} = 10^{-3}$ is used, and the $\underset{\sim}{Q}$ matrix is partitioned as shown by Eq. (6.1) in which $\underset{\sim}{Q}_{21}$ and $\underset{\sim}{Q}_{22}$

are (2x9) matrices. The following values are assigned to elements of these two matricies for illustrative purposes:

$$\underset{\sim}{Q}_{21} = \begin{bmatrix} -33.5 & -67. & -100.5 & -134. & -167.5 & -201. & -234.5 & -268. & -375.6 \\ -33.5 & -67. & -100.5 & -134. & -167.5 & -201. & -234.5 & -268. & 32.2 \end{bmatrix}$$

$$\underset{\sim}{Q}_{22} = \begin{bmatrix} 67.5 & 135.0 & 202.5 & 270.0 & 338.5 & 405.0 & 472.5 & 540.0 & 32.2 \\ 5.8 & 11.6 & 17.6 & 23.2 & 29.0 & 34.7 & 40.5 & 46.3 & 5.7 \end{bmatrix}$$

A value of 67.0 is chosen for α, Eq. (6.1), such that the top floor relative displacement is reduced approximately by 60%

Using the Riccati closed-loop control algorithm, the building response quantities and required active control force are displayed in Fig. 21. With the application of any one of three instantaneous optimal control algorithms, the corresponding quantities are displayed in Fig. 22. The maximum values of the time histories shown in Fig. 21 and 22 are tabulated in Table 2.

Finally, it should be mentioned that the control efficiency for each of three instantaneous optimal control algorithms is quite different when a system time delay or an estimation error for structural parameters is introduced. Numerical examples will be presented in the next subsections.

6.2 Structural Control With System Uncertainty: When the system identification involves uncertainty, the actual system matrix $\underset{\sim}{A}$ is unknown and the estimated system matrix $\underset{\sim}{A}^*$ is used for control operation. Various degrees of estimation error in stiffness and damping will be introduced to illustrate the effect of system uncertainty on the control system. The error in stiffness estimation for every story unit, denoted by Δk, is

represented by the percentage of the true stiffness. The corresponding estimation error in the fundamental frequency ω_f, denoted by $\Delta\omega$, is expressed in terms of the percentage of ω_f. The estimation error in damping coefficient for every story unit, denoted by Δc, is similarly defined. The estimation error for the damping ratio, ξ, in the first mode is expressed in terms of the percentage of ξ, as denoted by $\Delta\xi$.

Example 3: Active Tendon Control System

Example 1 is reconsidered and various estimation errors for structural parameters are introduced. Using the Riccati closed-loop control algorithm, the time histories of structural response quantities and active control force from the first controller are presented in Figs. 23-25. In these figures, ±40% estimation errors in stiffness or damping have been introduced. The maximum response quantities and control force in the entire time histories of 30 seconds are summarized in the upper part of Table 3. The control force shown in the table is the one from the controller in the lowest story unit. It is observed from Table 3 that in comparison with the results under ideal control environments, the response quantities may increase or decrease depending on whether the structural properties are under or over estimated. However, as the response quantities increase, the corresponding active control force always decreases and vice versa. This indicates that the degradation of the control efficiency is not quite significant. The control system is moderately sensitive to the stiffness estimation error (or natural frequency), whereas it is not sensitive the estimation error of damping coefficient. In general, an estimation error within 20% for stifffness and 50% for damping is quite acceptable, when the Riccati closed-loop control algorithm is used.

With the application of the instantaneous optimal-open-loop control algorithm, the time histories of the structural response quantities and the

active control force from the first controller for various degrees of stiffness estimation error are shown in Figs. 26-28. The maximum response quantities and the maximum active control force are summarized in the upper part of Table 4. It is observed from Table 4 that the control system is quite sensitive to the estimation error for the stiffness as compared to the Riccati closed-loop control algorithm. An estimation error for stiffness may result in a considerable degradation of the control effectiveness. Further, it is observed from Fig. 26 that the response quantities beyond 17 seconds do not die down as rapidly as that of the ideal system without uncertainty. On the other hand, the control system is not sensitive to the estimation error for damping as shown in Fig. 29-31 and Table 4.

It is concluded that the instantaneous optimal open-loop control algorithm is quite sensitive to the system uncertainty in stiffness or natural frequency, and the control efficiency can deteriorate considerably if the stiffness estimation error is more than 10%. This situation may have been expected, because in open-loop control no feedback state vector is measured. Note that the feedback state vector reflects to some extent the behavior of true system parameters.

Using the instantaneous optimal closed-open-loop control algorithm, the time histories of the structural response quantities and active control force are depicted in Figs. 32-34. In these figures, estimation errors of ±40% for stiffness and damping are introduced. The maximum response quantities and active control force in 30 seconds of the time history are summarized in the upper part of Table 5. Table 5 and Figs. 32-34 indicate that the instantaneous optimal closed-open-loop control algorithm is practically insensitive to system uncertainties.

Finally, it has been shown in Section III that the instantaneous optimal closed-loop control algorithm is independent of structural parameters or system uncertainty.

Example 4: Active Mass Damper

Example 2 is reconsidered and various estimation errors of structural parameters are taken into account. With the Riccati closed-loop control algorithm, time histories of the response quantities and control force are shown in Figs. 35-37 for different degrees of estimation errors. The maximum values in these time histories are summarized in the lower part of Table 3. A comparison between the upper part and lower part of Table 3 shows that the active mass damper is less sensitive to the uncertainties (or errors) in system identification. An estimation error of 40% for stiffness is acceptable when the Riccati closed-loop control algorithm is used. Again, the error in damping estimation has a negligible effect on the efficiency of the control system.

With the application of the instantaneous optimal open-loop control algorithm, the time histories of the response quantities and active control force are depicted in Figs. 38-43. The corresponding maximum response quantities and control force are summarized in the lower part of Table 4. As observed from Table 4, the control system is sensitive to the uncertainty in stiffness estimation, in particular, when the stiffness is over-estimated. An over-estimation of the stiffness for more than 10% will result in a significant degradation of the control efficiency. Again, the control system is not sensitive to the estimation error for damping.

With the application of instantaneous optimal closed-open-loop control, the time histories of response quantities and control force are shown in Figs. 44-46. The corresponding maximum values are displayed in the lower part of Table 5. It is observed from the table that the instantaneous

optimal closed-open-loop control algorithm is not sensitive to the estimation errors for structural parameters.

6.3 **Structural Control With System Time Delay**: To demonstrate the effect of system time delay on the control system, the same examples worked out in Section 6.1 under ideal control environments will be considered, in which various degrees of time delay τ will be introduced. The system time delay, τ, is expressed in 10^{-3} seconds and also in percentage of the fundamental period of the structure $T_f = 1.085$ sec.

Example 5: Active Tendon Control System

Example 1 will be reconsidered herein except that a time delay τ is taken into account. The solutions for the structural response quantities and active control forces have been derived in Section V.

By use of the Riccati closed-loop control algorithm, time histories of the response quantities and active control forces are computed for various degrees of time delay τ. Some results are displayed in Figs. 49 to 51. The absolute maximum value within the entire time history of 30 seconds of earthquake episode for the response and control force is considered as a measure for the effect of system time delay. In particular, the deviation of the absolute maximum value from that obtained without system delay. Let Y_8 be the maximum top floor relative displacement with respect to the ground in the time history of 30 seconds with a system time delay, and $\bar{Y}_8$ be the corresponding quantity under ideal control environments without a time delay. Then, the deviation, $Y_8 - \bar{Y}_8$, measured in terms of the percentage of $\bar{Y}_8$, is plotted in Fig. 47(a) as a solid curve. In other words, the solid curve represents the deviation, $(Y_8 - \bar{Y}_8)/\bar{Y}_8$, as a function of time delay

As observed from the figure, the deviation increases as the time delay τ increases. With a time delay τ, the maximum control force from the controller installed in the lowest story unit is denoted by U_1, whereas the corresponding maximum control force without a time delay is denoted by $\bar{U}_1$. The deviation of the maximum control force measured in terms of the percentage of $\bar{U}_1$, i.e., $(U_1 - \bar{U}_1)/\bar{U}_1$, is plotted in Fig. 47(a) as a dashed curve. Again, the deviation increases as the magnitude of time delay τ increases.

From Fig. 47(a), two observations made in the following are significant. (1) As the time delay τ increases, the maximum response quantities increase whereas the required maximum control forces are always larger than that without a system time delay. This indicates that the control efficiency degrades monotonically with respect to the time delay τ. (2) The absolute maximum values of response quantities increase drastically as the time delay τ is over 5% of the fundamental structural period T_f. In other words, the slope of the solid curve increases rapidly for $\tau > 5\%\ T_f$.

The structural response quantities and required active control forces have been computed for various degrees of time delay τ using three instantaneous optimal control algorithms. The deviations of the absolute maximum of the top floor relative displacement and control force are displayed in Figs. 47(b) and 48, when three instantaneous optimal control algorithms are used. Further, the time histories of response quantities and active control force are displayed in Figs. 52 to 60. Again, the two conclusions described previously for Riccati closed-loop control hold for instantaneous optimal control algorithms.

It is observed that time delay is most serious for instantaneous optimal open-loop control. Riccati closed-loop control and instantaneous

optimal closed-loop control are less sensitive to system time delay than instantaneous optimal closed-open-loop control. A time delay within 3% of the fundamental natural frequency, $T_f = 1.085$ seconds, is tolerable for the instantaneous optimal open-loop control algorithm, whereas a time delay of 4.5% of T_f is acceptable for other control algorithms. Beyond these limits described above, the degradation of the control efficiency is quite significant.

The fact that open-loop control may be susceptible to system time delay can be explained in the following. The control force is regulated by the measured input excitation rather than the feedback state vector in the case of open-loop control. The predominant frequency of the input excitation is usually quite different from that of the structure. Theoretically, the frequency content of the control force is expected to be close to that of the structural response. Since the frequency of the structural response is contributed by the frequencies of the input excitation and the structure, a time delay may result in a significant phase shift for the control force with respect to the response. This is particularly true when the magnitude of time delay is large.

Example 6: Active Mass Damper

Example 2 is reconsidered in which a system time delay τ is introduced. The deviation of the absolute maximum top floor relative displacement and that of the absolute maximum control force are presented in Figs. 61 and 62 as functions of time delay τ. For different control algorithms, the time histories of the structural response quantities and control force are displayed in Figs. 63 to 74.

From the results presented above, the effect of time delay on the active tendon control system and active mass damper is comparable, although

the active mass damper is slightly less sensitive. The observations made previously hold for the active mass damper also.

6.4 Truncation of Small Control forces: The sensitivity and criticality of truncating small control forces on the control system will be illustrated using the following numerical examples. The truncation level ϵ is expressed in term of KN and also in term of the percentage of maximum control force from the first controller under ideal control environments obtained in Section 6.1.

Example 7: Active Tendon Control System

Example 1 will be reconsidered in which different truncation levels, ϵ, for active control forces will be made. Numerical results for the time histories of the top floor relative displacement, the base shear force, and the active control force from the first controller are presented in Figs. 75 to 77 when the Riccati closed-loop control algorithm is used. With the application of three instantaneous optimal control algorithms, the corresponding results are displayed in Figs. 78 to 86.

For the particular earthquake ground acceleration input considered, the structural response and the active control force have a most intense segment roughly from 3 to 17 seconds. The active control forces outside this region are quite small. Thus, a majority of small control forces truncated are outside this region. As such, the structural response quantities do not die down after 17 seconds as rapidly when the small control forces are truncated. However, the truncation effect on the maximum structural response that occurs in the most intense segment is extremely limited as evidenced by Figs. 75 to 86. The truncation effect may become significant when the truncation level is high enough such that some control forces in the most intense segment are eliminated.

The maximum structural response is of great concern, whereas the rate of decay of the response beyond the most intense segment may not be important. Consequently, the maximum response quantities and the maximum control force within the time period of 30 seconds are tabulated in Tables 6-9 for different truncation levels, ϵ, and different control algorithms. The first column in the table indicates the actual truncation level ϵ in KN, and the second column shows the truncation level expressed in terms of the percentage of the maximum control force under ideal control environments as given in the first row of the table. For different truncation levels, the maximum response quantities and maximum control force are also expressed in terms of the percentage of the corresponding quantity obtained without a truncation, i.e., $\epsilon = 0$.

It is observed from Tables 7 to 9 and Figs. 78 to 86 that a truncation of all control forces smaller than 20% of the maximum control force practically does not affect the maximum response quantities. However, the response quantities do not die down as rapidly as the results obtained without a truncation of small control forces. The conclusion holds for all control algorithms considered.

Example 8: Active Mass Damper

Example 2 is reconsidered in which different levels of truncation for control forces have been made. The time histories of the top floor relative displacement, the base shear force, and the control force are presented in Figs. 87 to 98 for different control algorithms. The maximum response quantities and control force are tabulated in Tables 10-13. As observed from Figs. 87 to 98 and Tables 10 to 13, a truncation of all control forces smaller than 20% of the maximum control force has an insignificant effect of the active mass damper system.

Unlike the system uncertainty and time delay, the effect of truncation of small control forces is not sensitive to different control algorithms. Likewise, the sensitivity for active tendon control system is almost identical to that of the active mass damper.

Table 1: Maximum Structural Responses and Control Force for an 8-Story Building with Active Tendon Control System

CONTROL LAW	TOP FLOOR DISPLACEMENT (cm)	BASE SHEAR FORCE (KN)	CONTROL FORCE FROM FIRST CONTROLLER (KN)
Uncontrolled	4.10	2,506	------
Riccati Closed-Loop Control	1.36	853	437
Instantaneous Optimal Control	1.34	847	421

Table 2: Maximum Structural Responses and Control Force for an 8-Story Building with an Active Mass Damper

CONTROL LAW	TOP FLOOR DISPLACEMENT (cm)	BASE SHEAR FORCE (KN)	CONTROL FORCE (KN)
Uncontrolled	4.10	2,506	------
Riccati Closed-Loop Control	1.61	1,075	250
Instantaneous Optimal Control	1.54	1,045	232

Table 3: Maximum Structural Responses and Control Force for an 8-Story Building Using Riccati Closed-Loop Control Algorithm.

ACTIVE TENDON CONTROL SYSTEM									
ESTIMATION ERROR				TOP FLOOR DISPLACEMENT (CM)	DIFFERENCE IN % OF 1.36 CM	BASE SHEAR FORCE (KN)	DIFFERENCE IN % OF 853 KN	CONTROL FORCE (KN)	DIFFERENCE IN % OF 437 KN
Δk %	$\Delta\omega$ %	Δc %	$\Delta\zeta$ %						
0	0	0	0	1.36	----	853	----	437	----
40	18.3	0	0	1.53	12.5	965	13.1	389	-11.0
20	9.6	0	0	1.43	5.1	899	5.4	413	-5.5
-20	-10.5	0	0	1.32	-2.9	792	-7.1	460	5.3
-40	-22.6	0	0	1.27	-8.4	698	-18.1	502	14.9
0	0	40	40	1.43	5.4	901	5.6	416	-4.8
0	0	-40	-40	1.33	-2.2	812	-4.8	443	1.4
ACTIVE MASS DAMPER									
ESTIMATION ERROR				TOP FLOOR DISPLACEMENT (CM)	DIFFERENCE IN % OF 1.61 CM	BASE SHEAR FORCE (KN)	DIFFERENCE IN % OF 1,070 KN	CONTROL FORCE (KN)	DIFFERENCE IN % OF 250 KN
Δk %	$\Delta\omega$ %	Δc %	$\Delta\zeta$ %						
0	0	0	0	1.61	----	1,070	----	250	----
40	18.3	0	0	1.71	6.2	1,047	-2.1	254	1.6
20	9.6	0	0	1.65	2.5	1,052	-1.7	255	2.0
-20	-10.5	0	0	1.59	-1.2	1,096	2.4	253	1.2
-40	-22.6	0	0	1.58	-1.8	1,096	2.4	278	11.2
0	0	40	40	1.64	1.8	1,085	1.4	240	-4.0
0	0	-40	-40	1.59	-1.2	1,054	-1.4	259	3.6

Table 4: Maximum Structural Responses and Control Force for an 8-Story Building Using Instantaneous Optimal Open-Loop Control Algorithm.

ACTIVE TENDON CONTROL SYSTEM									
ESTIMATION ERROR				TOP FLOOR DISPLACEMENT (CM)	DIFFERENCE IN % OF 1.34 CM	BASE SHEAR FORCE (KN)	DIFFERENCE IN % OF 847 KN	CONTROL FORCE (KN)	DIFFERENCE IN % OF 421 KN
Δk %	Δω %	Δc %	Δζ %						
0	0	0	0	1.34	----	847	----	421	----
20	9.6	0	0	1.64	22.4	996	17.6	415	-1.4
10	4.9	0	0	1.51	12.7	866	2.2	403	-4.3
-10	-5.1	0	0	1.43	6.7	910	7.4	439	4.3
-20	-10.5	0	0	1.71	27.6	1,022	20.7	457	8.6
0	0	40	40	1.37	2.2	884	4.4	409	-2.8
0	0	-40	-40	1.33	-0.7	799	-5.6	441	4.7
ACTIVE MASS DAMPER									
ESTIMATION ERROR				TOP FLOOR DISPLACEMENT (CM)	DIFFERENCE IN % OF 1.54 CM	BASE SHEAR FORCE (KN)	DIFFERENCE IN % OF 1,045 KN	CONTROL FORCE (KN)	DIFFERENCE IN % OF 232 KN
Δk %	Δω %	Δc %	Δζ %						
0	0	0	0	1.54	----	1,045	----	232	----
20	9.6	0	0	1.96	27.3	1,202	15.0	217	-6.5
10	4.9	0	0	1.77	14.9	1,094	4.7	223	-3.9
-10	-5.1	0	0	1.52	-1.3	1,031	-1.3	246	6.0
-20	-10.5	0	0	1.55	0.6	1,082	3.5	274	18.1
0	0	40	40	1.56	1.3	1,045	---	230	-0.9
0	0	-40	-40	1.54	----	1,047	0.2	234	0.9

Table 5: Maximum Structural Responses and Control Force for an 8-Story Building Using Instantaneous Optimal Closed-Open-Loop Control Algorithm.

ACTIVE TENDON CONTROL SYSTEM									
ESTIMATION ERROR				TOP FLOOR DISPLACEMENT (CM)	DIFFERENCE IN % OF 1.34 CM	BASE SHEAR FORCE (kn)	DIFFERENCE IN % OF 847 KN	CONTROL FORCE (KN)	DIFFERENCE IN % OF 421 KN
Δk %	$\Delta\omega$ %	Δc %	$\Delta\zeta$ %						
0	0	0	0	1.34	----	847	----	421	----
40	18.3	0	0	1.39	3.7	829	-2.1	438	4.0
20	9.6	0	0	1.37	2.2	838	-1.1	428	1.6
-20	-10.5	0	0	1.34	----	856	1.1	414	-1.6
-40	-22.6	0	0	1.38	3.0	878	3.6	413	-1.9
0	0	40	40	1.34	---	852	0.5	418	-0.7
0	0	-40	-40	1.35	0.7	843	-0.4	425	1.4
ACTIVE MASS DAMPER									
ESTIMATION ERROR				TOP FLOOR DISPLACEMENT (CM)	DIFFERENCE IN % OF 1.54 CM	BASE SHEAR FORCE (KN)	DIFFERENCE IN % OF 1,045 KN	CONTROL FORCE (KN)	DIFFERENCE IN % OF 232 KN
Δk %	$\Delta\omega$ %	Δc %	$\Delta\zeta$ %						
0	0	0	0	1.54	---	1,045	---	232	---
40	18.3	0	0	1.55	0.7	1,046	0.1	232	---
20	9.6	0	0	1.54	---	1,045	---	232	---
-20	-10.5	0	0	1.54	---	1,045	---	232	---
-40	-22.6	0	0	1.54	---	1,046	0.1	232	---
0	0	40	40	1.54	---	1,046	0.1	232	---
0	0	-40	-40	1.54	---	1,046	0.1	232	---

Table 6: Maximum Response Quantities and Control Force for an 8-Story Building with Tendon Control System Using Riccati Closed-Loop Control Algorithm.

ϵ IN KN	ϵ IN % of 437KN	TOP FLOOR DISPLACEMENT (CM)	CHANGE IN % OF 1.36 CM	BASE SHEAR FORCE (KN)	CHANGE IN % OF 853 KN	CONTROL FORCE (KN)	CHANGE IN % OF 437 KN
0	0.0	1.36	----	853	-----	437	-----
50	11.44	1.36	----	844	-1.0	439	0.4
75	17.16	1.36	----	847	-0.7	442	1.1
100	22.88	1.37	0.7	848	-0.6	444	1.6

Table 7: Maximum Response Quantities and Control Force for an 8-Story Building with Tendon Control System Using Instantaneous Optimal Closed-Loop Control Algorithm.

ϵ IN KN	ϵ IN % OF 421KN	TOP FLOOR DISPLACEMENT (CM)	CHANGE IN % OF 1.34 CM	BASE SHEAR FORCE (KN)	CHANGE IN % OF 847 KN	CONTROL FORCE (KN)	CHANGE IN % OF 421 KN
0	0.0	1.34	----	847	-----	421	-----
50	11.87	1.34	----	848	0.1	421	-----
75	17.81	1.33	-0.7	850	0.3	424	0.7
100	23.75	1.32	-1.5	853	0.7	426	1.1

Table 8: Maximum Response Quantities and Control Force for an 8-Story Building with Tendon Control System Using Instantaneous Optimal Open-Loop Control Algorithm.

ϵ IN KN	ϵ IN % OF 421KN	TOP FLOOR DISPLACEMENT (CM)	CHANGE IN % OF 1.34 CM	BASE SHEAR FORCE (KN)	CHANGE IN % OF 847 KN	CONTROL FORCE (KN)	CHANGE IN % OF 421 KN
0	0.0	1.34	----	847	-----	421	-----
50	11.87	1.33	-0.7	849	0.2	422	0.2
75	17.81	1.33	-0.7	852	0.6	424	0.7
100	23.75	1.33	-0.7	853	0.7	426	1.1

Table 9: Maximum Response Quantities and Control Force for an 8-Story Building with Tendon Control System Using Instantaneous Optimal Closed-Open-Loop Control Algorithm.

ϵ IN KN	ϵ IN % OF 421KN	TOP FLOOR DISPLACEMENT (CM)	CHANGE IN % OF 1.34 CM	BASE SHEAR FORCE (KN)	CHANGE IN % OF 847 KN	CONTROL FORCE (KN)	CHANGE IN % OF 421 KN
0	0.0	1.34	----	847	-----	421	-----
50	11.87	1.34	----	848	0.1	421	-----
75	17.81	1.33	-0.7	852	0.6	424	0.7
100	23.75	1.33	-0.7	853	0.7	426	1.1

Table 10: Maximum Response Quantities and Control Force for an 8-Story Building with an Active Mass Damper Using Riccati Closed-Loop Control Algorithm.

ϵ IN KN	ϵ IN % OF 250KN	TOP FLOOR DISPLACEMENT (CM)	CHANGE IN % OF 1.61 CM	BASE SHEAR FORCE (KN)	CHANGE IN % OF 1,070 KN	CONTROL FORCE (KN)	CHANGE IN % OF 250 KN
0	0	1.61	----	1,070	-----	250	-----
50	20	1.66	3.1	1,073	0.2	249	-0.4
75	30	1.74	8.1	1,088	1.7	237	-5.2

Table 11: Maximum Response Quantities and Control Force for an 8- Story Building with an Active Mass Damper Using Instantaneous Optimal Closed-Loop Control Algorithm.

ϵ IN KN	ϵ IN % OF 232KN	TOP FLOOR DISPLACEMENT (CM)	CHANGE IN % OF 1.54 CM	BASE SHEAR FORCE (KN)	CHANGE IN % OF 1,047 KN	CONTROL FORCE (KN)	CHANGE IN % OF 232 KN
0	0	1.54	----	1,047	-----	232	-----
50	21.55	1.56	1.2	1,036	-1.0	225	-3.0
75	32.32	1.60	3.9	977	-6.7	203	-12.5

Table 12: Maximum Response quantities and Control Force for an 8-Story Building with an Active Mass Damper Using Instantaneous Optimal Open-Loop Control Algorithm.

ϵ IN KN	ϵ IN % OF 232KN	TOP FLOOR DISPLACEMENT (CM)	CHANGE IN % OF 1.54 CM	BASE SHEAR FORCE (KN)	CHANGE IN % OF 1,047 KN	CONTROL FORCE (KN)	CHANGE IN % OF 232 KN
0	0	1.54	----	1,047	-----	232	-----
50	21.55	1.56	1.2	1,035	-1.1	224	-3.4
75	32.32	1.62	5.2	977	-6.7	205	-11.6

Table 13: Maximum Response Quantities and Control Force for an 8-Story Building with an Active Mass Damper Using Instantaneous Optimal Closed-Open-Loop Control Algorithm ϵ: Maximum Control Force U_{max} = 232 KN.

ϵ IN KN	ϵ IN % OF 232KN	TOP FLOOR DISPLACEMENT (CM)	CHANGE IN % OF 1.54 CM	BASE SHEAR FORCE (KN)	CHANGE IN % OF 1,047 KN	CONTROL FORCE (KN)	CHANGE IN % OF 232 KN
0	0	1.54	----	1,047	-----	232	-----
50	21.55	1.55	0.6	1,035	-1.1	224	-3.4
75	32.32	1.61	4.5	976	-6.8	204	-12.0

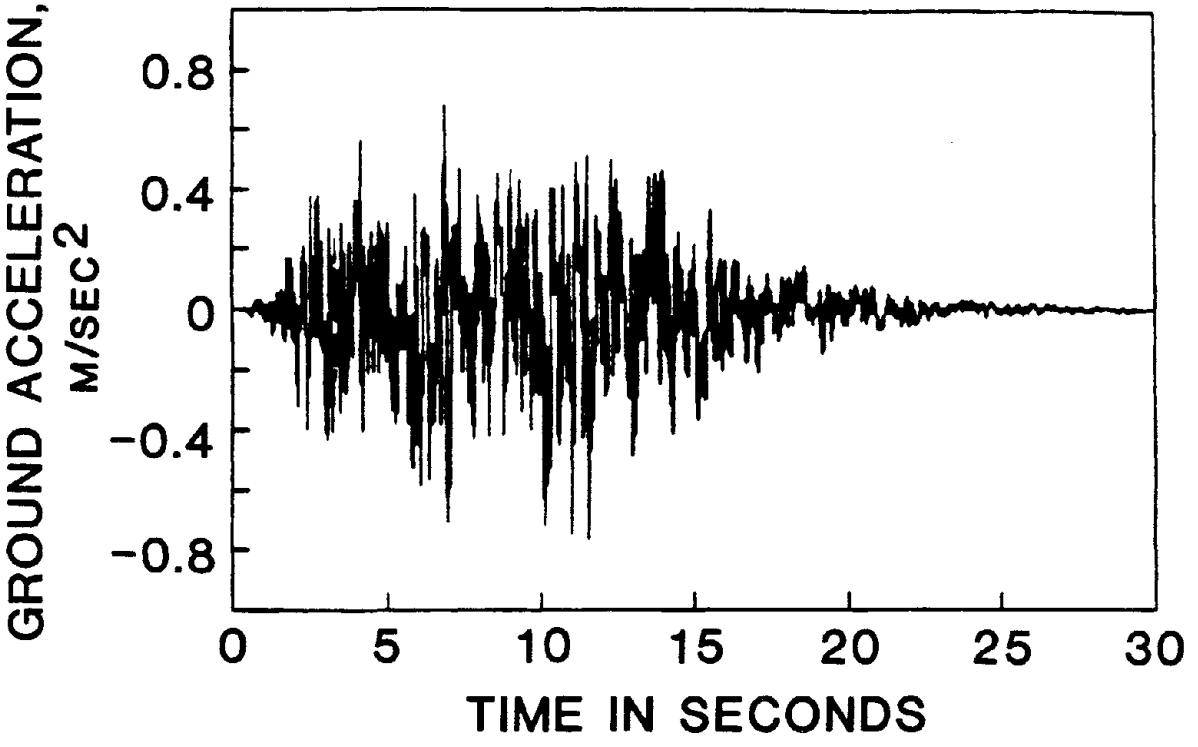

Fig. 17: Simulated Ground Acceleration

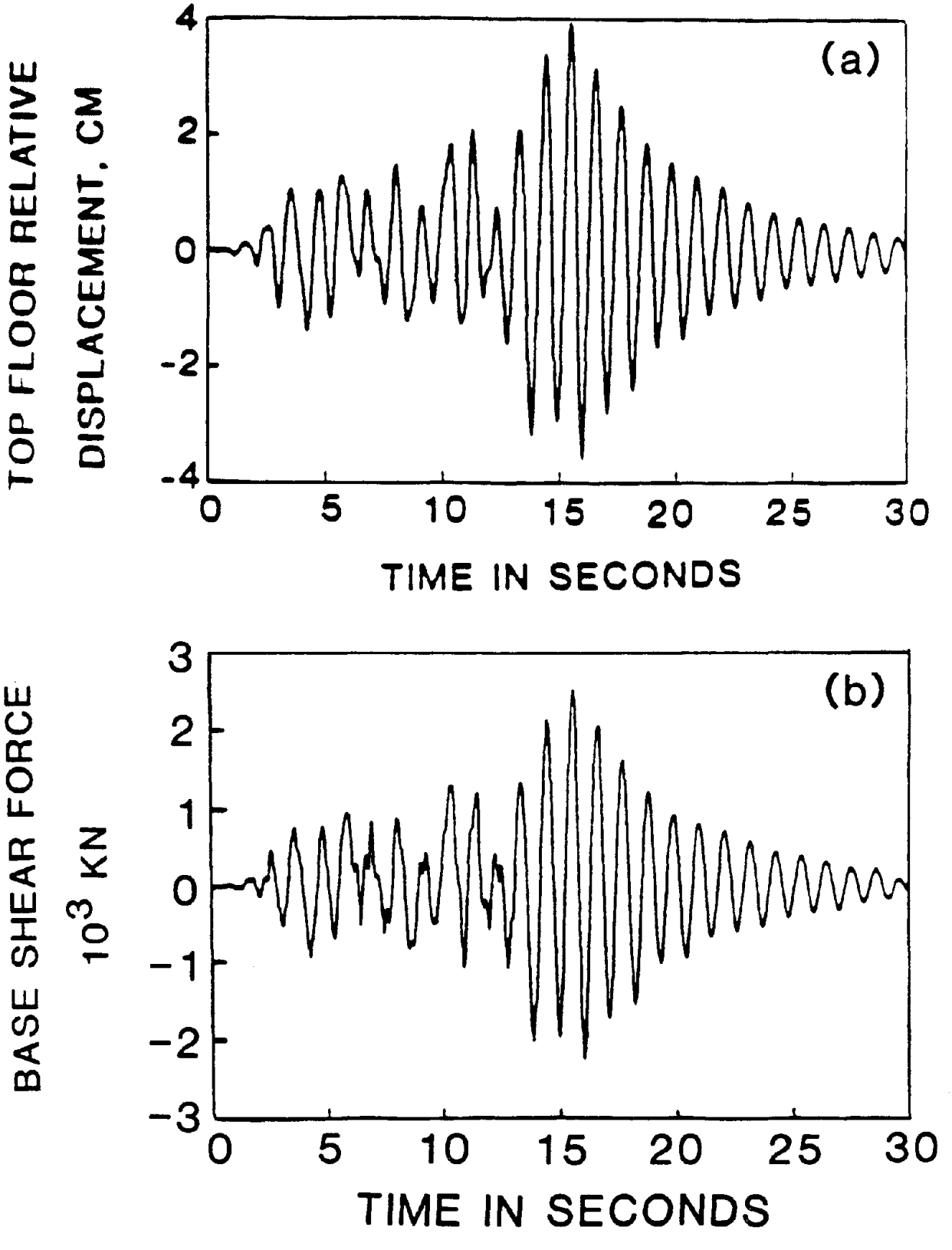

Fig. 18: Uncontrolled Response Quantities: (a) Top Floor Relative Displacement, (b) Base Shear Force

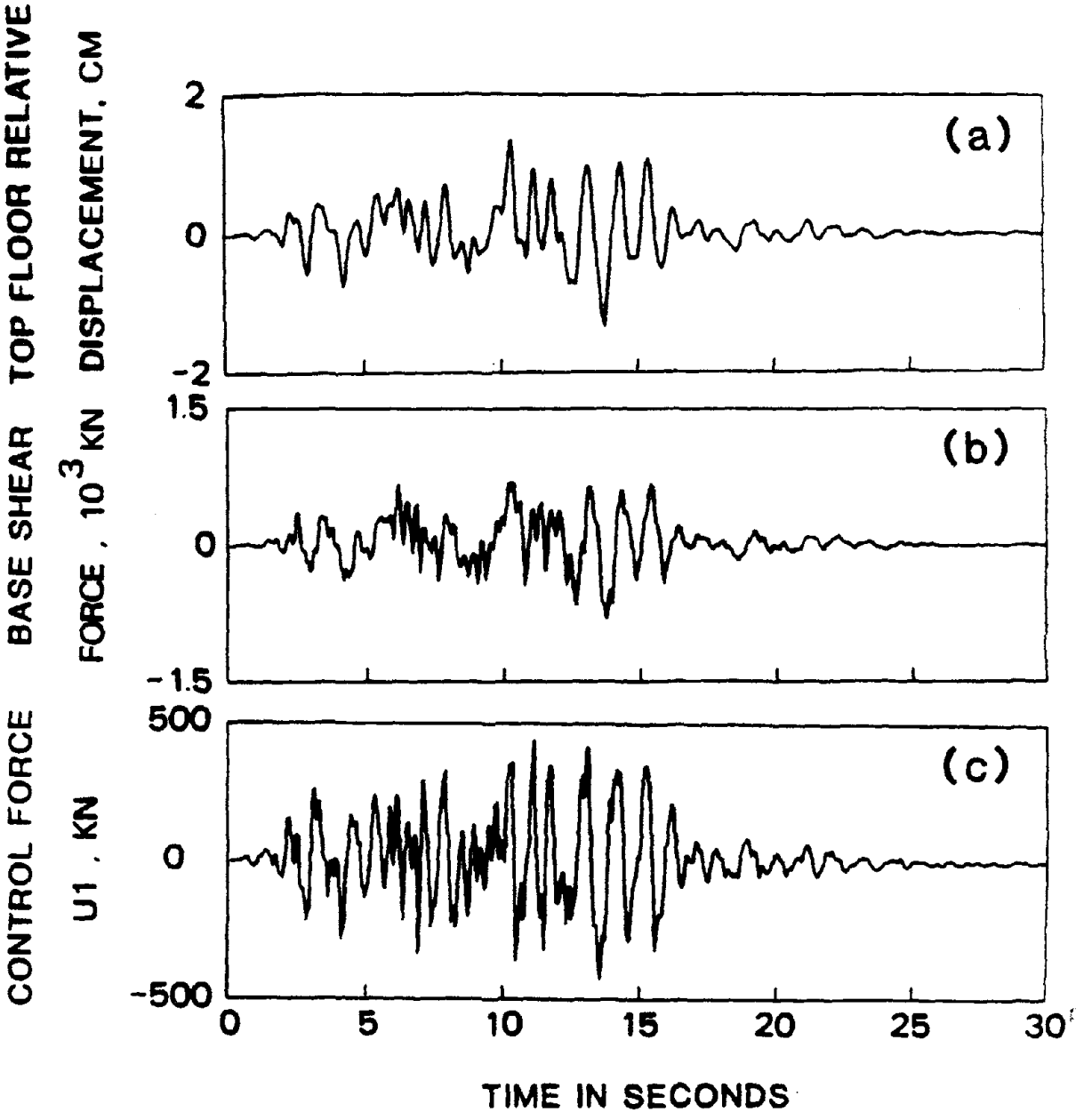

Fig. 19: Response Quantities and Active Control Force Using Tendon Control System and Riccati Closed-Loop Control Algorithm: (a) Top Floor Relative Displacement, (b) Base Shear Force, (c) Active Control Force.

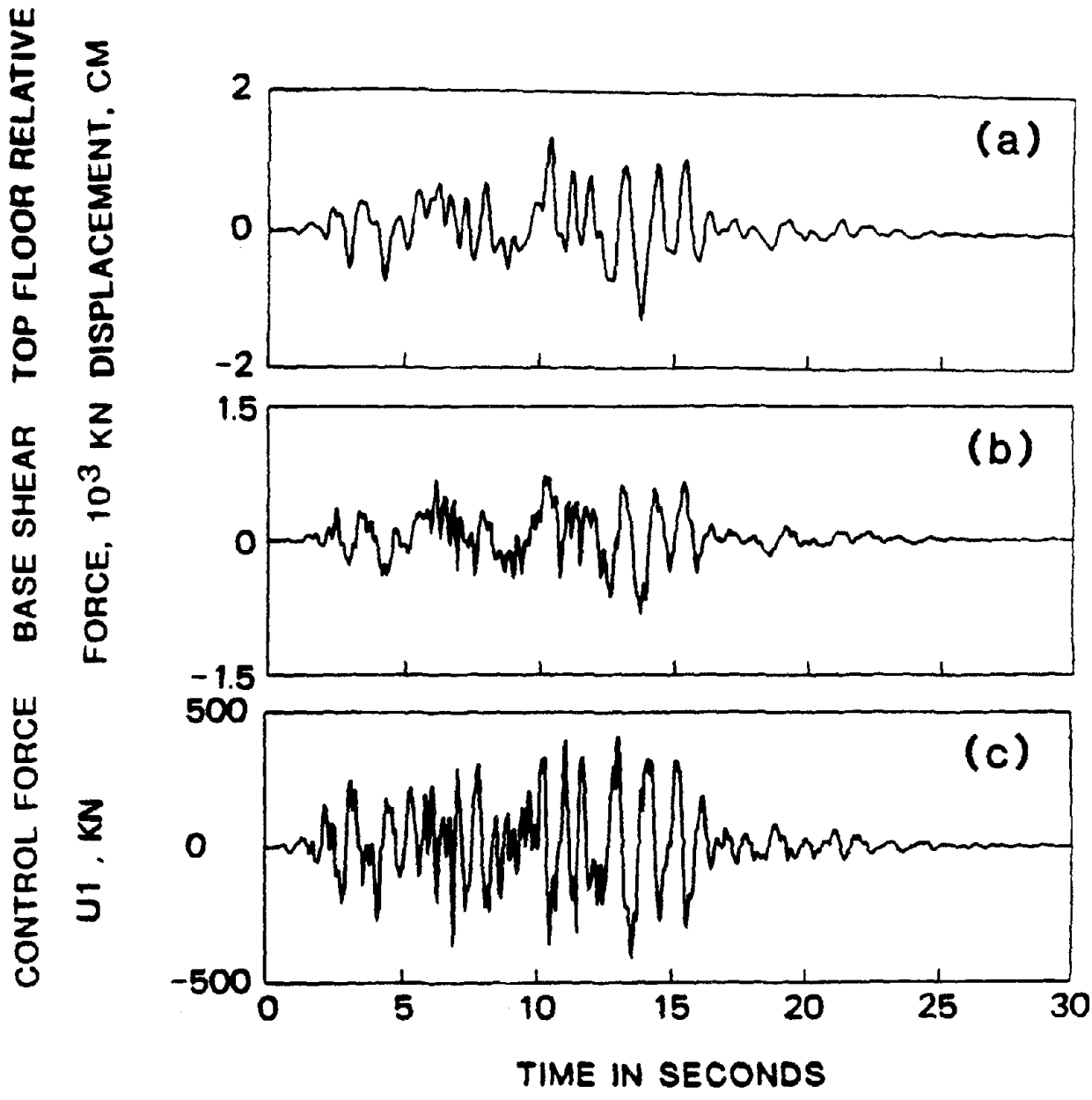

Fig. 20: Response Quantities and Active Control Force Using Tendon Control System and Instantaneous Optimal Control Algorithm: (a) Top Floor Relative Displacement, (b) Base Shear Force, (c) Active Control Force.

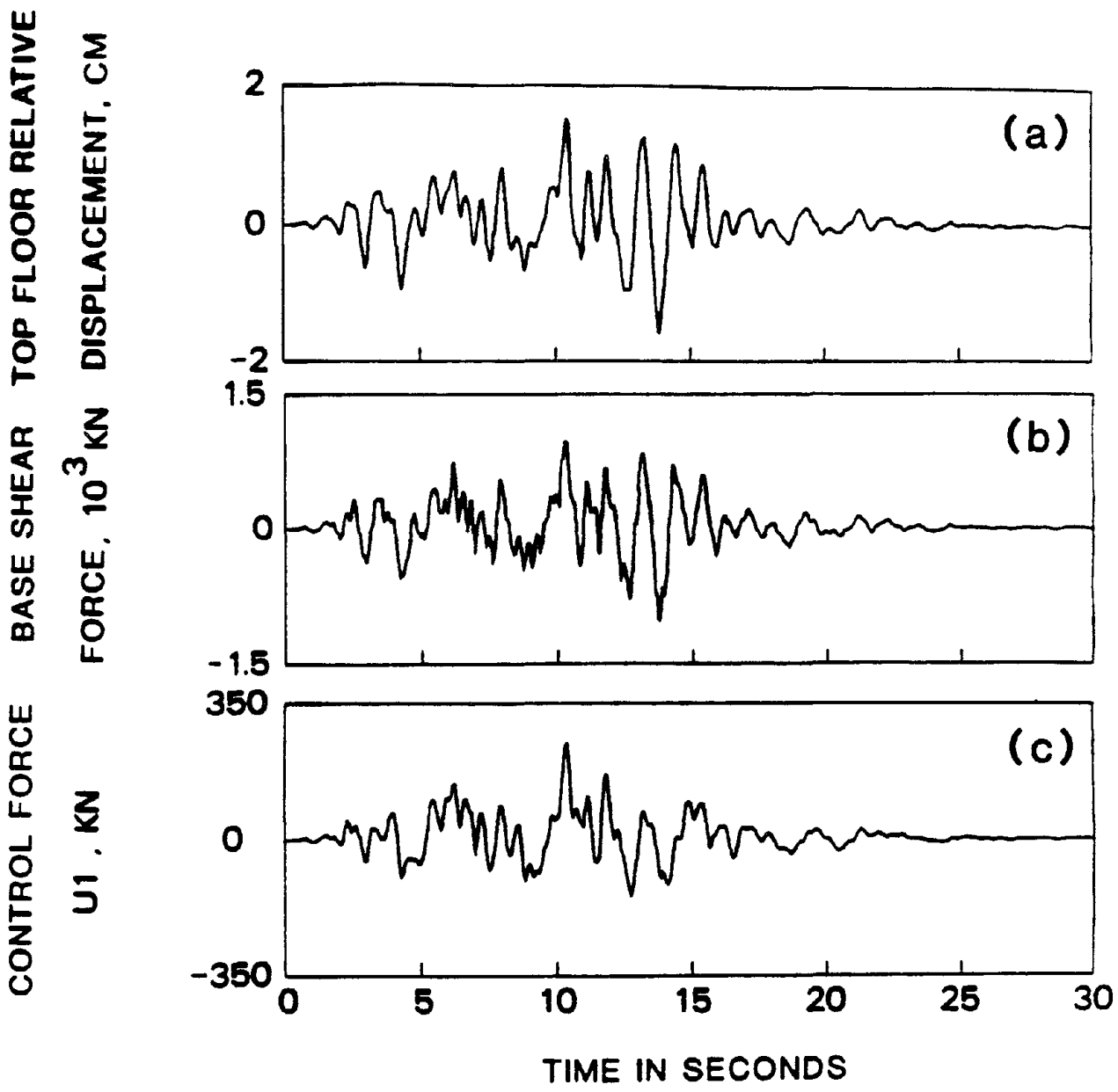

Fig. 21: Response Quantities and Active Control Force Using an Active Mass Damper and Riccati Closed-Loop Control Algorithm: (a) Top Floor Relative Displacement, (b) Base Shear Force, (c) Active Control Force.

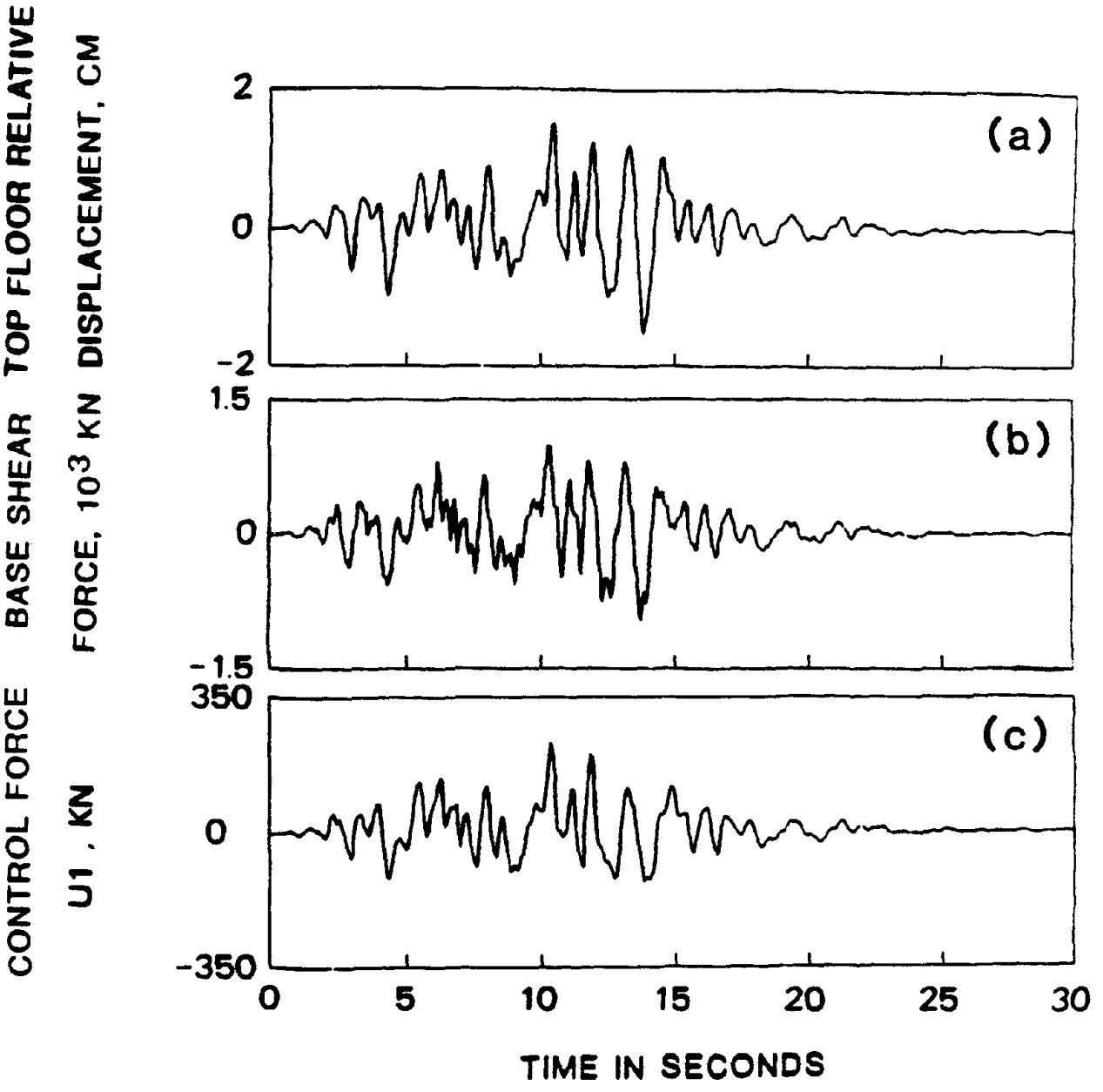

Fig. 22: Response Quantities and Active Control Force Using an Active Mass Damper and Instantaneous Optimal Control Algorithm: (a) Top Floor Relative Displacement, (b) Base Shear Force, (c) Active Control Force.

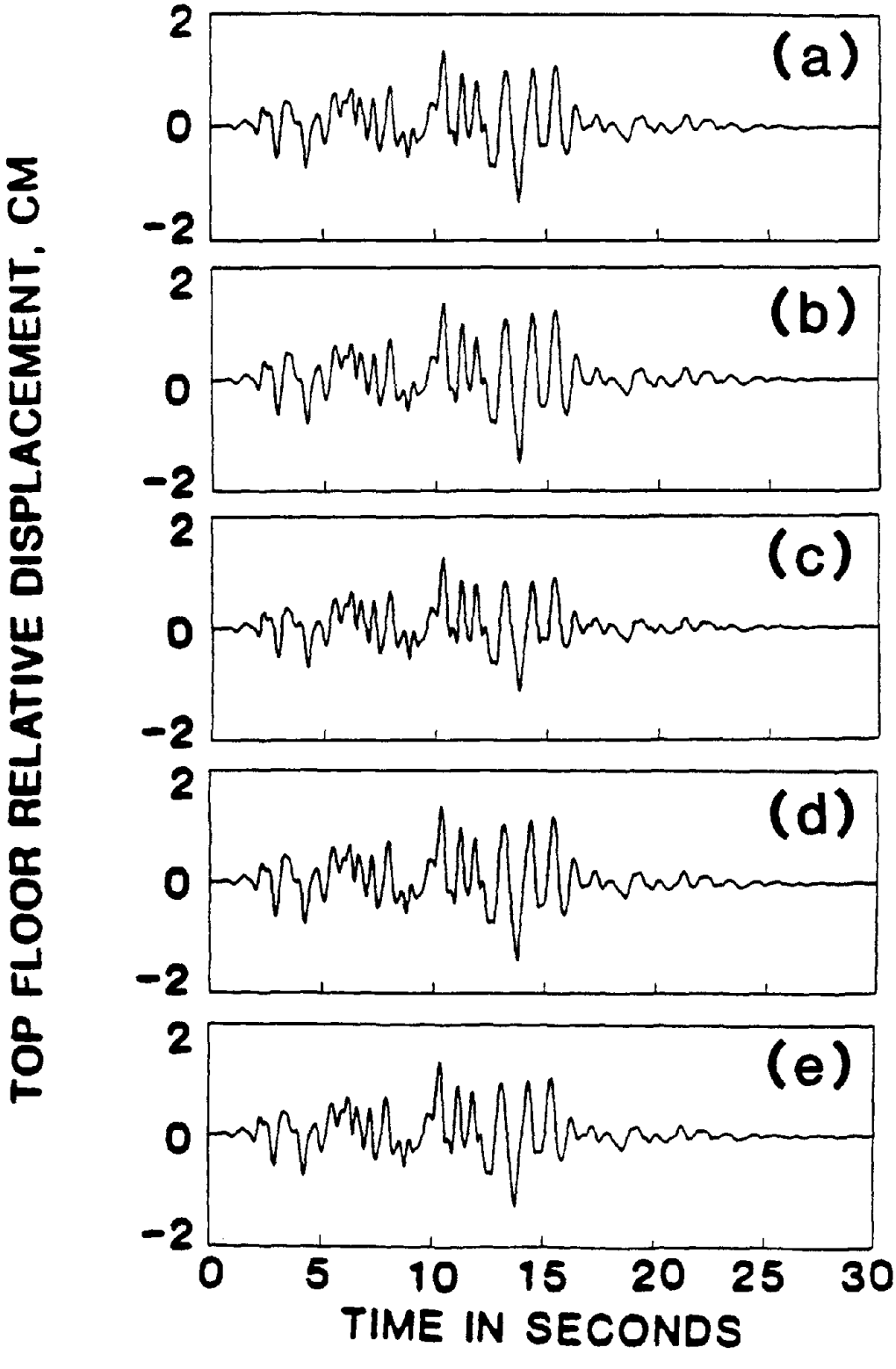

Fig. 23 : Top Floor Relative Displacement for an 8-Story Building using Tendon Control System and Riccati Closed-Loop Control Algorithm:(a) No System Uncertainty, (b) $\Delta K = 40\%$, (c) $\Delta K = -40\%$, (d) $\Delta C = 40\%$, (e) $\Delta C = -40\%$.

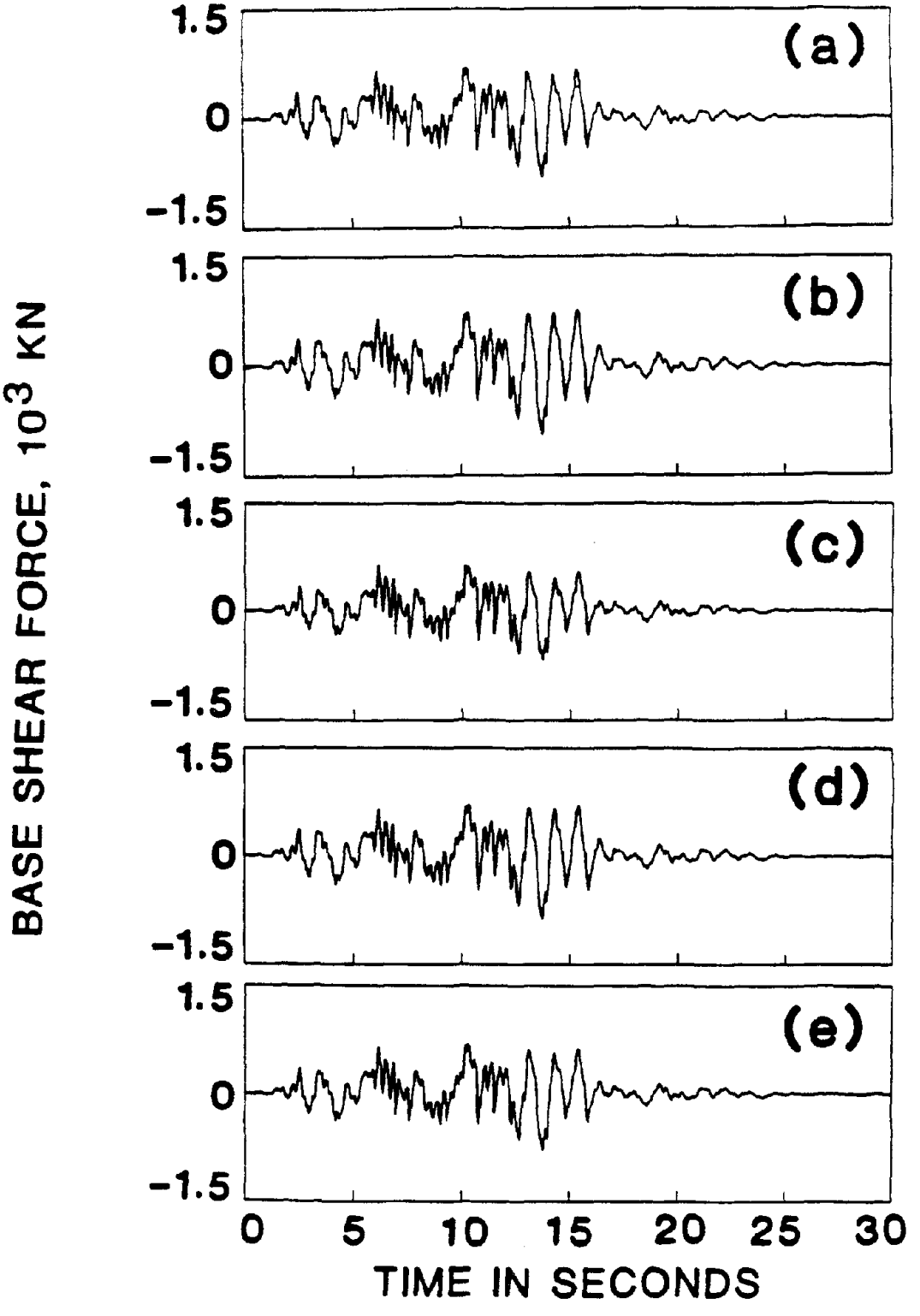

Fig. 24 : Base Shear Force for an 8-Story Building Using Tendon Control System and Riccati Closed-Loop Control Algorithm: (a) No System Uncertainty, (b) $\Delta K = 40\%$, (c) $\Delta K = -40\%$, (d) $\Delta C = 40\%$, (e) $\Delta C = -40\%$.

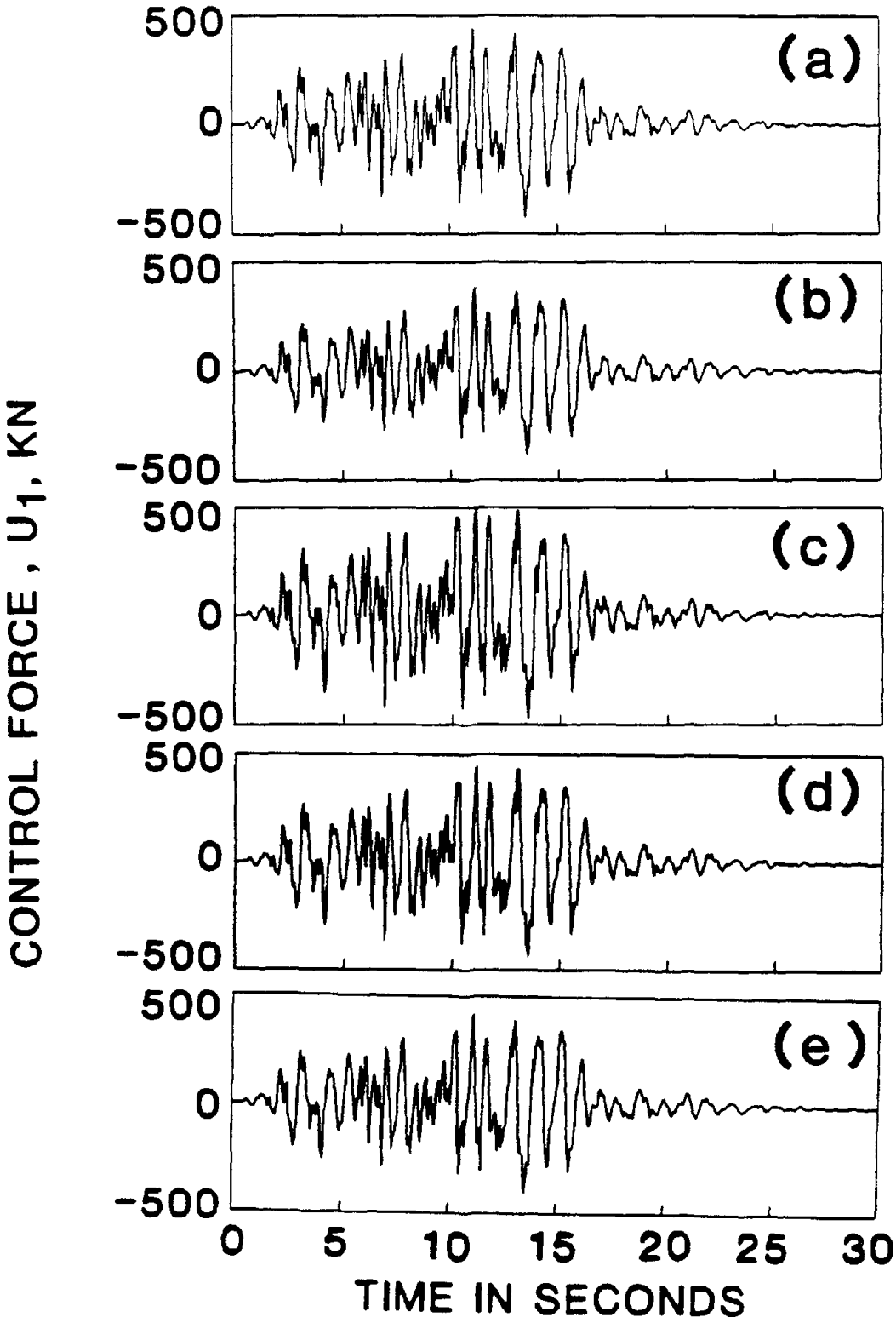

Fig. 25 : Active Control Force From the First Controller for an 8-Story Building Using Tendon Control System and Riccati Closed-Loop Control Algorithm: (a) No System Uncertainty, (b) $\Delta K = 40\%$, (c) $\Delta K = -40\%$, $\Delta C = 40\%$, (e) $\Delta C = -40\%$.

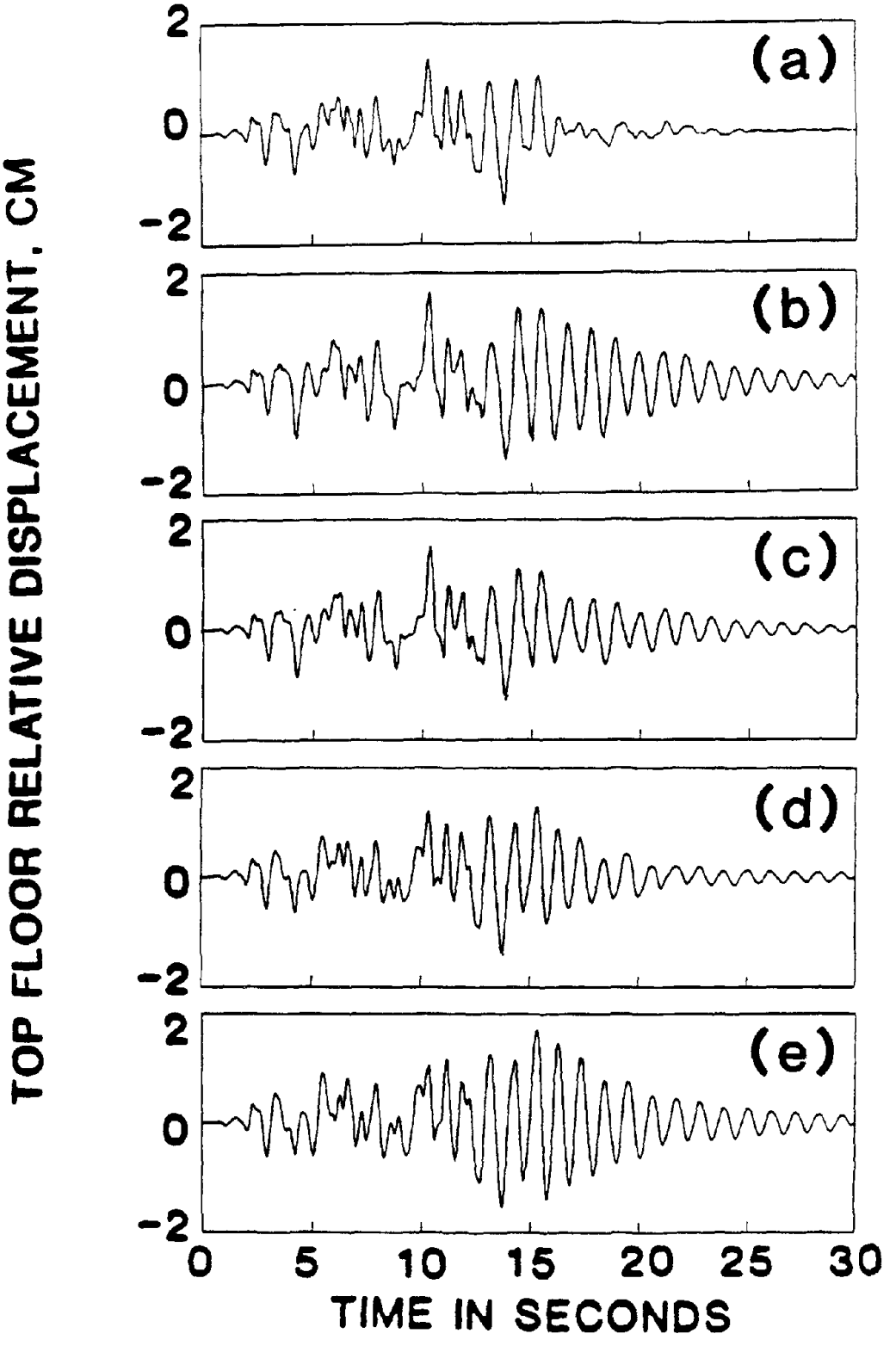

Fig. 26: Top Floor Relative Displacement for an 8-Story Building Using Tendon Control System and Instantaneous Optimal Closed-Loop Control Algorithm : (a) No System Uncertainty, (b) $\Delta K = 40\%$, (c) $\Delta K = -40\%$, (d) $\Delta C = 40\%$, (e) $\Delta C = -40\%$.

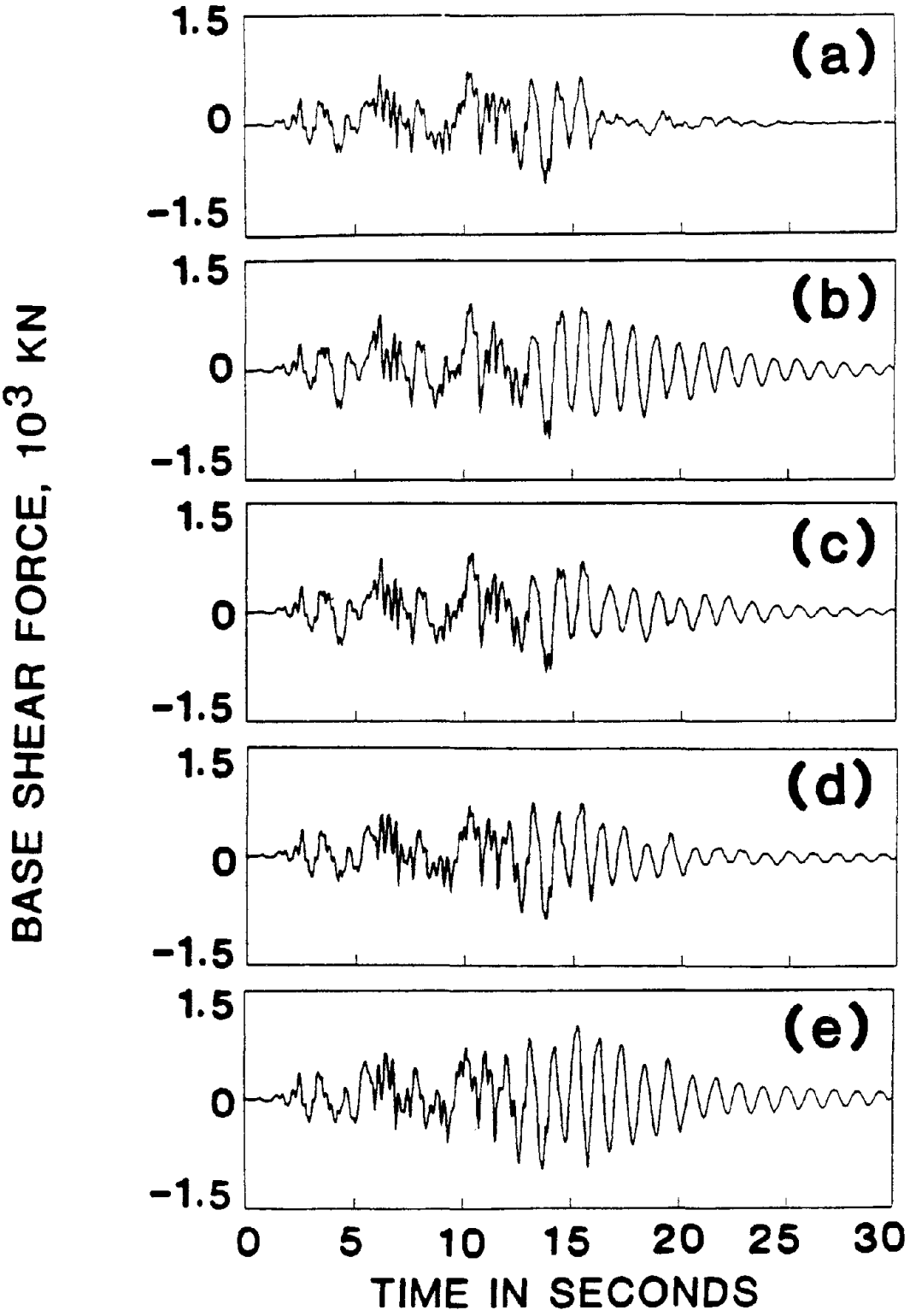

Fig. 27: Base Shear Force for an 8-Story Building Using Tendon Control System and Instantaneous Optimal Closed-Loop Control Algorithm: (a) No System Uncertainty, (b) $\Delta K = 40\%$, (c) $\Delta K = -40\%$, (d) $\Delta C = 40\%$, (e) $\Delta C = -40\%$.

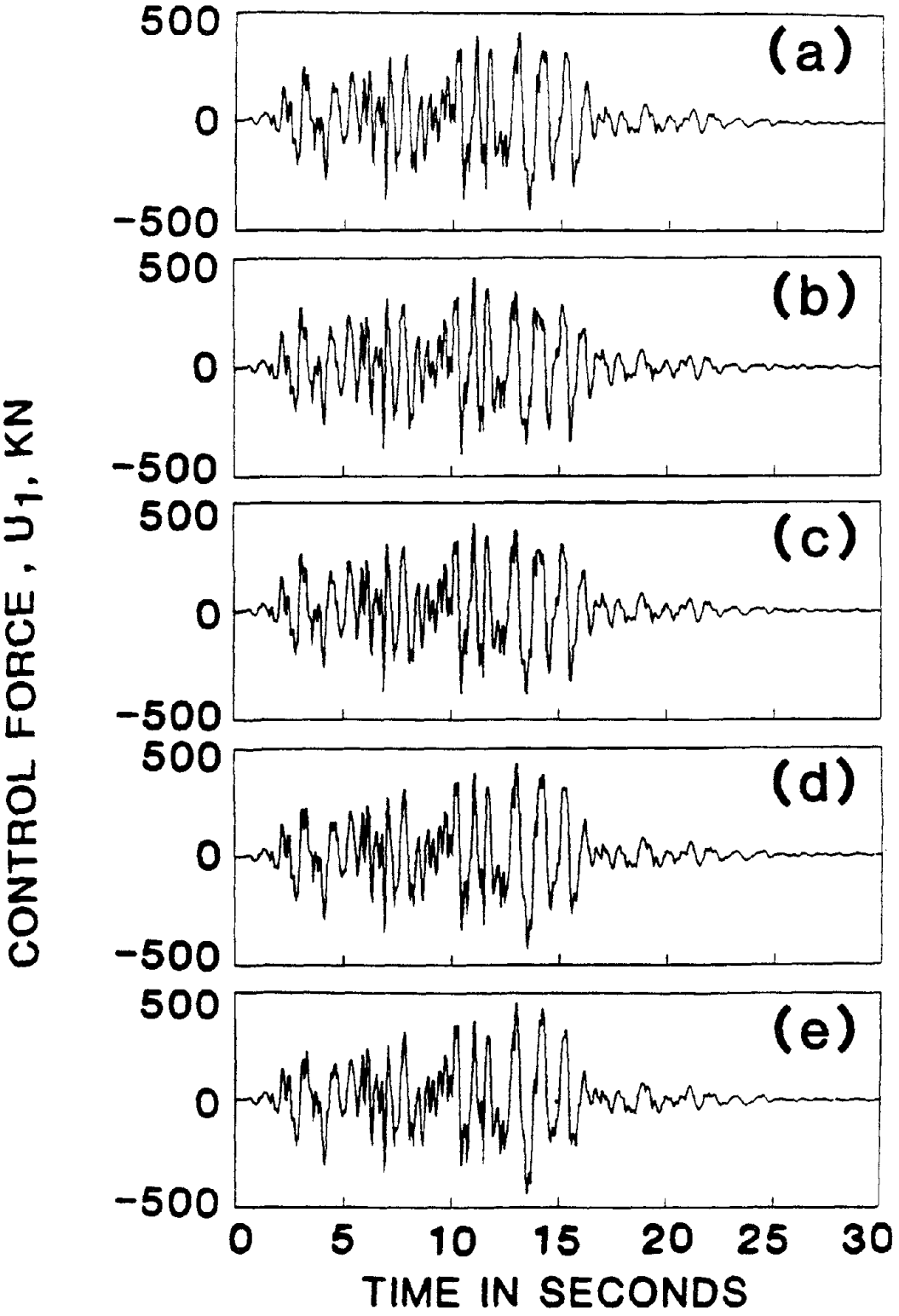

Fig. 28: Active Control Force from the First Controller for an 8-Story Building Using Tendon Control System and Instantaneous Optimal Closed-Loop Control Algorithm: (a) No System Uncertainty, (b) $\Delta K = 40\%$, $\Delta K = -40\%$, $\Delta C = 40\%$, $\Delta C = -40\%$.

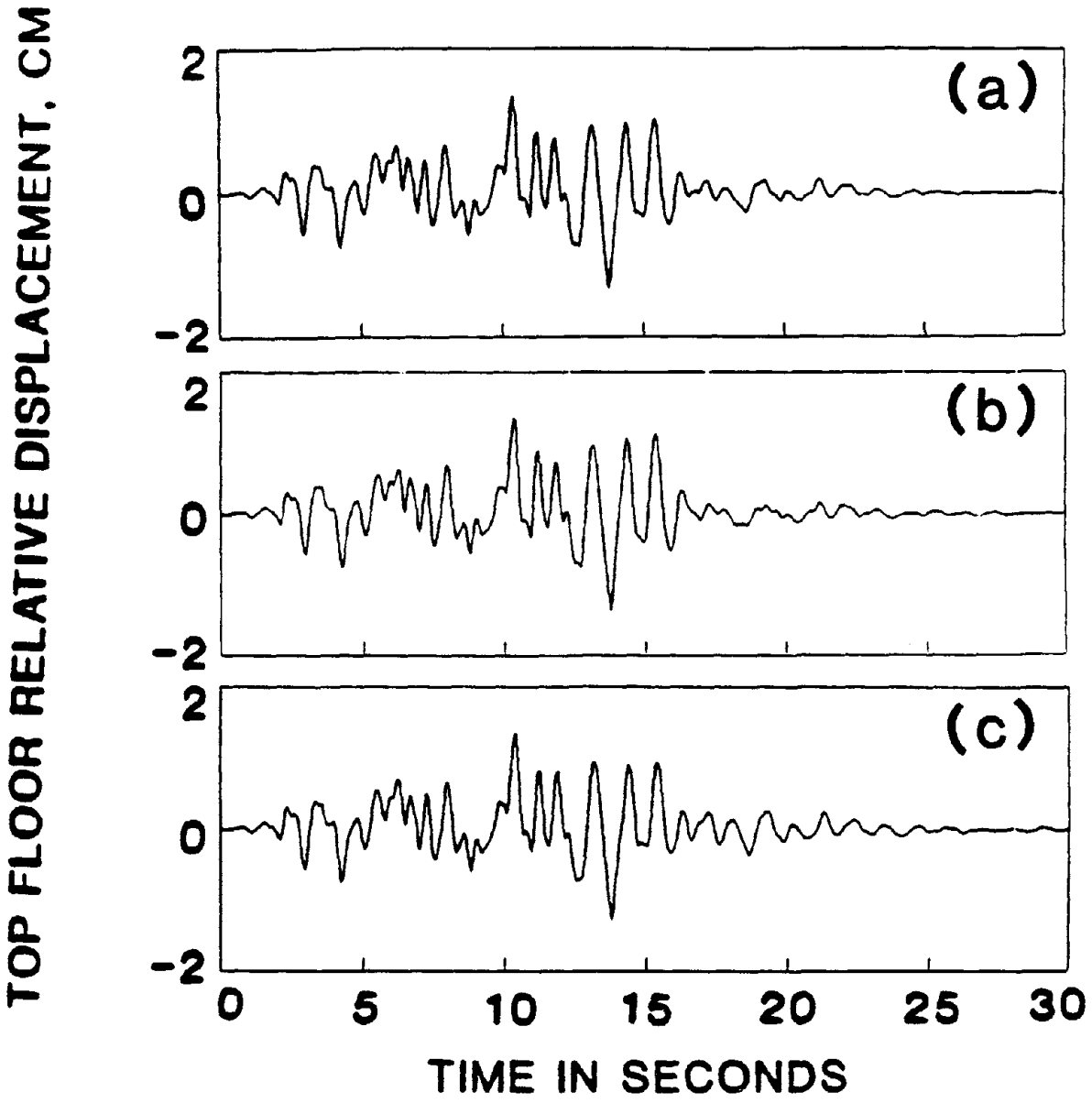

Fig. 29: Top Floor Relative Displacement for an 8-Story Building Using Tendon Control System and Instantaneous Optimal Open-Loop Control Algorithm: (a) No System Uncertainty, (b) $\Delta C = 40\%$, (c) $\Delta C = -40\%$.

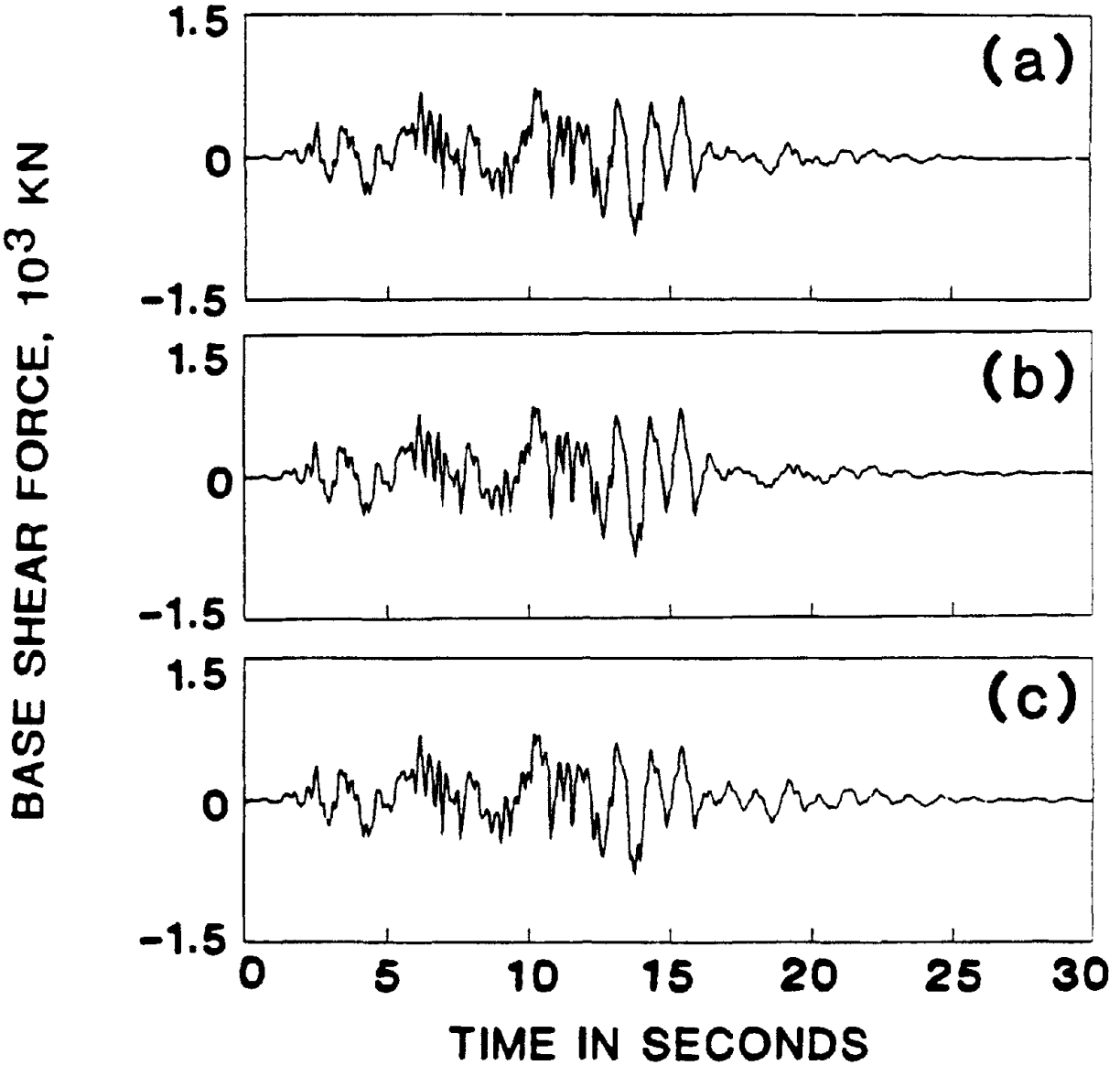

Fig. 30: Base Shear Force for an 8-Story Building Using Tendon Control System and Instantaneous Optimal Open-Loop Control Algorithm: (a) No System Uncertainty, (b) $\Delta C = 40\%$, (c) $\Delta C = -40\%$.

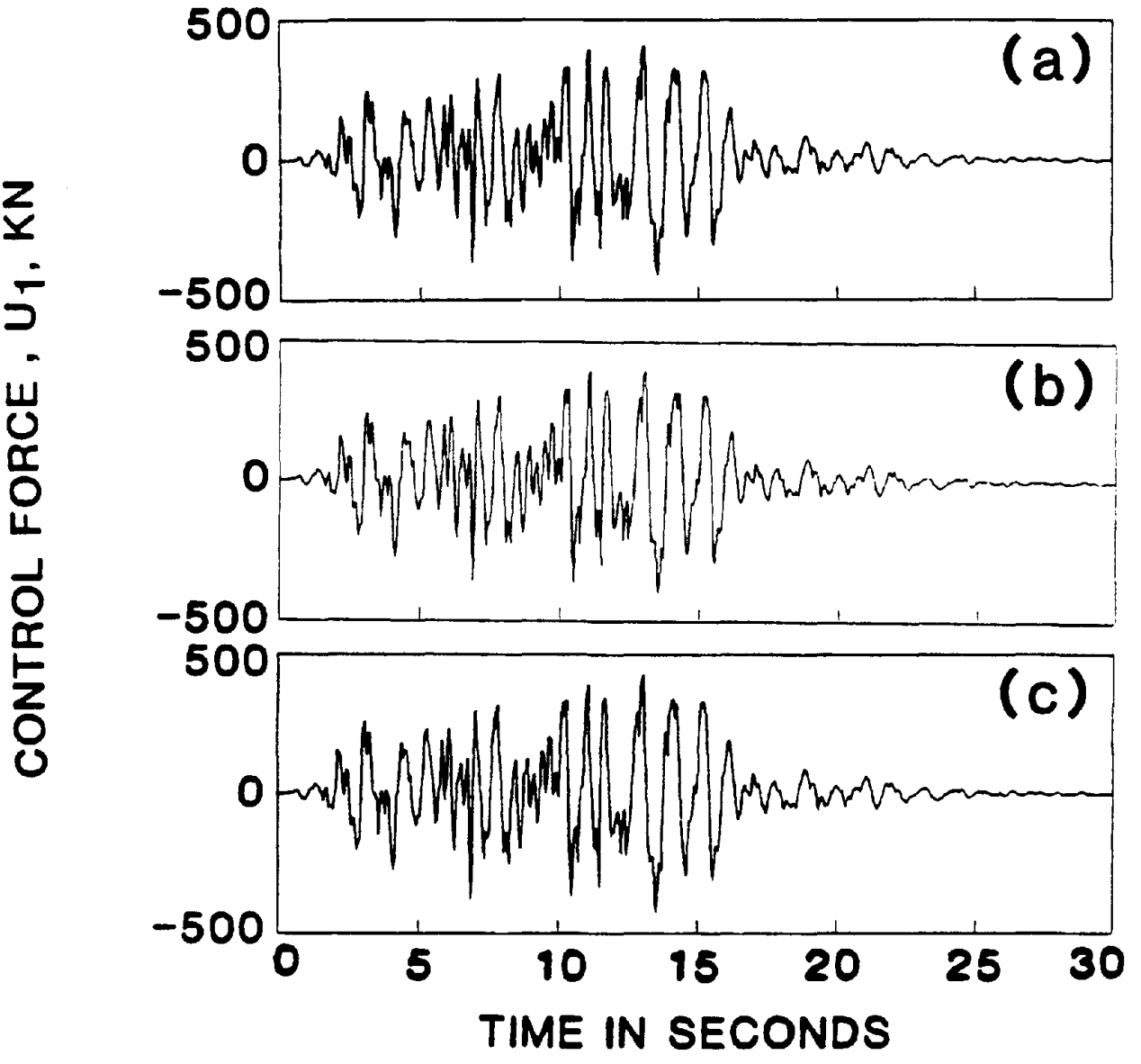

Fig. 31: Active Control Force from the First Controller for an 8-Story Building Using Tendon Control System and Instantaneous Optimal Open-Loop Control Algorithm: (a) No System Uncertainty, (b) ΔC = 40%, (c) ΔC = 40%.

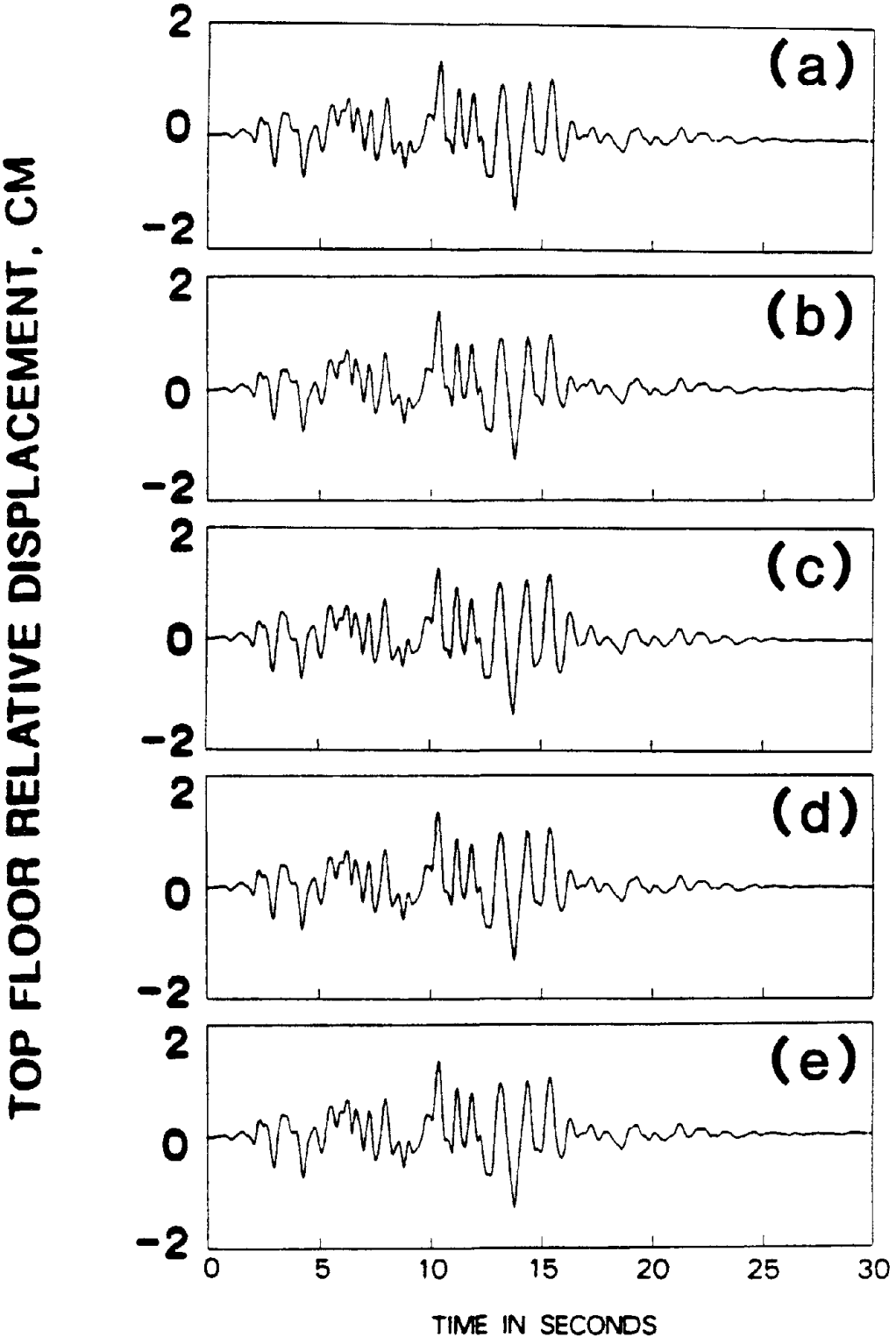

Fig. 32: Top Floor Relative Displacement for an 8-Story Building Using Tendon Control System and Instantaneous Optimal Closed-Open-Loop Control Algorithm: (a) No System Uncertainty, (b) $\Delta K = 40\%$, (c) $\Delta K = -40\%$, (d) $\Delta C = 40\%$, (e) $\Delta C = -40\%$.

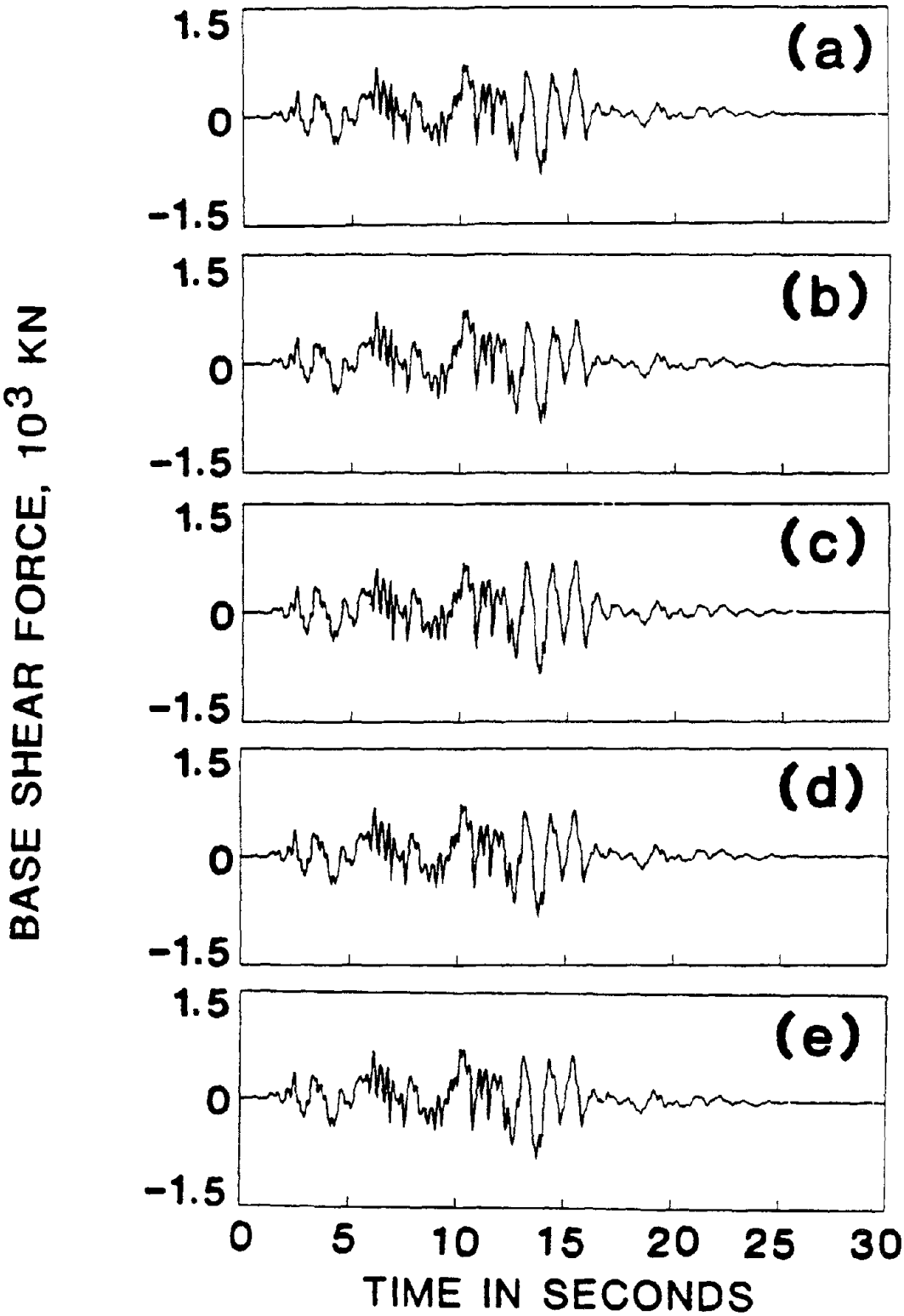

Fig. 33: Base Shear Force for an 8-Story Building Using Tendon Control System and Instantaneous Optimal Closed-Open-Loop Control Algorithm: (a) No System Uncertainty, (b) $\Delta K = 40\%$, (c) $\Delta K = -40\%$, (d) $\Delta C = 40\%$, (e) $\Delta C = -40\%$.

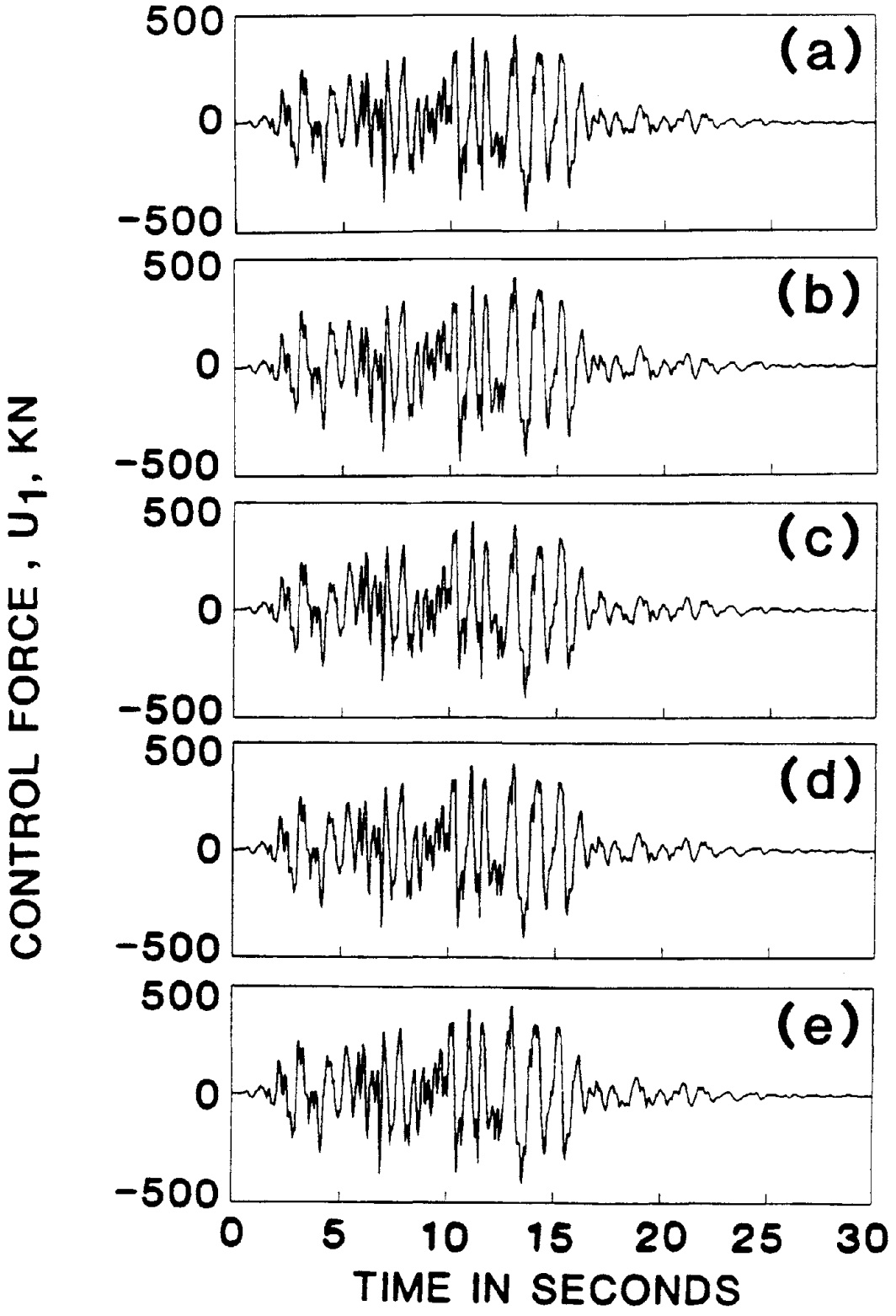

Fig. 34: Active Control Force from the First Controller for an 8-Story Building Using Tendon Control System and Instantaneous Optimal Closed-Open-Loop Control Algorithm: (a) No System Uncertainty, (b) ΔK = 40%, (c) ΔK = -40%, (d) ΔC = 40%, (e) ΔK = -40%.

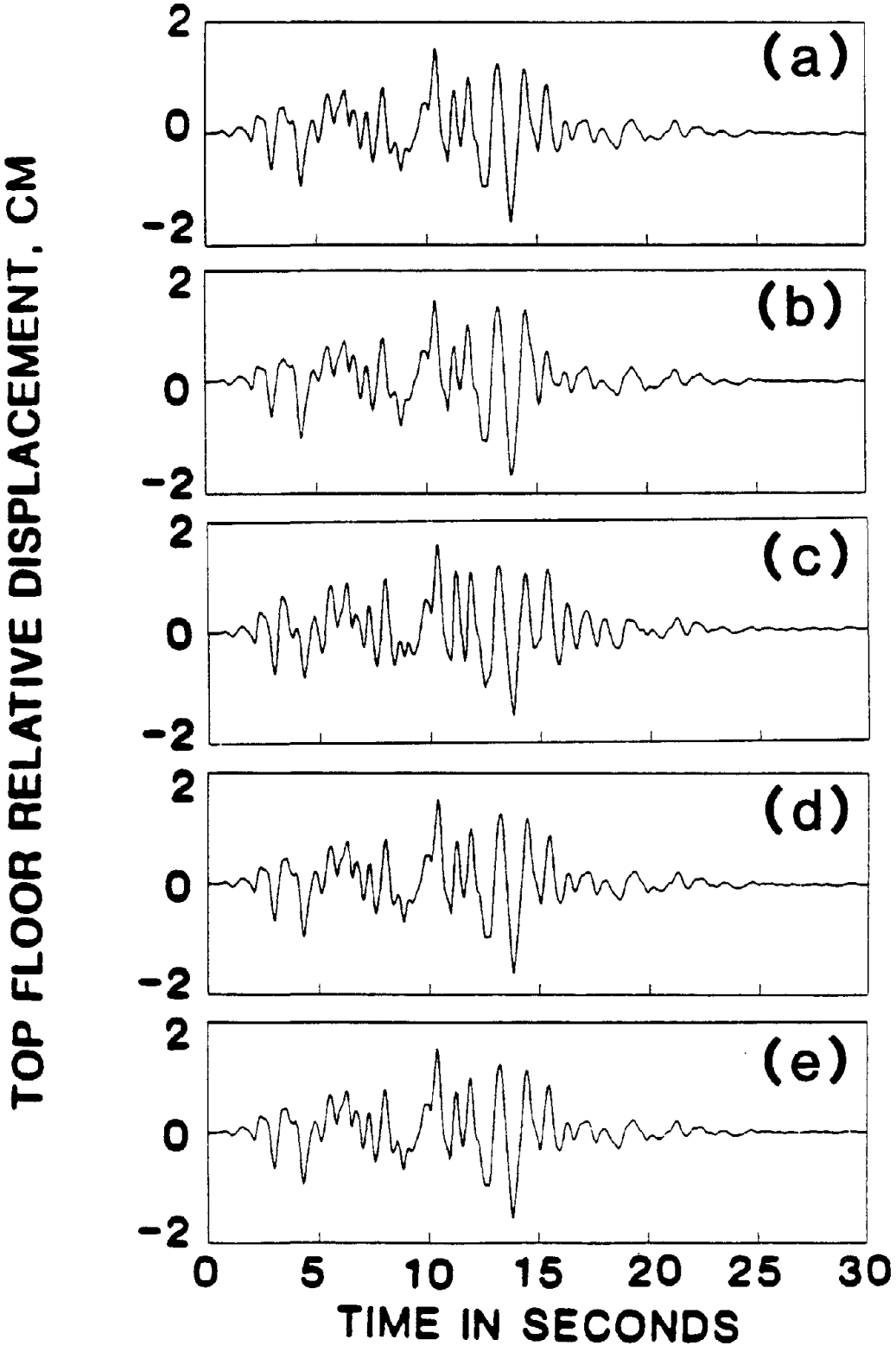

Fig. 35: Top Floor Relative Displacement for an 8-Story Building Using Active Mass Damper and Riccati Closed-Loop Control Algorithm: (a) No System Uncertainty, (b) $\Delta K = 40\%$, (c) $\Delta K = -40\%$, (d) $\Delta C = 40\%$, (e) $\Delta C = -40\%$.

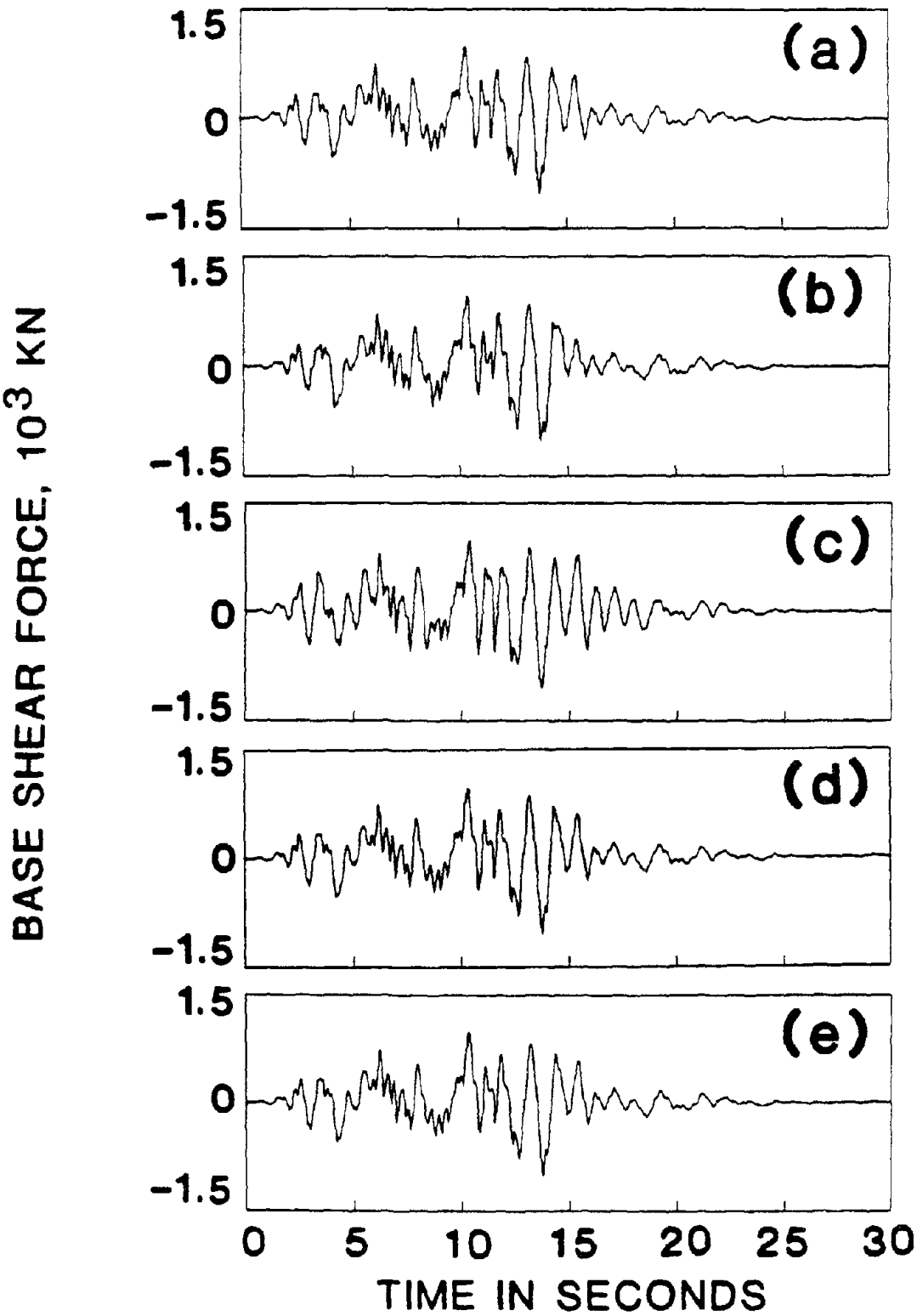

Fig. 36: Base Shear Force for an 8-Story Building Using Active Mass Damper and Riccati Closed-Loop Control Algorithm: (a) No System Uncertainty, (b) $\Delta K = 40\%$, (c) $\Delta K = -40\%$, (d) $\Delta C = 40\%$, (e) $\Delta C = -40\%$.

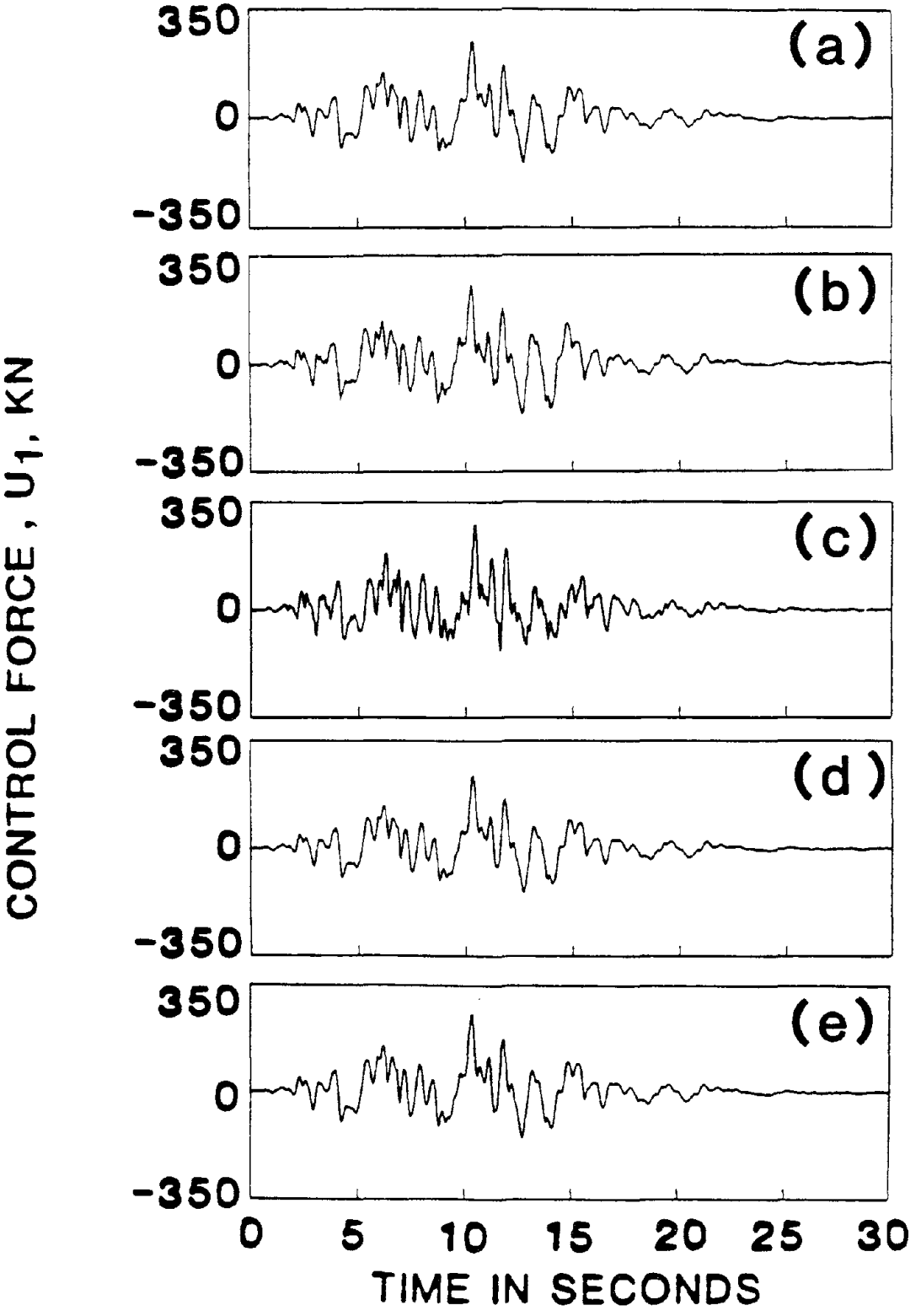

Fig. 37: Active Control Force for an 8-Story Building Using Active Mass Damper and Riccati Closed-Loop Control Algorithm: (a) No System Uncertainty, (b) ΔK = 40%, (c) ΔK = -40%, (d) ΔC = 40%, (e) ΔC = -40%.

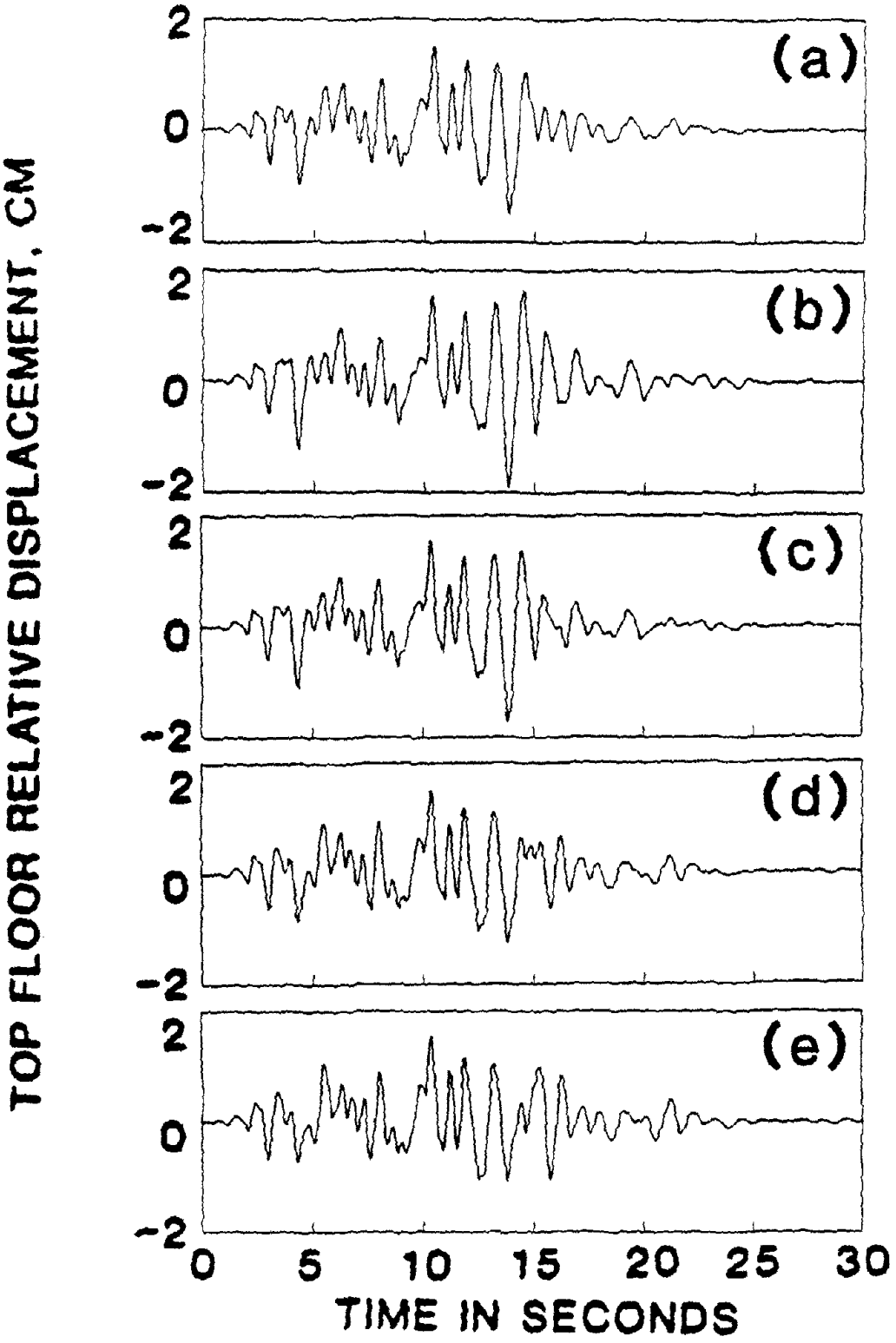

Fig. 38: Top Floor Relative Displacement for an 8-Story Building Using Active Mass Damper and Instantaneous Optimal Open-Loop Control Algorithm: (a) No System Uncertainty, (b) $\Delta K = 20\%$, (c) $\Delta K = 10\%$, (d) $\Delta K = -10\%$, (e) $\Delta K = -20\%$.

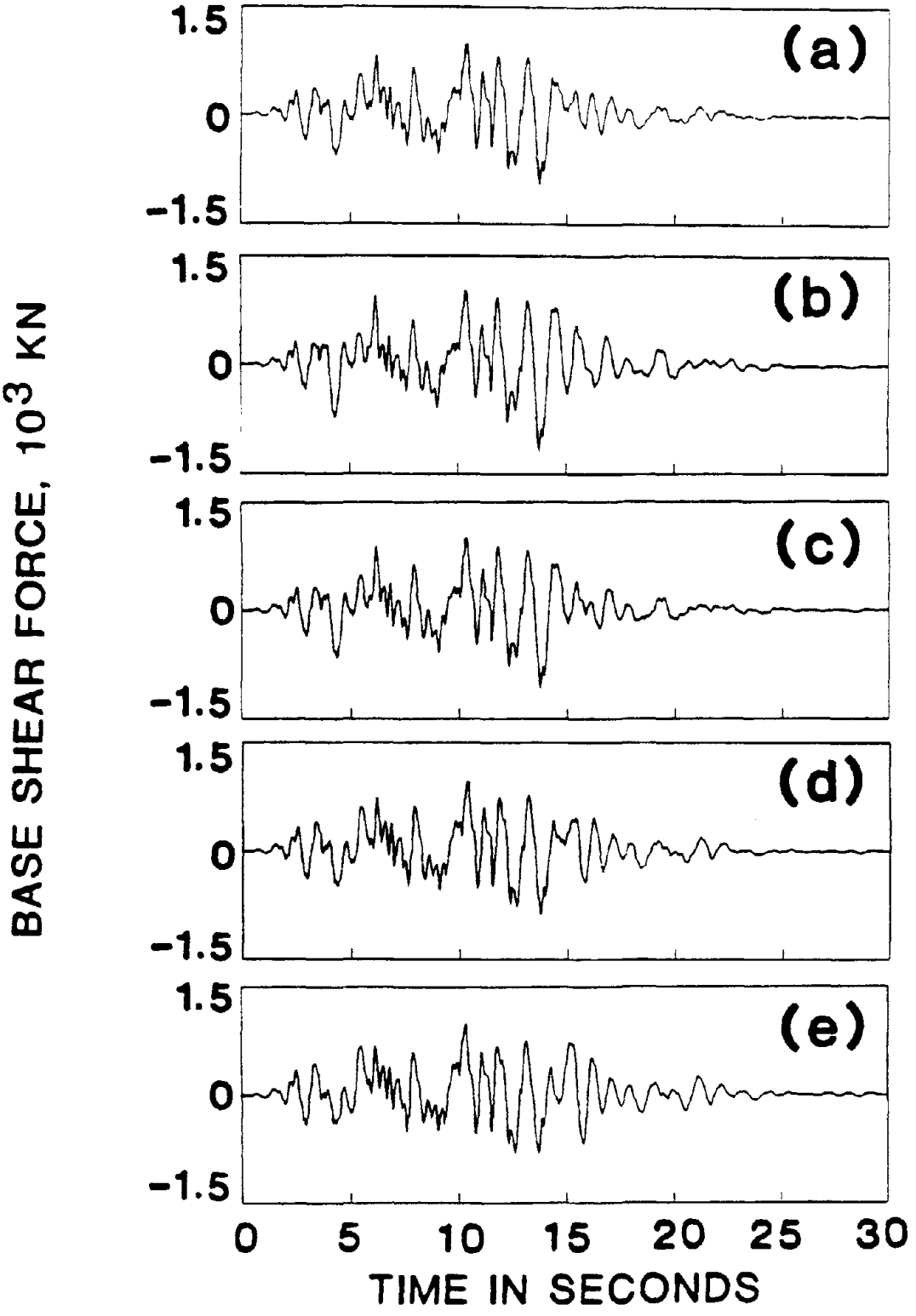

Fig. 39: Base Shear Force an 8-Story Building Using Active Mass Damper and Instantaneous Optimal Open-Loop Control Algorithm: (a) No System Uncertainty, (b) ΔK = 20%, (c) ΔK = 10%, (d) ΔK = -10%, (e) ΔK = -20%.

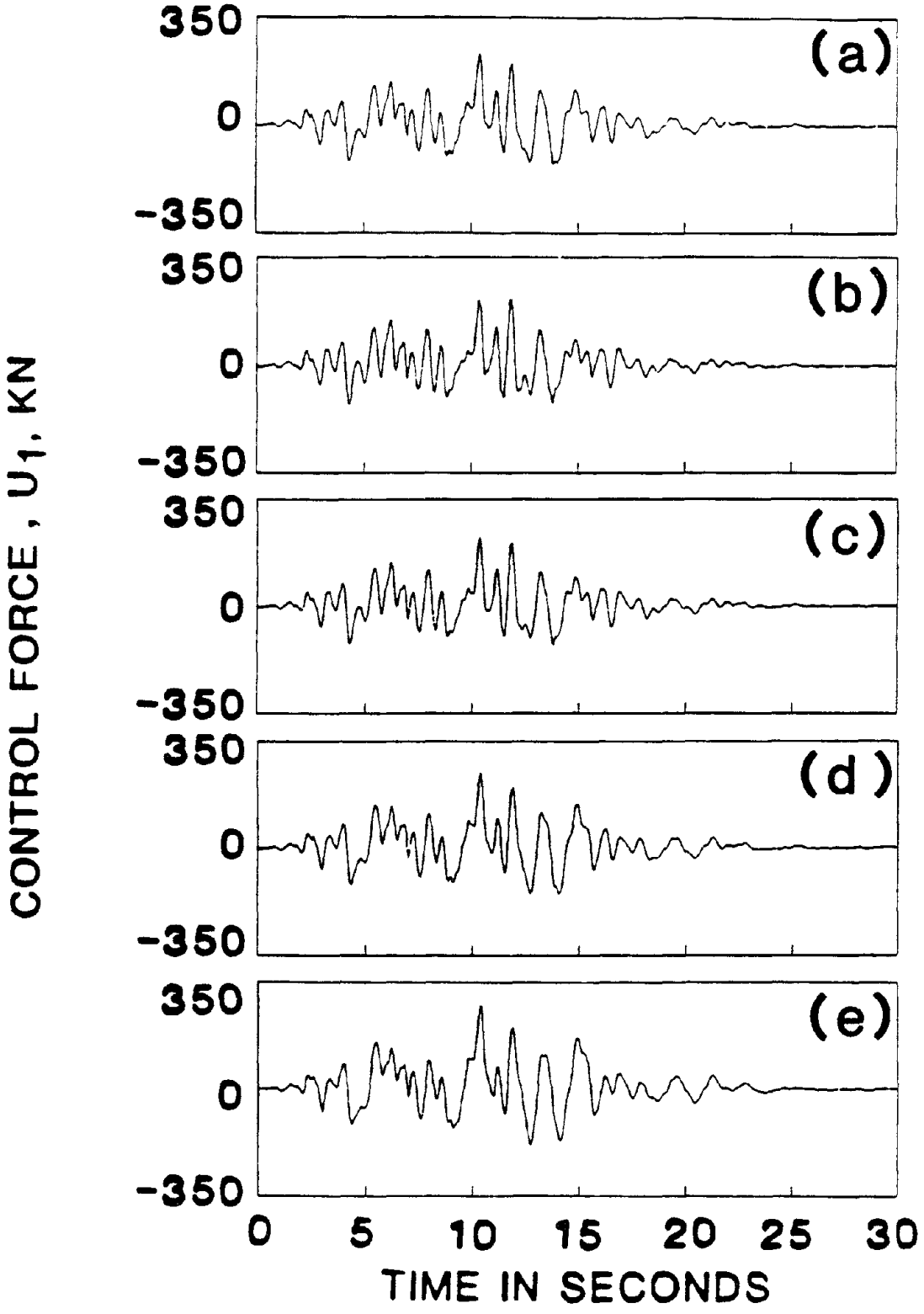

Fig. 40: Active Control Force an 8-Story Building Using Active Mass Damper and Instantaneous Optimal Open-Loop Control Algorithm: (a) No System Uncertainty, (b) ΔK = 20%, (c) ΔK = 10%, (d) ΔK = -10%, (e) ΔK = -20%.

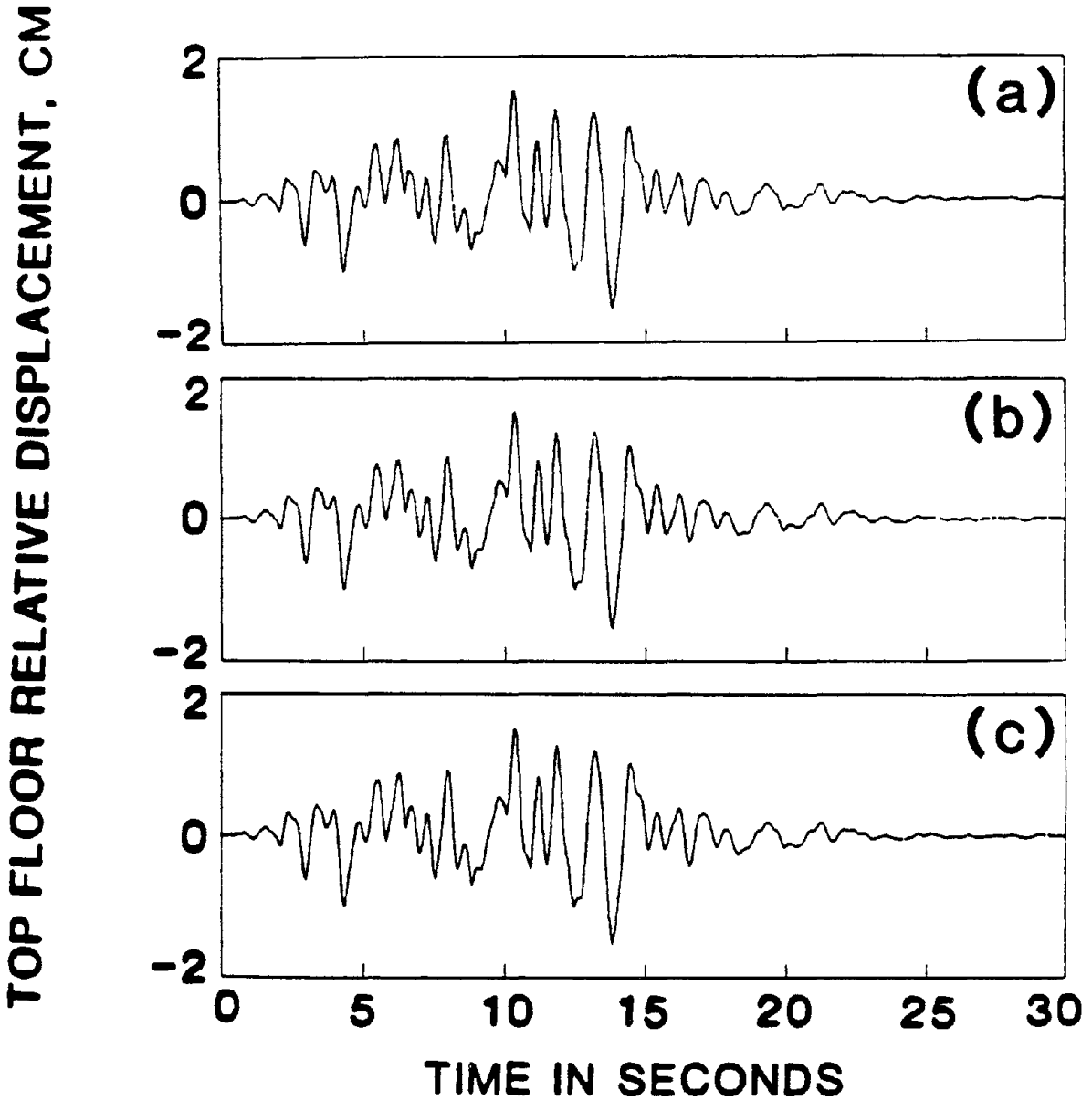

Fig. 41: Top Floor Relative Displacement for an 8-Story Building Using Active Mass Damper and Instantaneous Optimal Open-Loop Control Algorithm: (a) No System Uncertainty, (b) $\Delta C = 40\%$, (c) $\Delta C = -40\%$.

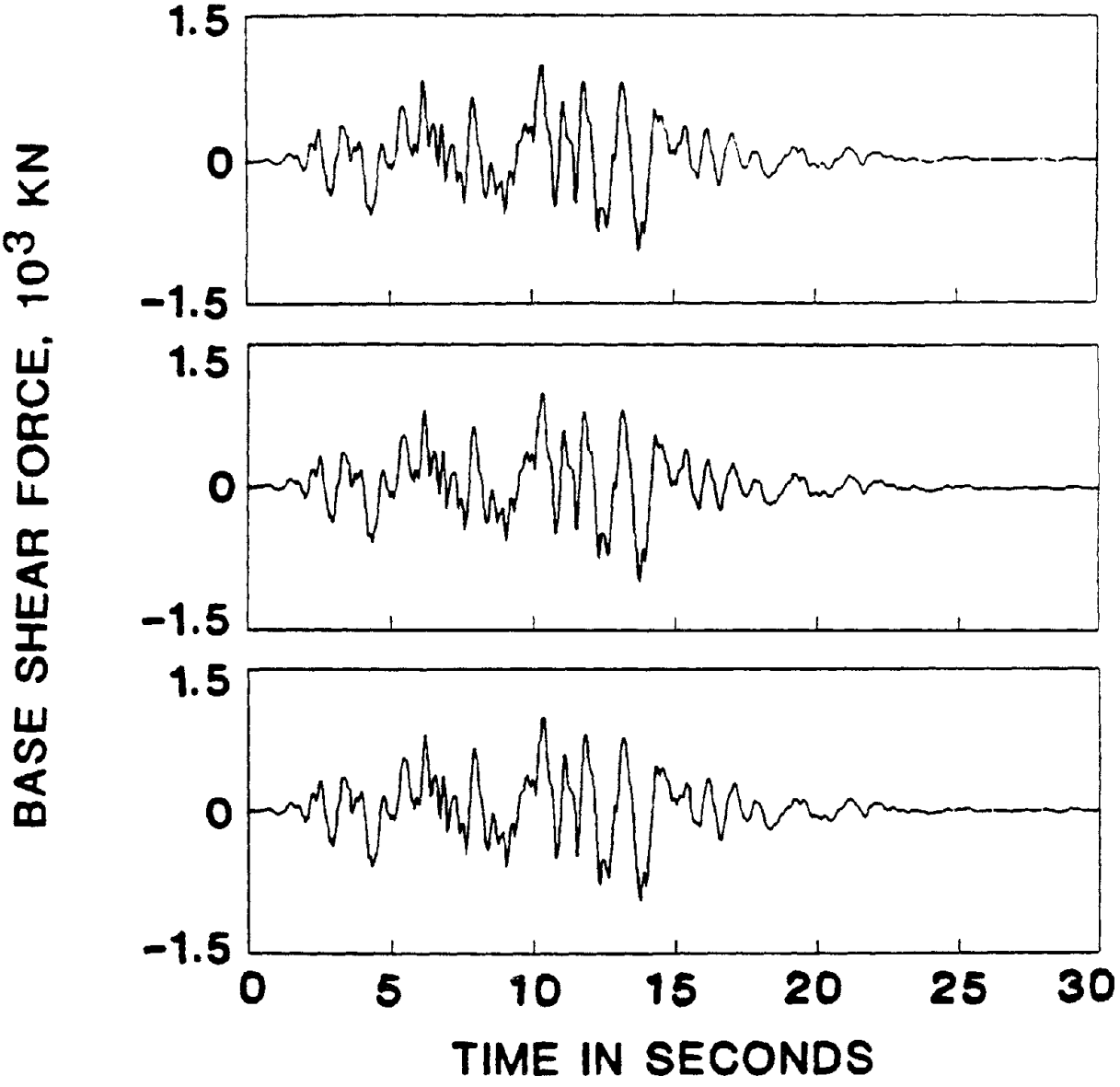

Fig. 42: Base Shear Force for an 8-Story Building Using Active Mass Damper and Instantaneous Optimal Open-Loop Control Algorithm: (a) No System Uncertainty, (b) $\Delta C = 40\%$, (c) $\Delta C = -40\%$.

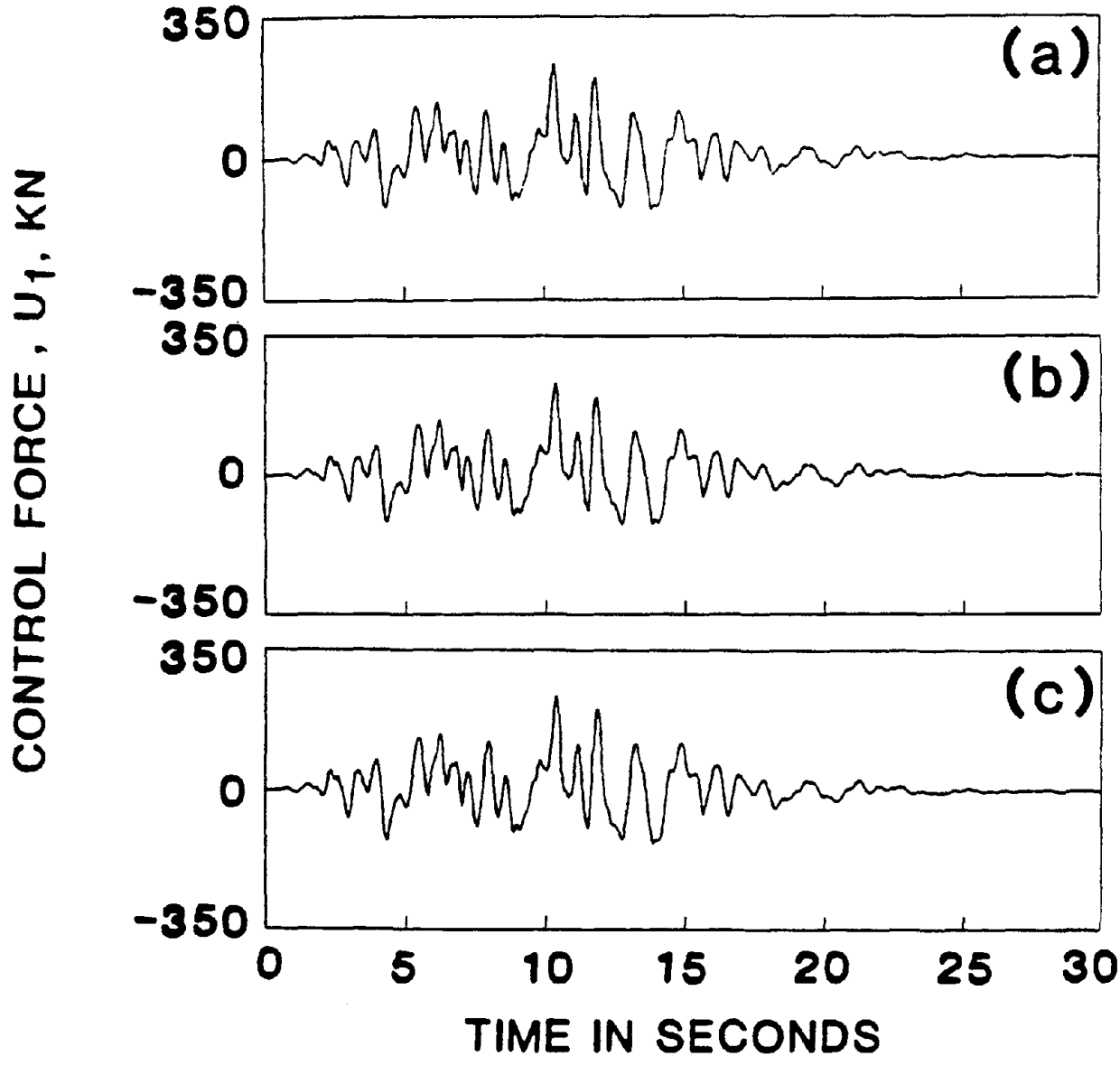

Fig. 43: Active Control Force for an 8-Story Building Using Active Mass Damper and Instantaneous Optimal Open-Loop Control Algorithm: (a) No System Uncertainty, (b) $\Delta C = 40\%$, (c) $\Delta C = -40\%$.

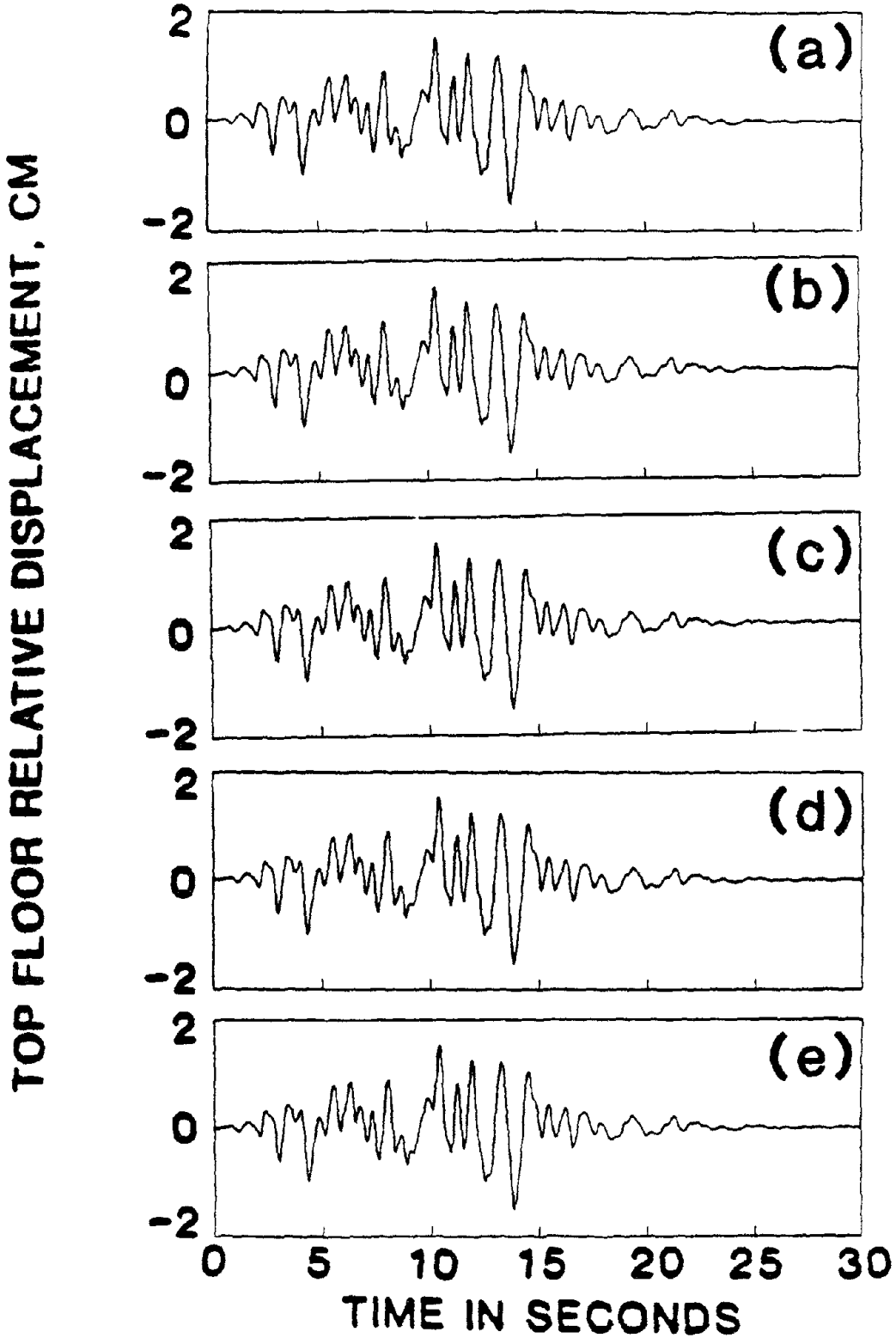

Fig. 44: Top Floor Relative Displacement for an 8-Story Building Using Active Mass Damper and Instantaneous Closed-Open-Loop Control Algorithm: (a) No System Uncertainty, (b) $\Delta K = 40\%$, (c) $\Delta K = -40\%$, (d) $\Delta C = 40\%$, (e) $\Delta C = -40\%$.

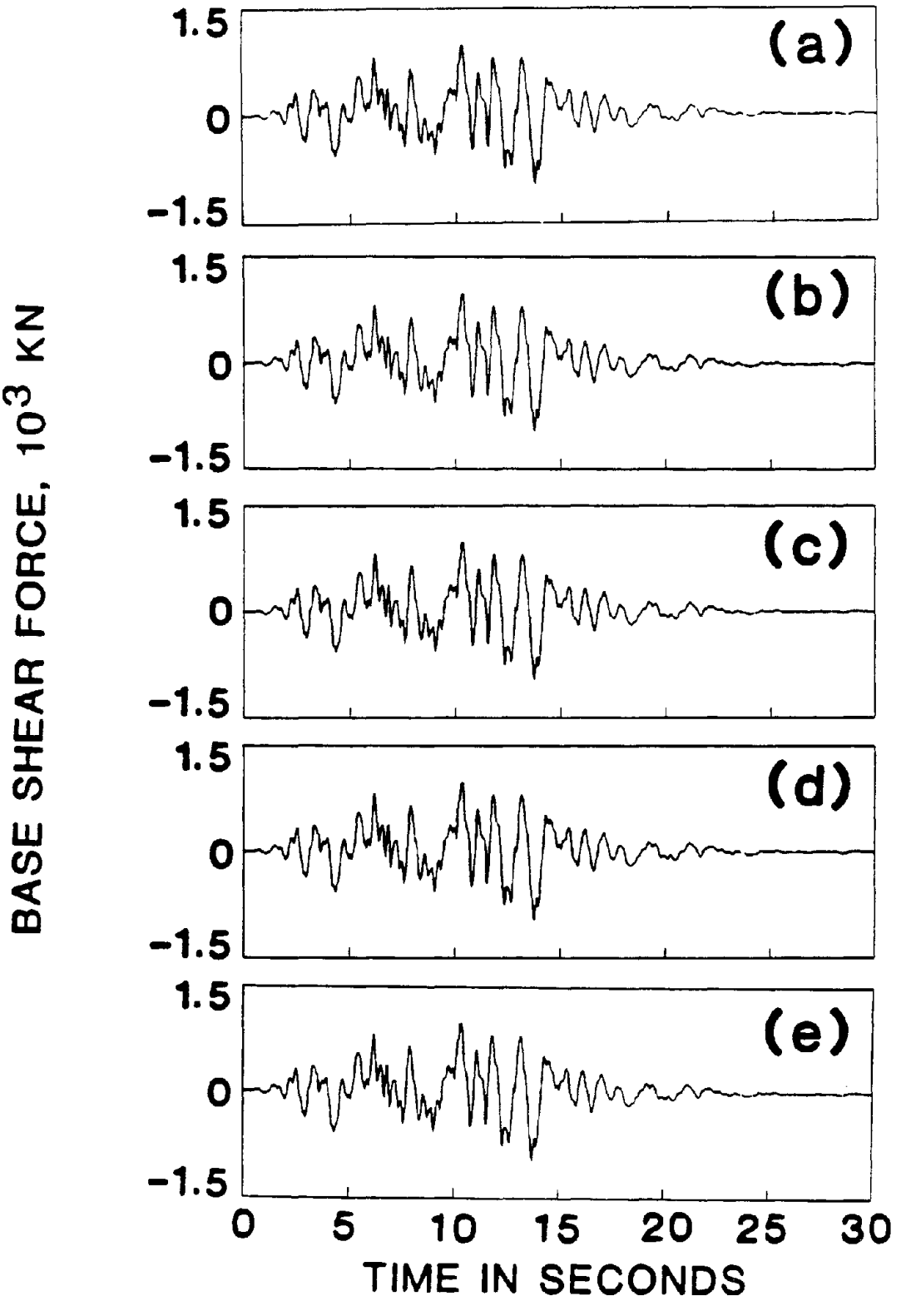

Fig. 45: Base Shear Force for an 8-Story Building Using Active Mass Damper and Instantaneous Closed-Open-Loop Control Algorithm: (a) No System Uncertainty, (b) $\Delta K = 40\%$, (c) $\Delta K = -40\%$, (d) $\Delta C = 40\%$, (e) $\Delta C = -40\%$.

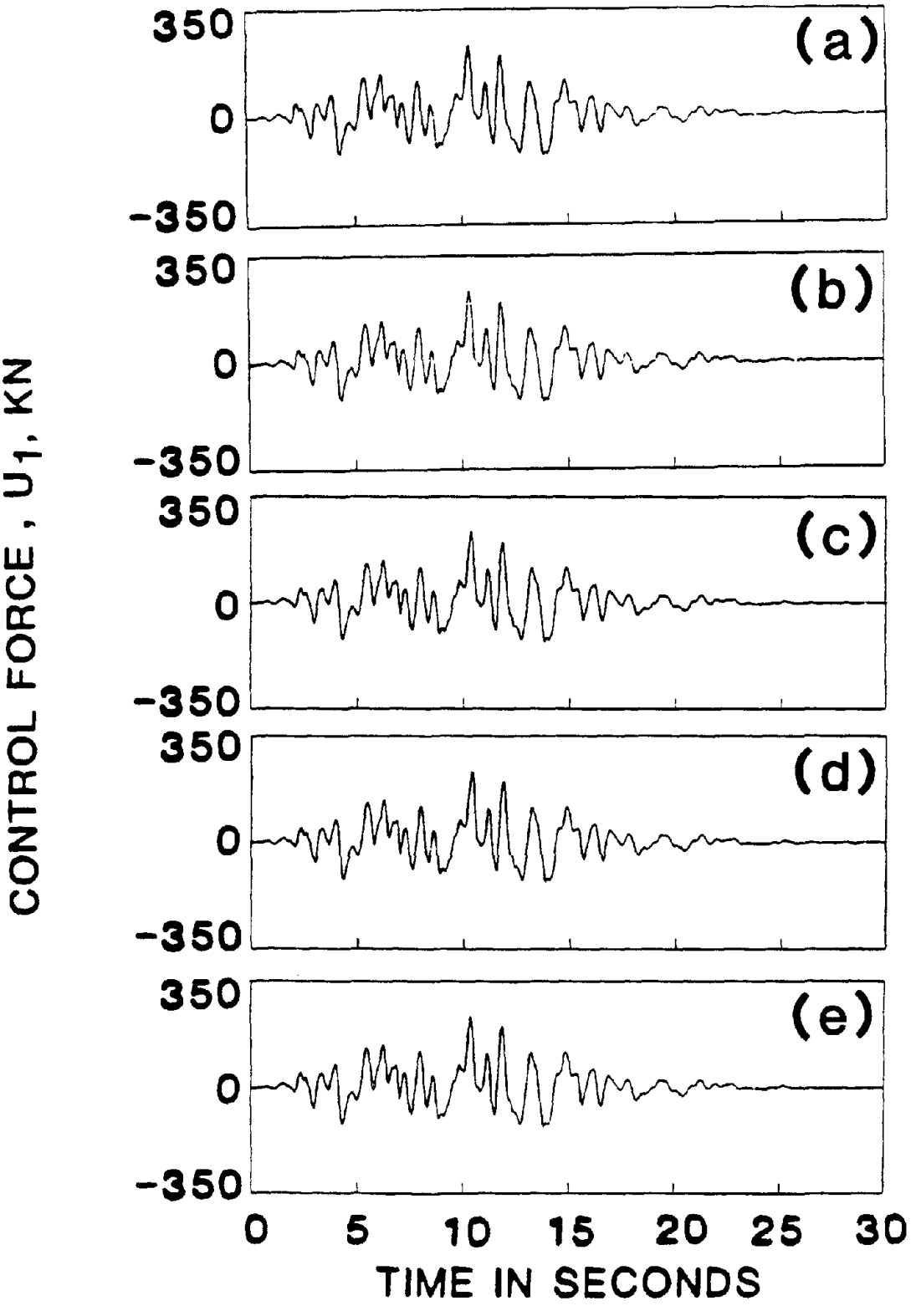

Fig. 46: Active Control Force for an 8-Story Building Using Active Mass Damper and Instantaneous Closed-Open-Loop Control Algorithm: (a) No System Uncertainty, (b) $\Delta K = 40\%$, (c) $\Delta K = -40\%$, (d) $\Delta C = 40\%$, (e) $\Delta C = -40\%$.

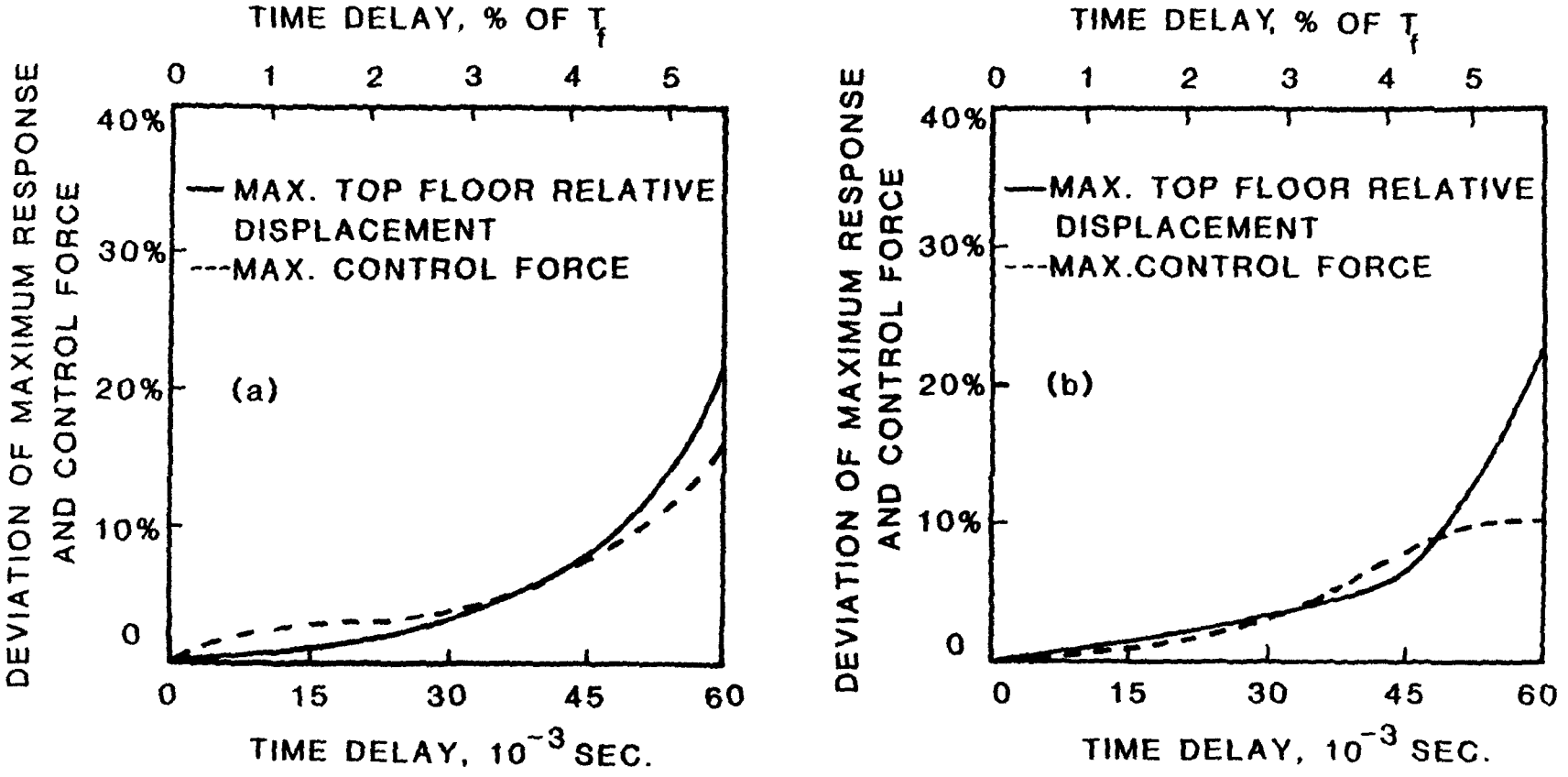

FIG. 47: EFFECT OF TIME DELAY, τ, ON MAXIMUM TOP FLOOR RELATIVE DISPLACEMENT AND CONTROL FORCE FOR BUILDING WITH TENDON CONTROL SYSTEM; (a) RICCATI CLOSED-LOOP CONTROL, (b) INSTANTANEOUS OPTIMAL CLOSED-LOOP CONTROL.

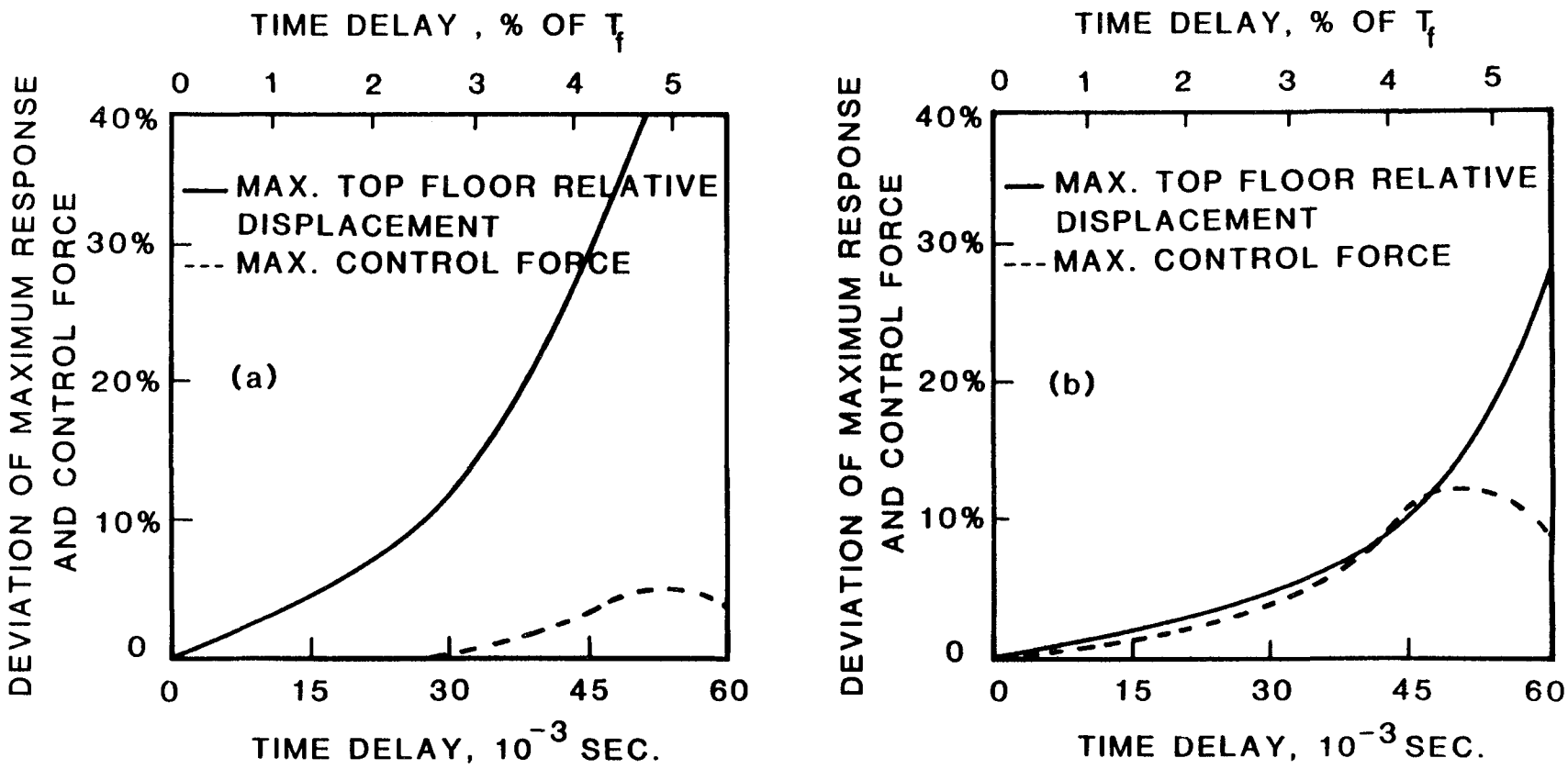

FIG. 48: EFFECT OF TIME DELAY, τ, ON MAXIMUM TOP FLOOR RELATIVE DISPLACEMENT AND CONTROL FORCE FOR BUILDING WITH TENDON CONTROL SYSTEM; (a) INSTANTANEOUS OPTIMAL OPEN-LOOP CONTROL, (b) INSTANTANEOUS OPTIMAL CLOSED-OPEN-LOOP CONTROL.

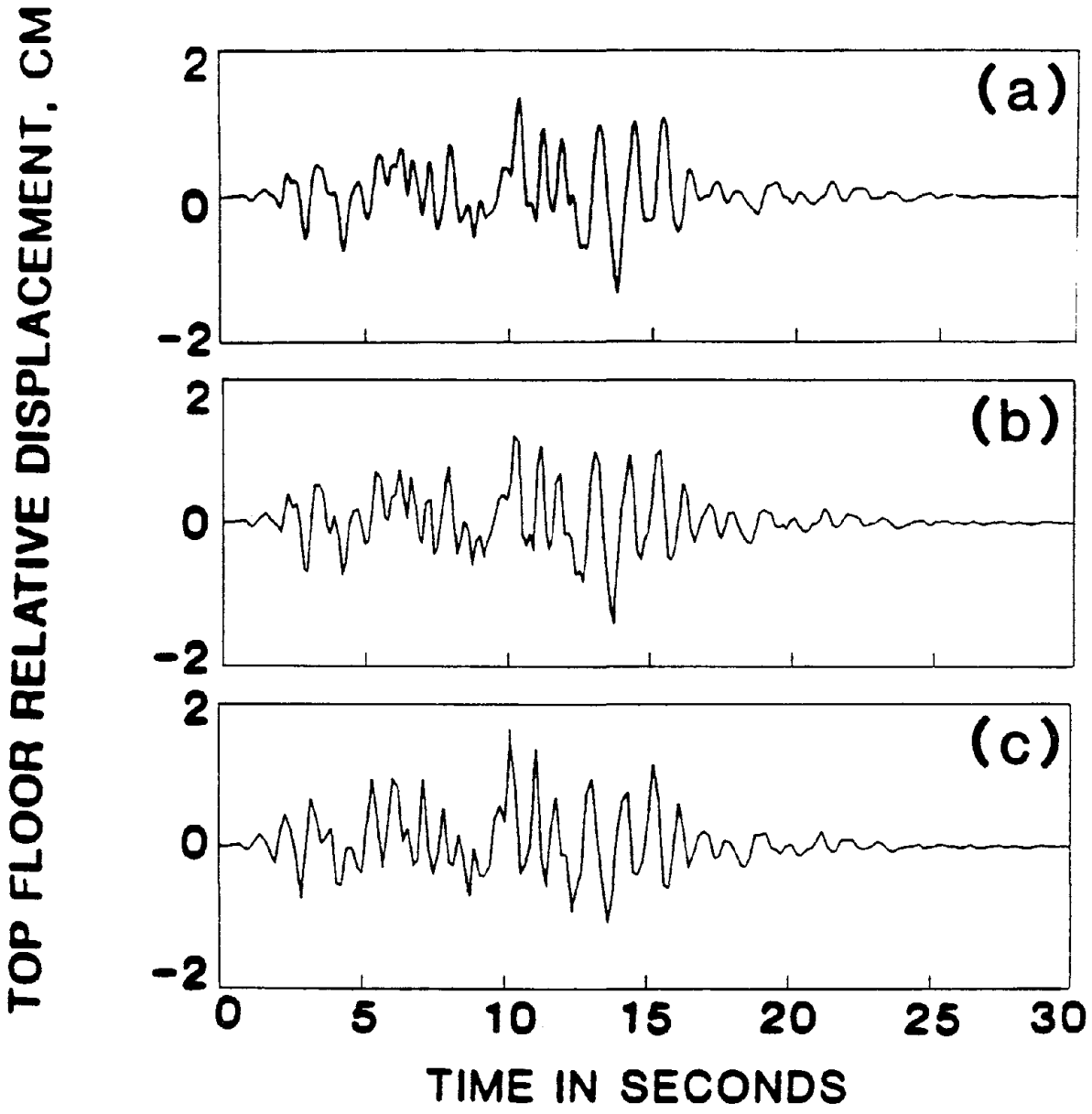

Fig. 49: Effect of Time Delay, τ, on Top Floor Relative Displacement for an 8-Story Building Using Tendon Control System and Riccati Closed-Loop Control Algorithm: (a) τ =0 (No Delay), (b) $\tau = 45 \times 10^{-3}$ sec., (c) $\tau = 60 \times 10^{-3}$ sec.

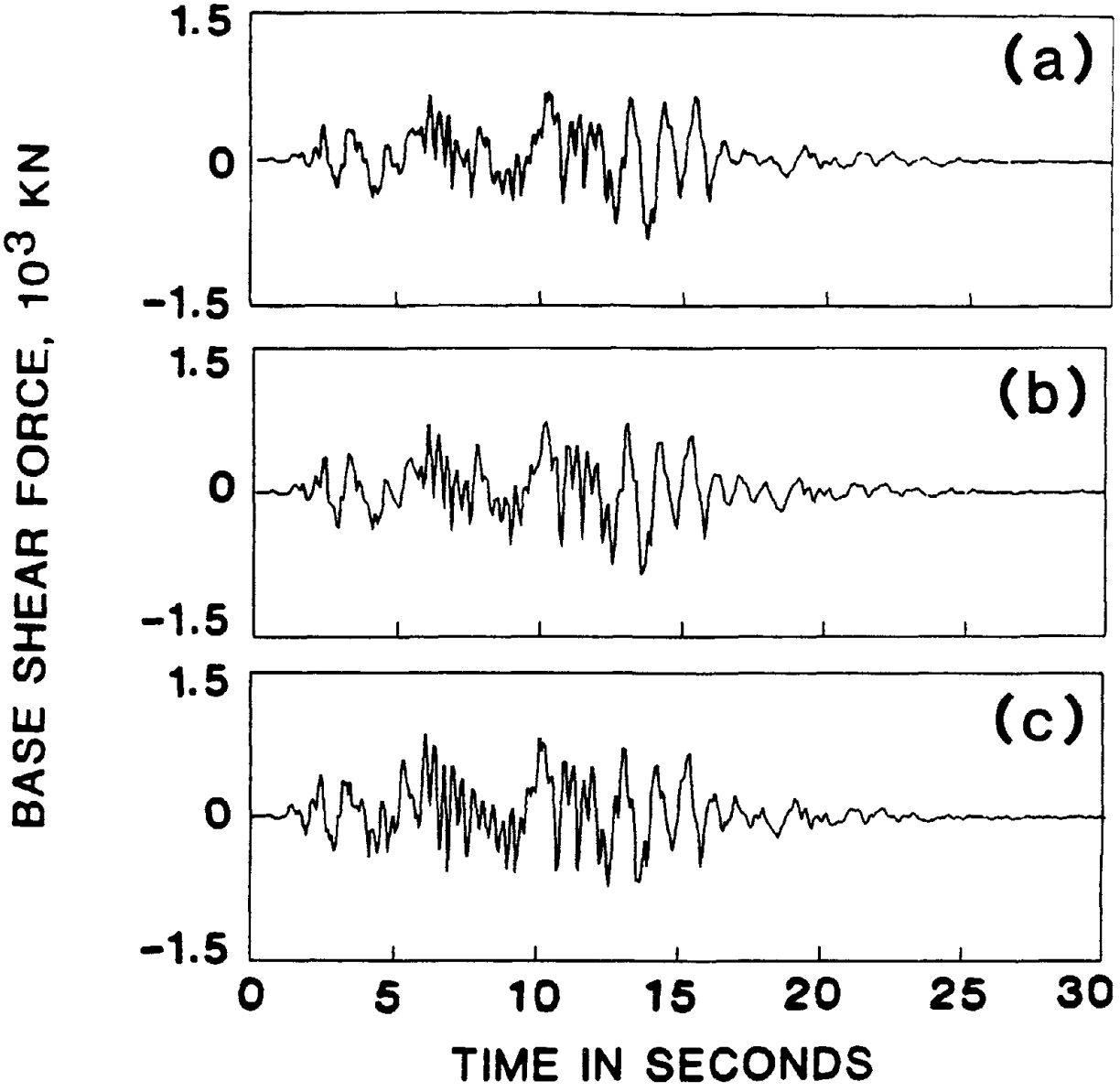

Fig. 50: Effect of Time Delay, τ, on Base Shear Force for an 8-Story Building Using Tendon Control System and Riccati Closed-Loop Control Algorithm: (a) τ =0 (No Delay), (b) $\tau = 45 \times 10^{-3}$ sec., (c) $\tau = 60 \times 10^{-3}$ sec.

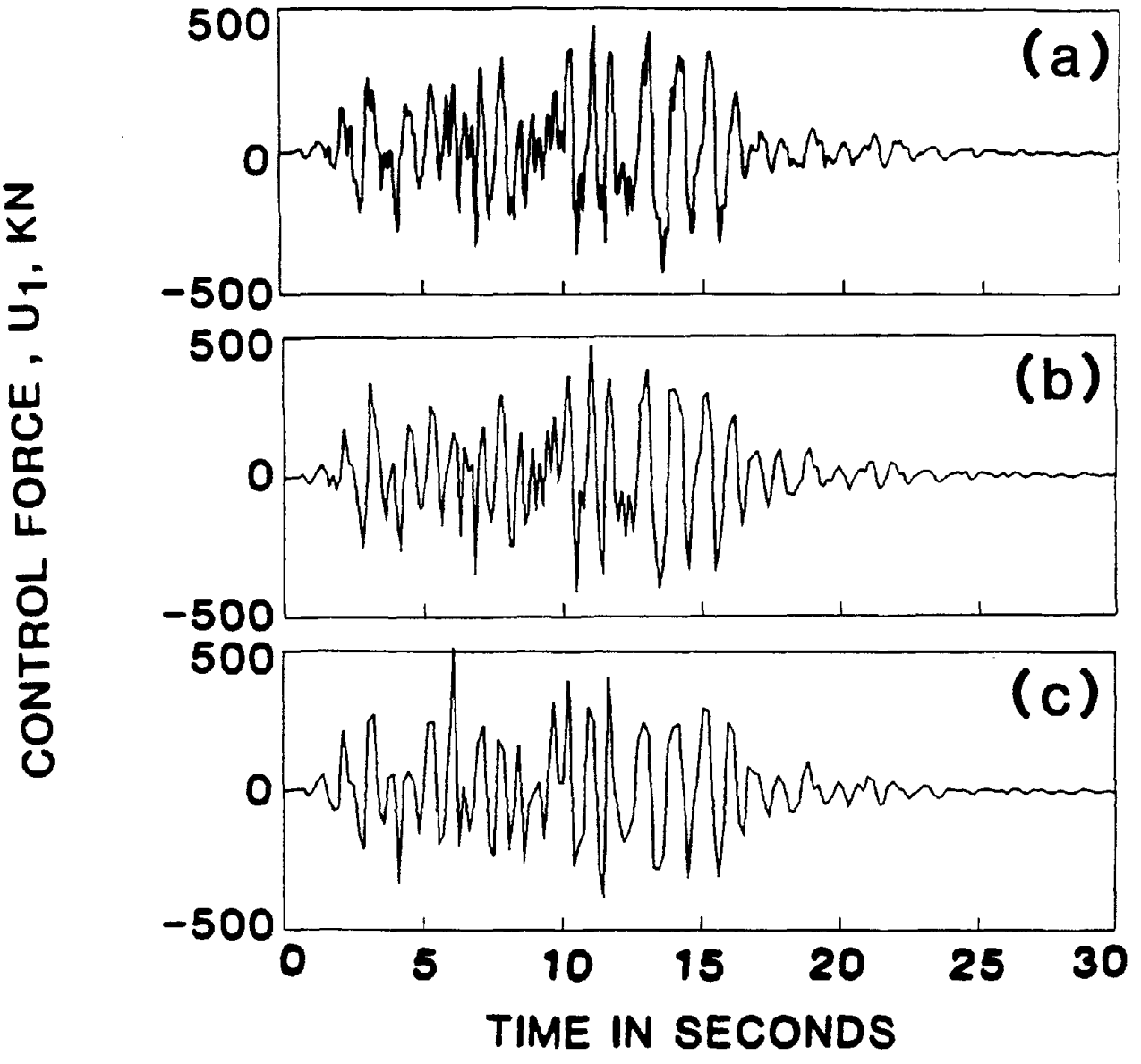

Fig. 51: Effect of Time Delay, τ, on Control Force from the First Controller for an 8-Story Building Using Tendon Control System and Riccati Closed-Loop Control Algorithm: (a) τ =0 (No Delay), (b) τ = 45 x 10^{-3} sec., (c) τ = 60 x 10^{-3} sec.

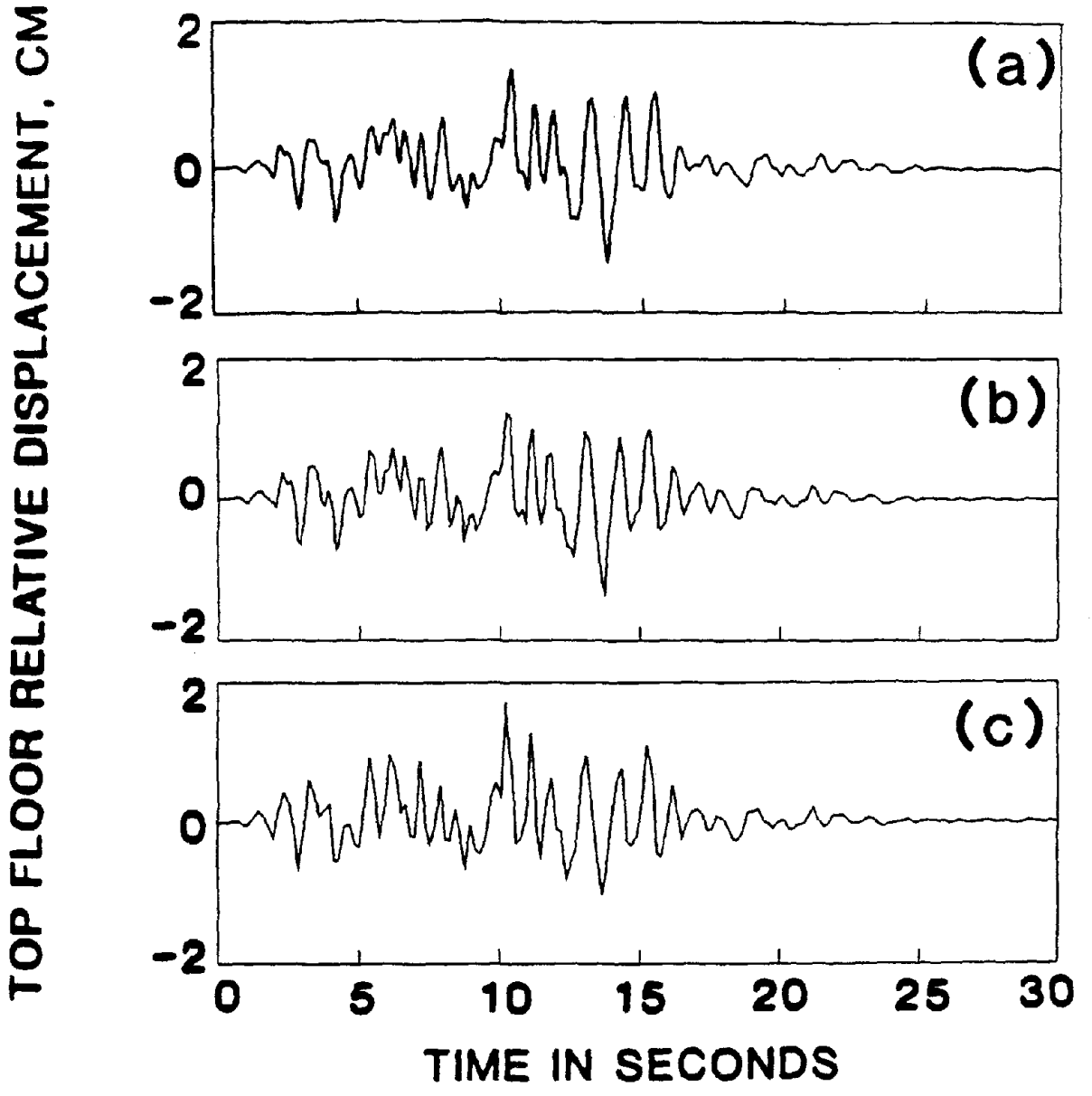

Fig. 52: Effect of Time Delay, τ, on Top Floor Relative Displacement for an 8-Story Building Using Tendon Control System and Instantaneous Optimal Closed-Loop Control Algorithm: (a) τ =0 (No Delay), (b) τ = 45×10^{-3} sec., (c) τ = 60×10^{-3} sec.

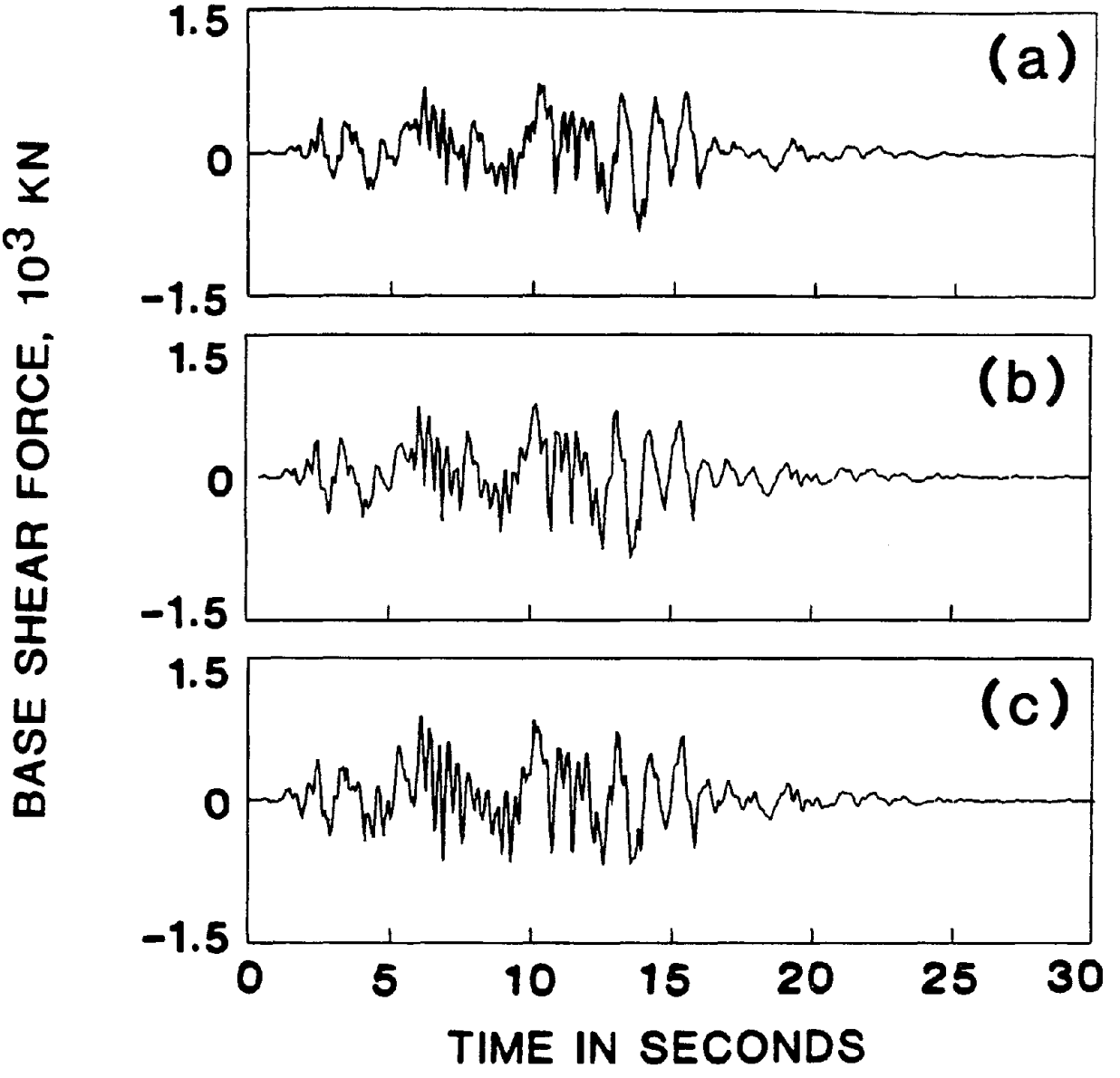

Fig. 53: Effect of Time Delay, τ, on Base Shear Force for an 8-Story Building Using Tendon Control System and Instantaneous Optimal Closed-Loop Control Algorithm: (a) τ =0 (No Delay), (b) τ = 45 x 10^{-3} sec., (c) τ = 60 x 10^{-3} sec.

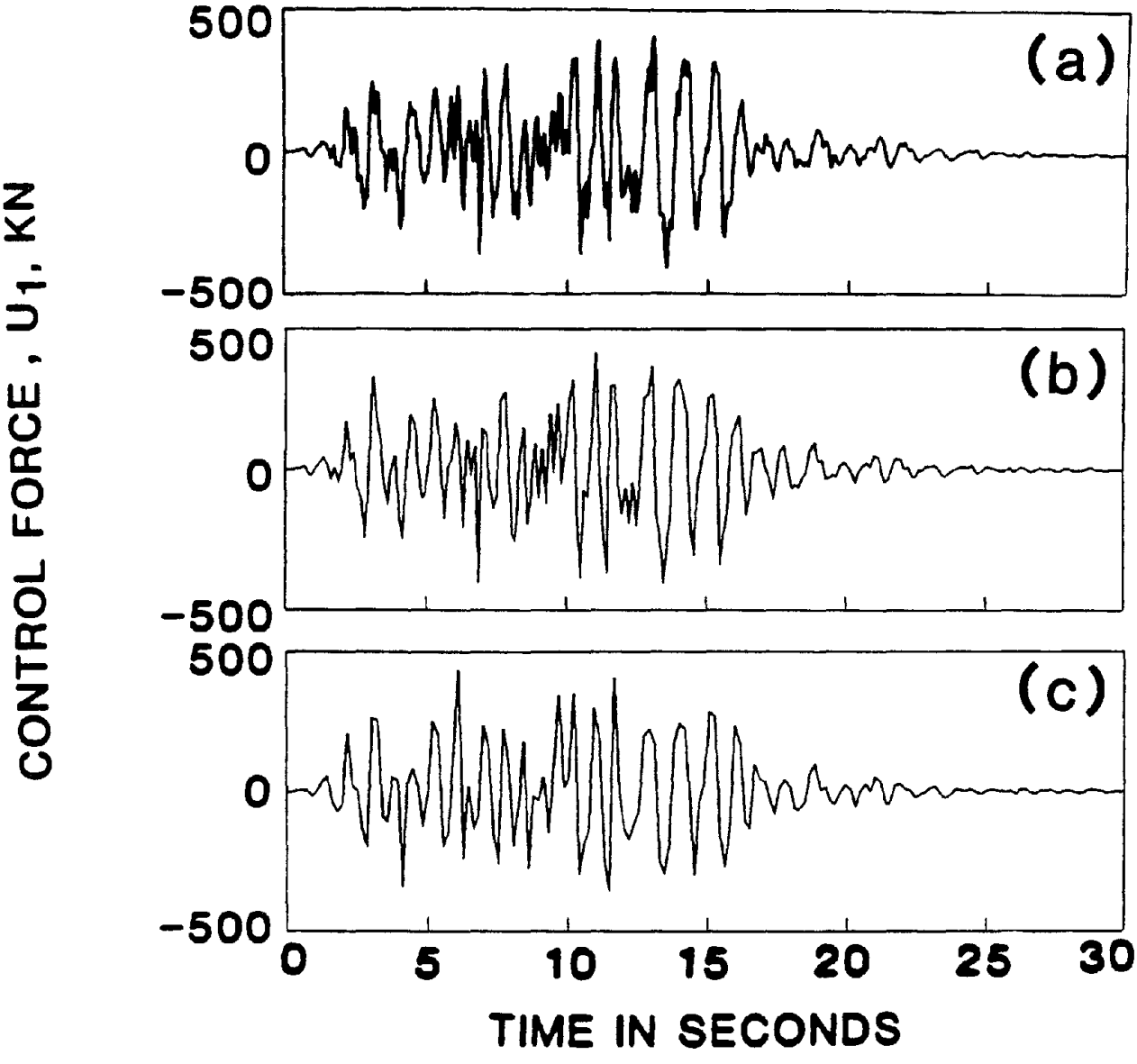

Fig. 54: Effect of Time Delay, τ, on Control Force from the First Controller for an 8-Story Building Using Tendon Control System and Instantaneous Optimal Closed-Loop Control Algorithm: (a) τ =0 (No Delay), (b) $\tau = 45 \times 10^{-3}$ sec., (c) $\tau = 60 \times 10^{-3}$ sec.

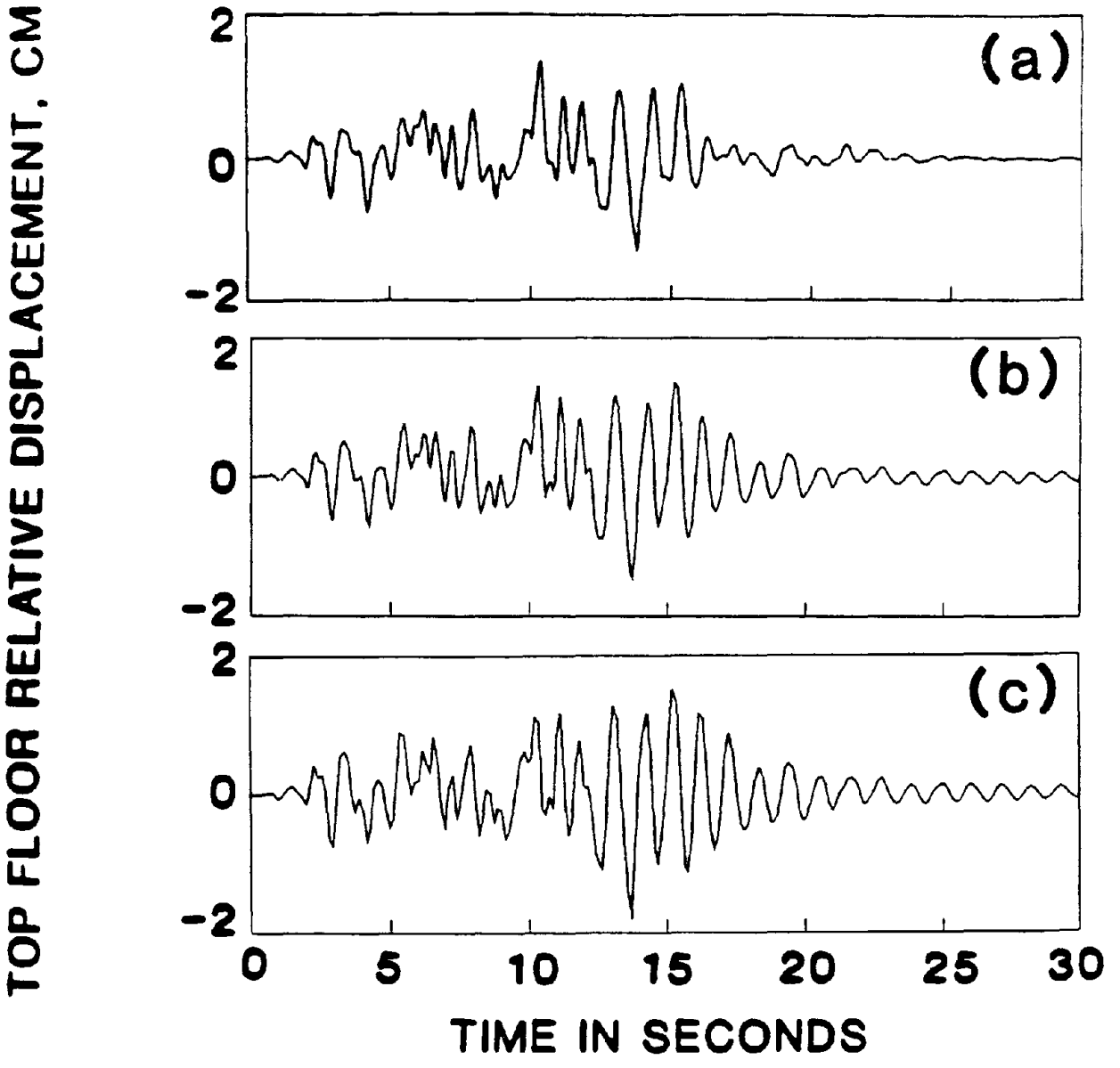

Fig. 55: Effect of Time Delay, τ, on Top Floor Relative Displacement for an 8-Story Building Using Tendon Control System and Instantaneous Optimal Open-Loop Control Algorithm: (a) τ =0 (No Delay), (b) τ = 30×10^{-3} sec., (c) τ = 45×10^{-3} sec.

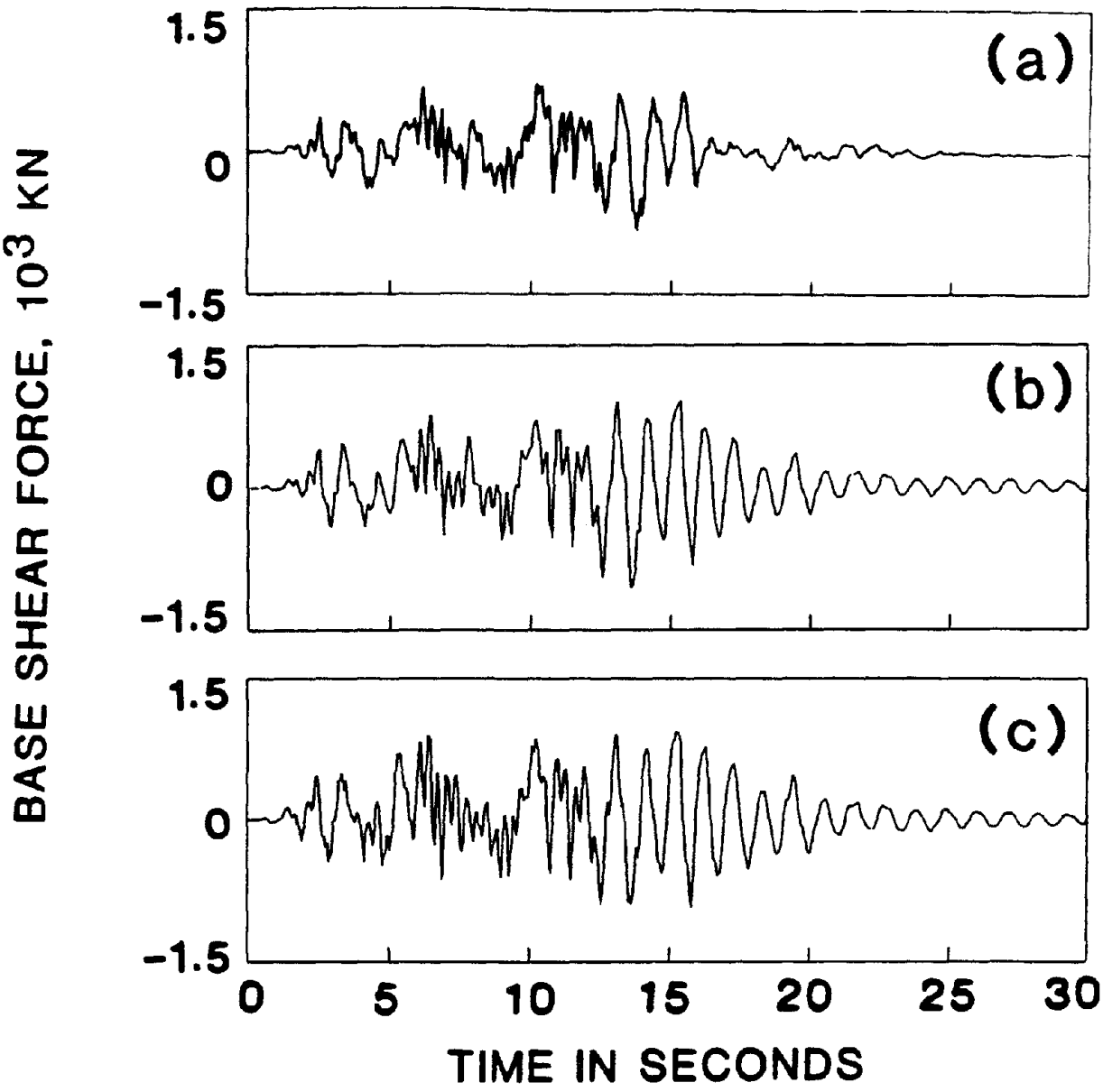

Fig. 56: Effect of Time Delay, τ, on Base Shear Force for an 8-Story Building Using Tendon Control System and Instantaneous Optimal Open-Loop Control Algorithm: (a) τ =0 (No Delay), (b) τ = 30 x 10^{-3} sec., (c) τ = 45 x 10^{-3} sec.

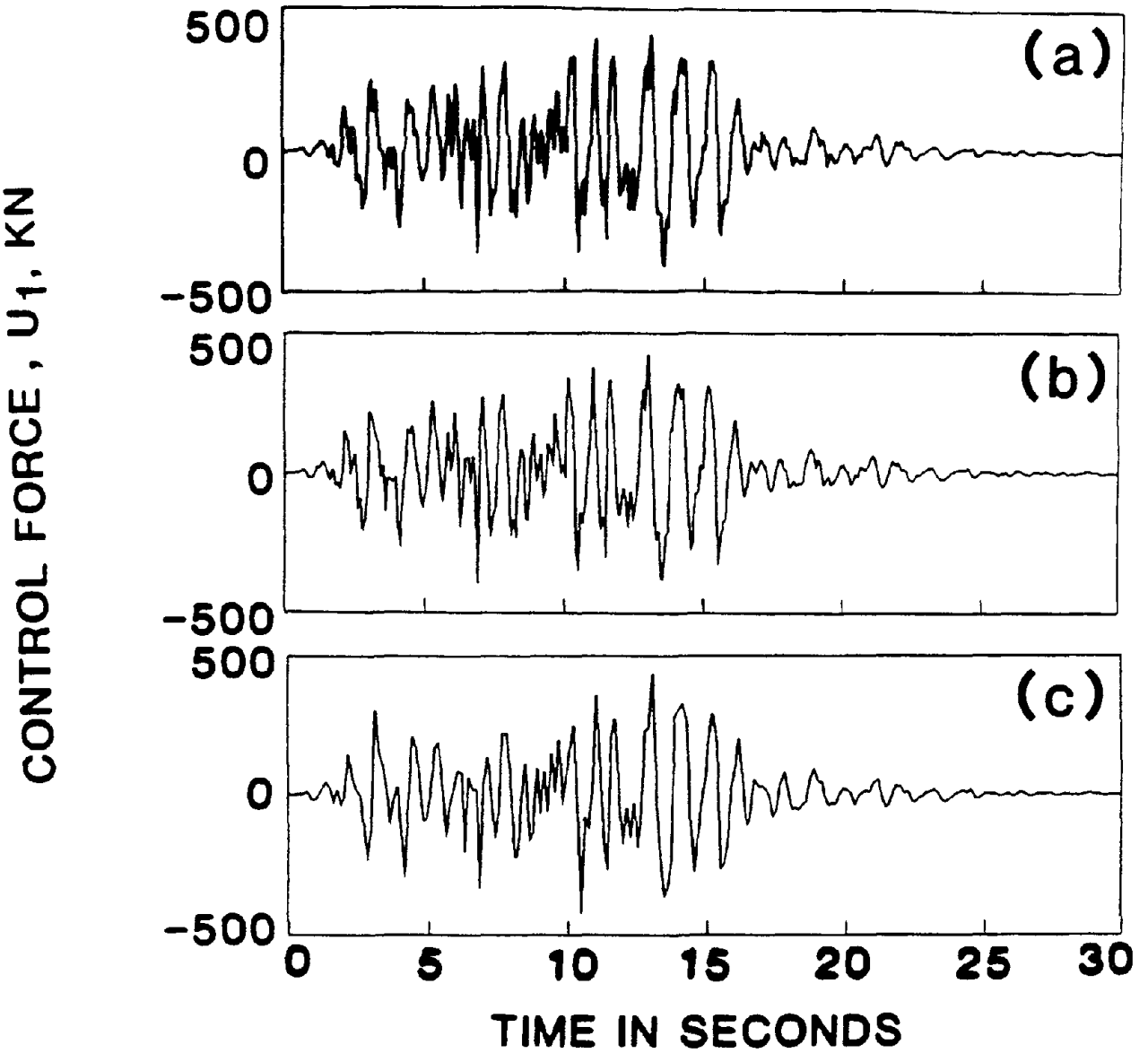

Fig. 57: Effect of Time Delay, τ, on Control Force from the First Controller for an 8-Story Building Using Tendon Control System and Instantaneous Optimal Open-Loop Control Algorithm: (a) τ =0 (No Delay), (b) $\tau = 30 \times 10^{-3}$ sec., (c) $\tau = 45 \times 10^{-3}$ sec.

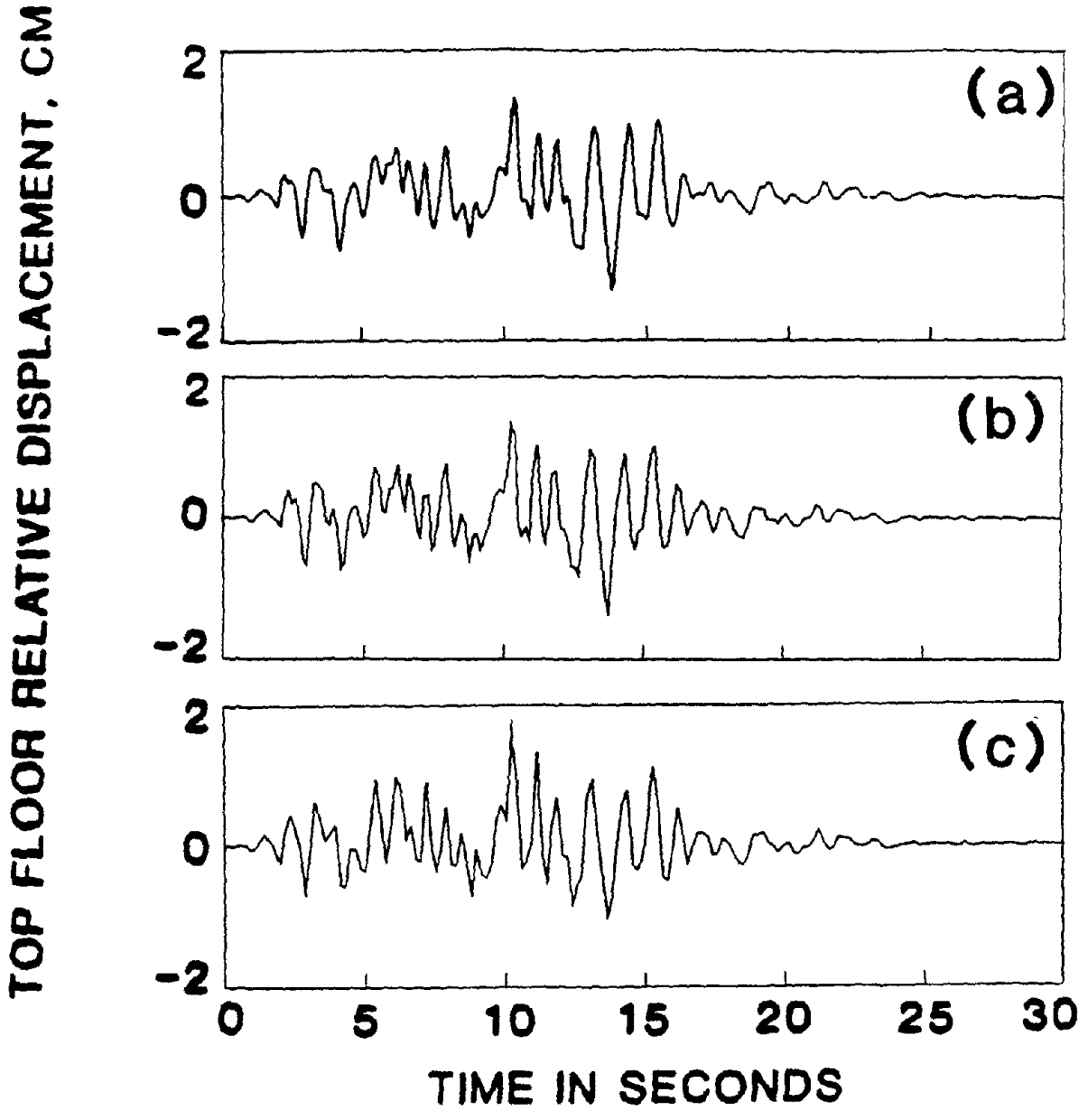

Fig. 58: Effect of Time Delay, τ, on Top Floor Relative Displacement for an 8-Story Building Using Tendon Control System and Instantaneous Optimal Closed-Open-Loop Control Algorithm: (a) τ =0 (No Delay), (b) $\tau = 45 \times 10^{-3}$ sec., (c) $\tau = 60 \times 10^{-3}$ sec.

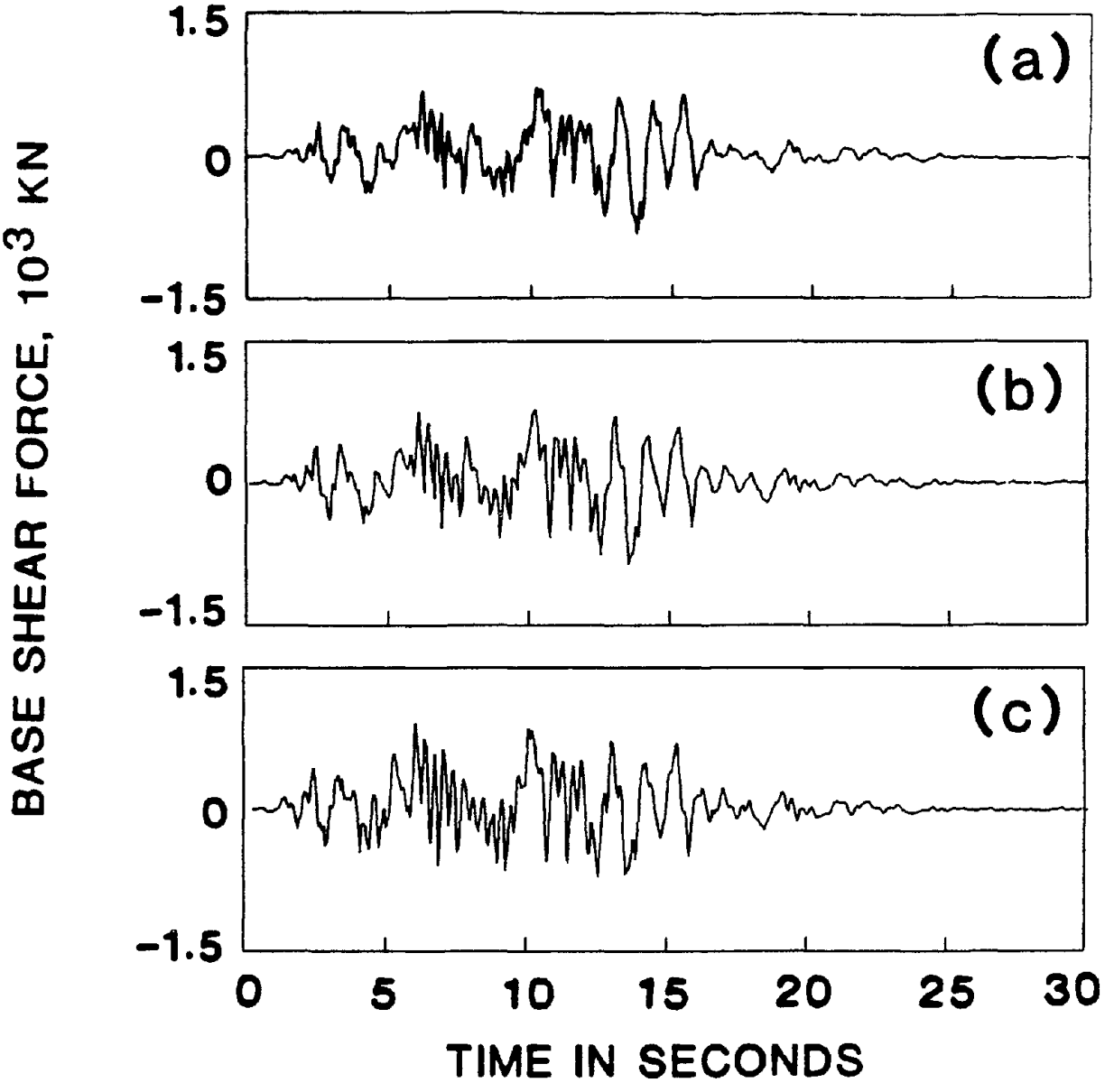

Fig. 59: Effect of Time Delay, τ, on Base Shear Force for an 8-Story Building Using Tendon Control System and Instantaneous Optimal Closed-Open-Loop Control Algorithm: (a) τ =0 (No Delay), (b) τ = 45 x 10^{-3} sec., (c) τ = 60 x 10^{-3} sec.

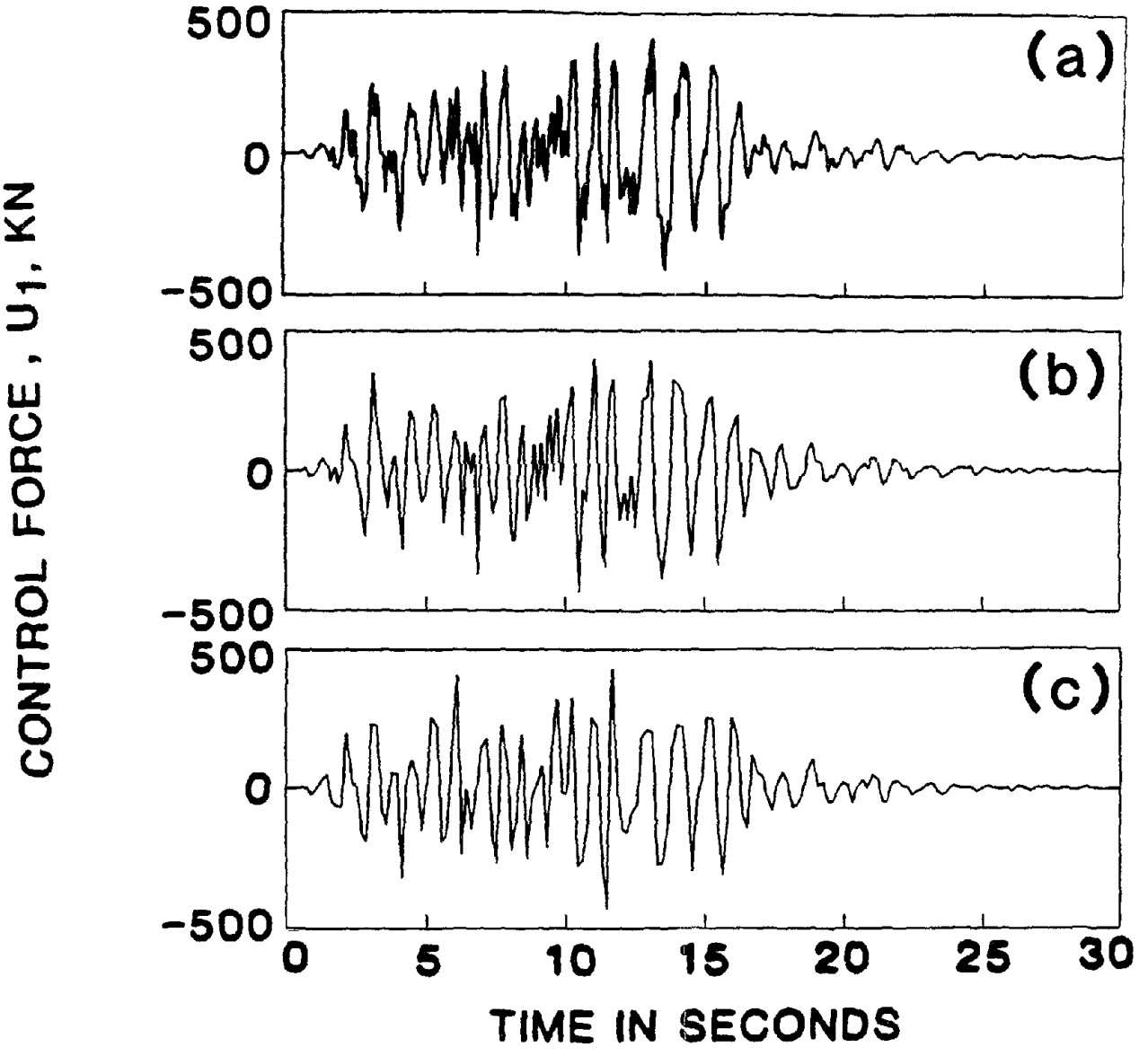

Fig. 60: Effect of Time Delay, τ, on Control Force from the First Controller for an 8-Story Building Using Tendon Control System and Instantaneous Optimal Closed-Open-Loop Control Algorithm: (a) τ -0 (No Delay), (b) $\tau = 45 \times 10^{-3}$ sec., (c) $\tau = 60 \times 10^{-3}$ sec.

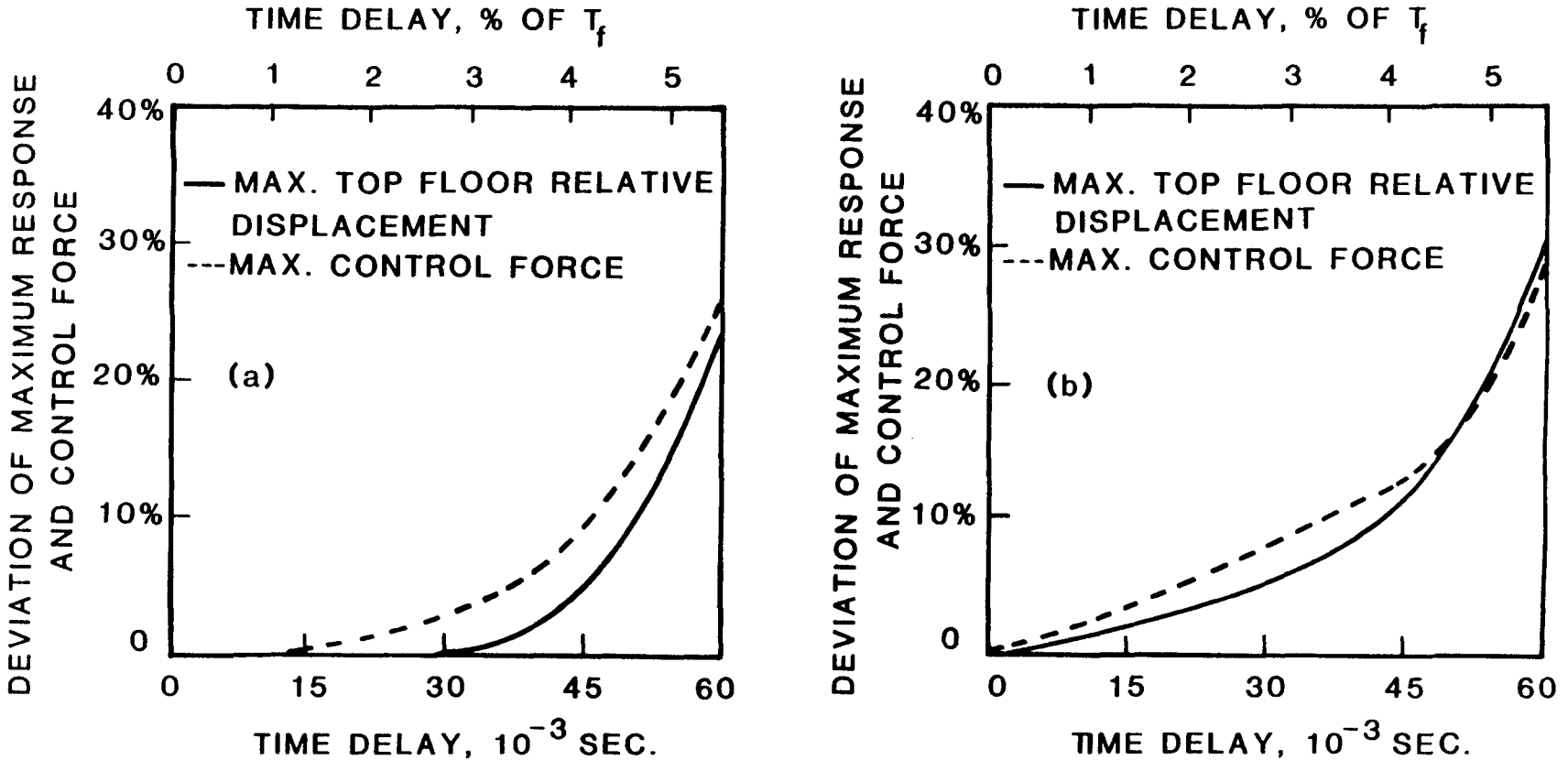

FIG. 61: EFFECT OF TIME DELAY, τ, ON MAXIMUM TOP FLOOR RELATIVE DISPLACEMENT AND CONTROL FORCE FOR BUILDING WITH ACTIVE MASS DAMPER USING; (a) RICCATI CLOSED-LOOP CONTROL, (b) INSTANTANEOUS OPTIMAL CLOSED-LOOP CONTROL.

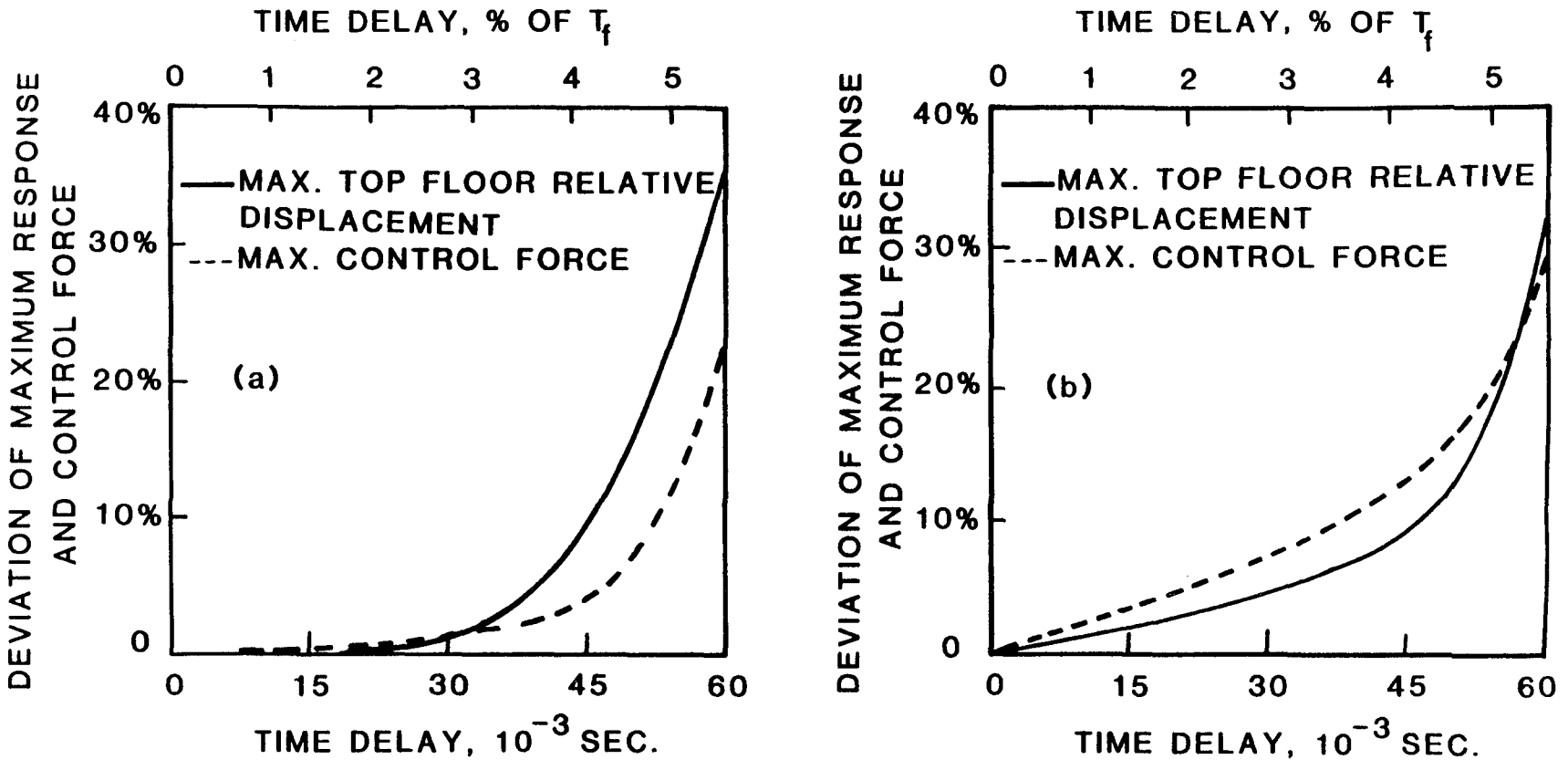

FIG. 62: EFFECT OF TIME DELAY, τ, ON MAXIMUM TOP FLOOR RELATIVE DISPLACEMENT AND CONTROL FORCE FOR BUILDING WITH ACTIVE MASS DAMPER USING; (a) INSTANTANEOUS OPTIMAL OPEN-LOOP CONTROL, (b) INSTANTANEOUS OPTIMAL CLOSED-OPEN-LOOP CONTROL.

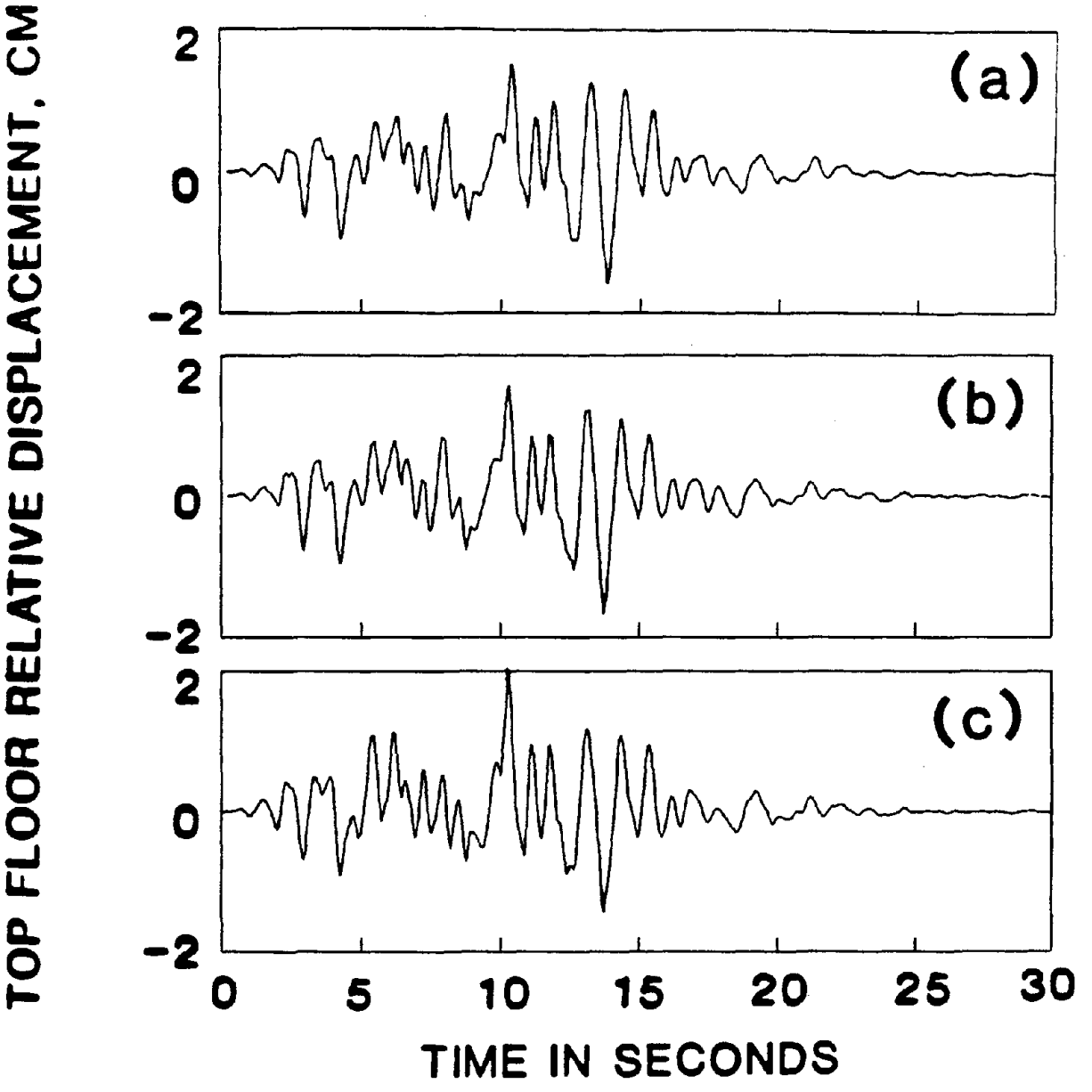

Fig. 63: Effect of Time Delay, τ, on Top Floor Relative Displacement for an 8-Story Building Using an Active Mass Damper and Riccati Closed-Loop Control Algorithm: (a) $\tau = 0$ (No Delay), (b) $\tau = 45 \times 10^{-3}$ sec., (c) $\tau = 60 \times 10^{-3}$ sec.

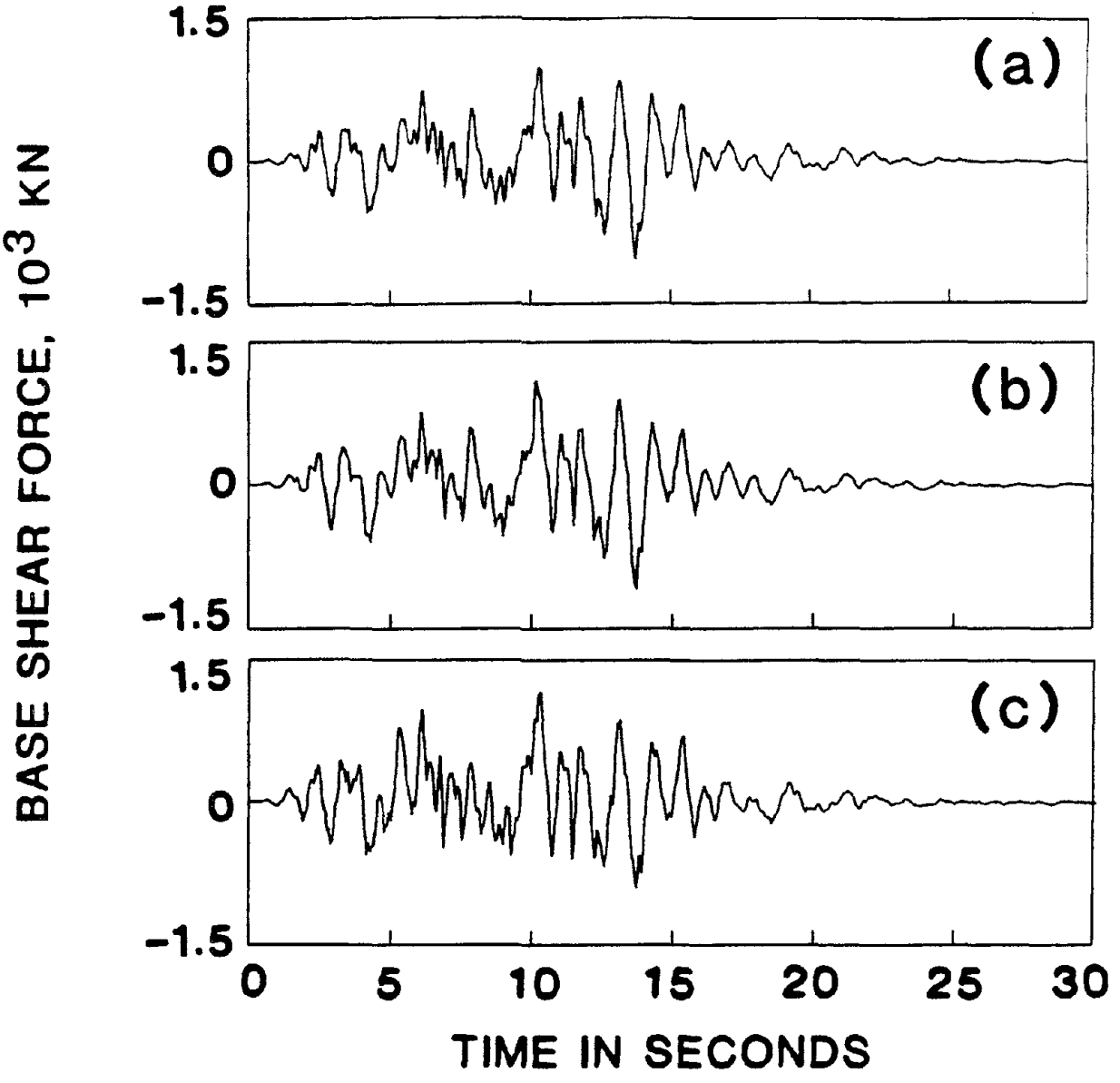

Fig. 64: Effect of Time Delay, τ, on Base Shear Force for an 8-Story Building Using an Active Mass Damper and Riccati Closed-Loop Control Algorithm: (a) $\tau = 0$ (No Delay), (b) $\tau = 45 \times 10^{-3}$ sec., (c) $\tau = 60 \times 10^{-3}$ sec.

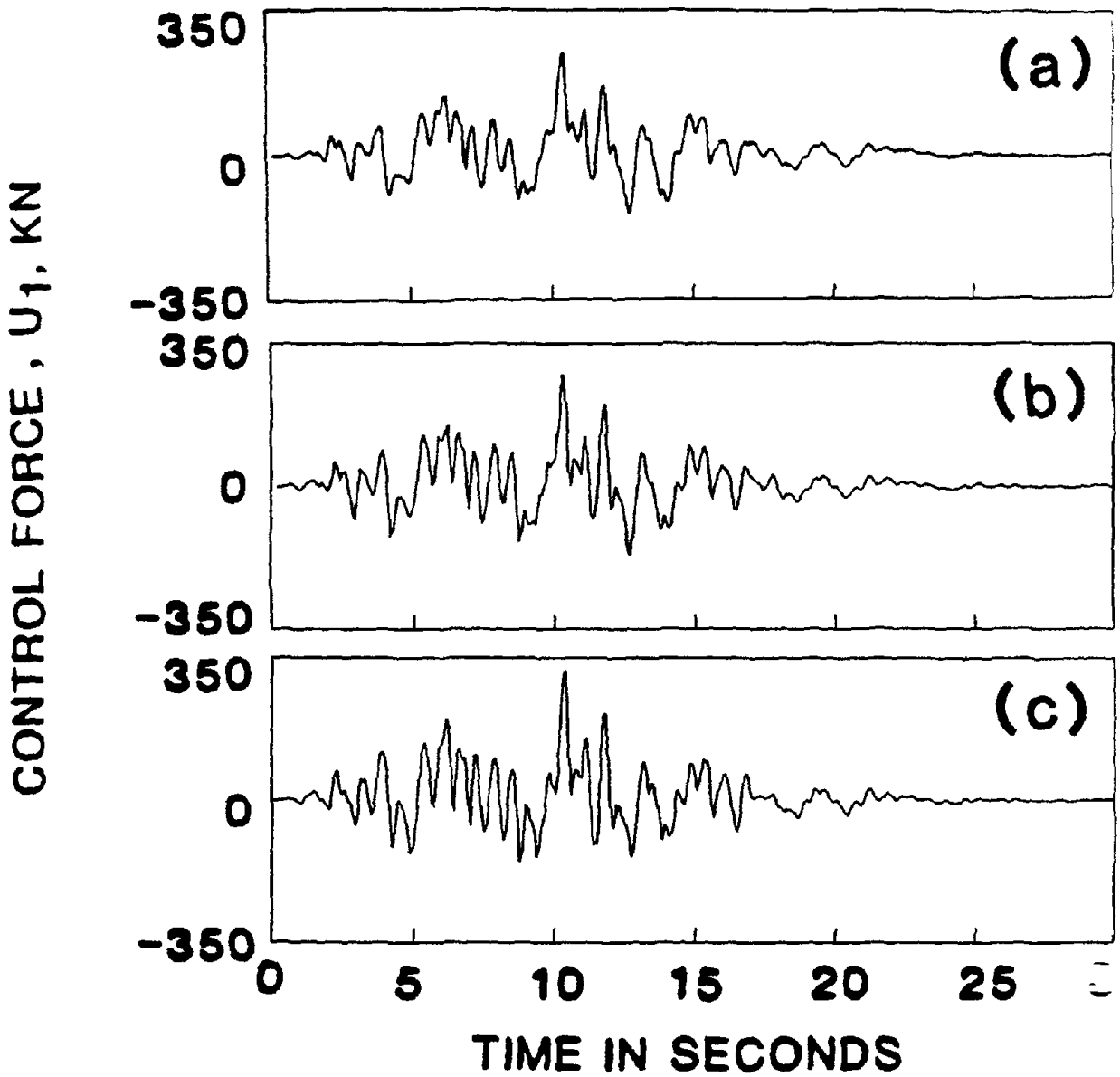

Fig. 65: Effect of Time Delay, τ, on Control Force for an 8-Story Building Using an Active Mass Damper and Riccati Closed-Loop Control Algorithm: (a) $\tau = 0$ (No Delay), (b) $\tau = 45 \times 10^{-3}$ sec., (c) $\tau = 60 \times 10^{-3}$ sec.

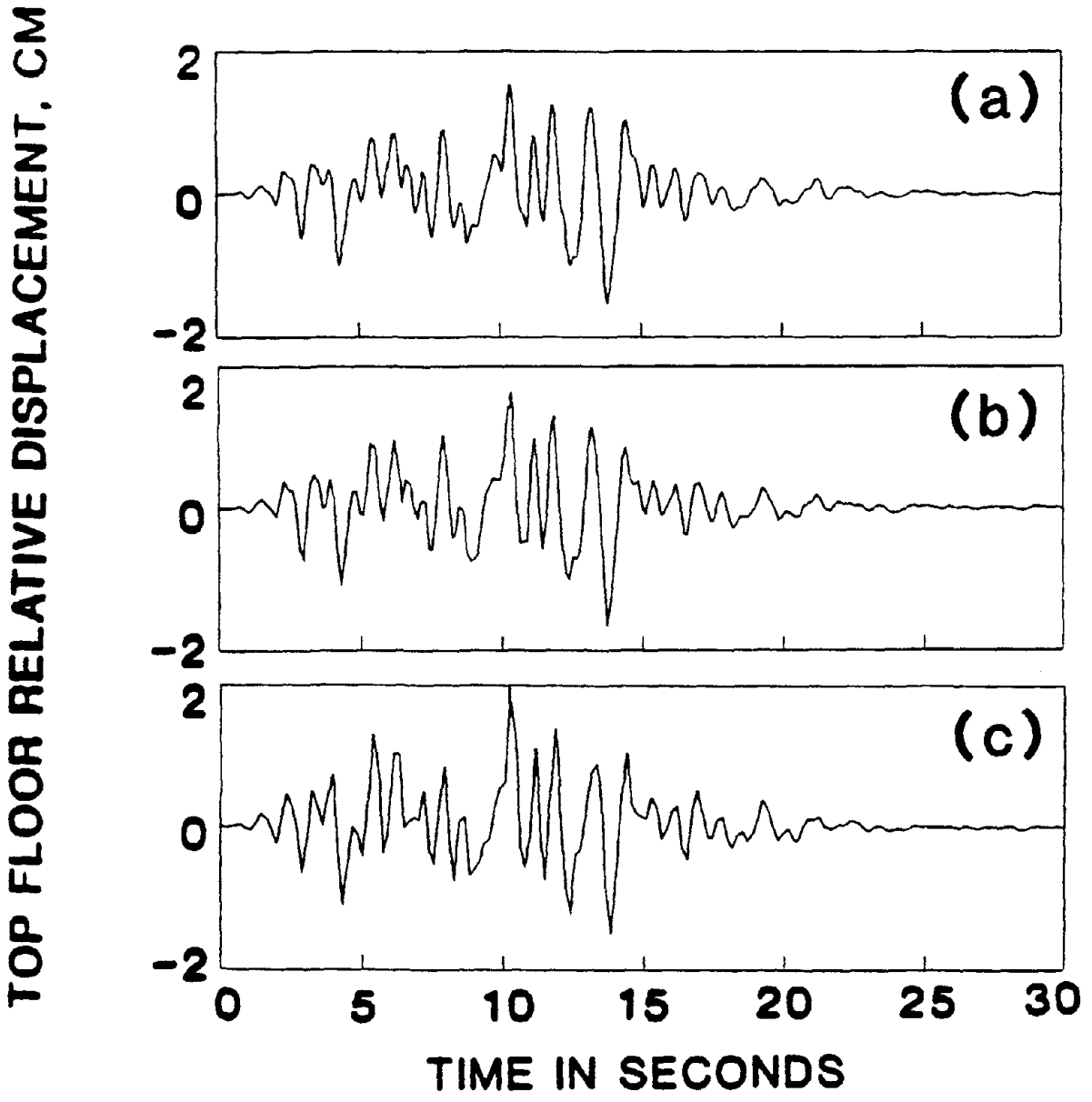

Fig. 66: Effect of Time Delay, τ, on Top Floor Relative Displacement for an 8-Story Building Using an Active Mass Damper and Instantaneous Optimal Closed-Loop Control Algorithm: (a) $\tau = 0$ (No Delay), (b) $\tau = 45 \times 10^{-3}$ sec., (c) $\tau = 60 \times 10^{-3}$ sec.

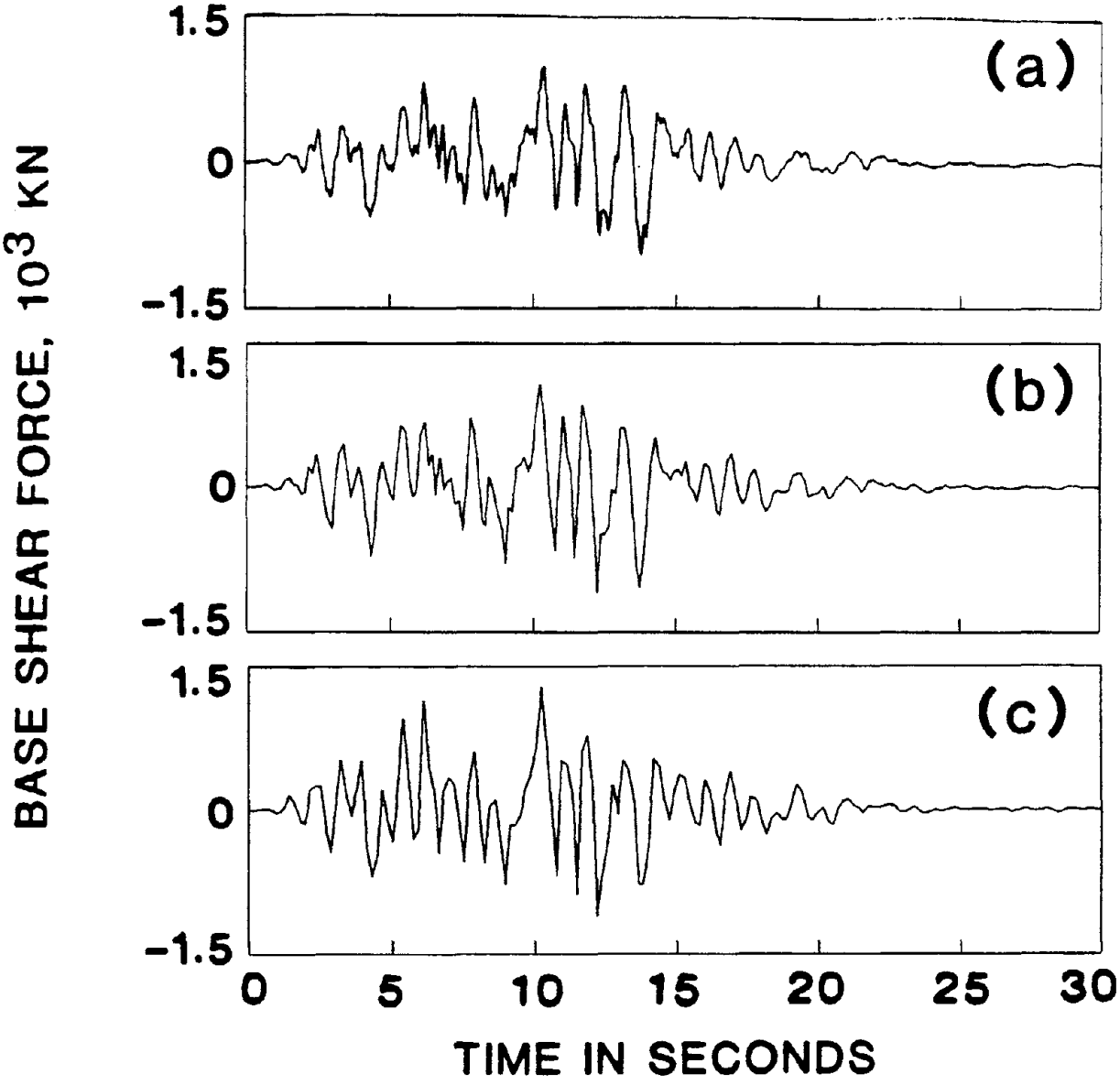

Fig. 67: Effect of Time Delay, τ, on Base Shear Force for an 8-Story Building Using an Active Mass Damper and Instantaneous Optimal Closed-Loop Control Algorithm: (a) $\tau = 0$ (No Delay), (b) $\tau = 45 \times 10^{-3}$ sec., (c) $\tau = 60 \times 10^{-3}$ sec.

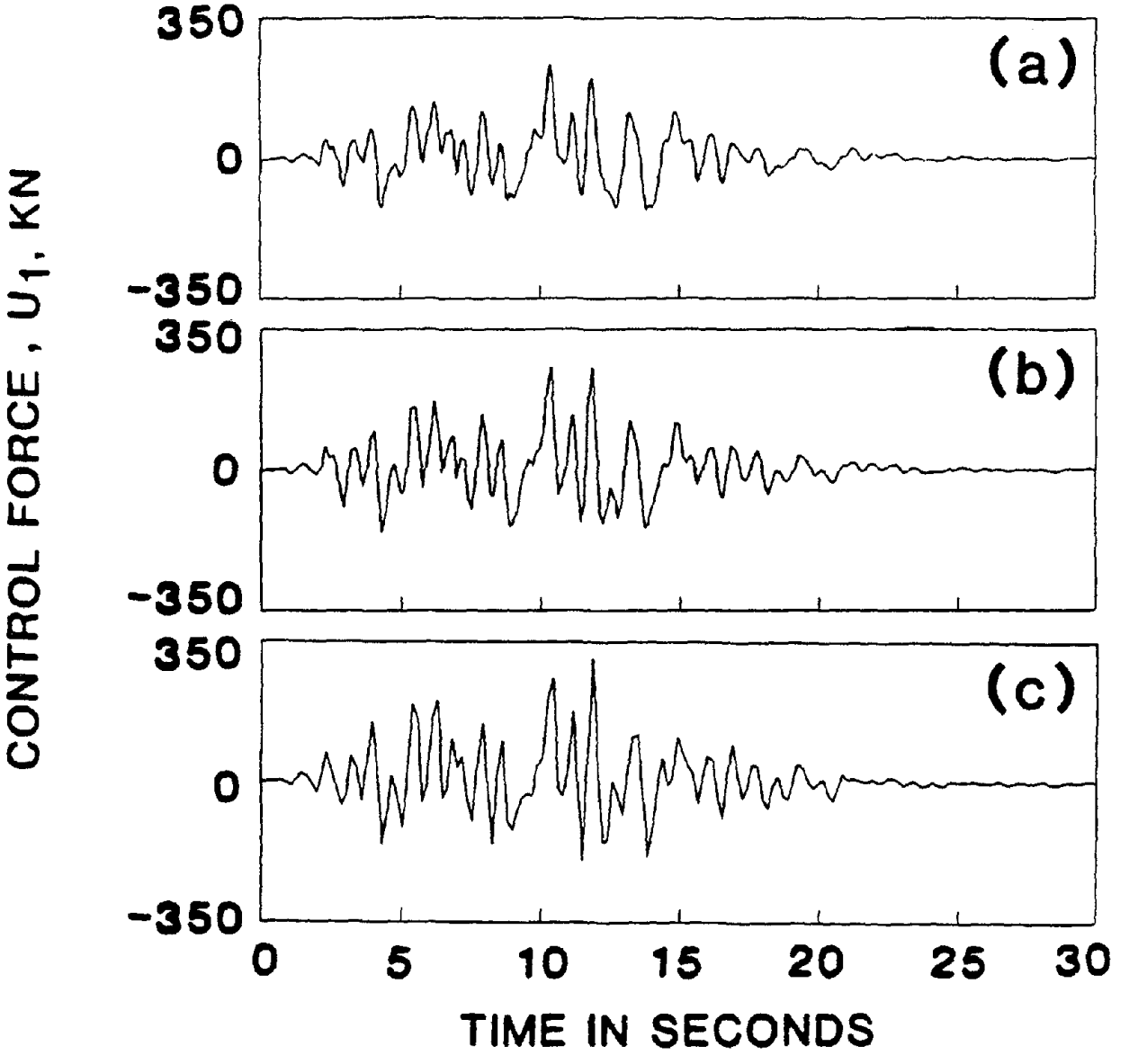

Fig. 68: Effect of Time Delay, τ, on Control Force for an 8-Story Building Using an Active Mass Damper and Instantaneous Optimal Closed-Loop Control Algorithm: (a) $\tau = 0$ (No Delay), (b) $\tau = 45 \times 10^{-3}$ sec., (c) $\tau = 60 \times 10^{-3}$ sec.

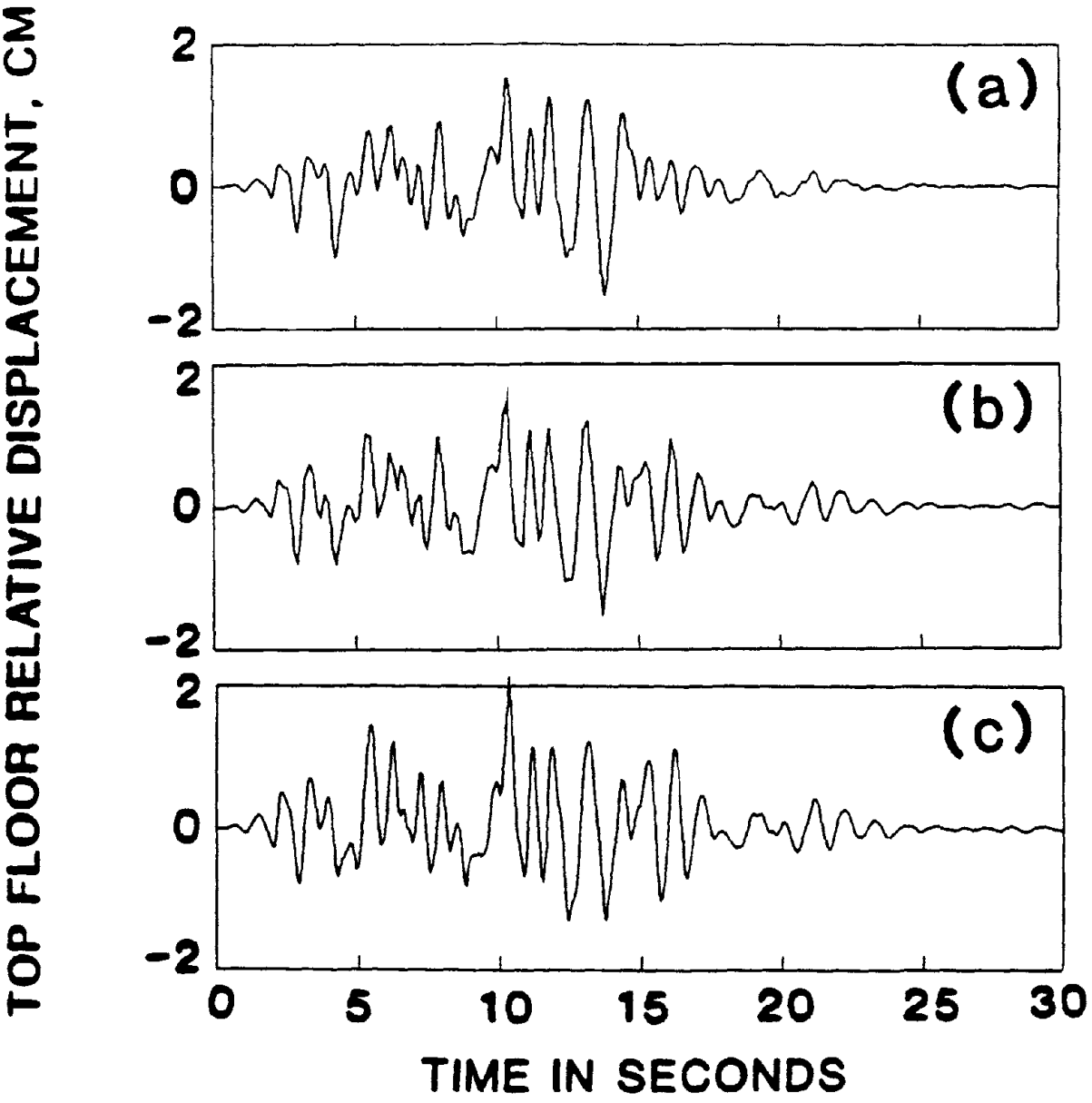

Fig. 69: Effect of Time Delay, τ, on Top Floor Relative Displacement for an 8-Story Building Using an Active Mass Damper and Instantaneous Optimal Open-Loop Control Algorithm: (a) $\tau = 0$ (No Delay), (b) $\tau = 45 \times 10^{-3}$ sec., (c) $\tau = 60 \times 10^{-3}$ sec.

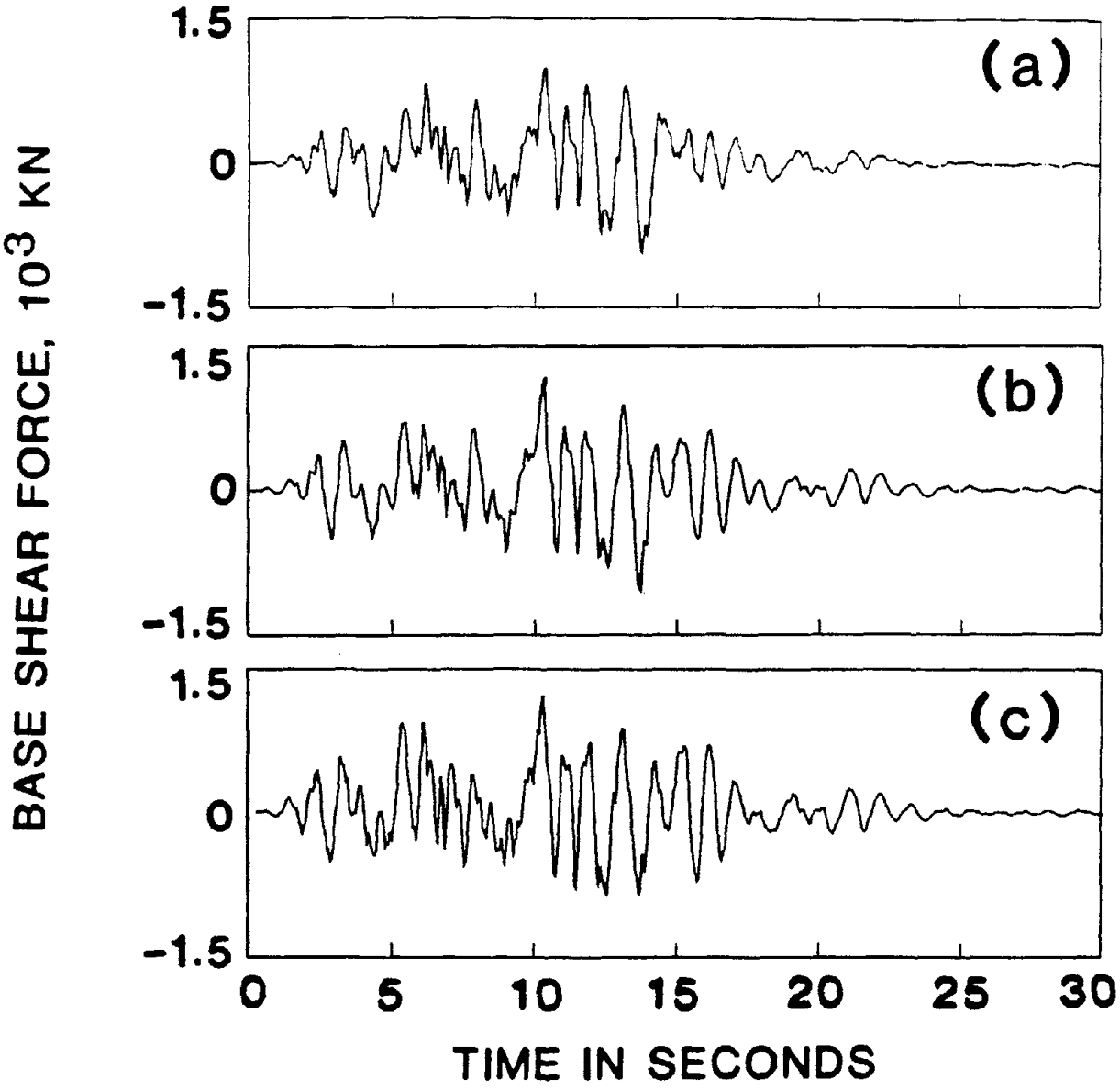

Fig. 70: Effect of Time Delay, τ, on Base Shear Force an 8-Story Building Using an Active Mass Damper and Instantaneous Optimal Open-Loop Control Algorithm: (a) $\tau = 0$ (No Delay), (b) $\tau = 45 \times 10^{-3}$ sec., (c) $\tau = 60 \times 10^{-3}$ sec.

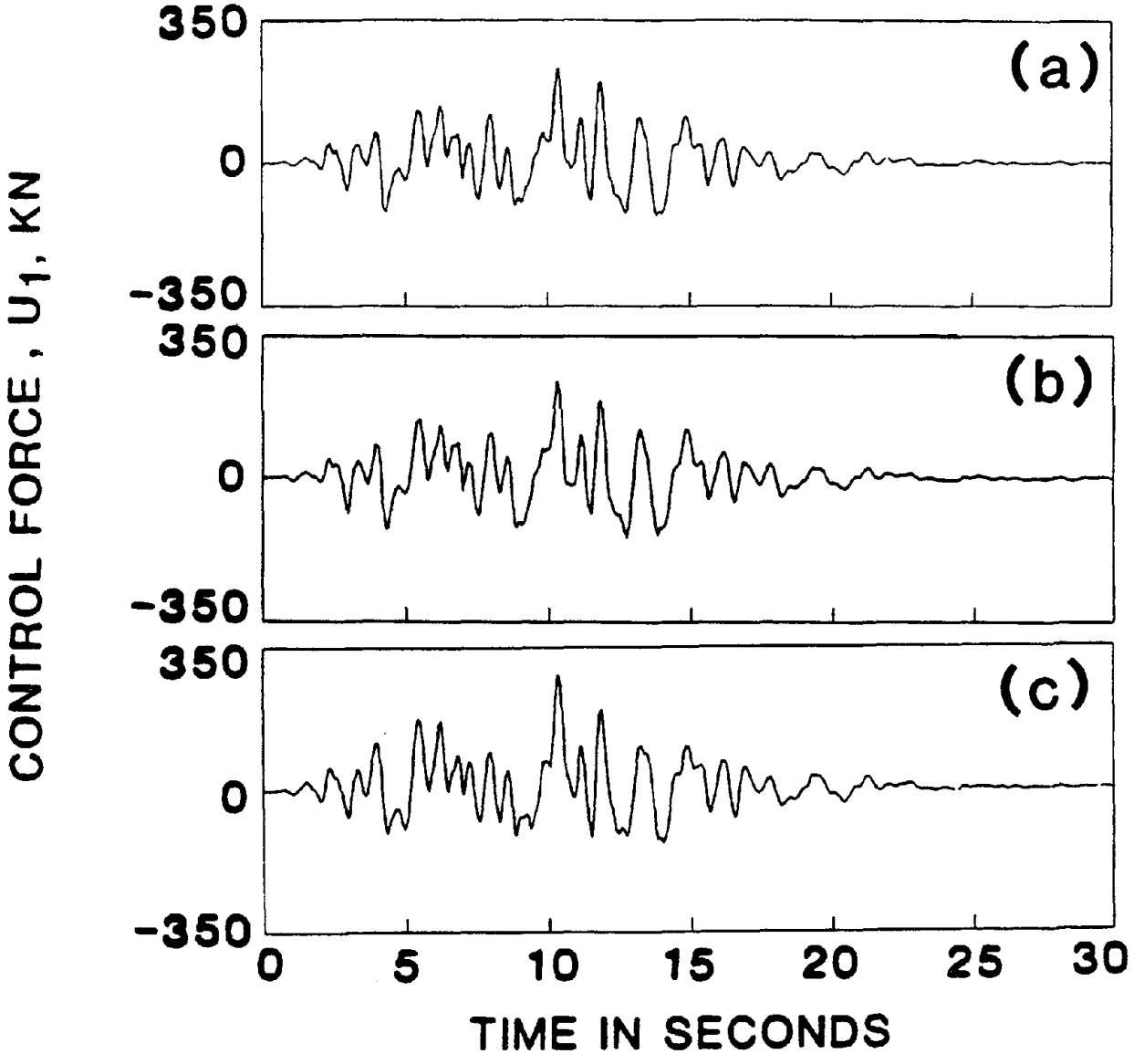

Fig. 71: Effect of Time Delay, τ, on Control Force for an 8-Story Building Using an Active Mass Damper and Instantaneous Optimal Open-Loop Control Algorithm: (a) $\tau = 0$ (No Delay), (b) $\tau = 45 \times 10^{-3}$ sec., (c) $\tau = 60 \times 10^{-3}$ sec.

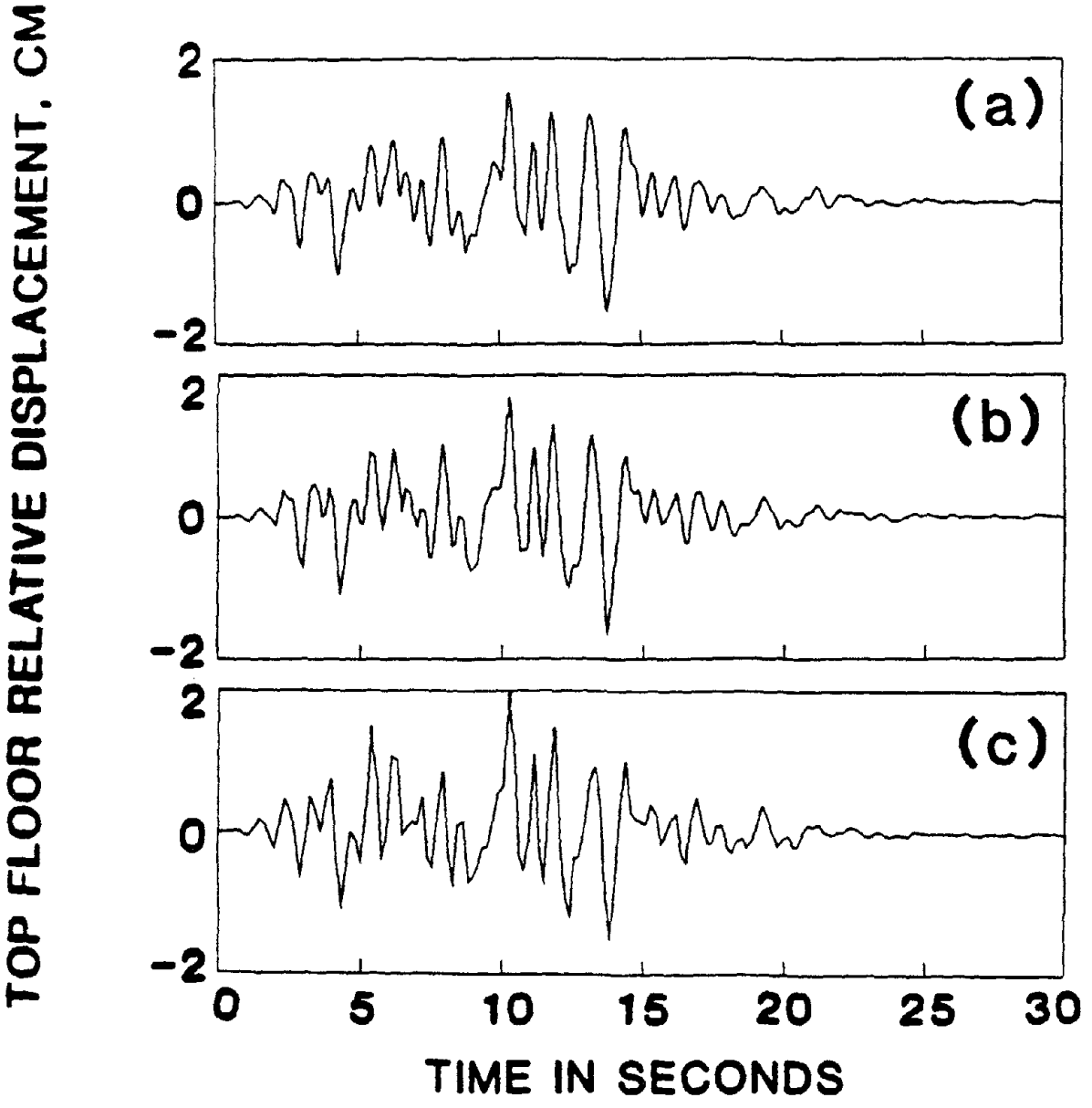

Fig. 72: Effect of Time Delay, τ, on Top Floor Relative Displacement for an 8-Story Building Using an Active Mass Damper and Instantaneous Optimal Closed-Open-Loop Control Algorithm: (a) $\tau = 0$ (No Delay), (b) $\tau = 45 \times 10^{-3}$ sec., (c) $\tau = 60 \times 10^{-3}$ sec.

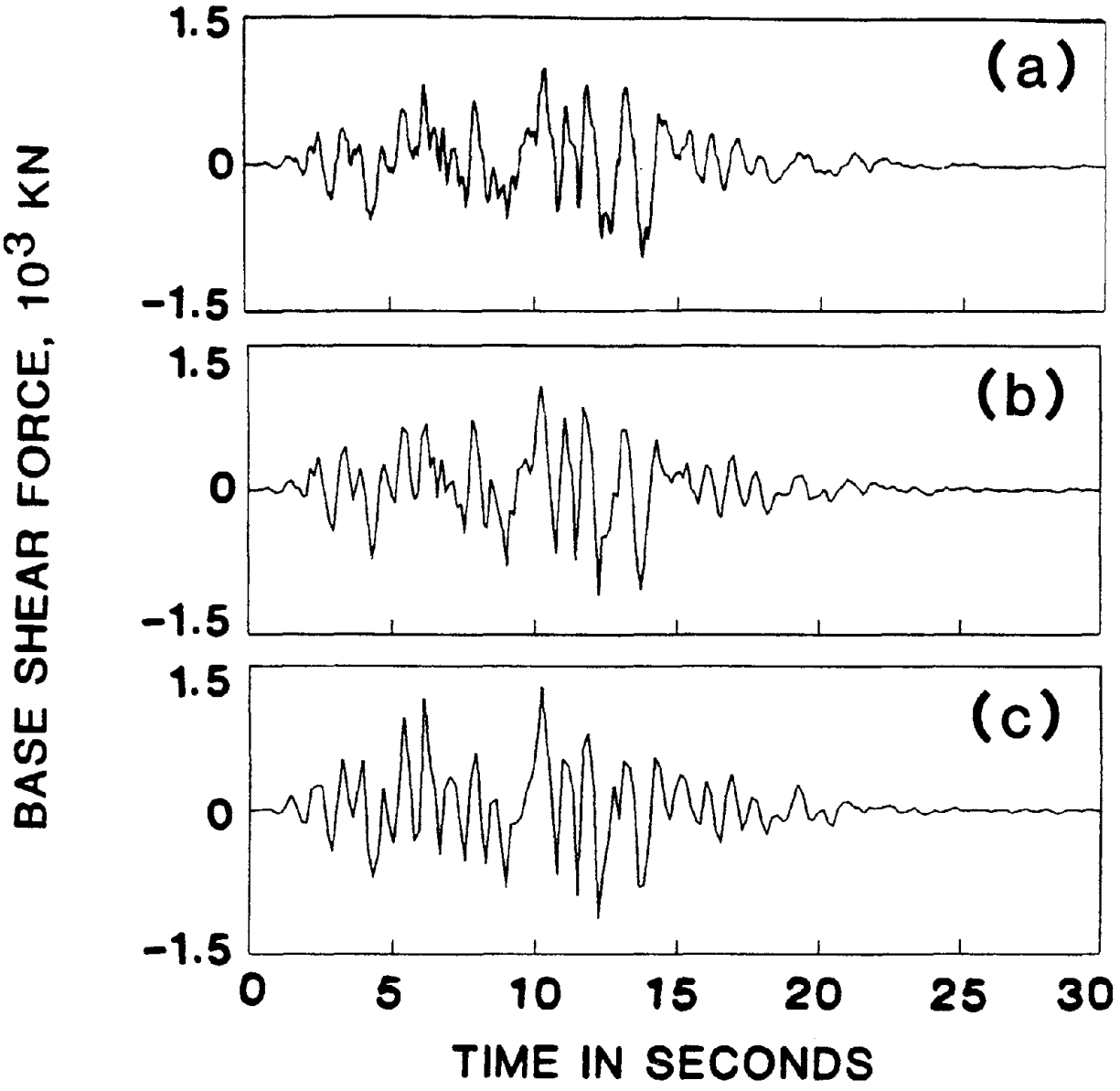

Fig. 73: Effect of Time Delay, τ, on Top Floor Relative Displacement for an 8-Story Building Using an Active Mass Damper and Instantaneous Optimal Closed-Open-Loop Control Algorithm: (a) $\tau = 0$ (No Delay), (b) $\tau = 45 \times 10^{-3}$ sec., (c) $\tau = 60 \times 10^{-3}$ sec.

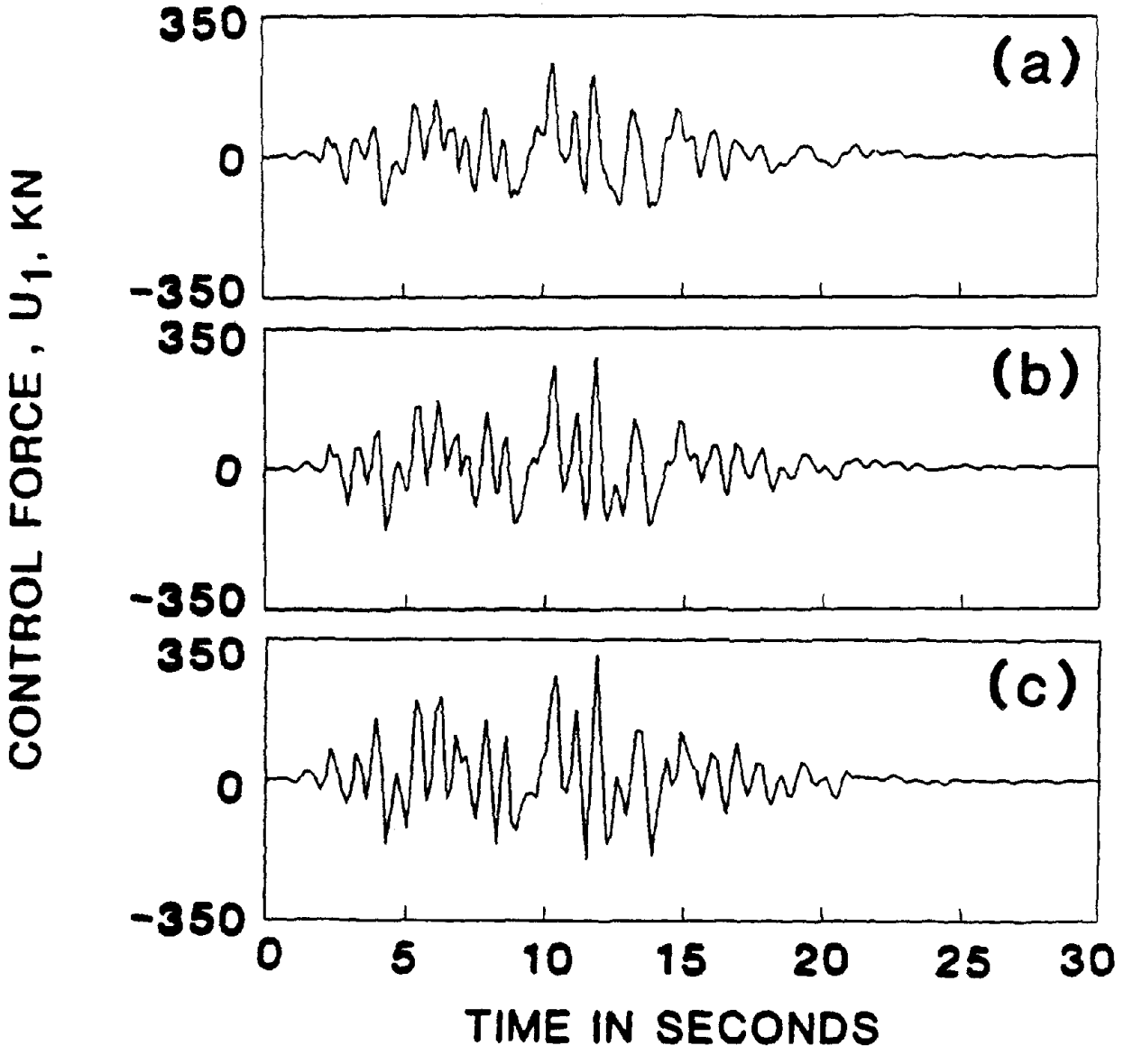

Fig. 74: Effect of Time Delay, τ, on Control Force for an 8-Story Building Using an Active Mass Damper and Instantaneous Optimal Closed-Open-Loop Control Algorithm: (a) $\tau = 0$ (No Delay), (b) $\tau = 45 \times 10^{-3}$ sec., (c) $\tau = 60 \times 10^{-3}$ sec.

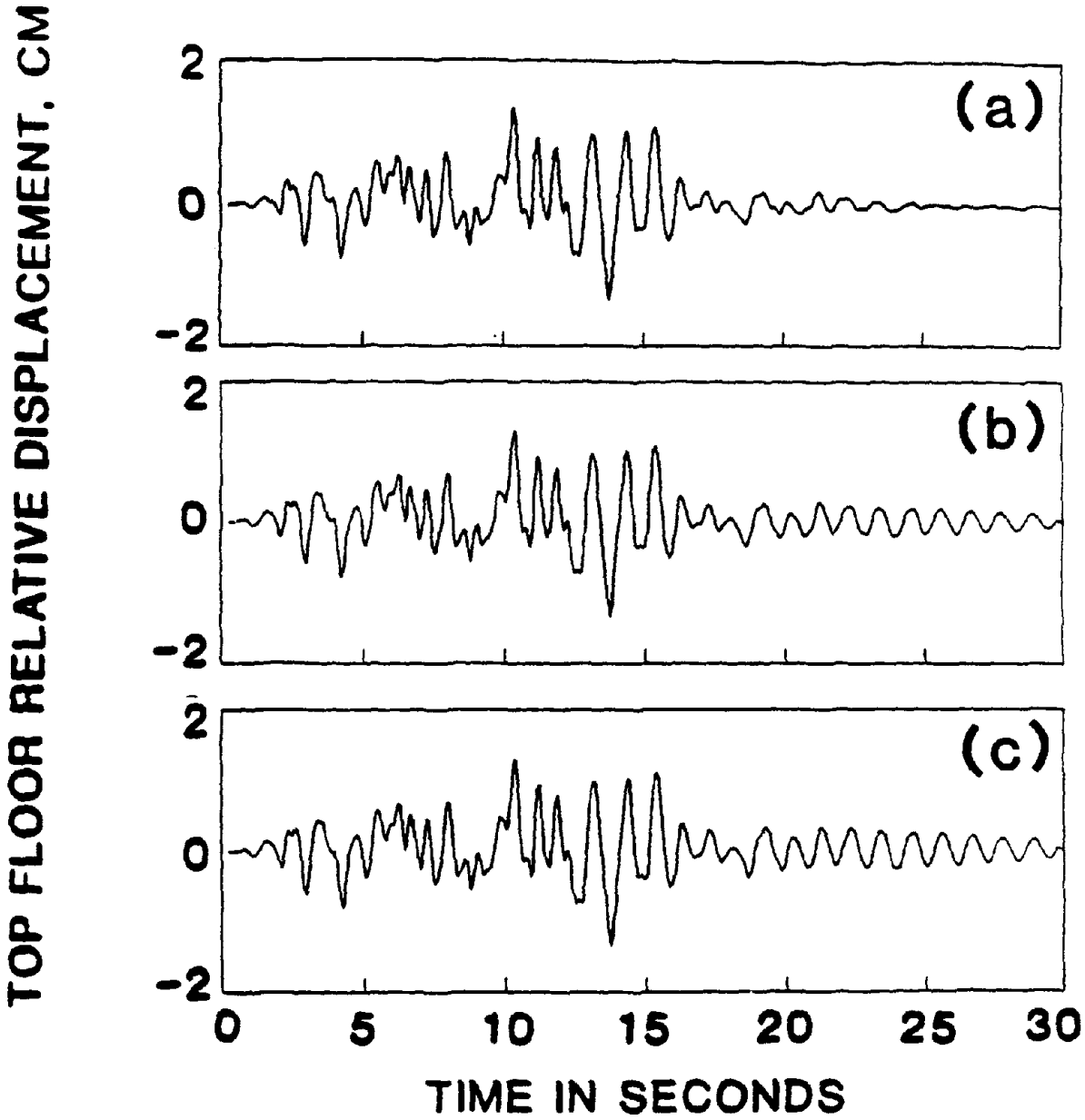

Fig. 75: Effect of Truncation of Small Control Forces on Top Floor Relative Displacement for an 8-Story Building with Tendon Control System Using Riccati Closed-Loop Control Algorithm for Different Truncation Levels ϵ: (a) No Truncation $\epsilon = 0$, (b) $\epsilon = 75$ KN (17.16%), (c) $\epsilon = 100$ KN (22.88%).

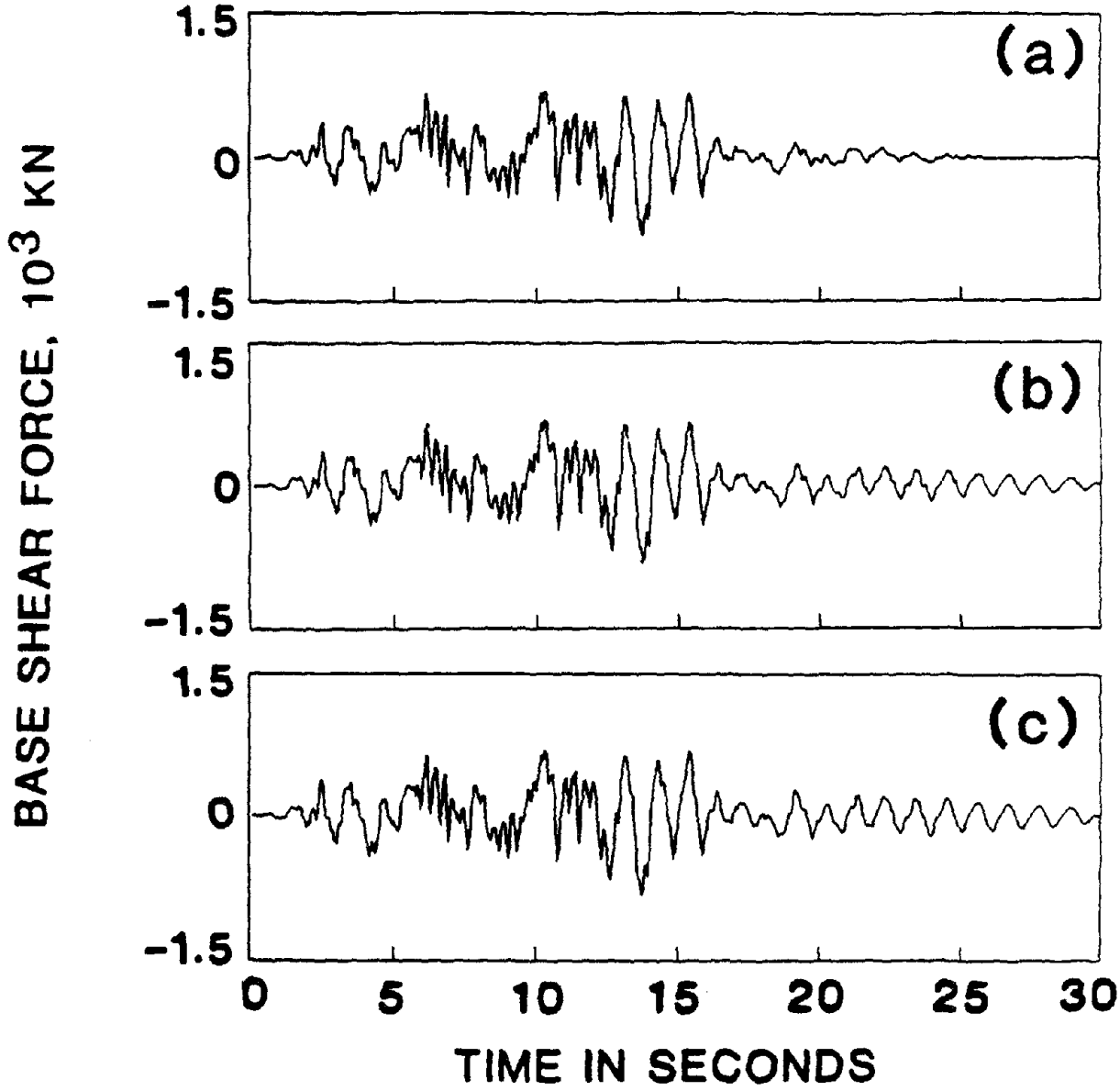

Fig. 76: *Effect of Truncation of Small Control Forces on Base Shear Force for an 8-Story Building with Tendon Control System Using Riccati Closed-Loop Control Algorithm for Different Truncation Levels ϵ: (a) No Truncation $\epsilon = 0$, (b) $\epsilon = 75$ KN (17.16%), (c) $\epsilon = 100$ KN (22.88%).*

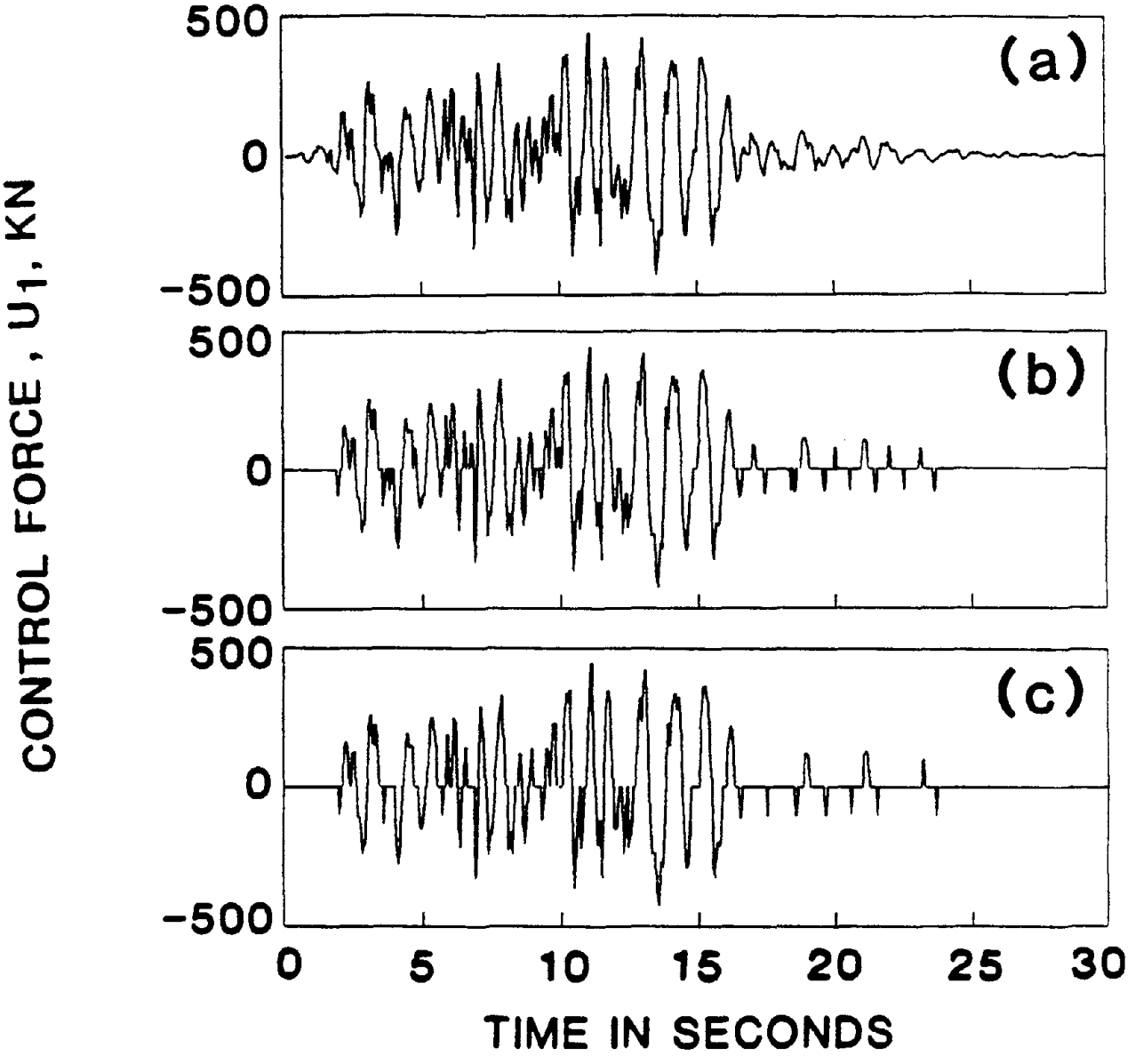

Fig. 77: Effect of Truncation of Small Control Forces on Control Force from First Controller for an 8-Story Building with Tendon Control System Using Riccati Closed-Loop Control Algorithm for Different Truncation Levels: (a) No Truncation $\epsilon = 0$, (b) $\epsilon = 75$ KN (17.16%), (c) $\epsilon = 100$ KN (22.88%).

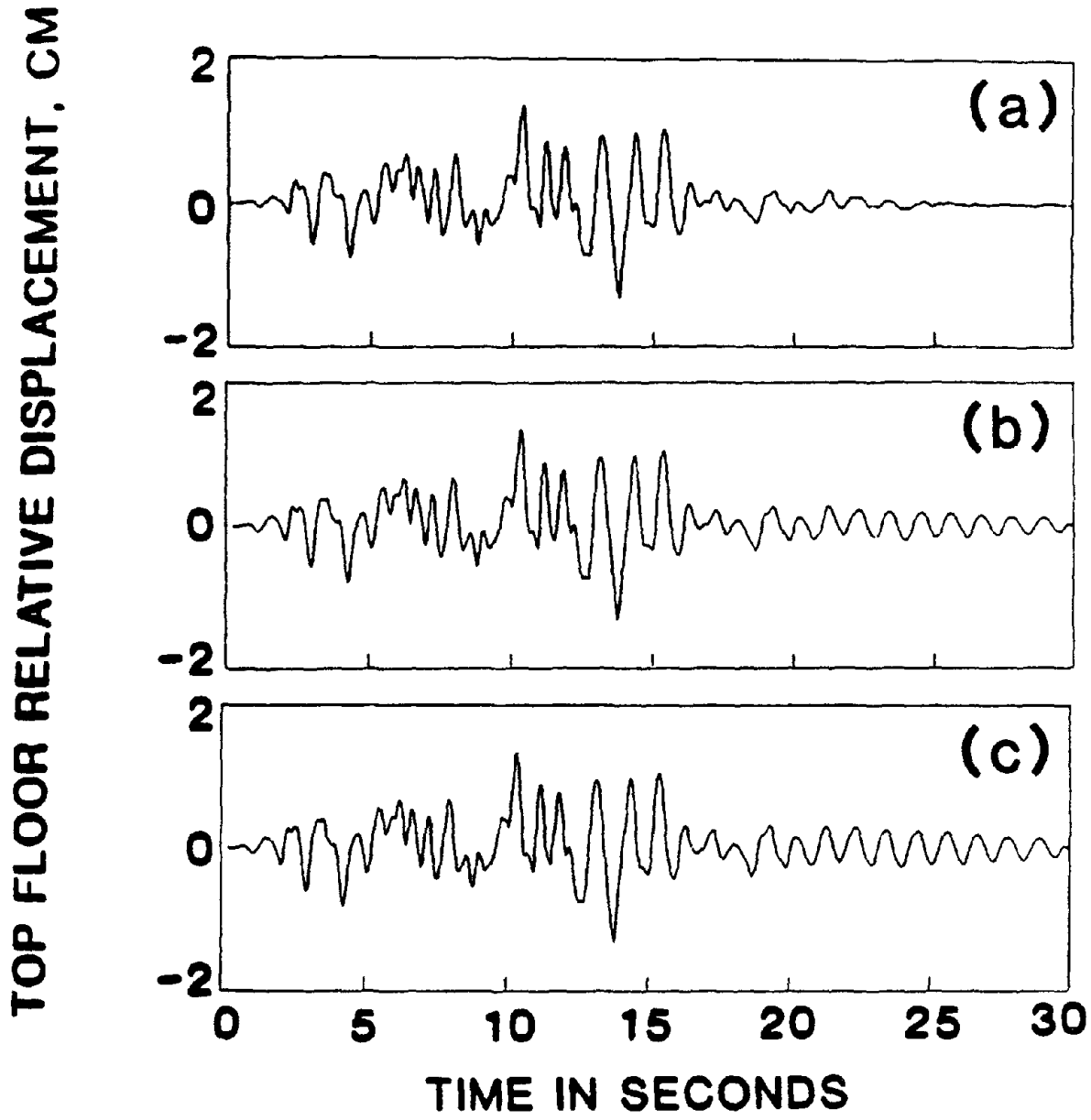

Fig. 78: Effect of Truncation of Small Control Forces on Top Floor Relative Displacement for an 8-Story Building with Tendon Control System Using Instantaneous Optimal Closed-Loop Control Algorithm for Different Truncation Levels ϵ: (a) No Truncation $\epsilon = 0$, (b) $\epsilon = 75$ KN (17.81%), (c) $\epsilon = 100$ KN (23.85%).

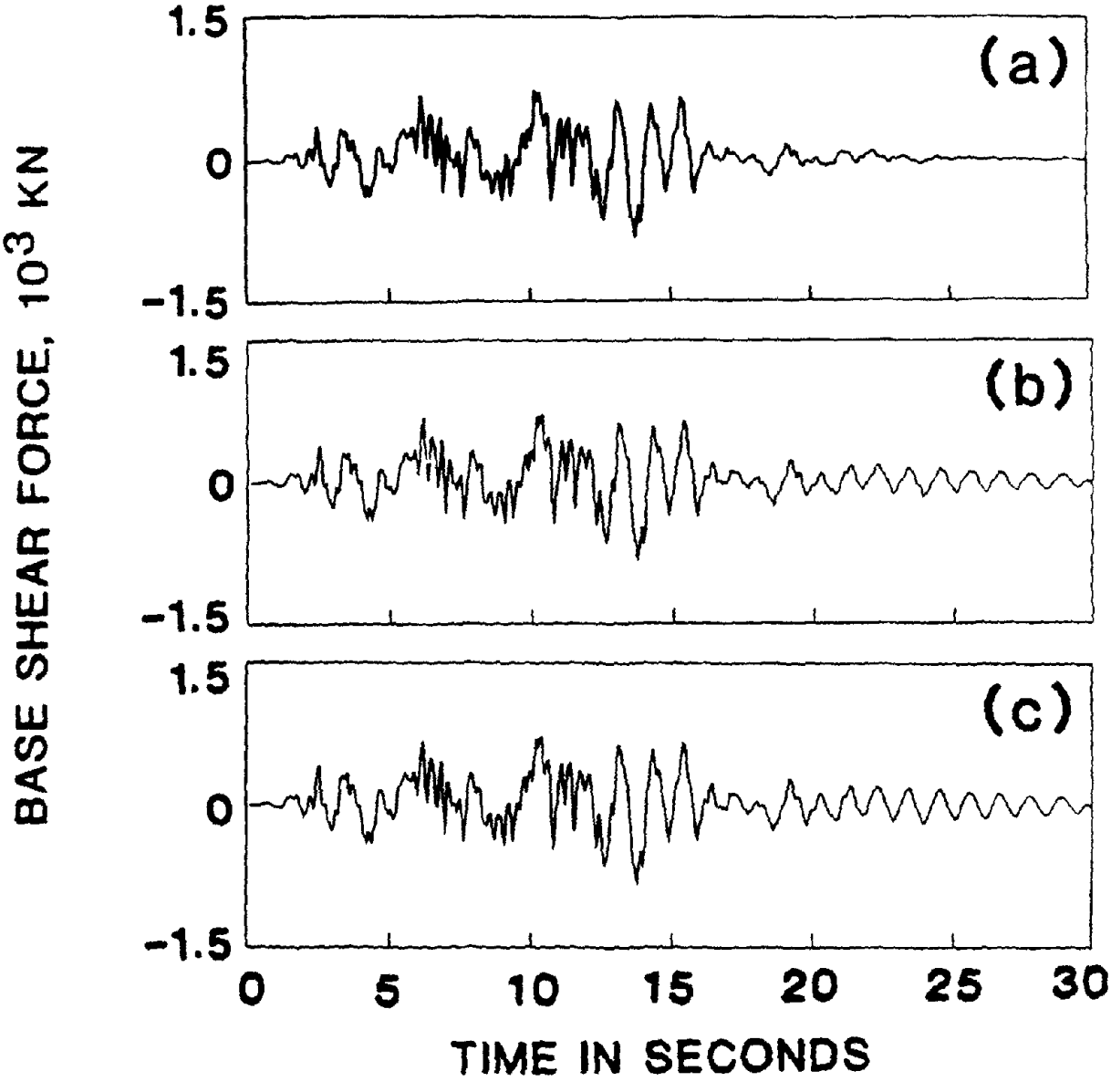

Fig. 79: Effect of Truncation of Small Control Forces on Base Shear Force for an 8-Story Building with Tendon Control System Using Instantaneous Optimal Closed-Loop Control Algorithm for Different Truncation Levels ϵ: (a) No Truncation $\epsilon = 0$, (b) $\epsilon = 75$ KN (17.81%), (c) $\epsilon = 100$ KN (23.75%).

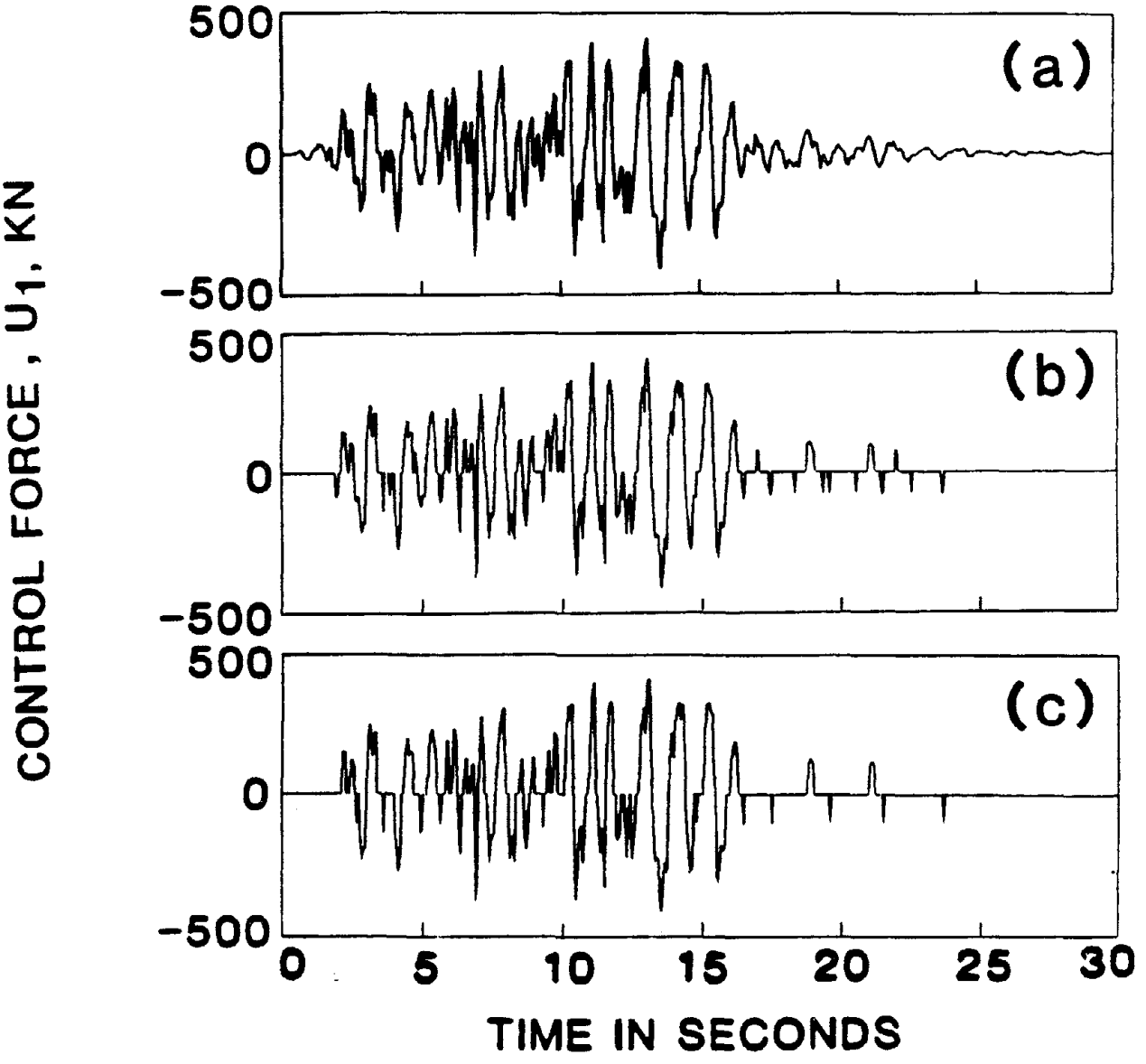

Fig. 80: Effect of Truncation of Small Control Forces on Control Force from First Controller for an 8-Story Building with Tendon Control System Using Instantaneous Optimal Closed-Loop Control Algorithm for Different Truncation Levels ϵ: (a) No Truncation $\epsilon = 0$, (b) $\epsilon = 75$ KN (17.81%), (c) $\epsilon = 100$ KN (23.75%).

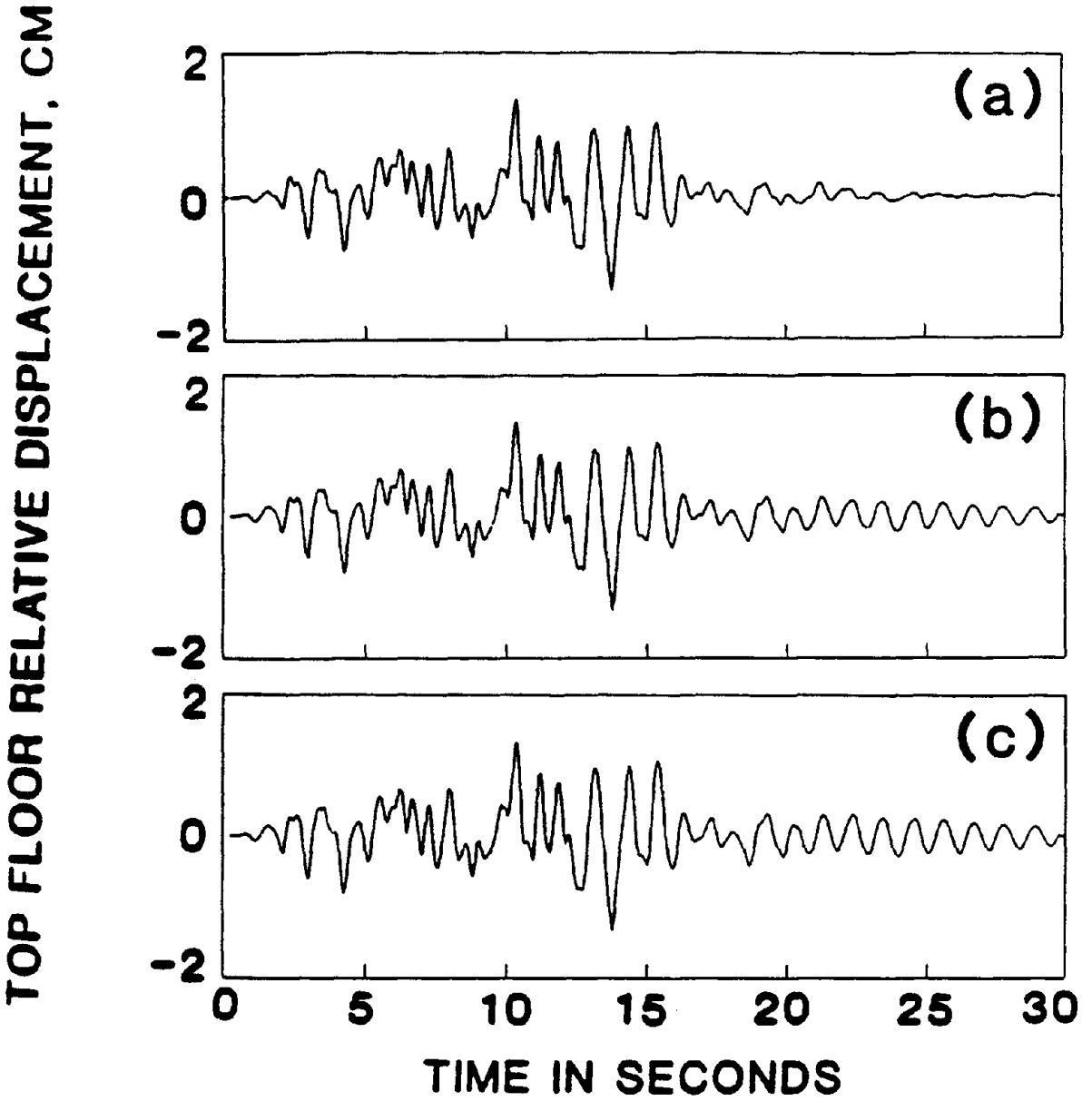

Fig. 81: Effect of Truncation of Small Control Forces on Top Floor Relative Displacement for an 8-Story Building with Tendon Control System Using Instantaneous Optimal Open-Loop Control Algorithm for Different Truncation Levels ϵ: (a) No Truncation $\epsilon = 0$, (b) $\epsilon = 75$ KN (17.81%), (c) $\epsilon = 100$ KN (23.75%).

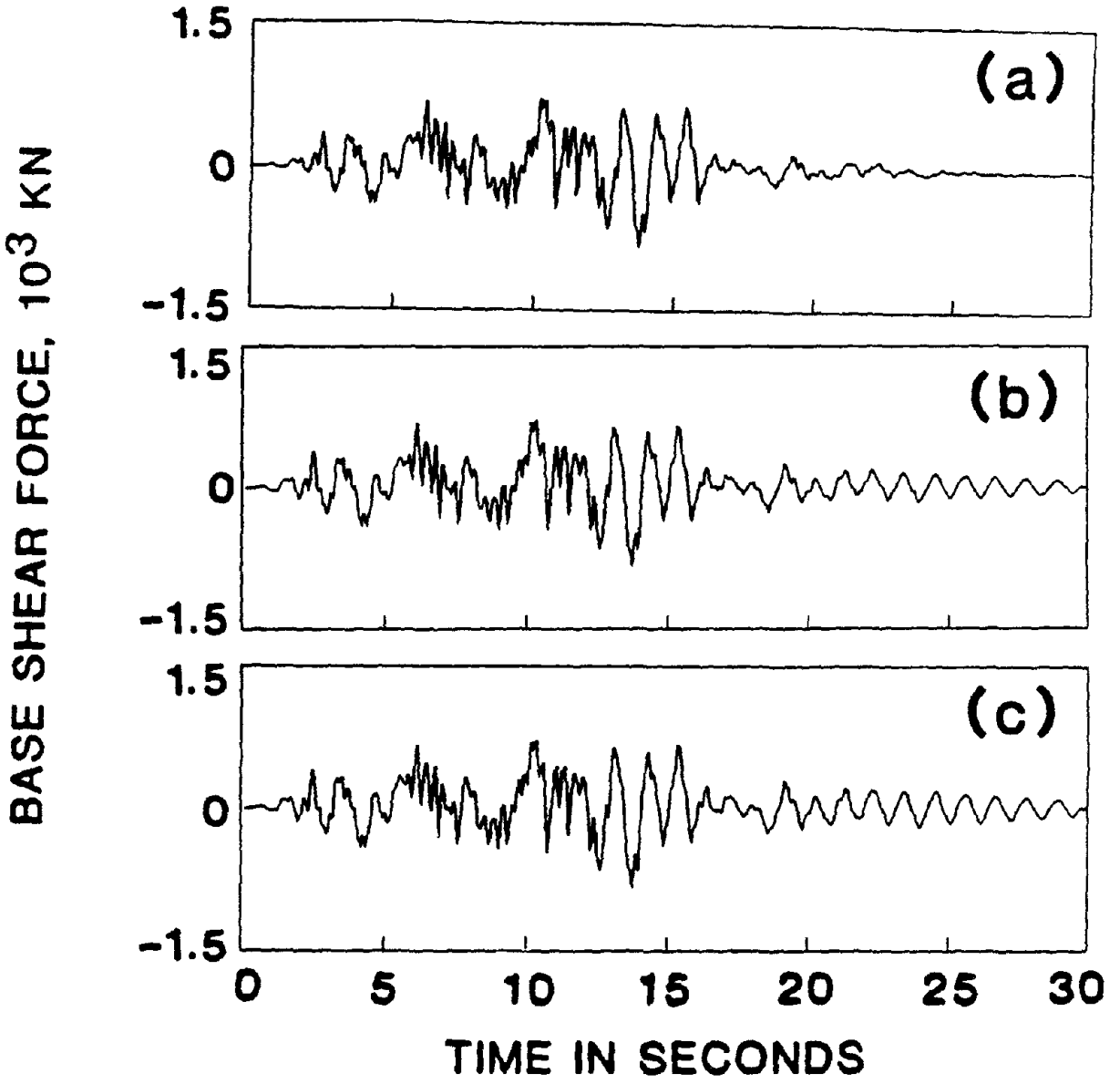

Fig. 82: Effect of Truncation of Small Control Forces on Base Shear Force for an 8-Story Building with Tendon Control System Using Instantaneous Optimal Open-Loop Control Algorithm for Different Truncation Levels ϵ: (a) No Truncation $\epsilon = 0$, (b) $\epsilon = 75$ KN (17.81%), (c) $\epsilon = 100$ KN (23.75%).

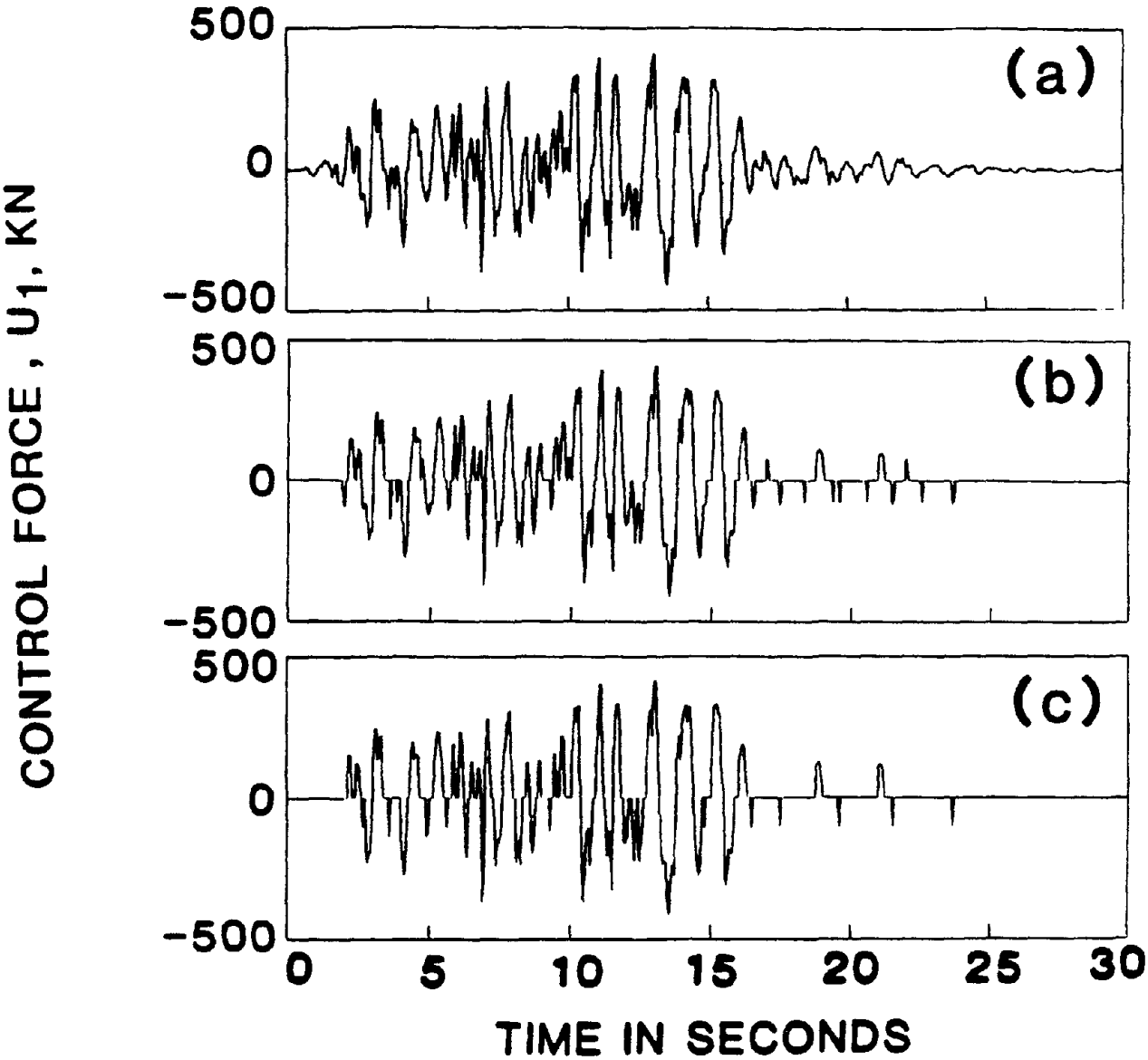

Fig. 83: Effect of Truncation of Small Control Forces on Control Force from First Controller for an 8-Story Building with Tendon Control System Using Instantaneous Optimal Open-Loop Control Algorithm for Different Truncation Levels ϵ: (a) No Truncation $\epsilon = 0$, (b) $\epsilon = 75$ KN (17.81%), (c) $\epsilon = 100$ KN (25.75%).

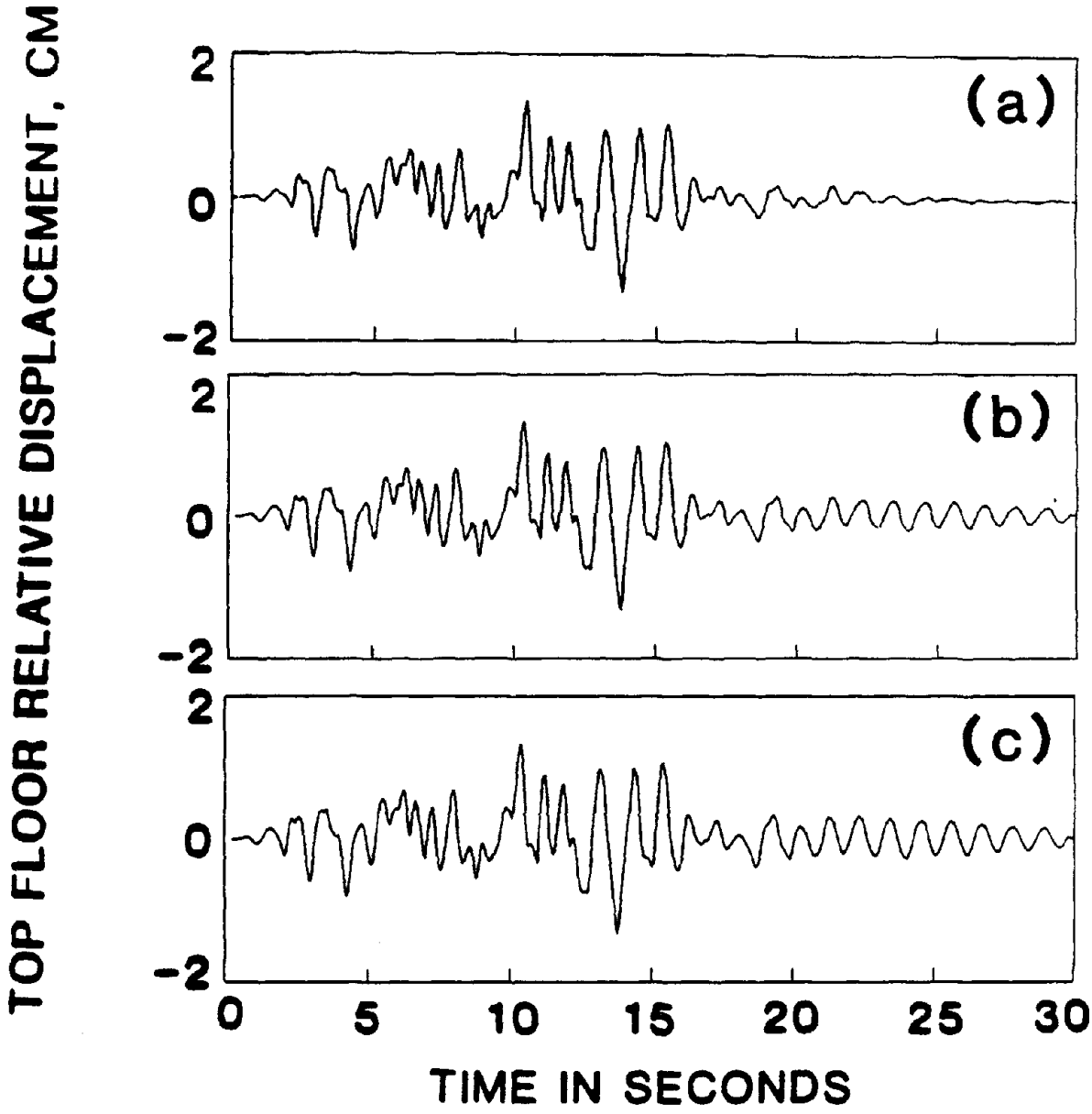

Fig. 84: Effect of Truncation of Small Control Forces on Top Floor Relative Displacement for an 8-Story Building with Tendon Control System Using Instantaneous Optimal Closed-Open-Loop Control Algorithm for Different Truncation Levels ϵ: (a) No Truncation ϵ - 0, (b) ϵ - 75 KN (17.81%), (c) ϵ - 100 KN (23.75%).

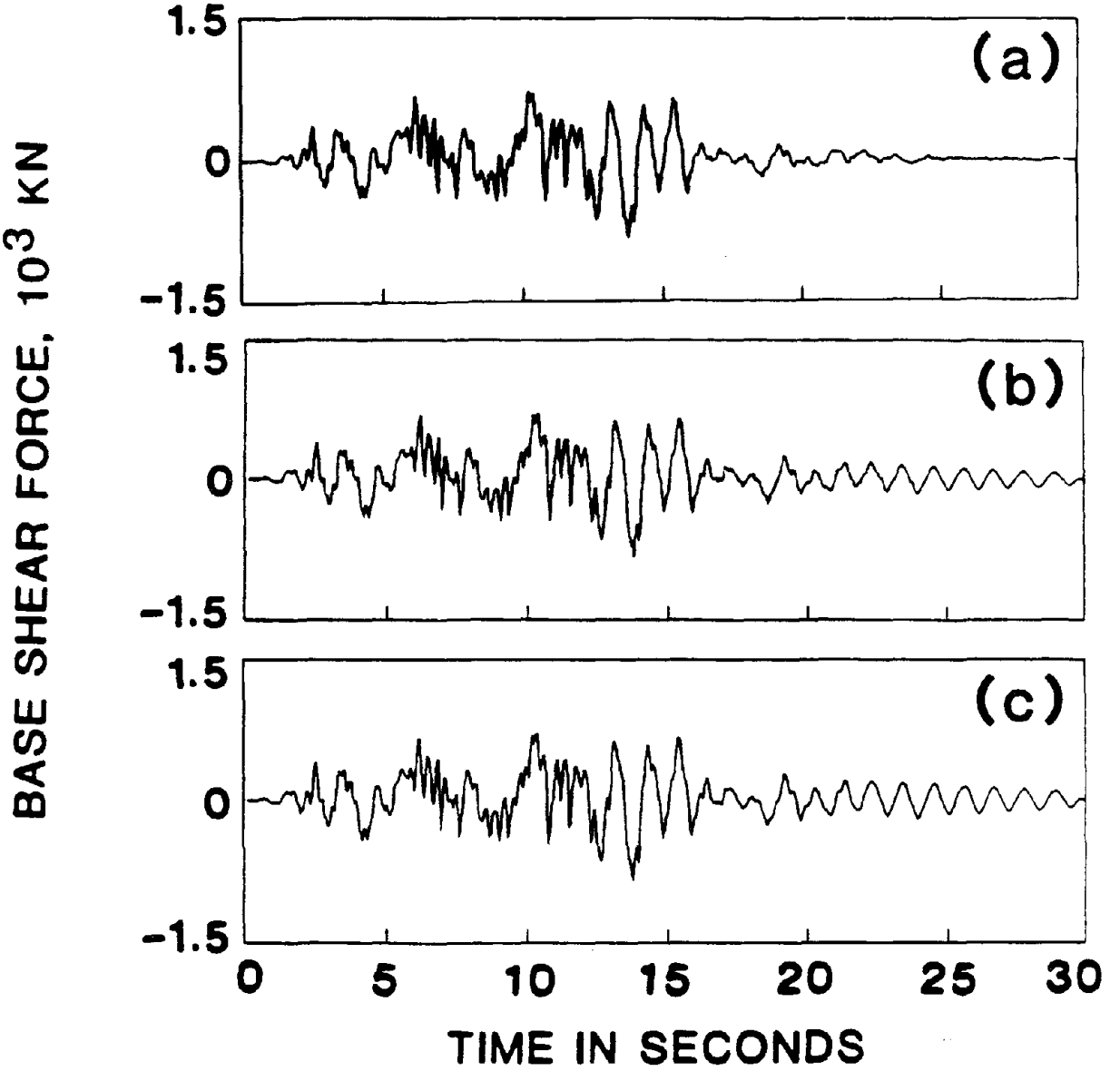

Fig. 85: Effect of Truncation of Small Control Forces on Base Shear Force for an 8-Story Building with Tendon Control System Using Instantaneous Optimal Closed-Open-Loop Control Algorithm for Different Truncation Levels ϵ: (a) No Truncation $\epsilon = 0$, (b) ϵ = 75 KN (17.81%), (c) ϵ = 100 KN (23.75%).

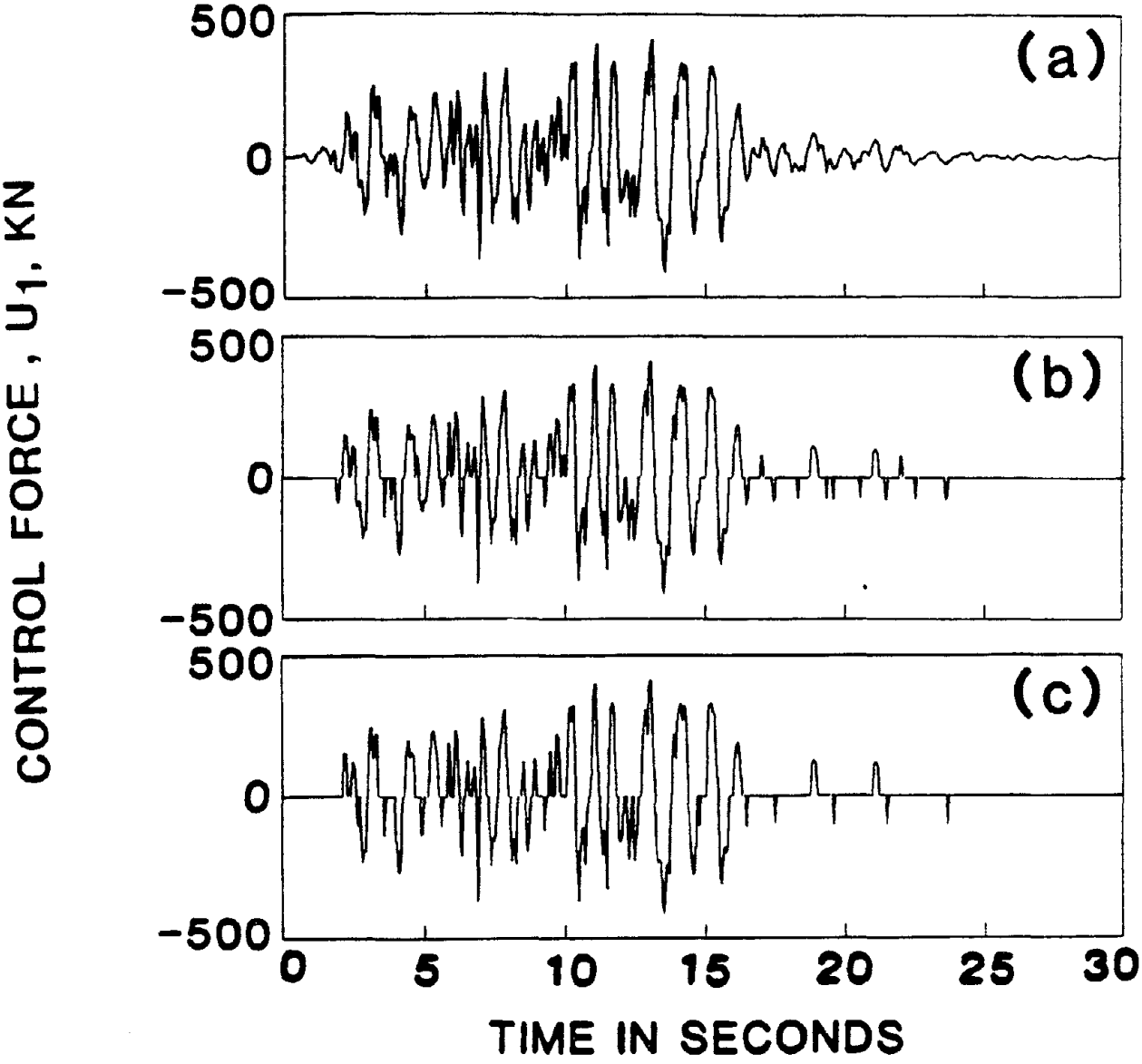

Fig. 86: Effect of Truncation of Small Control Forces on Control Force from First Controller an 8-Story Building with Tendon Control System Using Instantaneous Optimal Closed-Open-Loop Control Algorithm for Different Truncation Levels ϵ: (a) No Truncation ϵ = 0, (b) ϵ = 75 KN (17.81%), (c) ϵ = 100 KN (23.75%).

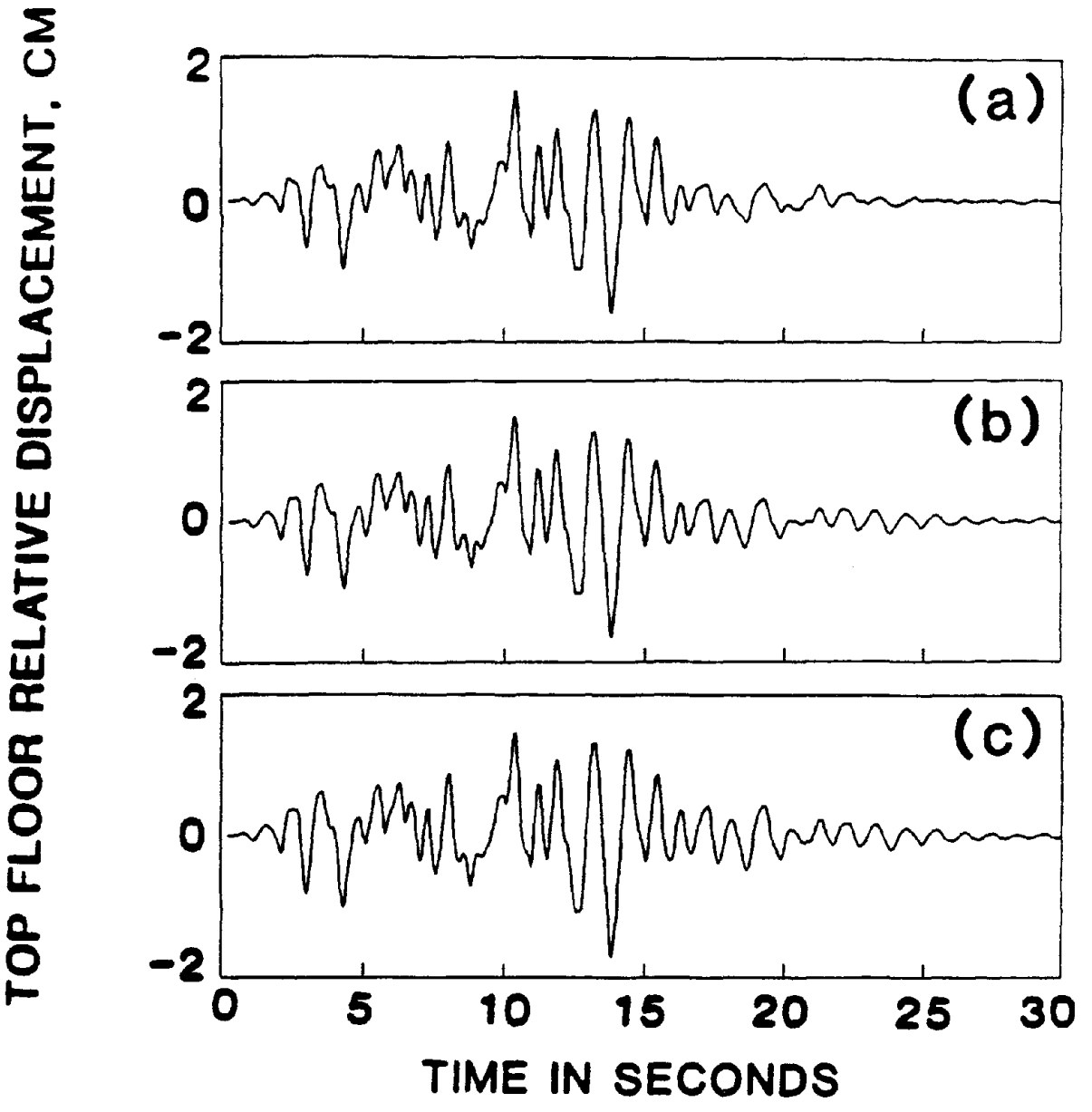

Fig. 87: Effect of Truncation of Small Control Forces on Top Floor Relative Displacement for an 8-Story Building with an Active Mass Damper Using Riccati Closed-Loop Control Algorithm for Different Truncation Levels ϵ: (a) No Truncation $\epsilon = 0$, (b) $\epsilon = 50$ KN (20%), (c) $\epsilon = 75$ KN (30%).

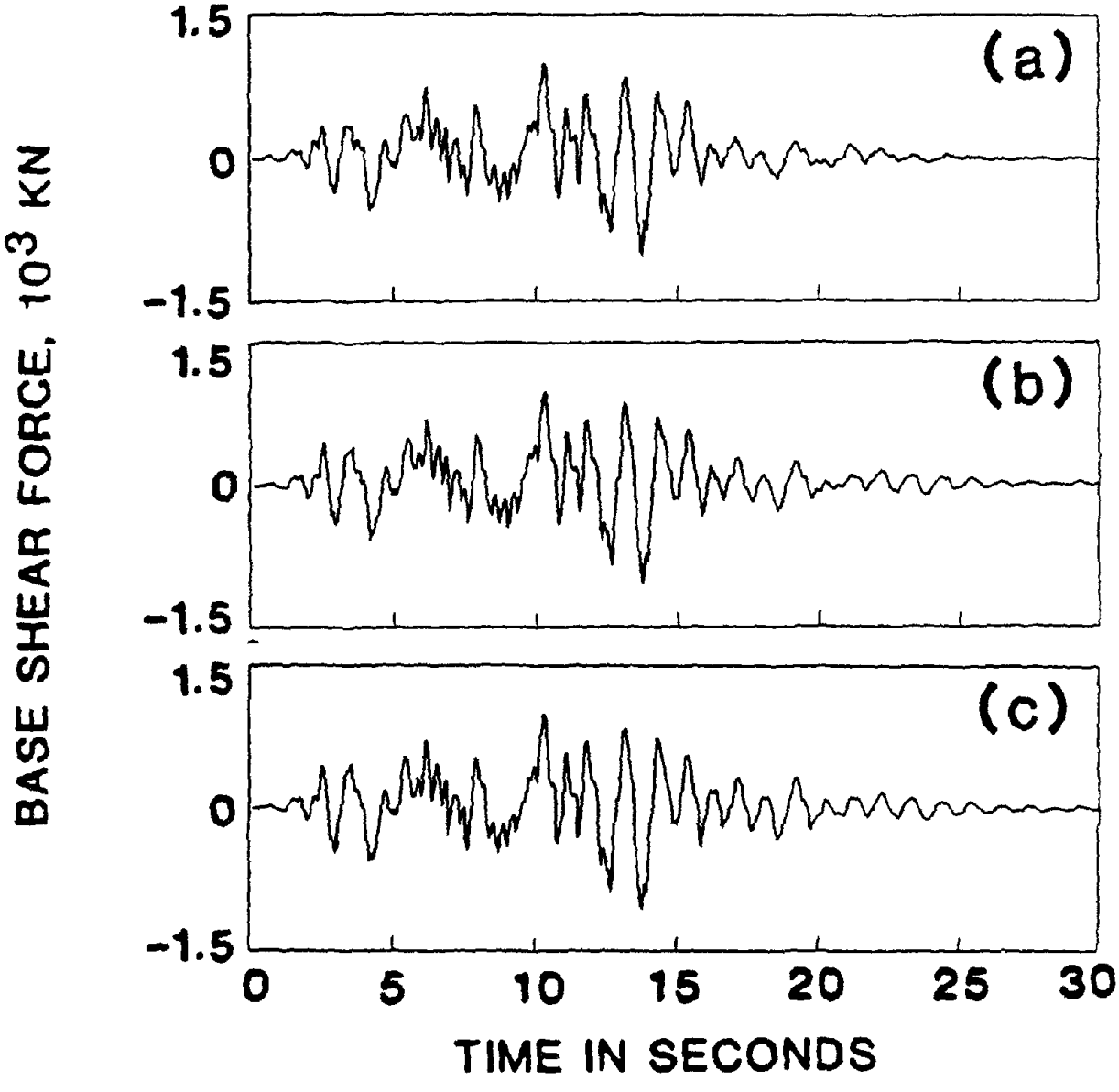

Fig. 88: Effect of Truncation of Small Control Forces on Base Shear Force for an 8-Story Building with an Active Mass Damper Using Riccati Closed-Loop Control Algorithm for Different Truncation Levels ϵ: (a) No Truncation $\epsilon = 0$, (b) $\epsilon = 50$ KN (20%), (c) $\epsilon = 75$ KN (30%).

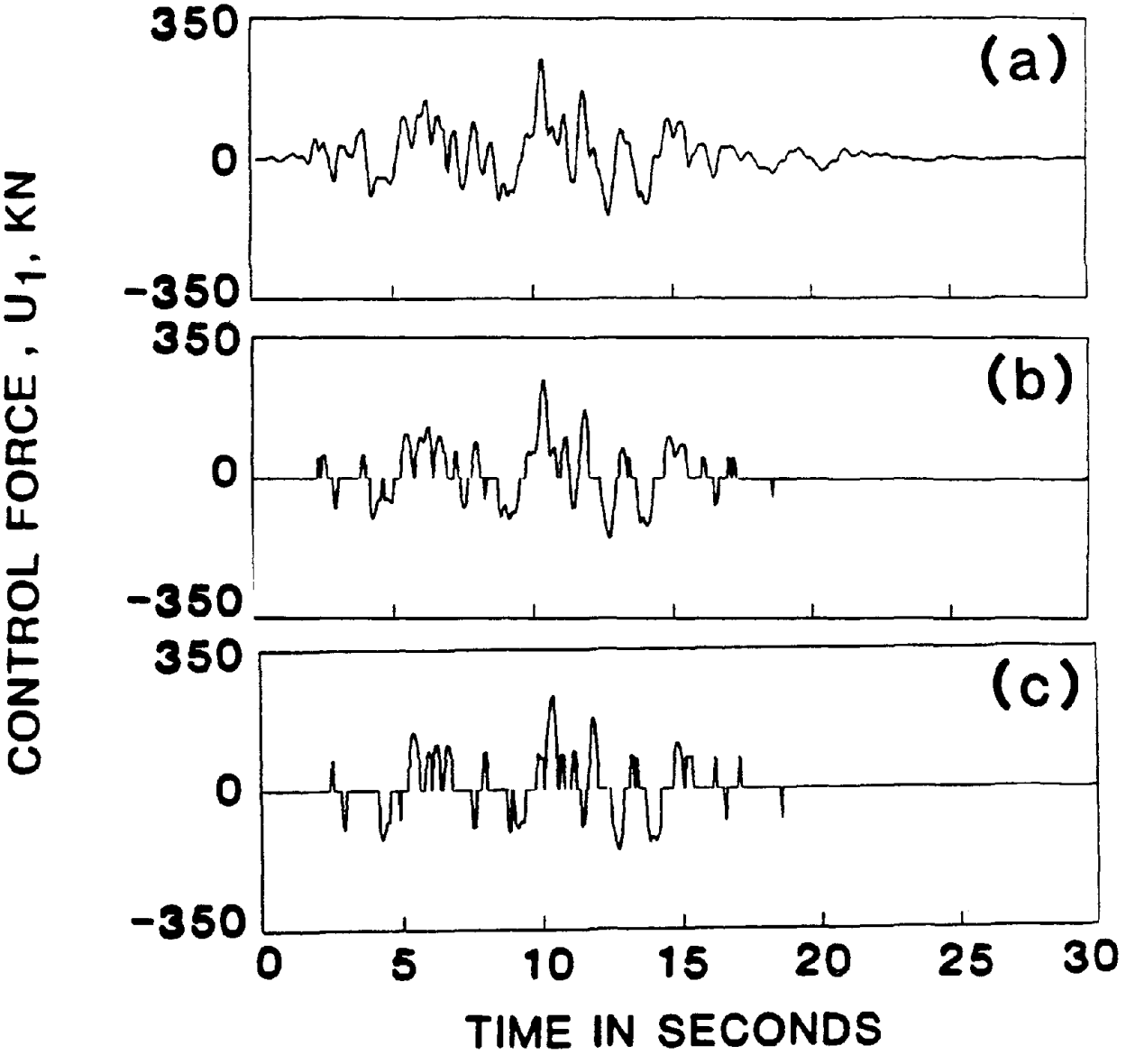

Fig. 89: Effect of Truncation of Small Control Forces for an 8-Story Building with Active Mass Damper Using Riccati Closed-Loop Control Algorithm for Different Truncation Levels ϵ: (a) No Truncation ϵ = 0, (b) ϵ = 50 KN (20%), (c) ϵ = 75 KN (30%).

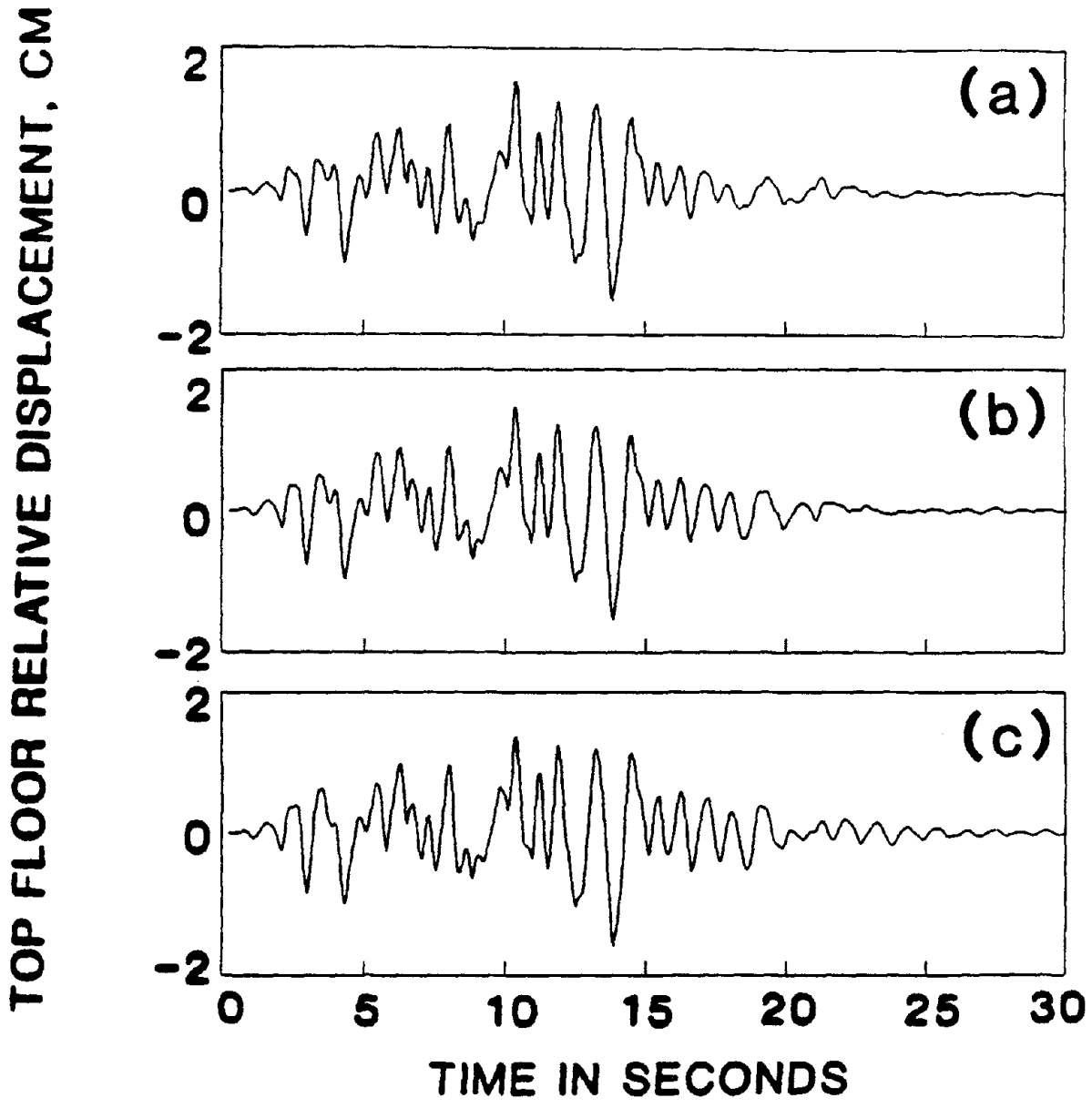

Fig. 90: Effect of Truncation of Small Control Forces on Top Floor Relative Displacement for an 8-Story Building with Active Mass Damper Using Instantaneous Optimal Closed-Loop Control Algorithm for Different Truncation Levels ϵ: (a) No Truncation $\epsilon = 0$, (b) ϵ = 50 KN (21.55%), (c) ϵ = 75 KN (32.32%).

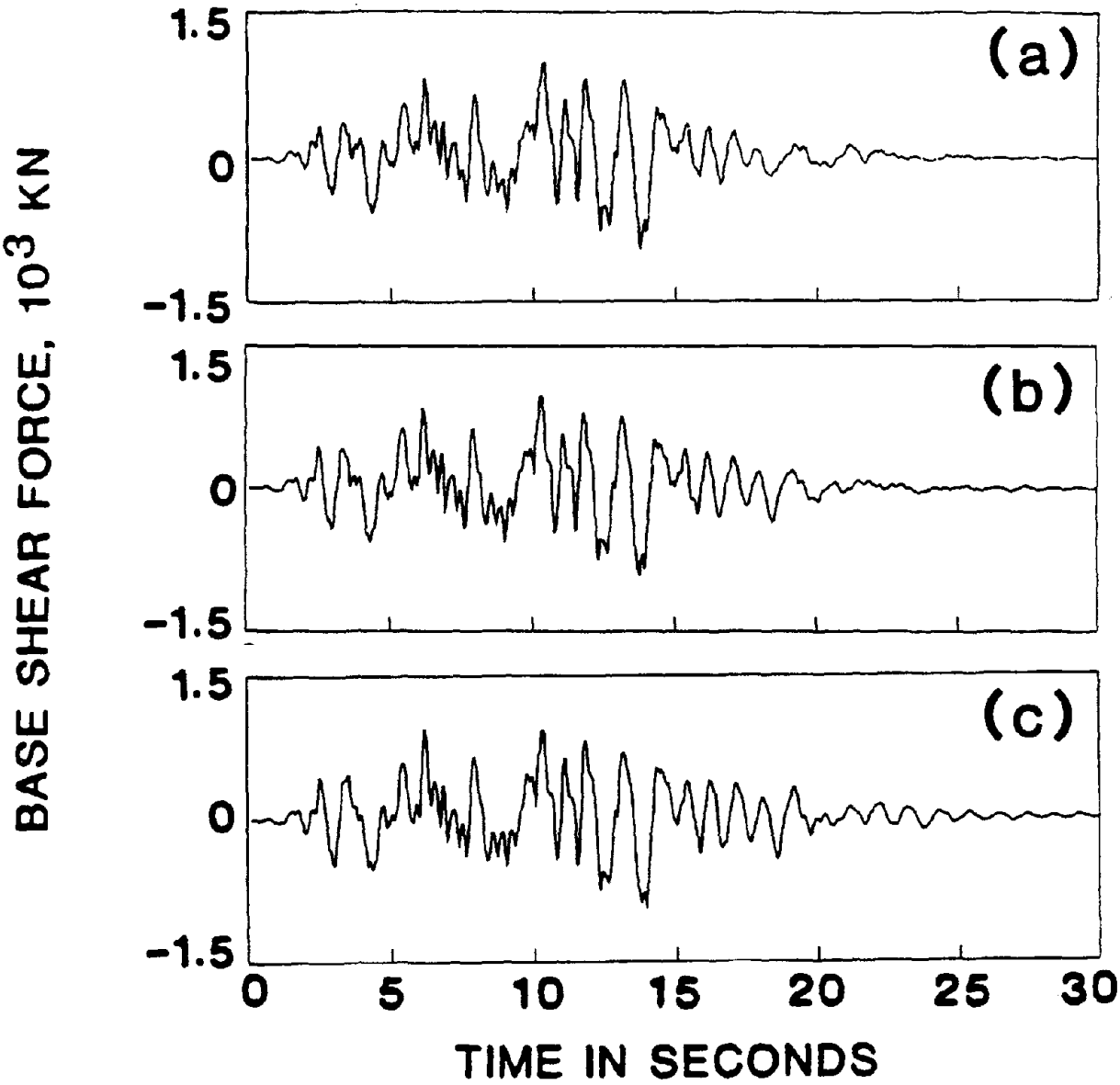

Fig. 91: Effect of Truncation of Small Control Forces on Base Shear Force for an 8-Story Building with Active Mass Damper Using Instantaneous Optimal Closed-Loop Control Algorithm for Different Truncation Levels ϵ: (a) No Truncation $\epsilon = 0$, (b) $\epsilon = 50$ KN (21.55%), (c) $\epsilon = 75$ KN (32.32%).

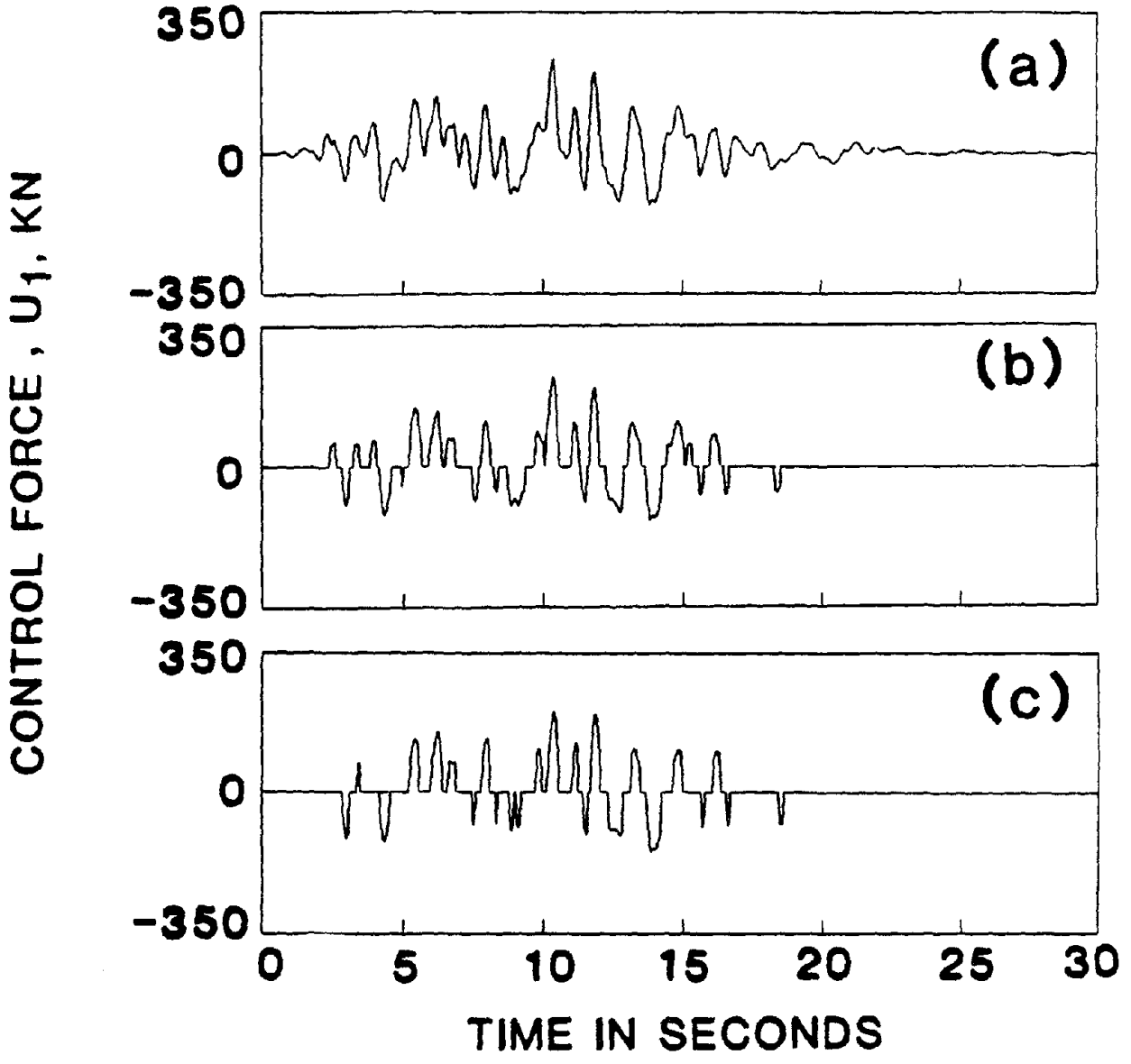

Fig. 92: Effect of Truncation of Small Control Forces for an 8-Story Building with Active Mass Damper Using Instantaneous Optimal Closed-Loop Control Algorithm for Different Truncation Levels ϵ: (a) No Truncation $\epsilon = 0$, (b) $\epsilon = 50$ KN (21.55%), (c) $\epsilon = 75$ KN (32.32%).

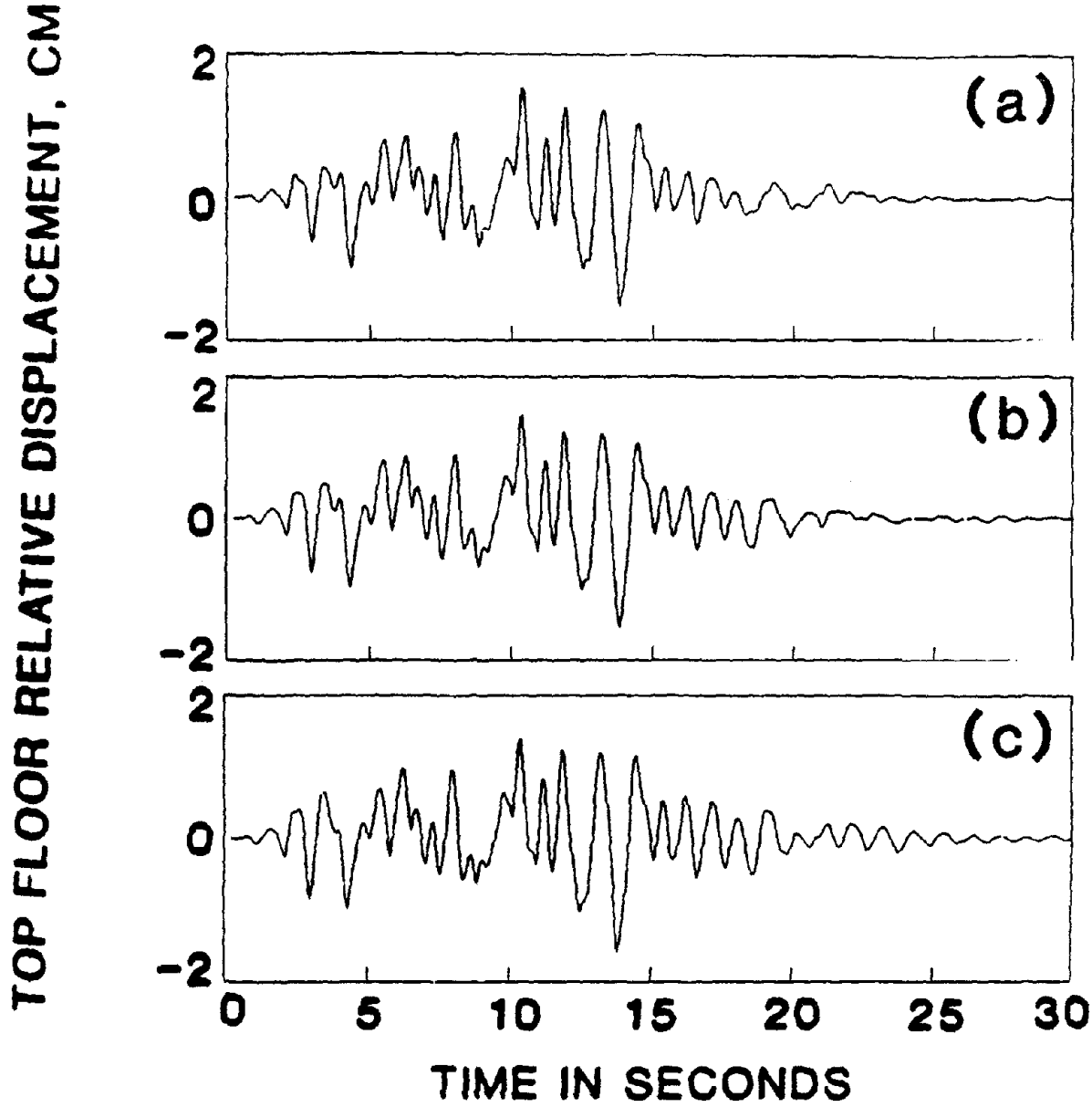

Fig. 93: Effect of Truncation of Small Control Forces on Top Floor Relative Displacement for an 8-Story Building with Active Mass Damper Using Instantaneous Optimal Open-Loop Control Algorithm for Different Truncation Levels ϵ: (a) No Truncation $\epsilon = 0$, (b) $\epsilon =$ 50 KN (21.55%), (c) $\epsilon = 75$ KN (32.32%).

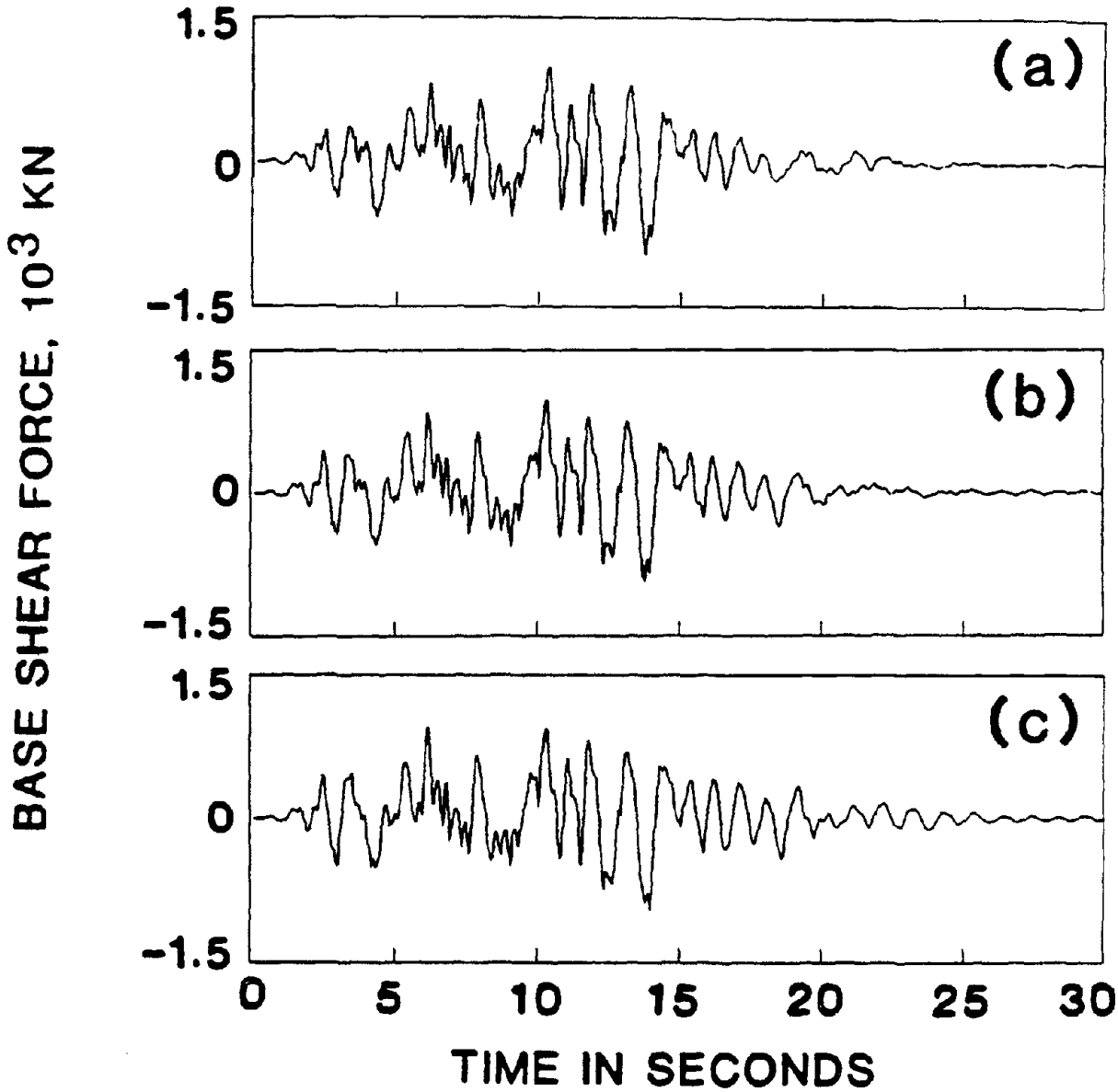

Fig. 94: Effect of Truncation of Small Control Forces on Base Shear Force for an 8-Story Building with Active Mass Damper Using Instantaneous Optimal Open-Loop Control Algorithm for Different Truncation Levels ϵ: (a) No Truncation $\epsilon = 0$, (b) $\epsilon = 50$ KN (21.55%), (c) $\epsilon = 75$ KN (32.32%).

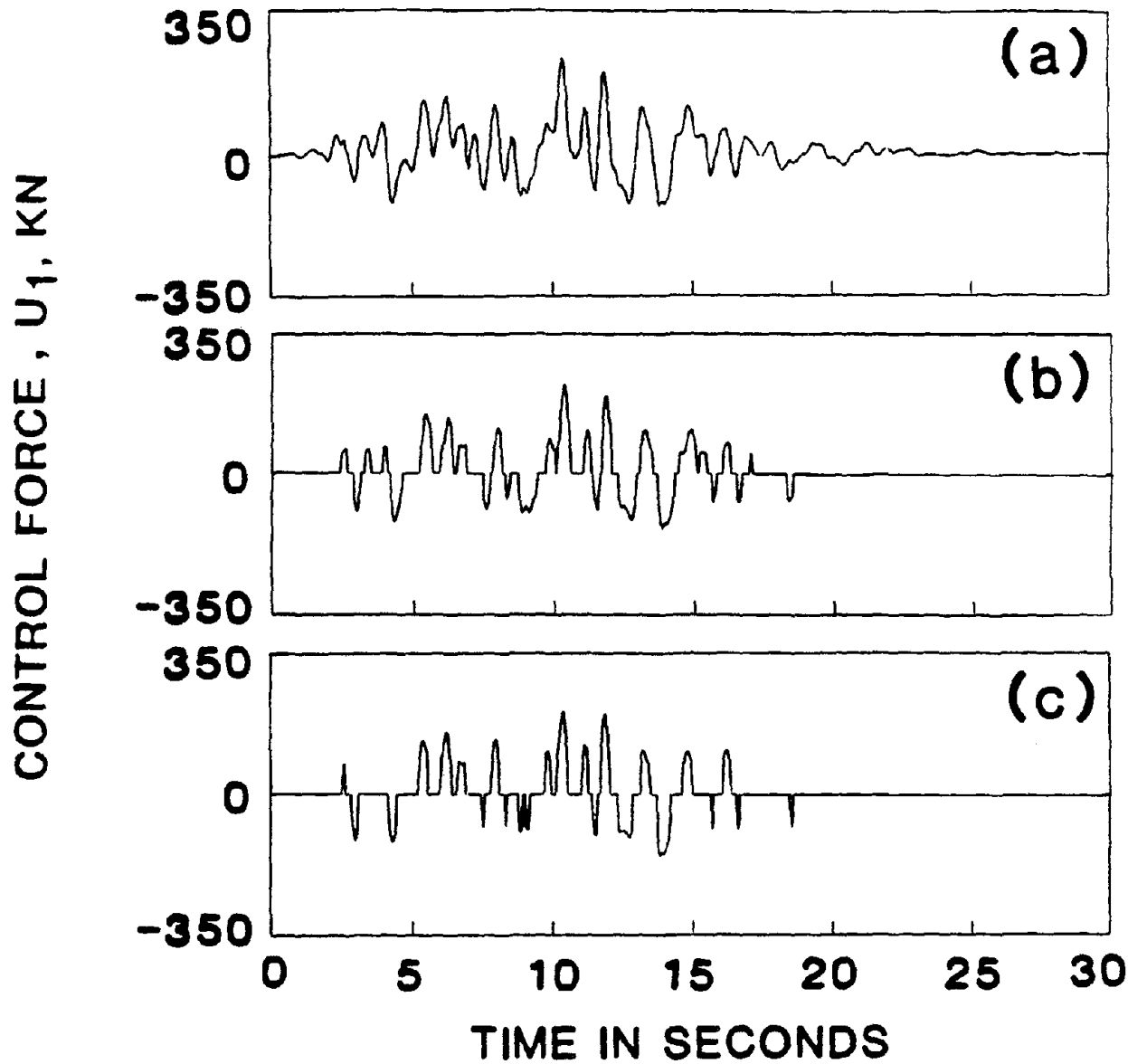

Fig. 95: Effect of Truncation of Small Control Forces for an 8-Story Building with Active Mass Damper Using Instantaneous Optimal Open-Loop Control Algorithm for Different Truncation Levels ϵ: (a) No Truncation $\epsilon = 0$, (b) $\epsilon = 50$ KN (21.55%), (c) $\epsilon = 75$ KN (32.32%).

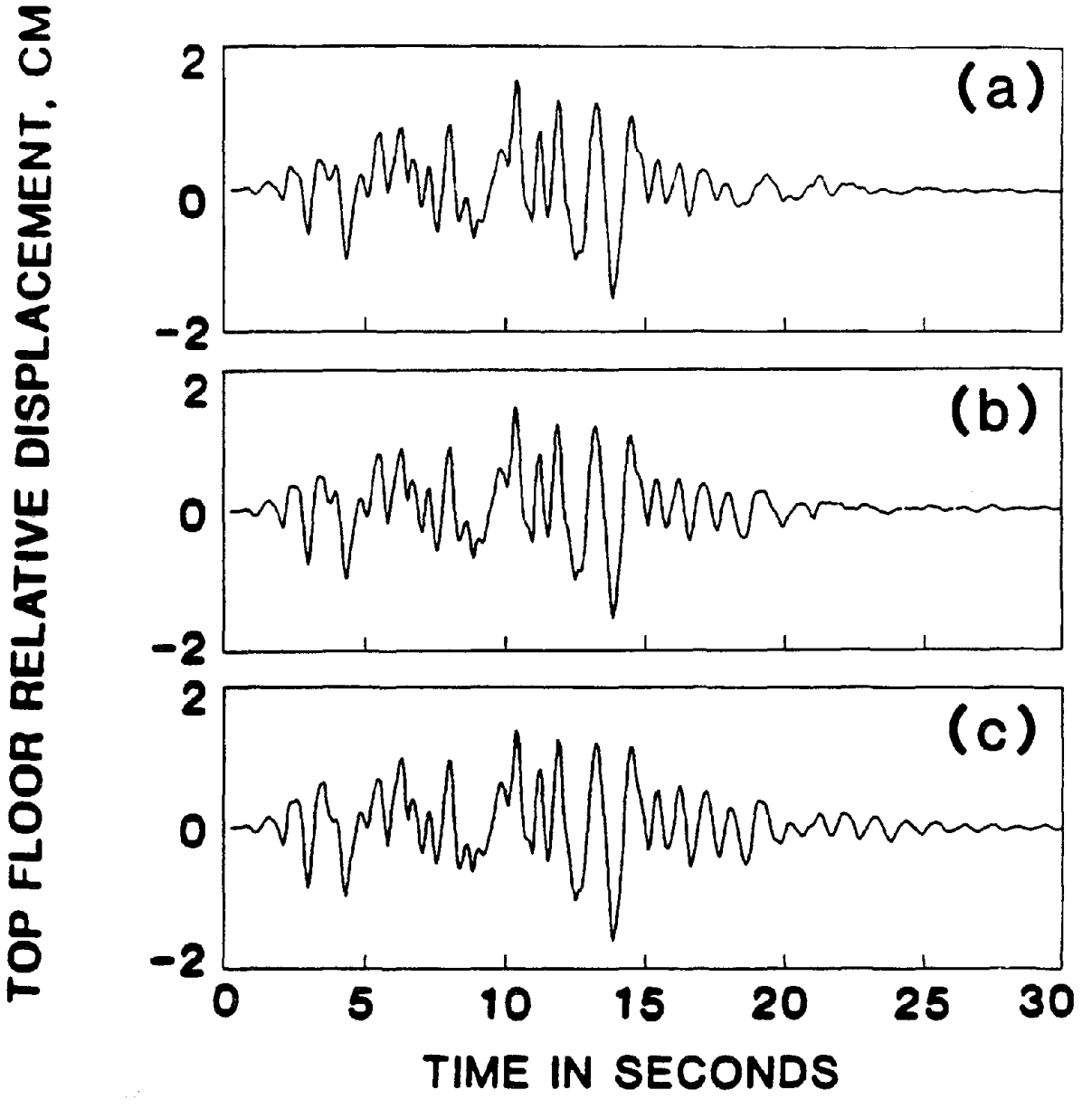

Fig. 96: Effect of Truncation of Small Control Forces on Top Floor Relative Displacement for an 8-Story Building with Active Mass Damper Using Instantaneous Optimal Closed-Open-Loop Control Algorithm for Different Truncation Levels ϵ: (a) No Truncation $\epsilon = 0$, (b) $\epsilon = 50$ KN (21.55%), (c) $\epsilon = 75$ KN (32.32%).

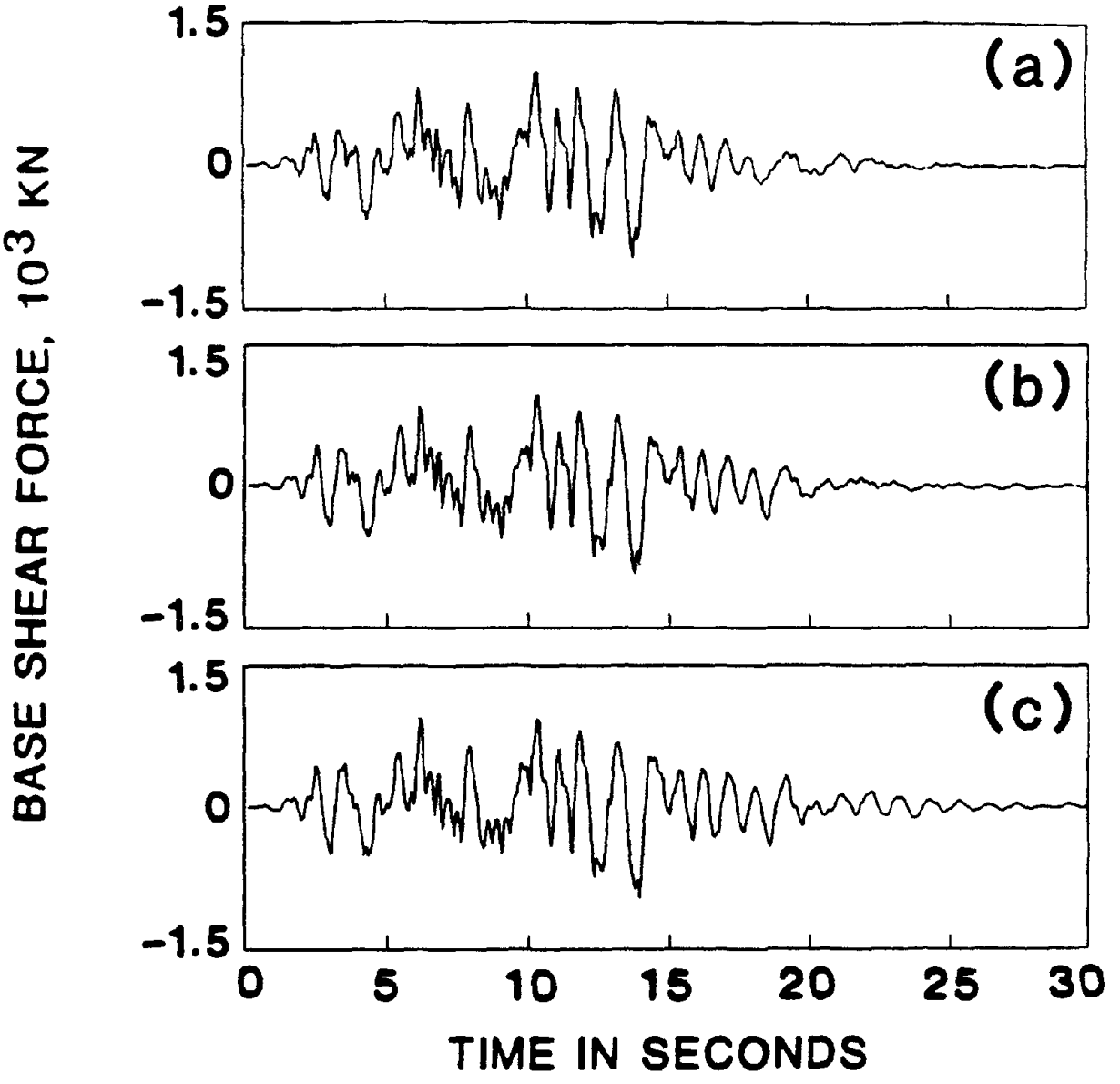

Fig. 97: Effect of Truncation of Small Control Forces on Base Shear Force for an 8-Story Building with Active Mass Damper Using Instantaneous Optimal Closed-Open-Loop Control Algorithm for Different Truncation Levels ϵ: (a) No Truncation $\epsilon = 0$, (b) $\epsilon =$ 50 KN (21.55%), (c) ϵ = 75 KN (32.32%).

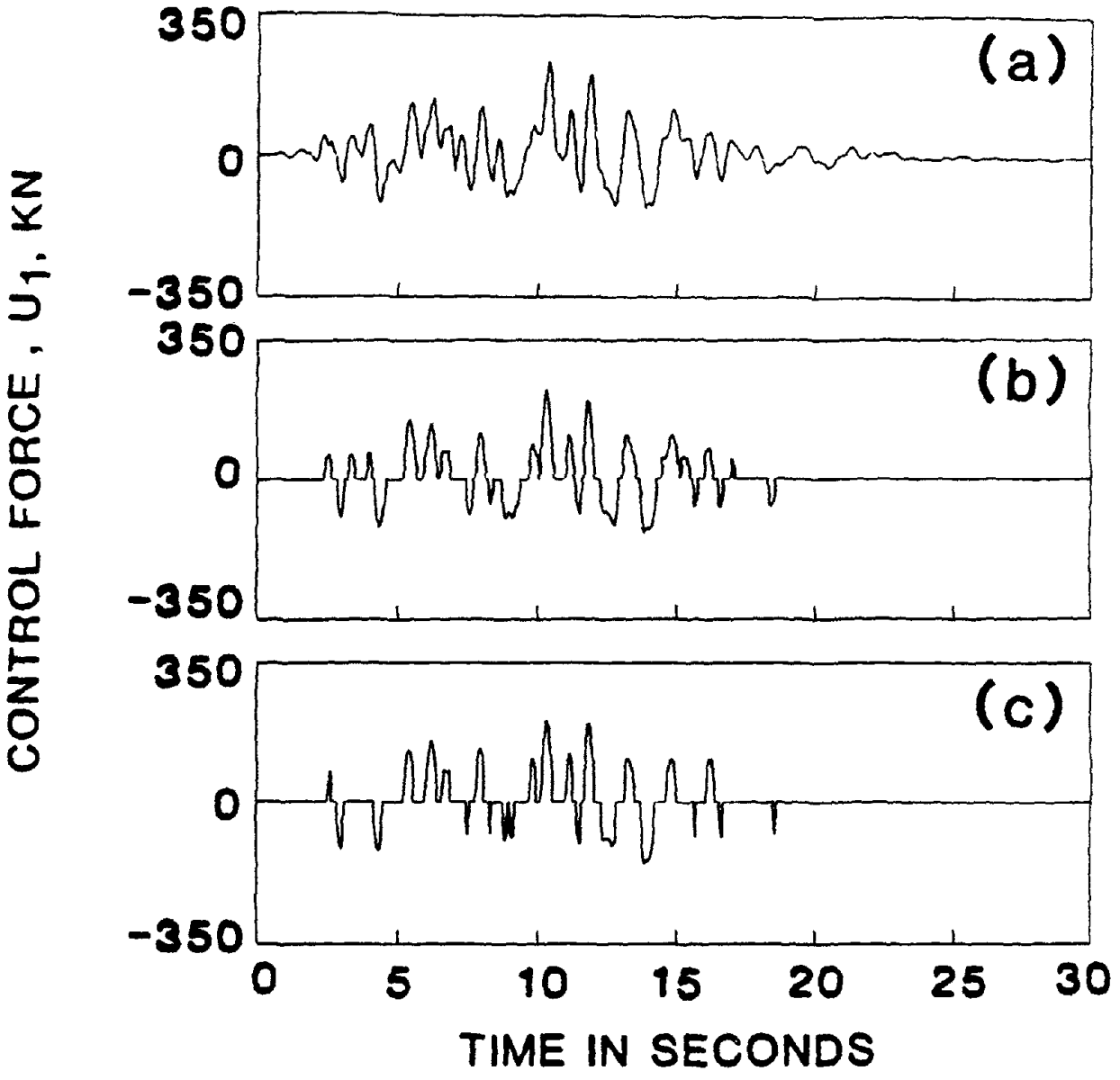

Fig. 98: Effect of Truncation of Small Control Forces for an 8-Story Building with Active Mass Damper Using Instantaneous Optimal Closed-Open-Loop Control Algorithm for Different Truncation Levels ϵ: (a) No Truncation $\epsilon = 0$, (b) $\epsilon = 50$ KN (21.55%), (c) $\epsilon = 75$ KN (32.32%).

VII. CONCLUSIONS

Under seismic excitations, the effect of system uncertainty, time delay, and truncation of small control forces on the structural control system have been investigated. The sensitivity, criticality and tolerance for system identification errors, time delay, and elimination of small control forces depend on the particular control algorithm used. Four control algorithms, which have been verified experimentally to be useful for earthquake-excited structures [4,5], have been studied. These include the Riccati closed-loop control algorithm, and three instantaneous optimal control algorithms recently proposed [17-18]. The method of sensitivity analysis for each control algorithm has been presented. Both active tendon control system and active mass damper have been investigated. Conclusions are summarized in the following.

(A) For uncertainty in system identification, the following conclusions are observed.

(i) The instantaneous optimal closed-loop control algorithm is independent of the system uncertainty. In other words, any estimation error in structural properties, such as damping, stiffness and natural frequency, does not affect the efficiency of the control system.

(ii) The instantaneous optimal closed-open-loop control algorithm is not sensitive to system uncertainties at all. A substantial estimation error for various structural parameters has an insignificant effect on the control system.

(iii) The instantaneous optimal open-loop control algorithm is quite sensitive to the system uncertainty in stiffness (or natrual frequency). An estimation error over 10% for the stiffness (or 5% for the first natural frequency) may result in a serious degradation for the control system. However, the control algorithm is not sensitive to the damping estimation.

In other words, a large estimation error for the structural damping does not affect the control system.

(iv) For the Riccati closed-loop control algorithm, the uncertainty in stiffness (or frequency) estimation has a moderate effect on the structural response and control force; however, its effect on the control efficiency is less prominent. A 20% estimation error for the stiffness (or 10% for the fundamental natrual frequency) is clearly acceptable. Again, the Riccati closed-loop control algorithm is not sensitive to the uncertainty in damping estimation. A 40% estimation error for damping is still acceptable.

From numerous sensitivity analysis results, it can be concluded, in general, that the control system is not sensitive at all to the statistical uncertainty involved in determining the dampings of the structure. The effect of damping estimation error on the control system is negligible. This is a very important and beneficial conclusion for the application of active control system, because the accurate identification of the damping coefficient for a structure is rather difficult. For some control algorithms, however, care should be taken in estimating the stiffness or natural frequencies in order to avoid excessive degradation of the control system.

(B) For system time delay, the following conclusions are obtained.

The instantaneous optimal open-loop control algorithm is most sensitive and critical to system time delay. It is followed by the instantaneous optimal closed-open-loop control algorithm. Two closed-loop control algorithms investigated are less sensitive to time delay because they depend exclusively on the feedback response state vector. In general, open-loop control is expected to be more critical and sensitive to system time delay. A system time delay always results in a degradation of control efficiency in the sense that both the response quantities and required active control

forces are larger than the corresponding results associated with no system time delay.

One important observation is that the tolerance for time delay is rather stringent, with 3% of the fundamental structural period for the instantaneous optimal open-loop control algorithm, and 4.5% of the fundamental structural period for other control algorithms. For the structure with a fundamental period, T_f, of 1.085 seconds considered in this report, the tolerances are 33×10^{-3} and 49×10^{-3} seconds, respectively. The problem becomes more critical when the period of the structure is shorter (or the fundamental frequency is higher). As a result, the system time delay may be an important issue for practical implementation of active control systems. In fact, such a conclusion has also been revealed experimentally [4, 5]. The experimental results using a scale structural model and excited by an earthquake record on a shaking table [4, 5] indicate that the response quantities and control force are always larger than those computed theoretically without a system time delay. In this regard, future research efforts are needed to establish methodologies for compensating system time delay, such as the preliminary study conducted in Ref. 9.

(C) For the truncation of small control forces, the following conclusions are obtained from extensive numerical results.

i) The active control systems investigated are not sensitive to the elimination of control forces that are smaller than 20% of the maximum control force.

(ii) With the truncation of small control forces, the structural response quantities do not die down as rapidly as in the case without truncation. However, the maximum response quantities remain practically unchanged, if the truncation level is within 20% of the maximum control force.

(iii) The conclusions obtained above hold for all control algorithms studied in this report. It is expected that these conclusions will hold for other control algorithms not investigated.

It should be emphasized that conclusions derived in this report are restricted to seismic-excited structures. Further studies are needed for other types of environmental loads.

ACKNOWLEDGEMENT

This research is supported in part by the National Science Foundation Grant No. ECE-85-21496 and National Center for Earthquake Engineering Research Grant No. NCEER-86-3021.

REFERENCES

1. Abdel-Rohman, M., and Leipholz, H.H., "Structural Control Considering Time Delay Effect," accepted for publication in Transactions of the Canadian Society of Mechanical Engineers, Oct. 1984.

2. Leipholz, H. H. (ed.), Structural Control, North-Holland Publishing Company, 1980, Proc. of First International Symposium on Structural Control, University of Waterloo, Waterloo, Canada, 1980.

3. Leipholz, H.H.E., (ed.), Structural Control, Martinus Nijhoff Publishing Co., Amsterdam, 1987, Proc. of Second International Symposium on Structural Control, University of Waterloo, Waterloo, Canada, July 15-17, 1985.

4. Lin, R.C., Soong, T.T., and Reinhorn, A.M., "Experimental Evaluation of Instantaneous Optimal Algorithms for Structural Control," National Center For Earthquake Engineering Research Technical Report No. NCEER-87-0002, April 1987.

5. Lin, R.C., Soong, T.T., and Reinhorn, A.M., "Active Stochastic Control of Seismic Structures," paper to appear in Proceedings of U.S.-Austria Joint Seminar on Stochastic Structural Mechanics, May 5-6, 1987, Florida Atlantic University, Boca Raton, FL.

6. Lund, R.A., "Active Damping of Large Structures in Winds," Structural Control, edited by H.H. Leipholz, North-Holland Publishing Company, 1980, pp. 459-470.

7. Masri, S.F., and Stafford, F.B., "Optimization Procedure for Pulse-Simulated Response," ASCE, J. Struc. Div., 107, ST9, pp. 1743-1761, 1981.

8. Masri, S.F., Bekey, G.A., and Caughey, T.K., "On-Line Control of Nonlinear Flexible Structures," J. Appl. Mech., Trans. ASME, 49 , pp. 877-884, 1982.

9. McGreevy, S., An Experimental Study of Time Delay Compensation in Active Structure Control, M.S. Thesis, State University of New York at Buffalo, N.Y., Jan. 1987.

10. Miller, R.K., Masri, S.F., Dehghanyar, T.J., and Caughey, T.K., "Active Vibration Control of Large Civil Structures," paper to appear in ASCE Journal.

11. Reinhorn, A.M., and Manolis, G.D., "Current State of Knowledge on Structure Control," The Shock and Vibration Digest, Vol. 17, No. 10, 1985, pp. 35-41.

12. Samali, B., Yang, J.N., and Liu, S.C., "Control of Lateral-Torsional Motion of Buildings Under Seismic Load," Journal of Structural Engineering, ASCE, Vol. 111, No. 10, Oct. 1985, pp. 2165-2180.

13. Sirlin, S., Paliou, C., Longman, R.W., Shinozuka, M., and Samara, E., "Active Control of Floating Structures," Journal of Engineering Mechanics, ASCE, Vol. 112, No. 9, Sept. 1986, pp. 947-965.

14. Soong, T. T., and Skinner, G. T., "Experimental Study of Active Structural Control," Journal of the Engineering Mechanics Division, ASCE, Vol. 107, No. EM6, Dec. 1981, pp. 1057-1068.

15. Soong, T. T., Reinhorn, A. M., and Yang, J. N., "A Standardized Model for Structural Control Experiments and Some Experimental Results," Second International Symposium on Structural Control, Univ. of Waterloo, Ontario, Canada, July 15-17; 1985, in Structural Control, (H.H.E. Leipholz, ed.), Martinus Nijhoff Publishing Co., Amsterdam, 1987, pp. 669-693.

16. Udwadia, F. E., and Tabaie, S., "Pulse Control of Structural and Mechanical Systems," Journal of the Engineering Mechanics Division, ASCE, Vol. 107, 1981, pp. 1011-1028.

17. Yang, J.N., Akbarpour, and Ghaemmaghami, P., "Instantaneous Optimal Control Algorithms For Tall Buildings Under Seismic Excitations," National Center For Earthquake Engineering Research Technical Report, NCEER-TR-87-0007, June 1987.

18. Yang, J.N., Akbarpour, A., and Ghaemmaghami, P., "New Optimal Control Algorithms For Structural Control," Journal of Engineering Mechanics, ASCE, Vol. 113, No. 9, Sept. 1987, pp. 1369-1386.

19. Yang, J.N., and Soong, T.T., "Recent Advances in Active Control of Civil Engineering Structures," paper to appear in Journal of Probabilistic Engineering Mechanics, Dec. 1987.

20. Yang, J.N., and Akbarpour, A., "Effect of System Uncertainty on Active Structural Control," paper presented at the Sixth Annual Structures Congress, ASCE, August 17-20, 1987, Orlando, FL.

21. Yang, J.N., and Akbarpour, A., "Structural Control With System Time Delay," paper presented at the 6th ASCE EMD Specialty Conference held on May 20-22, 1987, SUNY/Buffalo.

22. Yao, J. T. P., "Concept of Structural Control," Journal of the Structural Division, ASCE, Vol. 98, No. ST7, July 1972, pp. 1567-1574.

23. Yao, J. T. P., and Soong, T. T., "Importance of Experimental Studies in Structural Control," Reprint 84-010, ASCE, Atlanta Convention, May 14-18, 1984.

24. Yao, J. T. P., and Abdel-Rohman, M., "Research Topics for Practical Implementation of Structural Control," Second International Symposium on Structural Control, Univ. of Waterloo, Ontario, Canada, July 15-17, 1985; in Structural Control, (H.H.E. Leipholz, ed.), Martinus Nijhoff Publishing Co., Amsterdam, 1987.